

**Advanced Magnetic Resonance Imaging
and Quantitative Analysis Approaches
in Patients with Refractory Focal Epilepsy**

Barbara Anne Katharina Kreilkamp

Ph.D.

2017



UNIVERSITY OF
LIVERPOOL

INSTITUTE OF
TRANSLATIONAL
MEDICINE

The Walton Centre



NHS Foundation Trust

Excellence in Neuroscience



epilepsy *action*

**Advanced Magnetic Resonance Imaging
and Quantitative Analysis Approaches
in Patients with Refractory Focal Epilepsy**

This thesis is submitted in accordance with
the requirements of the University of
Liverpool for the Degree of Doctor in
Philosophy

by

Barbara Anne Katharina Kreilkamp
B.A., M.Sc. (*Distinction*)

September 2017

In loving memory of

Alice Amelia Augustitus and John Guy Augustitus, my dear grandparents

Declaration

This thesis is the result of my own work. The material contained in this thesis has not been presented, nor is currently being presented, either wholly or in part, for any other degree or qualification.

Date

Signature

Statement on Collaboration with Co-Workers

The work presented in this thesis was carried out at the Walton Centre Foundation Trust (WCFT), National Health Services, in Fazakerley, Liverpool, UK. It involved the analysis of a dataset that had been acquired at the Life and Brain Center Bonn, Germany and another collected at WCFT. Local ethics committees approved of all studies and all participants provided written informed consent. This research was supported by a PhD studentship award by the University of Liverpool and a student bursary by Epilepsy Action.

The data of the first cohort collected in Bonn, Germany was acquired between 2006 and 2011 by Dr Bernd Weber (principal investigator) and involved patients with temporal lobe epilepsy and associated hippocampal sclerosis undergoing pre-surgical evaluation with post-surgical follow-up 1-2 years later. For the second cohort, all analyses were performed on Magnetic Resonance Imaging (MRI), demographic, clinical and neuropsychological data of patients and controls collected within the WCFT project from September 2014 until April 2016. These patients were referred to the WCFT for MRI during pre-surgical evaluation for relief of intractable focal epilepsy while attending clinics with Dr Wiesmann, Dr Bracewell, Dr Nicholson, Professor Marson and Dr Auce. Control volunteers were recruited through the scientific team, medically screened and scanned by Kath Tyler, Sue Kiel, Sharon Gould and Lindsey Rankin. Barbara A. K. Kreilkamp was responsible for MRI acquisition with the definition of sequence parameters (only for data acquired at the WCFT), MRI processing, quality assurance, measurements (except for the hippocampal internal architecture measurements made by Dr Samia Elkommos and the manual tract tracing performed by Lucy Lisanti), data analysis and interpretation of the results.

Acknowledgements

The writing of this thesis has been challenging in many ways – personally and professionally. A topic as exciting as this one is not easily set aside during hours of recreation and play. My partner, friends and family have been as supportive as they could possibly be during my years of study and research. All of their love, faith, support and fun energy has accompanied me on my way to this final rewarding moment of holding my own Ph.D. thesis in my hands. It would not have been possible in this way without each one of you. I am especially indebted to my dear friends Noon, Amal, Christine, Ruth and Geoff for sharing their homes with me countless times during my time of travel and writing up.

Everything I have learnt in the last three years has been guided by my primary supervisor Dr Simon Keller. I thank him for sharing his experience, excitement and his own established excellent network of scientists with me. The high quality of supervision coupled with opportunities to learn embedded in such a friendly working relationship have made this time very special. All of this was more than I could have ever asked for. Thank you, Simon! I hope to continue working with you and your Liverpool team for many years in the future.

I would like to thank my secondary supervisor, Professor Anthony Marson, for all the encouragement before, during and after my PhD and for continuously showing his fascination about the novel MR analysis approaches. Dr Udo Wiesmann, Dr Kumar Das and Dr Shubhabrata Biswas have done this in the same way and I am very grateful for the time and practical support they provided as clinicians right from the outset of this PhD. I have learnt so much from all four of you!

Both of my supervisors, Dr Simon Keller and Professor Anthony Marson have been instrumental in securing funding for the entire 3-year PhD project. I am very grateful that this allowed me to work while being financially secured during times of research and conference attendance through the University of Liverpool PhD studentship and

the Epilepsy Action Postgraduate Study bursary.

So many aspects of this work would not have been possible to complete without the help and conversations with members of staff at the Magnetic Research and Imaging Centre and the WCFT and students at the University of Liverpool. Thank you, Dave Watling, Helen Leggett, Julie Lloyds, Jaki Wilson, Cerian Jackson, Dr Samia Elkommos, Dr Rasheed Zakaria, Dr Graeme Sills, Dr Jessica Atkinson, Dr Jennifer Weston, Dr Batil Alonazi, Amal Alorainy, Dr Fahad Alhazmi, Alanood Alsaleh, Dr Sarah Nevitt, Dr Pete Dixon, Rachael Kelly, Dr Silviya Balabanova, Nadia Al-Najjar, Graham Powell, Val Adams, Sue Monaghan, Bill Bimson, Dr Graham Kemp, Lucy Lisanti, Lorna Bryant, Yachin Chen, Mollie Neason, Dr Vanessa Sluming, Dr Martyn Bracewell, Dr Andrew Nichols and Dr Pauls Auce. I especially would like to thank the superintendent MR radiographer, Kath Tyler and radiographers Sharon Gould, Susan Kiel and Lindsey Rankin in the WCFT involved in the research for acquiring the high-quality data and telling funny stories.

Last but not least, I would like to say a big thank you to my collaborators. I'm very grateful for all the opportunities and guidance Professor Mark Richardson and Dr Bernd Weber provided during preparation of our manuscript, which has now been published in *Neuroimage: Clinical*. This would not have been possible in the final form without Sarah's support with some of the statistics involved. Thank you, Russell, for devoting a whole fun week at MUSC in Charleston, USA to teach me a new image analysis technique and sharing many of your MATLAB scripts with me!

Advanced Magnetic Resonance Imaging and Quantitative Analysis Approaches in Patients with Refractory Focal Epilepsy

Barbara Anne Katharina Kreilkamp

Abstract

Background

Epilepsy has a high prevalence of 1%, which makes it the most common serious neurological disorder. The most difficult to treat type of epilepsy is temporal lobe epilepsy (TLE) with its most commonly associated lesion being hippocampal sclerosis (HS). About 30-50% of all patients undergoing resective surgery of epileptogenic tissue continue to have seizures postoperatively. Indication for this type of surgery is only given when lesions are clearly visible on magnetic resonance images (MRI). About 30% of all patients with focal epilepsy do not show an underlying structural lesion upon qualitative neuroradiological MRI assessment (MRI-negative).

Objectives

The work presented in this thesis uses MRI data to quantitatively investigate structural differences between brains of patients with focal epilepsy and healthy controls using automated imaging preprocessing and analysis methods.

Methods

All patients studied in this thesis had electrophysiological evidence of focal epilepsy, and underwent routine clinical MRI prior to participation in this study. There were two datasets and both included a cohort of age-matched controls: (i) Patients with TLE and associated HS who later underwent selective amygdalahippocampectomy (cohort 1) and (ii) MRI-negative patients with medically refractory focal epilepsy (cohort 2). The participants received high-resolution routine clinical MRI as well as additional sequences for gray and white matter (GM/WM) structural imaging. A neuroradiologist reviewed all images prior to analysis. Hippocampal subfield volume and automated tractography analysis was performed in patients with TLE and HS and related to post-surgical outcomes, while images of MRI-negative patients were analyzed using voxel-based morphometry (VBM) and manual/automated tractography. All studies were designed to detect quantitative differences between patients and controls, except for the hippocampal subfield analysis as control data was not available and comparisons were limited to patients with persistent postoperative seizures and those without.

Results

1. Automated hippocampal subfield analysis (cohort 1):

The high-resolution hippocampal subfield segmentation technique cannot establish a link between hippocampal subfield volume loss and post-surgical outcome. Ipsilateral and contralateral hippocampal subfield volumes did not correlate with clinical variables such as duration of epilepsy and age of onset of epilepsy.

2. Automated WM diffusivity analysis (cohort 1):

Along-the-tract analysis showed that ipsilateral tracts of patients with right/left TLE and HS were more extensively affected than contralateral tracts and the affected regions within tracts could be specified. The extent of hippocampal atrophy (HA) was not related to (i) the diffusion alterations of temporal lobe tracts or (ii) clinical characteristics of patients, whereas

diffusion alterations of ipsilateral temporal lobe tracts were significantly related to age at onset of epilepsy, duration of epilepsy and epilepsy burden. Patients without any postoperative seizure symptoms (excellent outcomes) had more ipsilaterally distributed WM tract diffusion alterations than patients with persistent postoperative seizures (poorer outcomes), who were affected bilaterally.

3. Automated epileptogenic lesion detection (cohort 2):

Comparison of individual patients against the controls revealed that focal cortical dysplasia (FCD) can be detected automatically using statistical thresholds. All sites of dysplasia reported at the start of the study were detected using this technique. Two additional sites in two different patients, which had previously escaped neuroradiological assessment, could be identified. When taking these statistical results into account during re-assessment of the dedicated epilepsy research MRI, the expert neuroradiologist was able to confirm these as lesions.

4. Manual and automated WM diffusion tensor imaging (DTI) analysis (cohort 2):

The analysis of consistency across approaches revealed a moderate to good agreement between extracted tract shape, morphology and space and a strong correlation between diffusion values extracted with both methods. While whole-tract DTI-metrics determined using Automated Fiber Quantification (AFQ) revealed correlations with clinical variables such as age of onset and duration of epilepsy, these correlations were not found using the manual technique. The manual approach revealed more differences than AFQ in group comparisons of whole-tract DTI-metrics. Along-the-tract analysis provided within AFQ gave a more detailed description of localized diffusivity changes along tracts, which correlated with clinical variables such as age of onset and epilepsy duration.

Conclusions

While hippocampal subfield volume loss in patients with TLE and HS was not related with any clinical variables or to post-surgical outcomes, WM tract diffusion alterations were more bilaterally distributed in patients with persistent postoperative seizures, compared to patients with excellent outcomes. This may indicate that HS as an initial precipitating injury is not affected by clinical features of the disorder and automated hippocampal subfield mapping based on MRI is not sufficient to stratify patients according to outcome. Presence of persisting seizures may depend on other pathological processes such as seizure propagation through WM tracts and WM integrity. Automated and time-efficient three-dimensional voxel-based analysis may complement conventional visual assessments in patients with MRI-negative focal epilepsy and help to identify FCDs escaping routine neuroradiological assessment. Furthermore, automated along-the-tract analysis may identify widespread abnormal diffusivity and correlations between WM integrity loss and clinical variables in patients with MRI-negative epilepsy. However, automated WM tract analysis may differ from results obtained with manual methods and therefore caution should be exercised when using automated techniques.

Publications

Only the publications related to work presented within this thesis are listed.

Kreilkamp, B. A. K., Weber, B., Richardson, M. P., Keller, S. S. (2017). Automated tractography in patients with temporal lobe epilepsy using TRActs Constrained by UnderLying Anatomy (TRACULA). *NeuroImage: Clinical*, 14, 67-76. <http://doi.org/10.1016/j.nicl.2017.01.003>

Kreilkamp, B. A. K., Weber, B., Elkommos, S. B., Richardson, M. P., Keller, S. S. (2018). Hippocampal Subfield Segmentation in Temporal Lobe Epilepsy: Relation to Outcomes. *Acta Neurologica Scandinavica*. Under Revision.

Keller, S. S., Richardson, M. P., Schoene-Bake, J.-C., O’Muircheartaigh, J., Elkommos, S., **Kreilkamp, B.**, Weber, B. (2015). Thalamotemporal alteration and postoperative seizures in temporal lobe epilepsy. *Annals of Neurology*, 77(5), 760-774. <http://doi.org/10.1002/ana.24376>

Keller, S.S., Glenn, G.R., Weber, B., **Kreilkamp, B.A.K.**, Jensen, J.H., Helpert, J.A., Barker, G.J. (2017). Preoperative automated fibre quantification predicts postoperative seizure outcome in temporal lobe epilepsy. *Brain*, Volume 140, Issue 1, 1 January 2017, 68–82, doi:<http://dx.doi.org/10.1093/brain/aww280>

Kreilkamp, B.A.K., Das, K., Wieshmann, U.C., Tyler, K., Kiel, S., Gould, S., Marson, A.G., Keller, S.S. (2017) Voxel-based MRI Analysis Can Assist Clinical Diagnostics in Patients with MRI-negative Epilepsy. Organization of Human Brain Mapping, Vancouver, British Columbia, Canada, June 2017 (abstract).

Kreilkamp, B.A.K., Das, K., Wieshmann, U.C., Tyler, K., Kiel, S., Gould, S., Marson, A.G., Keller, S.S. (2016) Voxel-based Myelinometry in Patients with MRI-negative Temporal Lobe Epilepsy. Geneva, Switzerland, Organization of Human Brain Mapping, June 2016 (abstract).

Kreilkamp, B.A.K., Das, K., Parkes, L.M., Wieshmann, U.C., Tyler, K., Kiel, S., Gould, S., Marson, A.G., Keller, S.S. (2016) Statistical Cerebral Blood Flow Mapping in Patients with Temporal Lobe Epilepsy. 12th European Congress on Epileptology, International League Against Epilepsy, Prague, Czech Republic, September 2016 (abstract).

Kreilkamp, B.A.K., Weber, B., Richardson, M.P., Keller, S.S. (2015) Automated Tractography using TRACULA for the Investigation of White Matter Tracts in Patients with Temporal Lobe Epilepsy. Festival of Neuroscience, The British Neuroscience Association, Edinburgh, United Kingdom, April 2015 (abstract).

Kreilkamp, B.A.K., Weber, B., Richardson, M.P., Keller, S.S. (2015) TRACULA versus TBSS: Comparing DTI Analysis Approaches in Patients with Temporal Lobe Epilepsy. Organization of Human Brain Mapping, Honolulu, Hawaii, United States of America, June 2015 (abstract).

Speaker

Kreilkamp, B.A.K. (2017) MRI-Analysis in Patients with 'non-lesional' Epilepsy. Annual Meeting of the Association of British Neurologists, Liverpool, United Kingdom, May 2017.

Kreilkamp, B.A.K. (2016) Translating MRI Research into Clinical Practice: Applications in Refractory Epilepsy. The Walton Centre Research Panel Meeting, Liverpool, United Kingdom, September 2016.

Kreilkamp, B.A.K. (2015) Principles of Diffusion Tensor Imaging and Applications in Science. Neuroimaging Group Meeting, University of Liverpool, Liverpool, United Kingdom, October 2015.

Kreilkamp, B.A.K. (2014) Sophisticated MR Imaging and Quantitative Analyses in Refractory Epilepsy. North-West Epilepsy Group Meeting, Liverpool, United Kingdom, November 2014.

Awards

1. Three-year PhD Studentship at the University of Liverpool, United Kingdom
2. Post-graduate Study Bursary Epilepsy Action of 2014/2015 £3000

Thesis Contents

List of Tables.....	xiii
List of Figures.....	xvii
Keywords, Glossary and Definitions.....	xxvii
Abbreviations.....	xxxii
Chapter 1: Introduction.....	1
1.1 Context and Outline of Thesis.....	1
1.2 Background.....	7
1.2.1 Epileptic Seizures.....	8
1.2.2 Epilepsy Syndromes.....	9
1.3 Surgical Intervention.....	10
1.4 Pre-surgical Evaluation.....	12
1.4.1 Surface Inter-ictal EEG.....	14
1.4.2 Assessment of Preoperative Functional Skills.....	15
1.4.3 Invasive Inter-ictal and Ictal EEG.....	16
1.4.4 Standard Diagnostic MRI.....	17
1.5 Rationale for Advanced MRI of the Brain.....	19
1.5.1 Additional Research Sequences.....	19
1.5.2 Quantitative Techniques.....	21
1.6 Motivation and Goals of this Thesis.....	23
1.6.1 Patients with TLE and Associated HS: Outcome Analysis.....	24
1.6.2 Patients with MRI-negative Focal Epilepsy.....	27
Chapter 2: Materials and Objectives.....	30
2.1 Organization of Chapter 2.....	30
2.2 Refractory Temporal Lobe Epilepsy with Hippocampal Sclerosis.....	31
2.2.1 Introduction.....	31
2.2.2 Methodology.....	32
2.2.2.1 Materials and Participants.....	32
2.2.2.2 Applied MR Sequences.....	33
2.2.2.3 Quantitative MRI Analysis.....	34
2.2.3 Objectives and Hypotheses.....	34
2.2.3.1 Automated Quantitative MRI of the Hippocampus: Study 1.....	34
2.2.3.2 Automated Quantitative MRI of Temporal Lobe Tracts: Study 2.....	36
2.3 Focal 'Non-lesional' and Lesional Epilepsy.....	37
2.3.1 Introduction.....	37
2.3.2 Methodology.....	38
2.3.2.1 Materials and Participants.....	38
2.3.2.2 Applied MR Sequences.....	38
2.3.2.3 Quantitative MRI Analysis.....	40
2.3.3 Objectives and Hypotheses.....	41
2.3.3.1 Neuroradiological Assessment and Clinical Findings: Study 3.....	41
2.3.3.2 Automated Epileptogenic Lesion Detection: Study 4.....	42
2.3.3.3 Automated Tract Reconstruction: Study 5.....	42
Chapter 3: Neuroanatomy.....	45
3.1 Organization of Chapter 3.....	45
3.2 Neuroanatomy of the Cerebrum.....	46

3.2.1 Divisions.....	46
3.2.2 Brain Development.....	50
3.2.3 Malformations of Cortical Development.....	52
3.3 Temporal Lobe.....	57
3.3.1 Hippocampus.....	57
3.3.2 Hippocampal Internal Architecture.....	58
3.3.3 Hippocampal Functions and Projections.....	60
3.4 Temporal Lobe Connectivity.....	65
3.4.1 Fimbria and Fornix.....	66
3.4.2 Parahippocampal Cingulum.....	68
3.4.3 Inferior Longitudinal Fasciculus.....	68
3.4.4 Superior Longitudinal Fasciculus.....	69
3.4.5 Uncinate Fasciculus.....	69
Chapter 4: Review on MR Physics.....	72
4.1 Introduction.....	72
4.2 Basic Principles of MR Image Acquisition.....	73
4.3 3D Volume T1-weighted Imaging.....	76
4.3.1 Principles.....	76
4.3.2 Applications.....	78
4.4 3D Volume T2-weighted Imaging.....	78
4.4.1 Principles.....	78
4.4.2 Applications.....	80
4.5 3D Volume T2FLAIR.....	81
4.5.1 Principles.....	81
4.5.2 Applications.....	83
4.6 High-resolution Coronal FLAIR Sequences.....	83
4.6.1 Principles.....	83
4.6.2 Applications.....	84
4.7 Diffusion Tensor Imaging.....	85
4.7.1 Principles.....	85
4.7.2 Analysis Approaches.....	89
4.7.2.1 Manual Methods.....	89
4.7.2.2 Automated Methods.....	90
Chapter 5: Automated Multi-sequence Hippocampal Subfield Segmentation in Refractory Temporal Lobe Epilepsy: Relation to Clinical Outcomes.....	93
5.1 Introduction.....	93
5.2 Methods.....	97
5.2.1 Participants.....	97
5.2.2 MRI Acquisition.....	97
5.2.3 MRI Analysis.....	98
5.2.4 Statistical Analysis.....	100
5.3 Results.....	101
5.3.1 Volumes and Clinical Correlations.....	101
5.3.2 Outcome.....	103
5.4 Summary.....	107
Chapter 6: TRActs Constrained by UnderLying Anatomy (TRACULA) in Patients with Refractory Epilepsy: Relation to Post-surgical Outcome.....	108
6.1 Introduction.....	108

6.1.1 Objectives and Hypotheses.....	111
6.1.2 Organization of Chapter.....	112
6.2 Methods.....	113
6.2.1 Participants.....	113
6.2.2 MR Acquisition.....	114
6.2.3 Data Pre-processing.....	114
6.2.4 Quality Assessment after Pre-processing.....	115
6.2.5 Extraction of Volumes and Tracts.....	116
6.2.6 Statistical Analysis.....	117
6.3 Results.....	120
6.3.1 Data Quality Assessment.....	120
6.3.2 Patients vs Controls	121
6.3.2.1 Volumes.....	121
6.3.2.2 Whole-tract Diffusion Metric Analysis.....	121
6.3.2.3 Waypoint Diffusion Metric Analysis.....	124
6.4 Summary.....	128
Chapter 7: Neuroradiological Findings in Patients with 'non-lesional' Focal Epilepsy Revealed by Research Protocol.....	130
7.1 Introduction.....	130
7.2 Materials and Methods.....	132
7.3 Results.....	133
7.4 Discussion.....	143
Chapter 8: Automated Multimodal MRI Analysis for Diagnostic Purposes in Patients with MRI-negative Epilepsy	147
8.1 Introduction.....	147
8.2 Methods.....	152
8.2.1 Participants.....	152
8.2.2 MRI Acquisition.....	152
8.2.3 Data Pre-processing.....	152
8.2.4 Generation of Feature Maps	153
8.2.5 Statistical Analysis.....	156
8.3 Results.....	158
8.3.1 Data Quality Assessment.....	158
8.3.2 Neurological Assessment and Statistical Analysis of Feature Maps.....	158
8.3.3 Multi-modal Analysis Based on MAP Clusters.....	160
8.4 Summary.....	164
Chapter 9: Manual and Automated Tractography Approaches in Patients with 'non-lesional' and lesional Temporal Lobe Epilepsy.....	166
9.1 Introduction.....	166
9.1.1 Objectives.....	169
9.1.2 Organization of Chapter	170
9.2 Materials and Methods.....	170
9.2.1 Participants.....	170
9.2.2 Data Preprocessing and Quality Assurance.....	171
9.2.3 Manual and Automated Tractography.....	173
9.2.4 Statistical Analysis.....	175
9.3 Results.....	177
9.3.1 Statistics: Demographic and Clinical Information.....	177

9.3.2 Manual versus Automated Tractography.....	178
9.3.2.1 Quality Control.....	178
9.3.2.2 DTI-metrics.....	178
9.3.2.3 Consistency of Tracts.....	180
9.3.2.4 Correlations Between Whole-tract DTI Metrics and Clinical Variables.....	180
9.3.3 Tract Profile Analysis (AFQ)	181
9.4 Summary	185
Chapter 10: Discussion and Conclusion.....	187
10.1 Organization of Chapter 10.....	187
10.2 Summary of Results	188
10.2.1 Automatic Hippocampal Subfield Segmentation in Patients with TLE and HS.....	188
10.2.2 Automated Tractography Analysis in Patients with TLE and HS.....	188
10.2.3 Neuroradiological Findings in Patients with 'Non-lesional' Focal Epilepsy.....	189
10.2.4 Automatic Detection of Focal Cortical Dysplasia.....	189
10.2.5 Automatic Fiber Quantification in Patients with TLE.....	190
10.3 Methodology, Strengths and Limitations.....	191
10.3.1 Cross-Sectional Study Design.....	191
10.3.2 Clinical Variables.....	192
10.3.3 In Vivo Hippocampal Subfield Mapping.....	193
10.3.4 Automated Tractography of Temporal Lobe Tracts.....	194
10.3.5 Voxel-based Analysis.....	197
10.4 Interpretations and Clinical Implications.....	200
10.4.1 Hippocampus and TLE.....	200
10.4.2 Temporal Lobe WM Tracts and TLE.....	202
10.4.3 Manual and Automated Tractography in Lesional and 'Non-lesional' TLE.....	207
10.4.4 Dysplasia and Focal Epilepsy.....	212
10.5 Future Directions and Conclusions.....	216
10.5.1 Automatic Hippocampal Subfield Segmentation in Patients with TLE and HS.....	216
10.5.2 Automated Tractography Analysis in Patients with TLE and HS.....	216
10.5.3 Automatic Fiber Quantification in Patients with TLE.....	218
10.5.4 Automatic Detection of Focal Cortical Dysplasia.....	218
REFERENCES.....	220
APPENDIX I: Raw Data.....	261
APPENDIX II: Supplementary Material.....	265

List of Tables

Chapter 2: Materials and Objectives

Table 2.1. Demographic, clinical and MR imaging information for all participants of Studies 1 & 2.

Details of individual patients/controls can be found in Table 2.A (Appendix: Raw Data). TLE = temporal lobe epilepsy; SD = standard deviation; SGTCS = secondary-generalized tonic-clonic seizure; FC = febrile convulsions.

Table 2.2. Demographic and clinical information for all participants of Studies 3-5.

Patients with other onsets included (14 patients with a frontal lobe onset and five patients with other onsets: see text). All participants underwent the same imaging protocol. Details of individual patients/controls can be found in Table 2.B (Appendix: Raw Data). TLE = temporal lobe epilepsy; SD = standard deviation; SGTCS = secondary-generalized tonic-clonic seizure.

Table 2.A. Raw data for patients and controls (Studies 1 & 2). FC = febrile convulsions, l = left, HS = hippocampal sclerosis, CPS = complex partial seizure, SPS = simple partial seizure, SGTCS = secondary-generalized tonic-clonic seizure, m/f = male / female, Onset/Age/Duration in years, frequency per month. 0/1 = no/yes. Empty cells indicate missing data. DTI = diffusion tensor imaging, T2STIR = T2 Short TI Inversion Recovery, Boldface: DTI data only.

Table 2.A. (continued). Raw data for patients (Studies 1 & 2). FC = febrile convulsions, r = right, l = left, HS = hippocampal sclerosis, CPS = complex partial seizure, SPS = simple partial seizure, SGTCS = secondary-generalized tonic-clonic seizure, m/f = male / female, Onset/Age/Duration in years, frequency per month. 0/1 = no/yes. Empty cells indicate missing data. DTI = diffusion tensor imaging, T2STIR = T2 Short TI Inversion Recovery, Boldface: DTI data only.

Table 2.B. Raw data for patients (Studies 3-5). CB = Complications at birth, FC = febrile convulsions, SVD = small-vessel disease, r = right, l = left, HS = hippocampal sclerosis, FCD = focal cortical dysplasia, TL = temporal lobe, FL = frontal lobe, TP = temporoparietal, GS = generalized seizure, A = absence, CPS = complex partial seizure, SPS = simple partial seizure, SGTCS = secondary-generalized tonic-clonic seizure, m/f = male / female, Family = Family history of epilepsy. Onset/Age/Duration in years, frequency per week. 0/1 = no/yes. Boldface: presence of potentially epileptogenic lesion (neuroradiological assessment, epilepsy research dedicated MRI). The asterisks indicates dual pathology (HS and FCD).

Table 2.B. (continued). Raw data for controls (Studies 3-5). m/f = male / female, Family = family history of epilepsy. Age in years. 0 = no, 1 = yes.

Chapter 3: Neuroanatomy

Table 3.1. Brain Structures and Their Relation to Epilepsy.

Chapter 4: Review on MR Physics

Table 4.1. Summary of MRI sequences used within this study of patients with focal epilepsy.

SNR = signal-to-noise ratio; CNR = contrast-to-noise ratio; CSF = cerebrospinal fluid; HS = hippocampal sclerosis.

Chapter 5: Automated multi-sequence hippocampal subfield segmentation in refractory temporal lobe epilepsy: Relation to clinical outcomes

Table 5.1. Comparison of Subfield Volumes Corrected for ICV in Patients with Left/Right TLE.

Table 5.2. Clinical Variables According to Surgery Outcome.

TLE = Temporal Lobe Epilepsy; SGTCS = Secondary-Generalized Tonic-Clonic Seizures.

Table 5.3. Comparison of Subfield Volumes Corrected for ICV in Patients with Outcomes ILAE I versus ILAE II-VI.

Chapter 6: TRActs Constrained by UnderLying Anatomy (TRACULA) in Patients with Refractory Epilepsy: Relation to Post-surgical Outcome

Table 6.1. Demographic and Clinical Variables According to Seizure Laterality. Abbreviation: TLE = Temporal Lobe Epilepsy. The conducted statistical tests were Chi-Squared tests of independence for the first three variables; one-way ANOVA for age and unpaired two-tailed t-tests for all remaining clinical variables.

Table 6.2. Kruskal-Wallis ANOVA Comparing Volumes across all groups.

M = Mean; SD = Standard Deviation; TLE = Temporal Lobe Epilepsy; C = Control; r = right; l = left.

Table 6.3. Non-parametric ANCOVA Comparing FA across all groups.

M = Mean; SD = Standard Deviation; TLE = Temporal Lobe Epilepsy; C = Control; l = left; r = right; FA = fractional anisotropy; SLFt = superior longitudinal fasciculus (temporal segment); ILF = inferior longitudinal fasciculus; UF = uncinate fasciculus; CAB = cingulum angular bundle. Corrected p-values.

Table 6.4. Non-parametric ANCOVA Comparing MD across all groups.

M = Mean; SD = Standard Deviation; TLE = Temporal Lobe Epilepsy; C = Control; l = left; r = right; FA = fractional anisotropy; SLFt = superior longitudinal fasciculus

(temporal segment); ILF = inferior longitudinal fasciculus; UF = uncinate fasciculus; CAB = cingulum angular bundle. Corrected p-values.

Chapter 7: Neuroradiological Findings in Patients with 'non-lesional' Focal Epilepsy Revealed by Research Protocol

Table 7.1. Patient Demographic and Clinical Information and Recent MRI-findings. Bold patient IDs indicate that the previous MRI was available for assessment. f=female, m=male, SPS=Simple Partial Seizures, SGTCS=Secondary-Generalized Tonic-Clonic Seizures, A=Absence Seizures, CPS=Complex Partial Seizures, TL=Temporal Lobe, FL=Frontal Lobe, TP=temporoparietal, FT=frontotemporal.

Table 7.2. Lesions found in the most recent MRI and retrospective comparison to previous MRI and reports. Epilepsy dedicated research protocol: 2-D coronal FLAIR MRI with high in-plane resolution (~0.5 mm), 3D T1w/T2w/T2FLAIR imaging. Technical reasons for previous MRI-negative report in italics.

Chapter 8: Automated Multimodal MRI Analysis for Diagnostic Purposes in Patients with MRI-negative Epilepsy

Table 8.1. Results of statistical testing on T1w JCT/EXT images after application of $p < 0.01$ and $p < 0.05$ FWE cluster correction.

The results show that the false positive rate lies between 18% and 53%, while the true positive rate is high. It was at 100% for the combined JCT and EXT image analysis. JCT = junction image; EXT = extension image.

Table 8.2. Summary of multimodal statistical testing based on $>3.5 \text{ cm}^3$ cluster masks of T1w JCT/EXT testing.

Patients with neuroradiologically determined FCDs (first four rows) and all twelve patients with no previously identified FCDs with at least one significant result (at $p < 0.01$ and $p < 0.05$ FWE corrected) in one modality are presented. The arrowheads indicate an increased ($>$) and decreased ($<$) signal in the respective patients' image compared to controls. These were also the patients that were re-reviewed by a consultant neuroradiologist. For three patients (34/49/86), none of the images tested in the multimodal approach with their respective $>3.5 \text{ cm}^3$ cluster masks reached significance.

Chapter 9: Manual and Automated Tractography Approaches in Patients with 'non-lesional' and lesional Temporal Lobe Epilepsy

Table 9.1. Demographic and clinical information for all participants.

TLE = Temporal Lobe Epilepsy; SD = Standard Deviation; SGTCS = Secondary-Generalized Tonic-Clonic Seizure; HS = hippocampal sclerosis.

Table 9.2. Correlations of whole-tract FA/MD values with variables for both approaches.

Spearman rho values (R) are shown with FDR corrected p-values (p) for each type of analysis (manual and automated). Boldface indicates significant effects. UF = uncinate fasciculus; PHWM = parahippocampal white matter bundle; FA = fractional anisotropy; MD = mean diffusivity; ipsi = ipsilateral; contra = contralateral.

Table 9.A. Whole-tract diffusion measures for manual (top) versus AFQ (bottom) tractography.

Abbreviations: M = Mean; SD = Standard Deviation; TLE = Temporal Lobe Epilepsy; C = Control; l = left; r = right; AFQ = Automated Fiber Quantification; FA = fractional anisotropy; MD = mean diffusivity (in 10^{-3} mm²/s); UF = uncinate fasciculus; PHWM = parahippocampal white matter bundle

Table. 9.B. Comparison of FA/MD values from all tracts between patient groups according to sex, presence of HS, SGTCS and history of febrile seizures.

Mean and standard deviations (in brackets) are presented for each tract. No significant effects were observed for either manual or AFQ generated tracts. UF = Uncinate Fasciculus; PHWM = Parahippocampal White Matter Bundle; FA = fractional anisotropy; MD = mean diffusivity; ipsi = ipsilateral; contra = contralateral; HS = hippocampal sclerosis; SGTCS = secondary-generalized tonic-clonic seizures.

List of Figures

Chapter 1: Introduction

Figure 1.1. Clinical trajectory for patients presenting with seizures.
AED = anti-epileptic drug.

Figure 1.2. Pre-surgical Evaluation in TLE (from Immonen 2010). The trajectory of the pre-surgical evaluation process is presented from top to bottom. EEG = electroencephalography; MRI = magnetic resonance imaging; PET = positron-emission tomography; SPECT = single-photon emission computed tomography; MEG = magnetoencephalography; AED = anti-epileptic drug.

Figure 1.3. FCD in the left supramarginal gyrus (top) and superior parietal lobule (bottom).

The related signal appears dark on T1w and bright on T2w/T2FLAIR 3D volume images. The WCFT neuroradiologist's report stated that the two dysplastic sites may be interconnected. L = left.

Figure 1.4. Right HS shown on T2FLAIR and T1FLAIR.

The T2FLAIR image shows hyperintense signal in the hippocampal region, while the T1FLAIR demonstrates hypointensity of the hippocampal formation with a marked volume loss. The loss of internal architecture in the right hippocampus is only marginally visible in both images. T1- and T2FLAIR both show blurring of the parahippocampal WM, which is a frequent finding co-occurring with HS. Images were acquired at WCFT. L = left.

Chapter 3: Neuroanatomy

Figure 3.1. Left lateral view of the brain showing the four lobes of the left cortical hemisphere of the cerebrum, brain stem (light brown) and cerebellum (brown) (from Human Anatomy Wiki 2017)

Ventrally, the Sylvian fissure separates the frontal lobe (orange) from the temporal lobe (blue), while caudally this most anterior lobe (frontal lobe) is separated from the parietal lobe (green) by the central sulcus. The occipital lobe is situated at the very posterior end of the brain (red area), caudal to the temporal and parietal lobes and separated via the parietal-occipital sulcus. Separations between lobes are also indicated with the red lines.

Figure 3.2. Medial aspect of right limbic lobe with the hippocampus (from Duvernoy 2005).

The inset (modified from Krebs et al. 2014) shows the limbic lobe (white) with relation to frontal (orange), temporal (yellow), parietal (green) and occipital (pink) lobes.

Hippocampal body:

1. Dentate gyrus (margo denticulatus)
2. Cornu ammonis
3. Fimbria placed upwards (arrows) to show cornu ammonis

Hippocampal head (uncal part):

4. Apex of the uncus
5. Band of Giacomini (uncal extension of margo denticulatus (1))
- 5' Uncal sulcus
6. Gyrus uncinatus

The anterior part of the uncus, belonging to the parahippocampal gyrus (piriform lobe) is composed of:

7. Semilunar gyrus
8. Prepiriform cortex
9. Gyrus ambiens
10. Entorhinal area
11. Parahippocampal gyrus
12. Collateral sulcus

Hippocampal tail:

13. Gyri of Andreas Retzius (intralimbic gyrus)
14. Fasciola cinerea prolonging the dentate gyrus
15. Gyrus fasciolaris, extension of the cornu ammonis
16. The gyrus subsplenialis prolongs the gyrus fasciolaris and is itself continued by the indusium griseum (17) on the dorsum of the corpus callosum (18)
19. Isthmus
20. Anterior calcarine sulcus
21. Cingulate gyrus
22. Cingulate sulcus
23. Subcallosal area
24. Anterior perforated substance
25. Anterior commissure
26. Fornix
27. Crus of the fornix

The dotted area indicates the limbic lobe. The a-a line indicates the plane of the section of Figure 3.8.

Figure 3.3. Stages of brain development (from Tau and Peterson 2010).

A timeline of major developmental events occurring in the development of the human brain. Six stages are shown.

Figure 3.4. Cortical development (from Poduri et al. 2013)

(A) A neuroepithelial cell (red) at the VZ serves as progenitor for both a pyramidal neuron (green-blue) as well as a radial glial cell (gold). (B) A newly differentiated neuron (blue) migrates along a radial glial fiber. (C) Neurons (blue) continue to migrate along the outer radial glial cells' process (brown) as intermediate progenitor cells (small yellow) form. (D) Intermediate progenitor cells begin to generate neurons (blue). (E) The progenitor cells in the ventricular zone begin to give rise to astrocytes (dark green). Interneurons (purple) generated elsewhere migrate tangentially. CP = cortical plate; IZ = intermediate zone; VZ = ventricular zone; oRG = outer radial glial (outside of VZ).

Figure 3.5. FCD as a result of suspected somatic mutation in a progenitor cell (from Poduri et al. 2013).

Healthy progenitor cells (bottom row, blue) give rise to healthy neurons and glial cells (top five layers, blue), while a progenitor cell with a somatic mutation (red) generates unhealthy cells (top five layers, red), thus mutated cells are interspersed with healthy neurons and glial cells. The respective produced funnel-shaped lesion in the adult brain can be detected in the left frontal lobe on the axial T2w MRI as a FCD characterized by GM thickening, GM/WM blurring and a transmantle sign reflecting the funnel shape of the developmental process. However, the right frontal lobe and other regions of the brain present a sharp GM/WM boundary, healthy GM thickness and no transmantle sign. R = right.

Figure 3.6. Various types of malformations of cortical development shown on conventional axial T1w MR images in four different patients.

A detailed description of the images can be found in the right panel. R = right.

Figure 3.7. Illustration of the internal structure of the hippocampus (left, from Duvernoy et al. 2013) and a corresponding post-mortem view of the hippocampus after opening of the temporal horn of the lateral ventricle (right, from Duvernoy 1998).

The CA and dentate gyrus (GD) form two interlocking U-shaped laminae. 1 hippocampal body, 2 hippocampal head, 3 hippocampal tail, 4 terminal segment of the tail, 5 hippocampal digitations, 6 vertical digitations, 7 CA and GD in the medial surface of the uncus, 8 band of Giacomini, 9 margo denticulatus. A = anterior; L = lateral; M = medial; P = posterior.

Figure 3.8. Cross-sectional diagram (a) and 9.4T MRI (b) of the right human hippocampus (from Duvernoy et al. 2013).

The right side of the image is the medial, while the left side is the lateral aspect of the hippocampus. CA1–CA4, fields of the cornu ammonis with pyramidal cells. Cornu ammonis: 1 alveus, 2 stratum oriens, 3 stratum pyramidale, 3' stratum lucidum, 4 stratum radiatum, 5 stratum lacunosum, 6 stratum moleculare, 7 vestigial hippocampal sulcus (note a residual cavity, 7'); dentate gyrus (with granule cells) with 8 stratum moleculare, 9 stratum granulosum and 10 polymorphic layer; 11 fimbria, 12 margo denticulatus, 13 fimbriodentate sulcus, 14 superficial hippocampal sulcus, 15 subiculum (transition area of hippocampus and parahippocampal gyrus), 16 choroid plexuses, 17 tail of caudate nucleus, 18 temporal (inferior) horn of the lateral ventricle.

Figure 3.9. Projections of the hippocampal and parahippocampal regions (from Duvernoy et al. 2013).

A-E are parts of the neural chain forming the polysynaptic intrahippocampal pathway. Cornu ammonis: 1 alveus, 2 stratum pyramidale, 3 Schaffer collaterals, 4 axons of pyramidal neurons (mainly to septal nuclei), 5 strata lacunosum and radiatum, 6 stratum moleculare, 7 vestigial hippocampal sulcus. Dentate gyrus (GD): 8 stratum moleculare, 9 stratum granulosum. CA1, CA3 fields of the cornu ammonis, SUB subiculum. ENT (Layer II of the entorhinal area) is the origin of this chain; its large pyramidal neurons are grouped in clusters, giving a granular aspect at the

entorhinal surface.

Figure 3.10. Left lateral views of major temporal lobe connections with the rest of the brain (modified from Catani and de Schotten 2008, visualized through tractography).

Figure 3.11. Hippocampus with Fimbria and Fornix (from RANZCRPart1 2015)

1: hippocampus, 2: fimbria, originating from the alveus within cornu ammonis; 3: crus of the fornix; 4: hippocampal commissures; 5: body of the fornix; 6: column of the fornix, post-commissural fornix; 7: pre-commissural fornix; 8: anterior commissure; 9: mammillary body; S: superior; I = inferior; P = posterior; A = anterior.

Chapter 4: Review on MRI Physics

Figure 4.1. MR Scanner (A) and the Spinning Proton (B) (from Ajtai et al. 2015).

As the person is lying in the scanner, a magnetic field is applied parallel to the person's body (Z-axis), while a radio-frequency wave is applied, which deflects the proton from the main magnetic field. This makes it possible to encode the proton's phase (perpendicular Y-axis) while spinning about the axis of B₀ (B) and to determine the proton spin frequency (X-axis) (B, lower arrow) during precession. Gradually the proton returns to only rotating about its own axis along B₀ (steady state). The diagram in panel B and MR images in general have a different frame of reference than depicted in panel A (see inset 'diagrams').

Figure 4.2. Conventional MRI sequences with radio-frequency pulses (from Elster 2017).

In order to acquire the MR signal within a spin-echo sequence, a 90° radio pulse is applied. The echo (S) is caused by the 180° radio pulse, which acts like a magnetic barrier and reflects the echo of the first 90° decay signal. For an inversion recovery sequence another 180° radio pulse is added before the 90° and 180° pulses. The time between the added 180° pulse and the 90° pulse is called TI. Apart from nulling the signal from fat and water, the added 180° pulse also flips the sign of the magnetization vector from z to -z. In both sequences, the time between the two 90° excitation pulses is termed TR. S = Signal-readout/echo, TE = echo time, TR = repetition time, TI = inversion time.

Figure 4.3. T1 relaxation time at 3T and derived T1w grayscale image (from Farrall 2015).

T1 relaxation times, defined as the time where 63% of net magnetization has been regained (dashed line): Fat = 370 ms; WM = 830 ms; GM = 1330 ms; CSF = 3600 ms (Gold et al. 2004, Wansapura et al. 1999). A signal readout time at 800 ms reveals optimal contrast with the tissue-dependent T1 relaxation curves having an optimal distance between each other (distinct signal differences across tissue types). MRI was acquired at the WCFT. Figure used and modified with permission of Professor Andrew Farrall at the Edinburgh Imaging Academy (www.ed.ac.uk/edinburgh-imaging/academy). L = left; R = right.

Figure 4.4. T2 relaxation times at 3T and derived grayscale T2w image (from Farrall 2015).

T2 relaxation times, defined as the time where 37% of all protons in the tissue have lost precessional phase coherence: WM = 90 ms; GM = 100 ms; Fat = 180 ms; CSF = 190 ms. A signal readout time at 180 ms reveals contrast with T2 relaxation curves having an optimal distance between each other (distinct signal differences across tissue types). MRI was acquired at the WCFT. Figure used and modified with permission of Professor Andrew Farrall at the Edinburgh Imaging Academy (www.ed.ac.uk/edinburgh-imaging/academy). L = left; R = right.

Figure 4.5. T1w and T2w signal patterns at different time points during brain development (from National Institutes of Health 2012)

The GM/WM T1w and T2w signal patterns at an age of one week is the reverse of the pattern seen at an age of one year and older. Information on side of MRI was not provided in source.

Figure 4.6. Anatomical T1w (top row), T2w (middle row) and T2FLAIR (bottom row) images in axial, coronal and sagittal views (left to right).

The images were acquired at the WCFT as part of the epilepsy research dedicated protocol. L = left.

Figure 4.7. Coronal T1- and T2FLAIR images.

These images allow a very accurate depiction of brain tissue within the coronal plane due to the high in-plane resolution. Note the level of detail within the temporal lobe (box) and hippocampus (arrow). Images were acquired at the WCFT. L = left.

Figure 4.8. Diffusion Weighted Imaging Sequence (from Le Bihan et al. 2006).

A gradient pulse pair (G_{diff}) is used to cause spin phase shifts along their locations. As in a conventional spin-echo sequence, a 90° pulse is applied and during the application of another 180° pulse diffusing spins remain out of phase (pink circles) as they are at a different location with respect to the diffusion-sensitizing gradient. All other proton spins are brought to their initial phase (yellow circles) and emit higher signals than spins that are out of phase because these respective protons have moved. The signals of the spinning protons are measured by the readout gradient. G_{sl} = slice selection gradient, G_{read} = readout gradient, $G_{\text{ph-enc}}$ = phase-encoding gradient, G_{diff} = diffusion gradient, RF= radio-frequency pulse.

Figure 4.9. Axial sections of whole brain diffusion data.

The first two images on the left of the first row show b0 images (no diffusion weighting), while the remaining six pertain to volume imaging acquired with different diffusion gradients (diffusion-weighted images). Note how voxel intensities across b0 images are the same for the corresponding voxels in the other b0 image (both b0 images look the same). This is not the case in diffusion-weighted images, since the proton spins vary according to different diffusion gradients giving rise to different intensities in these volumes when compared to each other. This is a necessary feature for tensor estimation. Images were acquired at the WCFT (a subset of 2 out of 6 b0 and 6 out of 60 diffusion-weighted volumes is presented). L = left.

Chapter 5: Automated multi-sequence hippocampal subfield segmentation in refractory temporal lobe epilepsy: Relation to clinical outcomes

Figure 5.1. Anatomical locations of segmented subfields on T1w (left) and T2STIR images (right) in a patient with right TLE. The same slices are shown for both images in the hippocampal head (A) and hippocampal body (B). R = Right; CA = Cornu Ammonis; HATA = Hippocampus-Amygdala Transition Area.

Figure 5.2. Decreased contralateral hippocampal volumes in patients with right TLE compared to patients with left TLE (hippocampal tail) and vice versa (presubiculum/HATA). Blue boxplots indicate data distribution, with the median (red line) and 95% confidence intervals (red triangles). * $p_{(FDR-corr)} < 0.1$; ** $p_{(FDR-corr)} < 0.05$; *** $p_{(FDR-corr)} < 0.01$.

Figure 5.3. Significant correlations of ipsilateral hippocampal internal architecture (HIA) ratings and ipsilateral subfield volumes extracted via Freesurfer. Linear least-square lines were fitted to the data.

Chapter 6: TRActs Constrained by UnderLying Anatomy (TRACULA) in Patients with Refractory Epilepsy: Relation to Post-surgical Outcome

Figure 6.1. All reconstructed TRACULA tracts.

Estimated probability tracts from TRACULA are overlaid on T1w (native space, control) and shown in sagittal (A), axial (B) and coronal (C) views at 20% of maximum probability. TRACULA tracts analyzed: CAB, SLFt, ILF and UF. R=Right; L=Left; CC-MIN=corpus callosum (forceps minor); CC-MAJ=corpus callosum (forceps major); ATR=anterior thalamic radiations; UF=uncinate fasciculus; ILF=inferior longitudinal fasciculus; CAB=cingulum angular bundle; SLFt=superior longitudinal fasciculus (temporal segment); SLFp=superior longitudinal fasciculus (parietal segment); CST=corticospinal tract; CCG=cingulum–cingulate gyrus bundle.

Figure 6.2. FA Values from TRACULA Tracts ILF, SLFt, UF and CAB.

The plot shows mean center tract FA distributions along with error bars for left and right tracts of patients with left TLE (red bars), controls (gray bars) and patients with right TLE (blue bars). Asterisks and bars show significantly reduced FA values for patients when comparing to controls and between the two patient groups. * $p < 0.05$; ** $p < 0.01$; *** $p < 0.001$, corrected for multiple comparisons.

Figure 6.3. MD Values from TRACULA Tracts ILF, SLFt, UF and CAB.

The plot shows mean center tract MD distributions along with error bars for left and right tracts of patients with left TLE (red bars), controls (gray bars) and patients with right TLE (blue bars). Asterisks and bars show significantly reduced MD values for patients when comparing to controls. * $p < 0.05$; ** $p < 0.01$; *** $p < 0.001$, corrected for multiple comparisons.

Figure 6.4. Waypoint comparison p-values along the tracts.

Differences between the patient groups and controls are shown projected onto a T1w template. Red regions show significantly reduced FA (first row) and increased MD (second row) relative to controls. Changes are more pronounced in MD than in FA and patients with left TLE are more bilaterally affected than patients with right TLE. TLE = Temporal Lobe Epilepsy; FA = fractional anisotropy; MD = mean diffusivity; SLFt = superior longitudinal fasciculus - temporal segment; CAB = cingulum angular bundle; ILF = inferior longitudinal fasciculus; UF = uncinate fasciculus.

Figure 6.5. Waypoint correlation p-values along the tracts according to side of seizure onset.

Relationships between the DTI-metrics and clinical variables are shown projected onto a T1w template and mean tract pathways. Red regions show significant correlations with reduced FA (first row) and increased MD (second row). Relationships between duration (corrected for age) and FA/MD of ipsilateral anterior UF and ILF regions and correlations between age at onset (MD of UF/ILF) and seizure burden (FA of UF) were found. FA = fractional anisotropy; MD = mean diffusivity; SLFt = superior longitudinal fasciculus - temporal segment; CAB = cingulum angular bundle; ILF = inferior longitudinal fasciculus; UF = uncinate fasciculus.

Figure 6.6. Waypoint comparison p-values along the tracts according to outcome.

Differences between the patient groups and controls are shown projected onto a T1w template. Red regions show significantly reduced FA (first row) and increased MD (second row) relative to controls. Changes are more pronounced in MD than in FA and patients with ILAE II-VI are affected in the contralateral SLFt (increase of MD relative to controls) whereas patients with ILAE I did not show this change. TLE = Temporal Lobe Epilepsy; FA = fractional anisotropy; MD = mean diffusivity; SLFt = superior longitudinal fasciculus - temporal segment; CAB = cingulum angular bundle; ILF = inferior longitudinal fasciculus; UF = uncinate fasciculus.

Chapter 7: Neuroradiological Findings in Patients with 'non-lesional' Focal Epilepsy Revealed by Research Protocol

Figure 7.1. Patient 22: right HS and Small-Vessel Disease. In 2014 this patient received a dedicated epilepsy protocol at WCFT. Although the T1FLAIR coronal sequence shows a comparable quality relative to the most recent 2015 T1FLAIR, Small Vessel Disease and right HS were not detected by the neuroradiologist. HS and WM lesions related to small vessel disease are increasingly conspicuous on the most recent T2FLAIR image relative to the 2014 T2FLAIR image, the latter of which suffers from lower SNR. R = right.

Figure 7.2. Patient 24: right HS. While early images do not show clear evidence of HS, the expert neuroradiologist termed this as “small right hippocampus” without explicitly diagnosing HS. This was inappropriately documented and this information did not reach the consultant neurologist. In the later image right HS was re-diagnosed. R = right.

Figure 7.3. Patient 25: bilateral HS. The images from 2009 show bilateral HS as demonstrated by hyperintensity on T2FLAIR and volume loss on T1FLAIR; this was referred to as “bilateral small hippocampi” by the expert neuroradiologist. This was inappropriately documented and the information did not reach the consultant neurologist. In 2015 the patient was diagnosed with bilateral HS. R = right.

Figure 7.4. Patient 38: left HS. Despite signal hyperintensity on T2FLAIR and volume loss on T1FLAIR, HS was only diagnosed in 2015. Lesion conspicuity was similar for both MRI sessions. R = right.

Figure 7.5. Patient 66: left HS. This patient received comparable quality of epilepsy-dedicated imaging in March and November 2015. However, HS was only diagnosed on the later images, which show hyperintensity on T1FLAIR and HA on T1FLAIR. Lesion conspicuity was similar for both MRI sessions. R = right.

Figure 7.6. Patient 56: right HS with parahippocampal WM blurring. In 2012 this patient received imaging at a general hospital (left: T2w; right: T1w Inversion Recovery) with an angulation not orthogonal to the long axis of the hippocampus. HS and parahippocampal WM blurring are more conspicuous on the epilepsy research image of 2015 (left: T2FLAIR; right: T1FLAIR), particularly relative to the contralateral hemisphere. R = right.

Figure 7.7. Patient 61: left temporal encephalocele. Left temporal encephalocele was diagnosed based on a 3D volume T2w acquisition, which is not routinely acquired in the evaluation of patients with epilepsy at the WCFT but was part of the study's dedicated epilepsy research protocol. Note how the lesion is more conspicuous on the T2w image (below) compared to the T1w (top). Diagnosis was later confirmed with computed tomography imaging. Older MRIs (all 2D) with large slice thickness (~5 mm) from 2009 failed to reveal this abnormality. L = left; R = right.

Figure 7.8. Patient 65: FCD / gliosis in right superior frontal gyrus. Diagnosis was made based on the 3D T2FLAIR image of 2015 (green image borders). The abnormality was not reported on the previous 2D axial T2w image (red image borders) where only one slice showed the small abnormality. R = right.

Figure 7.9. Formerly 'non-lesional' cases showing lesions using the epilepsy dedicated research protocol. Numbers refer to patient IDs. Please refer to Table 7.1 for details on each lesion identified. R = right.

Chapter 8: Automated Multimodal MRI Analysis for Diagnostic Purposes in Patients with MRI-negative Epilepsy

Figure 8.1. Procedure for obtaining T1w junction and extension images (Huppertz et al. 2005).

Raw T1w images were intensity corrected, normalized and segmented into WM/GM maps. These were used to obtain GM/WM voxel intensity thresholds. Any voxels

with intensities of half a standard deviation higher/lower than the mean GM/WM intensities were saved to a binarized junction image, which was cortex-masked ('AAL' in SPM12). The GM segment was also masked and served as the extension image. Both resulting images were smoothed with a 6mm FWHM smoothing kernel. The data of patient 59 is featured here. L = left.

Figure 8.2. General workflow of the applied statistical tests in T1w JCT and EXT maps.

This graph shows the generation of the binarized cluster masks based on T1w used to restrict statistical testing for all other imaging modalities to regions that are potentially dysplastic. Patient 59 is given as an example (cluster in the JCT map). In the case that any one of the remaining imaging modalities showed a significant effect, the site was again reviewed by a neuroradiologist. TIV = total intracranial volume; JCT = T1w junction image; EXT = T1w extension image. FWE = family-wise error. T-scores: yellow/red bars. L = left.

Figure 8.3. Four patients with dysplasia and true positive findings: results from individual statistical testing against 40 controls using T1w JCT and EXT maps.

Green bars indicate single patients with two sites of dysplasia. T-scores are represented for JCT and EXT results. From top to bottom: patients with IDs 51, 56, 59 and 65. JCT = T1w junction image; EXT = T1w extension image. L = left.

Figure 8.4 Reduction of the false positive rate within the patient sample.

An example patient (59) is featured with all clusters found in EXT and these have been numbered (dorsal → ventral). Based on the statistical test with $p < 0.01$, FWE-cluster correction at $p < 0.05$, 23 patients presented with false positives (first box). Cluster extent thresholding at > 3500 ($> 3.5 \text{ cm}^3$) voxels reduced this number by eight patients (second box). Note the reduction of false positives within a single patient. Using the cluster masks derived from single patients, statistical testing was performed on other imaging modalities. Three patients had insignificant findings in all other imaging modalities and were deemed to be non-dysplastic sites (third box). Overall, the false positive rate was reduced from 53% to 28%. The sites found by the automated tool in these remaining twelve patients were re-reviewed by a neuroradiologist. EXT = extension; JCT = junction; FP = false positive; FA = fractional anisotropy; MD = mean diffusivity; GM/WM = gray/white matter; L = left.

Figure 8.5. Results of combined $> 3.5 \text{ cm}^3$ cluster masks based on T1w JCT/EXT analysis.

All clusters of the twelve patients are shown. The corresponding sites in T1w/T2w/T2FLAIR images were re-reviewed by a consultant neuroradiologist and clusters (in red) were used as masks in multimodal analysis. HS = hippocampal sclerosis; l = left; r = right; OL/PL/TL/FL = occipital/parietal/temporal/frontal lobe; JCT = junction; EXT = extension.

Chapter 9: Manual and Automated Tractography Approaches in Patients with 'non-lesional' and lesional Temporal Lobe Epilepsy

Figure 9.1. Manual delineation of UF (left) and PHWM (right) tracts.

Tracts were delineated using ROIs drawn on the subjects' FA image in native diffusion space. 'AND' ROIs (green, purple and orange) served as ROIs where tracts were allowed to pass through, while 'NOT' ROIs (red and blue) were used to define the end of tracts. Tract colors define the principle direction of diffusion for single fibers (red = left/right, blue = inferior/superior, green = anterior/posterior).

Figure 9.2. Dorsal views of the brain showing all bilateral cleaned (left) and clipped UF and PHWM AFQ tracts (right).

The colors of the tracts denote the principle direction of diffusion for the midpoint of the particular fiber (red = left/right, blue = inferior/superior, green = anterior/posterior). Image rendered in standard ICBM space with MRicroS tool, version 2015 (<https://www.nitrc.org/plugins/mwiki/index.php/mricros:MainPage>). L = left.

Figure 9.3. Whole-tract diffusion measures for manual (left) versus AFQ (right) tractography.

For each group and tract median FA/MD values are presented along with respective standard errors. Using manual tractography, patients with left TLE had significantly reduced FA values in the left UF and right PHWM and increased MD values in left and right UF and PHWM, while patients with right TLE had an increase in MD in the left PHWM compared to controls (top left and bottom left). AFQ was only able to identify the FA decrease in the right PHWM and MD increase in the right UF for patients with left TLE (bottom right). FA = fractional anisotropy; MD = mean diffusivity; UF = uncinate fasciculus; PHWM = parahippocampal white matter bundle; l = left; r = right. . * $p < 0.05$, corrected for multiple comparisons.

Figure 9.4. Comparison of Patients with right and left TLE versus controls.

The T1w overlay in standard space shows areas of the UF where patients had decreased FA (left, red areas) and increased MD (right and inset, red areas). rTLE = right TLE; lTLE = left TLE; FA = fractional anisotropy; MD = mean diffusivity.

Figure 9.5. Patients with HS compared to controls and patients without HS (inset).

The T1w overlay in standard space shows areas of the UF where patients with HS had decreased FA (top and inset, red areas) and increased MD (bottom, red areas). FA = fractional anisotropy; MD = mean diffusivity. HS = hippocampal sclerosis.

Figure 9.6. Correlations of DTI-metrics with demographic and clinical variables.

There were correlations between FA (top row) and age, age of onset, seizure burden and epilepsy duration corrected for age. All FA correlations were negative except for the correlation with age of onset, which was positive (marked with an asterisk, younger age of onset was associated with decrease in FA of the ipsilateral PHWM). There were also correlations between patient MD values (bottom row) and age of onset (negative, marked with an asterisk) and epilepsy duration corrected for age (positive).

Keywords, Glossary and Definitions

Atrophy

Atrophy is the reduction of brain tissue volume during neuropathological processes, characterized by decreased neuronal density due to degeneration of neuronal cells in the affected area.

Contralateral

Related to the opposite side of seizure onset / hippocampal sclerosis. See antonym “ipsilateral”.

Cryptogenic Focal Epilepsy

Synonymous with focal epilepsy (see below) with no known cause.

Cytoarchitecture

This is the arrangement of cells in cortical tissue. Cytoarchitectural investigations allow the characterization of every cell by location, function and the relation to other cells.

Diffusion Magnetic Resonance Imaging

Diffusion magnetic resonance imaging allows the non-invasive visualization of hydrogen proton movement (diffusion) in living internal body tissue. As white matter only allows diffusion in certain directions (anisotropic diffusion), the structure and anatomy of white matter tracts may be inferred by this imaging technique using the related computational method (tractography).

Electrophysiological Recordings

Electrophysiological recordings are part of pre-surgical evaluations to investigate intractable seizures. Non-invasive (scalp) and invasive EEG recordings are used to identify the source of epileptogenic ictal and interictal neuronal activity.

Epileptogenic Zone

The epileptogenic zone denotes the region of cortex that generates epileptic seizures.

Focal Epilepsy

Brain disorder characterized by origination of seizures from a single area of the brain causing the seizures (= epileptogenic area). Focal epilepsy may originate from an epileptogenic lesion such as hippocampal sclerosis or focal cortical dysplasia.

Focal Cortical Dysplasia

Circumscribed brain area characterized by abnormal appearance due to malformations during neuronal development giving rise to abnormal cytoarchitecture. Focal cortical dysplasia may appear as thickened/thinned cortex, cortical surface malformation and may have a blurred gray and white matter boundary.

Gray Matter

Gray matter is the darker tissue of the brain, consisting mainly of nerve cell bodies (somata), unmyelinated axons and branching dendrites. These cells make up three types of cortex arranged in concentric rings: allocortex (limbic cortex), mesocortex (neuronal layer between allocortex and neocortex forming the transitional zone between the two) and neocortex (makes up most of the cerebral cortex, also termed isocortex).

Gray Matter Volume Analysis

Gray matter volume of patients and healthy controls are compared via voxel-based morphometry based on T1w images.

Hippocampal Atrophy

Reduction of hippocampal volume, which may be qualitatively (by neuroradiologists) and quantitatively (using statistical MR image analysis) assessed. In patients with temporal lobe epilepsy, it may be an indicator of hippocampal sclerosis.

Hippocampal Axis

This is the long axis of the hippocampus, running parallel to the midline of the temporal lobe. In order to correctly diagnose hippocampal sclerosis characterized by atrophy, it is beneficial to realign the raw MR image perpendicular to this axis.

Hippocampal Sclerosis

Hippocampal sclerosis is a lesion to the hippocampus associated with temporal lobe seizures, the epileptogenic lesion is characterized by neuronal loss co-occurring with hippocampal subfield volume reduction and gliosis.

Hippocampus

The hippocampus is located in allocortex of the medial temporal lobe and serves memory and navigational functions. Frequently this structure is affected by a loss of neurons in patients with temporal lobe epilepsy and this lesion (hippocampal sclerosis) has been associated with causing seizures.

Ictal

Relating to a seizure.

Inter-ictal

Relating to an interval between seizures.

Ipsilateral

Related to the same side of seizure onset / hippocampal sclerosis. See antonym “contralateral”.

Modulation

Modulation is used during voxel-based morphometry analysis to compensate for warping effects that occur when non-linearly registering individual brain MR images to a standard space brain template (normalization). Specifically, the images are scaled according to the amount of contraction needed during normalization in order

to give a more accurate volume measurement.

Morphology

Form, shape, structure and size of the brain or any of its substructures.

Morphometry

Morphometry allows the three-dimensional statistical investigation of brain morphology using computer algorithms.

Magnetic Resonance Imaging

Magnetic Resonance imaging allows the non-invasive high-resolution visualization of living internal body tissue, structure and anatomy by measurements of physical responses of protons to a magnetic field and radio-frequency pulses.

Neuropathology

Neuropathology is the branch of medicine concerned with disorders of the nervous system characterized by anatomical or neurophysiological abnormalities (= neuropathological abnormalities).

Neuropsychology

Neuropsychology is a branch of psychology that aims to identify the relationship between an individual's behavior, emotion and cognition and his/her brain function.

Pre-surgical Evaluation

Pre-surgical evaluation is the medical and neuropsychological investigation of patients to determine the suitability for (resective) brain surgery to treat a neurological disorder such as epilepsy.

Spatial Normalization

Spatial normalization is the process of co-registering individual brain MR images to a template brain image. This is performed before group-wise voxel-based statistical comparisons can be made so that the MRI brain areas correspond across all study

participants.

Temporal Lobe Epilepsy

Temporal lobe epilepsy is a neurological disorder and the most common type of epilepsy. In these patients, the temporal lobe contains the epileptogenic tissue that generates seizures and this ictal activity may propagate to other regions within the temporal lobe and other extra-temporal lobe structures.

Voxel-Based Morphometry

Voxel-based morphometry is an automated statistical approach that allows three-dimensional analysis of whole brain morphology in individuals or in a group of patients compared to a control/patient cohort based on voxel-wise statistical testing.

Wada Test

The Wada test is a neuropsychological tool within the pre-surgical evaluation protocol that allows the assessment of language and memory lateralization in patients.

White Matter

White matter is the paler tissue of the brain, consisting mainly of nerve fibers with their myelin sheaths.

Abbreviations

2D Two-Dimensional	JCT Junction Image
3D Three-Dimensional	L Left
A Absence Seizure	M Male
ACPC Anterior Commissure Posterior Commissure Realignment of MRI	MAP Morphometric Analysis Program
AFQ Automated Fiber Quantification	MDT Multi-disciplinary Team
C Controls	MNI Montreal Neurological Institute
CA Cornu Ammonis	MR Magnetic Resonance
CAB Cingulum Angular Bundle (=PHWM)	MRI Magnetic Resonance Imaging
CB Complications at Birth	PET Positron Emission Tomography
CNR Contrast-to-Noise Ratio	PHWM Parahippocampal White Matter Bundle (=CAB)
CPS Complex Partial Seizure	R Right
CSF Cerebrospinal Fluid	ROI Region Of Interest
DTI Diffusion Tensor Imaging	SGTCS Secondary-Generalized Tonic-Clonic Seizure
EEG Electroencephalography	SLFt Superior Longitudinal Fasciculus (Temporal Segment)
EXT Extension Image	SNR Signal-to-Noise Ratio
F Female	SPGR Spoiled Gradient
FC Febrile Convulsions	SPM Statistical Parametric Mapping
FCD Focal Cortical Dysplasia	SPS Simple Partial Seizure
FDR False-Discovery-Rate	STIR Short TI Inversion Recovery
FF Fimbria-Fornix	SVD Small-Vessel Disease
FL Frontal Lobe	TIV Total intracranial volume (=ICV)
FLAIR Fluid Attenuated Inversion Recovery	TL Temporal Lobe
fMRI Functional Magnetic Resonance Imaging	TLE Temporal Lobe Epilepsy
FSE Fast Spin Echo	TMI Total Motion Index
GM Gray Matter	TP Temporoparietal
GS Generalized Seizure	UF Uncinate Fasciculus
HA Hippocampal Atrophy	VBM Voxel-Based Morphometry
HS Hippocampal Sclerosis	WCFT Walton Centre Foundation Trust
ICV Intracranial Volume (=TIV)	WM White Matter
ILAE International League Against Epilepsy	
ILF Inferior Longitudinal Fasciculus	

Chapter 1: Introduction

Chapter 1: Introduction.....	1
1.1 Context and Outline of Thesis.....	1
1.2 Background.....	7
1.2.1 Epileptic Seizures.....	8
1.2.2 Epilepsy Syndromes.....	9
1.3 Surgical Intervention.....	10
1.4 Pre-surgical Evaluation.....	12
1.4.1 Surface Inter-ictal EEG.....	14
1.4.2 Assessment of Preoperative Functional Skills.....	15
1.4.3 Invasive Inter-ictal and Ictal EEG.....	16
1.4.4 Standard Diagnostic MRI.....	17
1.5 Rationale for Advanced MRI of the Brain.....	19
1.5.1 Additional Research Sequences.....	19
1.5.2 Quantitative Techniques.....	21
1.6 Motivation and Goals of this Thesis.....	23
1.6.1 Patients with TLE and Associated HS: Outcome Analysis.....	24
1.6.2 Patients with MRI-negative Focal Epilepsy.....	27

1.1 Context and Outline of Thesis

Epilepsy forms an important challenge to scientific and clinical advancement since about 1% to 2% of the general population is affected by this disorder (WHO 2016, Neligan et al. 2012, Ngugi et al. 2010). This is especially true for patients with focal epilepsy, who continue to have seizures despite taking anti-epileptic drugs (AEDs). This is the case in approximately 30% of all patients (Kwan and Brodie 2000, Dichter and Brodie 1996). Some patients may be candidates to undergo resective surgery for removal of the epileptogenic tissue. Surgical resection may completely or substantially reduce seizure frequency (Wiebe et al. 2001). Patients with focal epilepsy are more likely to have an underlying structural abnormality, are more likely to be refractory to medical treatment (Kwan and Brodie 2000) and if the lesion has been identified on MRI and found to be consistent with the likely seizure onset zone, these patients are more readily referred for surgery (Wiebe and Jette 2012b).

However, again in about 30% of patients with focal epilepsy, who would otherwise be suitable candidates for resective surgery to alleviate seizure frequency, no underlying epileptogenic lesion is identified (Kwan and Brodie 2000, Dichter and Brodie 1996). Postoperative outcome is significantly worse in patients without an identifiable lesion on clinical MRI (Bien et al. 2009, Tellez-Zenteno et al. 2010, Jehi et al. 2007) and patients are less likely to be referred to surgery. However, despite careful evaluation of surgical candidacy, 30-40% of all patients will continue to experience seizures at a follow-up of five years (Annegers et al. 1979, Cockerell et al. 1995, Cockerell et al. 1997, Janszky et al. 2005). This number may be even higher (de Tisi et al. 2011) with only 38% of patients being completely seizure-free after one-year follow-up (Wiebe et al. 2001). It is not completely clear why this is the case, but recurrence of seizures may be due to occult epileptogenic lesions in the brain not previously seen on Magnetic Resonance Imaging (MRI).

This thesis presents different studies pertaining to advanced MRI analyses performed on data of patients with refractory focal epilepsy: (i) patients with temporal lobe epilepsy (TLE) who have presented with hippocampal sclerosis (HS) and have had a good/poor response to surgery; (ii) patients who are not considered for surgery as their MRI investigations remained inconclusive (MRI-negative). However, the research objectives for the studies based on two independent datasets are substantially different: the first project allowed the study of outcome correlates by analysis of pre-surgical structural changes between patients with excellent and poor response to surgery, while the latter facilitated a more detailed qualitative/quantitative MR analysis of patients with debilitating seizures despite being MRI-negative.

TLE is the most frequent form of medically refractory focal epilepsy (Almeida et al. 2012, Wiebe and Jette 2012a), but it may be amenable to resective surgery. A controlled trial of surgery for refractory TLE showed that after a 1-year postoperative

period, 58% of all patients were free from seizures impairing awareness, compared to only 8% of patients that had been treated medically (Wiebe et al. 2001). TLE is characterized by widespread GM/WM changes, which extend throughout the brain (Bernhardt et al. 2013, Keller and Roberts 2008, Richardson 2012, Bonilha and Keller 2015, Rodríguez-Cruces and Concha 2015, Gross 2011). Extensive brain changes like these have given rise to the notion that TLE may be considered a brain network disorder (Berg and Scheffer 2011). HS is the most common neuropathological correlate of TLE and the preoperative detection of HS on MRI is related to improved postoperative prognosis after temporal lobectomy (Spencer et al. 2005). Still, 40% of all patients with TLE and associated HS receiving resective surgery to alleviate seizure frequency do not benefit from surgery (Wiebe et al. 2001, Engel et al. 1993). It is unknown why some patients continue to experience seizures after the potentially epileptogenic lesion has been removed surgically. It is likely that some epileptogenic gray matter (GM) tissue has remained in the brain (Rosenow and Lüders 2001, Zachenhofer et al. 2011, Surges and Elger 2013). This assumption is supported by evidence from a study showing that post-surgical outcomes improved after re-operation where the new surgical lacuna also included residual lesions (Wyler et al. 1989). Other reasons may include incorrect localization of the seizure focus at first surgery or post-surgical progression of the underlying disorder (Surges and Elger 2013), which may also include brain network changes (Berg and Scheffer 2011). Histopathology studies have suggested that patients with HS type 1, which is associated with a volume loss in hippocampal subfields Cornu Ammonis 1 (CA1) and CA4 have an earlier initial precipitating injury such as a febrile seizure at an age of two to three years old and superior outcomes over patients with HS type 2 (neuronal loss only in CA1) and those with HS type 3 (CA4 subfield volume loss) who experience initial precipitating injuries at a later time point at age six and beyond (Blümcke et al. 2013, Blümcke et al. 2007). For neuroanatomical details on hippocampal subfields of healthy individuals see Chapter 3. However, apart from the fact that patients present with different types of HS preoperatively, it is likely that

patients have different epileptogenic networks linked to their individual clinical history (e.g. duration of epilepsy) and predisposing them to varying surgical outcomes. So far however, it is unclear whether HS is a driving factor for brain network changes or if the epileptogenic network is influenced by other clinical factors. It is therefore important to investigate, whether certain structural changes occurring in epilepsy are related to post-surgical outcomes or the severity/chronicity of the disorder. The objective of this study was to relate preoperative MR imaging markers to clinical information and post-surgical outcome in order to assess whether high-resolution preoperative imaging of the hippocampal formation can predict surgical outcomes (Study 1) or if network disruption is related to HS, certain clinical features of the disorder and postoperative outcome (Study 2). These correlations were performed using T1w data for hippocampal structural analysis and Diffusion Tensor Imaging (DTI) data was analyzed to reveal any disruption of white matter (WM) structural brain connectivity.

Patients with focal epilepsy presenting without MRI-visible lesions are classified as having cryptogenic focal epilepsy (older term, used within this thesis) or focal epilepsy with no known cause (newer term). The presence of a brain abnormality on MRI significantly predicts long-term (longer than five years) surgical outcomes (Berkovic et al. 1995). Both the fact that certain neurons are epileptogenic, therefore constituting the focal seizure onset zone, which is potentially discernible on preoperative MRI as an abnormal GM structural alteration (e.g. abnormal patterns of gyration, HS, GM/WM blurring, cortical thickening) and the fact that seizure activity propagates via WM connections (epileptogenic network) are important clinical factors. These should be used as a framework in order to develop neuroimaging markers for the determination of potential epileptogenic regions in individual patients. Lesion detection and conspicuousness using a dedicated epilepsy research MRI protocol at a specialist surgical center may aid in this endeavor (von Oertzen et al. 2002). However, many subtle image signal changes indicating FCDs may escape

visual assessment on structural MRI or indeed may not be visible at all. Furthermore, some MRI require quantitative analysis, as is the case with DTI data. The overall aim of this study was to identify possible epileptogenic lesions via expert neuroradiological reassessment of all images (Study 3) and supplementary automated quantitative analysis (Studies 4 + 5). T1w, T2w, T2FLAIR and DTI data were used to automatically quantify changes in individual patients as compared to healthy controls (Study 4) and validated against neuroradiological assessment. Furthermore, an automated tractography approach was used to identify disrupted structural networks in patients with TLE on a group level (Study 5), which were compared against a technique based on manual ROI placements considered the "gold standard" (Hammers et al. 2007, Van Leemput et al. 2009, Schoene-Bake et al. 2014, Keller et al. 2012) to identify temporal lobe tracts using tractography (Yeatman et al. 2012) when histology as a true gold standard is not available.

Chapter 1 provides background information concerning the clinical phenotypical manifestation regarding seizures/syndromes, diagnosis, pre-surgical evaluation and treatment of focal epilepsy. The later parts of this chapter comprise a brief review of the routine clinical sequences and advanced imaging techniques. The focus is on the development and application of structural MRI and justifications for the used analyses are provided.

Chapter 2 describes the methodology common to all studies (Chapters 5 to 9) while providing an overview on the materials (acquired data), objectives and hypotheses. The methodology specific to each individual study is detailed separately in the relevant chapter.

As this thesis focusses on MR analysis of patients with TLE in a large sample (total of 130 patients), **Chapter 3** provides a review on gross brain structure and neuroanatomy of the temporal lobe. In particular this chapter highlights the temporal lobe's GM substructures and WM structural connections. Since the next largest cohort of patients presented with potentially epileptogenic lesions, such as FCD

resulting from cortical malformations during brain development, healthy neurodevelopment is discussed.

Chapter 4 is a review chapter that provides information on general MR physics and the specific sequences applied in the clinical/scientific evaluation of patients with epilepsy. The sequences that form the basis for the studies are described in detail.

Chapter 5 describes the first study (Study 1) in patients with unilateral HS with a diagnosis of TLE on data collected at a specialized epilepsy center in Bonn, Germany. An automatic hippocampal subfield mapping technique is applied in order to assess how different substructures of the hippocampus are affected in patients with postoperative seizure freedom and those with persistent seizures.

Chapter 6 details a second study (Study 2) that is conducted on the same patient population as in Chapter 5. Here, WM tracts diffusivity measures of patients with left and right TLE were compared to controls and among these two patient groups. Additionally, correlations of WM tract diffusivity measures with volumetric and clinical data were investigated. This was done using automated probabilistic tractography (TRActs Constrained by UnderLying Anatomy, TRACULA) rather than time-consuming manual tract reconstruction methods.

Chapter 7 is the only qualitative study of this thesis (Study 3) and describes individual patient cases with a focal onset of epilepsy, these patients have been reported as presenting without a lesion on previous MRI (MRI-negative). This is the first study within the thesis on data collected at the Walton Centre Foundation Trust (WCFT) in Liverpool, United Kingdom. This study was conducted on patients that have been identified with an epileptogenic lesion in context of the advanced MR protocol used for this study and retrospectively earlier MRI reports were re-reviewed.

Chapter 8 details results pertaining to an automated quantitative detection procedure designed to identify focal cortical dysplasia (FCD) in the patients described in Chapter 7 (Study 4).

Chapter 9 describes diffusivity changes along WM tracts in the patient sample described in Chapter 7 with focal epilepsy using the automated tool Automated Fiber Quantification (AFQ) on a group level (Study 5).

Chapter 10 provides a discussion of the results together with relevant biological and clinical implications. Pertinent methodological strengths and limitations are discussed as well before it concludes with the implications of interpretations and indicates where future work is still needed.

1.2 Background

This literature review details the characteristics of epilepsy as a neurological disorder and information on the challenges epilepsy poses to the patients in its various forms is provided. Section 1.3 and 1.4 describe surgical intervention and pre-surgical evaluation using inter-ictal scalp electroencephalography (EEG), baseline neuropsychological assessment, diagnostic MRI, and invasive EEG. Section 1.5 focuses on the specific scientific techniques used in development and application of advanced structural and functional MRI. Section 1.6 describes the aims of this study.

Epilepsy is a neurological disorder characterized by recurrent unprovoked seizures, which are involuntary movements of the body that can last from a few milliseconds to several minutes. This is due to excessive or synchronous neuronal activity in the central nervous system that may be either genetically determined (McNamara 1999) or related to injury (Ramon y Cajal 1928). Epilepsy is a severe electrophysiological disorder of the brain and seizures can have a long-lasting adverse effect on quality of life of the affected patient (Lee et al. 2015b). Co-morbidities include psychiatric (Gaitatzis et al. 2004, Gilliam et al. 2003) and cognitive impairment (Braakman et al. 2012), sleep disorders (Jacoby et al. 2015) and migraine (Toldo et al. 2010). A significant proportion of patients with epilepsy are treated for a psychiatric disorder (Kanner 2009). Distinct seizure types have been described by the International

League Against Epilepsy (ILAE) based on characteristic symptoms and signs like seizure type, cause, age of onset and electroencephalographic patterns (ILAE 1981). For epilepsy to be diagnosed, the patient must have experienced a minimum of two unprovoked seizures.

1.2.1 Epileptic Seizures

Broadly the different epileptic seizure types may be classified as being either focal (with and without impairment of awareness) and generalized seizures (ILAE 1989, Berg et al. 2010, Morimoto et al. 2004). Focal seizures originate from excessive neuronal activity coming from one hemisphere of the brain and may be identified by electrophysiological recordings (EEG) and their semiology, which is the specific characteristic of the seizure to co-occur with specific movements and this allows lateralization/localization of the seizure focus (Berg et al. 2010). The focus remains the same for the recurrence of seizures in a given patient. These types of seizures may affect awareness (complex partial seizures) or they may not (simple partial seizures) (Morimoto et al. 2004, Berg et al. 2010). Focal seizures have the potential to develop into secondary-generalized/convulsive seizures, meaning that the excessive neuronal activity from the epileptogenic focus rapidly spreads to other parts of the brain (Morimoto et al. 2004, ILAE 1989). Primary generalized seizures cannot be located to one single focus as they show a bilateral ictal EEG discharge (ILAE 1989). Various subtypes of seizures exist, including tonic, atonic, myoclonic and absence seizures. Atonic seizures are characterized by a sudden loss of muscle tone while awareness is usually not impaired, they are typically very short, lasting between one and two seconds. The very brief and sudden involuntary shock-like muscle contraction is a manifestation of the *myoclonic seizure* (Kojovic et al. 2011). A *tonic-clonic seizure* may occur and manifests itself in ongoing (~1 minute) irregular jerking (clonic phase) and rigidity (tonic phase), while awareness may rarely be retained (ILAE 1989). *Status epilepticus* manifests itself in a similar manner, however it lasts much longer (>30 minutes). A *tonic-clonic seizure* may be followed

by atonia, resulting in a *myoclonic-atonic seizure*. A *negative myoclonic seizure* is a seizure where the sudden and brief loss of muscle tone is compensated with a voluntary movement (Kojovic et al. 2011). *Absence seizures* are characterized by a loss of awareness and memory during the duration of the seizure. It is possible for these seizures to last several minutes and develop into absence status epilepticus (Meierkord and Holtkamp 2007).

This thesis focuses on patients with a focal onset of epileptic seizures who do not respond to medical treatment (first line of treatment) and may benefit from resective surgery to attain seizure freedom. Consequences of having a seizure involve injuries and a negative impact on academic success as information cannot be processed by the brain during a seizure or recovery. A lot of time is spent on avoidance of seizures (medical treatment/appointments) and recovery, which may compromise the time otherwise needed to study etc. These aspects may severely impact the patient's quality of life it is therefore paramount to identify the most appropriate therapy for a given patient. Surgery may be the only treatment option for patients who do not respond to AED that may help these patients attain a worthwhile seizure reduction or even seizure freedom.

1.2.2 Epilepsy Syndromes

Various types of epilepsy syndromes exist and may be broadly classified as genetically/epigenetically determined (related to autoimmune responses or congenital malformation in the brain) or provoked after injury/infection of the brain that alters the brain structure and metabolism. Generally, epilepsy syndromes can either be idiopathic (have a significant genetic component), symptomatic (seizures are due to a brain lesion/injury) or cryptogenic (also thought to be symptomatic, but seizures have an unknown cause). A time period of a few weeks to several years may elapse between the brain insult and the emergence of the epilepsy (McNamara 1999).

According to the National Institute of Neurological Disorders and Stroke (2015), about 2-5% of all infants and young children aged 5 and younger may experience non-epileptic febrile convulsion, which is the occurrence of a seizure together with a fever. Febrile convulsions have been associated with a higher risk for developing epilepsy later in life (Walsh et al. 2017). Children in the first few decades of life may be affected by Rasmussen's encephalitis, which is a rare and progressive form of focal epilepsy (Rasmussen et al. 1958) that destroys one hemisphere through repeated seizures. This disorder causes a progressive decline of neurological functions that can stretch from a few months to years and the cause may lie in aberrant auto-immune processes targeting an infection in the brain (Rogers et al. 1994). Another type of epilepsy, which affects children, is Juvenile Myoclonic Epilepsy where multiple genes must be inherited to produce the phenotype (McNamara 1999). Epilepsy secondary to FCD usually begins early in life and is often refractory to AED therapy (Fonseca et al. 2012). The term FCD designates an entire spectrum of abnormalities of the laminar structure of the cortex (Blümcke et al. 2011). In patients with frontal lobe epilepsy, FCD is one of the most frequently found causes for epileptogenic neuronal activity (Kabat and Krol 2012) and may be amenable to resective surgery (Lemer et al. 2009). In other patients any other lobe of the brain may show epileptogenic activity (with or without detection of FCD) and the epilepsy is termed according to the affected lobe. The most difficult to treat type of epilepsy using AED is TLE, and the most common lesion associated with TLE is HS (Wiebe and Jette 2012a).

1.3 Surgical Intervention

Approximately 30% of all patients with focal epilepsy are refractory to medical treatment (Kwan and Brodie 2000). There is no single clear definition of refractoriness, although a failure of trialing two appropriate AEDs has been recommended (Berg 2009). Within this thesis, refractoriness was defined as a patient

having failed at least two AEDs during a minimum course of at least a one-year period after diagnosis. Consequently, alternative clinical treatments targeting a seizure reduction become necessary in these cases (Figure 1.1).

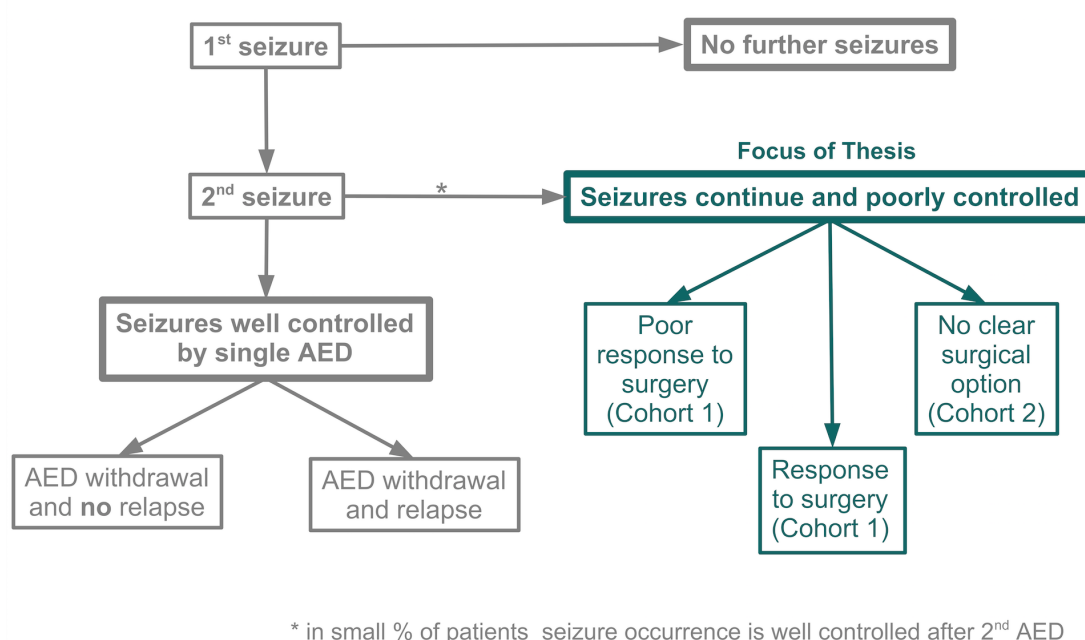


Figure 1.1. Clinical trajectory for patients presenting with seizures.
AED = anti-epileptic drug.

Resective surgery of epileptogenic tissue is the most common choice if treatment with AEDs has failed. A detailed interdisciplinary preoperative investigation initiated and conducted by the members of the multidisciplinary team (MDT, consisting of neurologists, neuropsychologists, electrophysiologists and surgeons) is necessary for accurate identification of the seizure focus. Surgical margins have to be carefully delineated so that a maximum of epileptogenic tissue is resected, while preserving the functions of eloquent cortex (e.g. memory and language functions). Implantation of a vagal nerve stimulator or brain stimulator may be considered instead if the targeted brain region's function involves critical skills such as control of limbs or production/understanding of language and resective surgery would severely impact

these. Although vagal nerve stimulator seizure reduction rates are inferior to resective surgery and complete seizure freedom is rarely achieved, results still show worthwhile seizure reduction rates of a 50% decrease in seizure frequency (Wheeler et al. 2011, Englot et al. 2011). In about 30% of all patients epilepsy may be potentially amenable to surgery and so these patients are considered for pre-surgical evaluation (Duncan 2010), while half of these patients are likely to have resective surgery (Lhatoo et al. 2003). The presence of postoperative seizure symptoms may be due to remaining epileptogenic tissue (Sisodiya et al. 1997). Further to conspicuous epileptogenic lesions, additional cortical and subcortical grey matter alterations (see reviews by Bernhardt et al. 2009, Keller and Roberts 2008, Richardson 2012, Bonilha and Keller 2015) and WM tract alterations (see reviews by Rodriguez-Cruces and Concha 2015, Gross 2011, Bernhardt et al. 2015) may reflect additional epileptogenic tissue/networks. In particular, patients with temporal plus epilepsy (primary temporal epileptogenic zone extending into other regions such as the neighboring insular cortex) seem to more likely to be refractory to surgical treatment and experience persistent postoperative seizure symptoms (Barba et al. 2017). It is therefore critical that pre-surgical evaluation identifies the epileptogenic focus and rules out additional lesions or bilateral involvement during seizure generation (Mansouri et al. 2012).

1.4 Pre-surgical Evaluation

In order to diagnose epilepsy, multiple steps are necessary (Figure 1.2). In a first step the patient's history is assessed and this includes information on complications at birth, previous neurological insult, any other illness and medication.

Neurological Assessment Patient history Neurological and psychiatric examination Seizure semiology Surface inter-ictal EEG High-resolution MRI Baseline neuropsychological assessment	
Structural Pathology (MRI-positive) Conclusive and concordant results in non-invasive evaluation	No Structural Pathology (MRI-negative) Non-conclusive or discordant results in non-invasive evaluation
Potential Use of Other Imaging Modalities PET / inter-ictal or ictal SPECT / MEG / EEG-videotelemetry	
Lateralization of Speech Dominance Wada, functional MRI	
Potential Use of Invasive Monitoring Evaluation with intracranial electrodes (Subdural strips, grid, depth electrodes) and EEG-videotelemetry	
Resective Surgery Tailored temporal lobe resection Selective amygdalohippocampectomy Only lesionectomy	No Indication for Resective Surgery Optimizing AED therapy Vagal Nerve Stimulation Re-evaluation, if new evidence of focal findings

Figure 1.2. Pre-surgical Evaluation in TLE (from Immonen 2010). The trajectory of the pre-surgical evaluation process is presented from top to bottom. EEG = electroencephalography; MRI = magnetic resonance imaging; PET = positron-emission tomography; SPECT = single-photon emission computed tomography; MEG = magnetoencephalography; AED = anti-epileptic drug.

In order to understand the nature of the seizures a neurological examination, assessment of seizure semiology, surface (scalp) inter-ictal EEG and high-resolution MRI are performed. Neuropsychological evaluation and psychiatric examination are performed in patients being considered for surgery to (i) identify the damaged brain region and (ii) to predict potential postoperative cognitive impairments and in some

cases to rule out psychogenic non-epileptic seizures provoked by emotional states rather than abnormal epileptogenic neuronal activity. Additional modalities for brain imaging such as Magnetoencephalography (MEG), Positron Emission Tomography (PET) and Single-Photon Emission Computed Tomography (SPECT) may be used when available and especially in cases where scalp EEG and MRI remain inconclusive.

Upon identification of the seizure onset zone (region of seizure origin), pre-surgical evaluation of language lateralization/localization (Wada test) and functional MRI are performed. Results of these investigations have critical importance in the success of surgery, as peri- and post-surgical damage to brain areas that are indispensable for defined cortical functions such as language, movement, vision and memory are to be avoided. If the investigation indicates that it is unlikely that eloquent cortex will be compromised, then surgery may be considered. Conversely, if the test does not indicate this, additional invasive monitoring may be warranted before resective surgery or implantation of stimulators is performed.

1.4.1 Surface Inter-ictal EEG

EEG is the true gold standard procedure for diagnosing epilepsy and allows electrophysiological recordings of various cortical brain areas through placement of measurement electrodes on the scalp. Inter-ictal scalp EEG relies on the occurrence of spikes (electrical activity) in the time period between the occurrence of one seizure to the next and as such demonstrates cortical hyperexcitability and hypersynchrony (Pillai and Sperling 2006). Hypersynchronicity refers to a synchronous bursts of action potentials involving several interconnected neurons and occurs as a consequence of characteristic membrane depolarization, while hyperexcitability refers to a state of neurons being unusually or excessively excitable. EEG has a high temporal resolution in the range of milliseconds, so that these electrophysiological recordings can simultaneously reflect underlying neuronal

activity. When a focal ictal discharge is detected, this offers clues about the location of the epileptogenic region and the specific epilepsy syndrome. Inter-ictal background rhythms of the brain activity may also indicate what type of epilepsy the patient may have (Pillai and Sperling 2006, Smith 2005). Additionally, baseline neuropsychological testing is performed and invasive inter-ictal EEG may be considered for clearer information on seizure focus localization (Figure 1.2). Cessation of AED treatment and sleep deprivation can help to induce seizures to increase the clinical yield of the subsequent EEG (Giorgi et al. 2014, Rizvi et al. 2014, Ellingson et al. 1984). It is not completely clear why sleep deprivation may elicit epileptogenic activity within the brain (Samsonsen et al. 2016), however, this procedure is common at clinical centers: surgery is only undertaken after long-term video monitoring of seizure onset with an appropriate informative outcome (Cascino 2002). Given that the characteristics of an inter-ictal spike can be occasionally misleading and difficult to localize (due to poor spatial resolution), it is essential to put EEG findings in clinical context and consider aetiology, physical examination, seizure semiology and neuroimaging findings (Pillai and Sperling 2006).

1.4.2 Assessment of Preoperative Functional Skills

Prior to surgery, baseline neuropsychological assessment and language lateralization are performed. These procedures can inform about preoperative functional skills or deficits and predict postoperative neuropsychological outcomes (Rosenow and Lüders 2001). Memory and language are the most important cognitive skills that need to be assessed and lateralized. This is especially true for TLE where verbal and visual memory may be tested. Loring (2007) reported that side of surgery, preoperative memory score and age can predict postoperative verbal memory performance six years after surgery. Impaired postoperative verbal and nonverbal memory skills have been reported in patients who had average or above average memory and language skills at baseline (Helmstaedter and Elger 1996, Bonelli et al. 2010). Hermann et al. (1992) reported that patients with histologically proven and

marked left mesial temporal sclerosis are less likely to show significant memory decline after surgery. The authors further suggest that surgically induced impairment of memory function can be avoided by using preoperative hippocampal volumetric MRI as memory decline correlates with the degree of HS. Apart from these psychometric tests prior to surgery, the invasive intracarotid sodium amobarbital procedure, also referred to as the Wada test (Wada and Rasmussen 1960), has traditionally been used to lateralize language function. The test results are essential for successful planning of resective surgery. However, many clinical centers have now replaced the invasive test with functional MRI testing as this forms a valid alternative to the invasive Wada testing (Klöppel and Büchel 2005, Dym et al. 2011, Binder 2010), which is still considered to be the clinical gold standard approach (Pelletier et al. 2007, Alonso et al. 2016). MRI data was not related to pre- and postoperative memory functions as this would have exceeded the scope of this thesis.

1.4.3 Invasive Inter-ictal and Ictal EEG

Invasive inter-ictal and ictal EEG may be performed when surface EEG does not yield sufficient information on seizure focus localization. This is the case in about 30% of all patients with TLE (Spencer et al. 1985). Information gained through this technique can contribute to avoidance of eloquent cortex during resective surgery and confirm deep cortical seizure onset zones by characteristic spike discharges (Spencer 2002). Furthermore, invasive EEG can detect unilateral seizure onset zones in the case of bilateral inter-ictal surface discharges. If the epileptogenic zone extends beyond visible lesions, inter-ictal EEG may even identify multifocal epileptogenic lesions (Raymond et al. 1995). The invasive inter-ictal and ictal EEG measurements are usually combined with simultaneous video recording, which is then termed EEG video telemetry. This offers the advantage that a seizure can be recorded on EEG with simultaneous video recordings of any related body movements and occurrence of speech. The patients who are undergoing video telemetry, visiting relatives or hospital personnel may mark the onset of a seizure as

soon as they become aware of it. Subsequently, the event recorded on a videocamera and any descriptions of the event can be directly related to the EEG recordings where electrophysiological discharges may be detectable if a seizure occurred.

1.4.4 Standard Diagnostic MRI

Patients presenting with focal seizures will undergo structural MRI at the start of the clinical investigation and if necessary also after standard EEG evaluation (to apply specialized MR imaging techniques). According to the commission report of the ILAE (Barkovich et al. 1998), neuroimaging for patients undergoing pre-surgical evaluation should provide data on: “(i) Delineation of structural and functional abnormalities in the putative epileptogenic region; (ii) Prediction of the nature of structural pathology in the putative epileptogenic region; (iii) Detection of abnormalities distant from the putative epileptogenic region and (iv) Identification of brain regions important for normal function including primary sensorimotor function, language and memory, and the relation of these regions to the epileptogenic region”. Neuroimaging can also provide information on lesions not related to epilepsy, which is important to rule out any other pathophysiological processes given that seizures may be related to vascular malformations, tumor, infection or neurodevelopmental structural alterations. Depending on the likely diagnosis, different MRI sequences may be employed to identify an epileptogenic lesion. For example, 3D MRI sequences T1-weighted (T1w), T2-weighted (T2w) and T2 fluid-attenuated inversion recovery (T2FLAIR) are indicated for neocortical epilepsies as FCD may be detected (Blümcke et al. 2011, Figure 1.3).

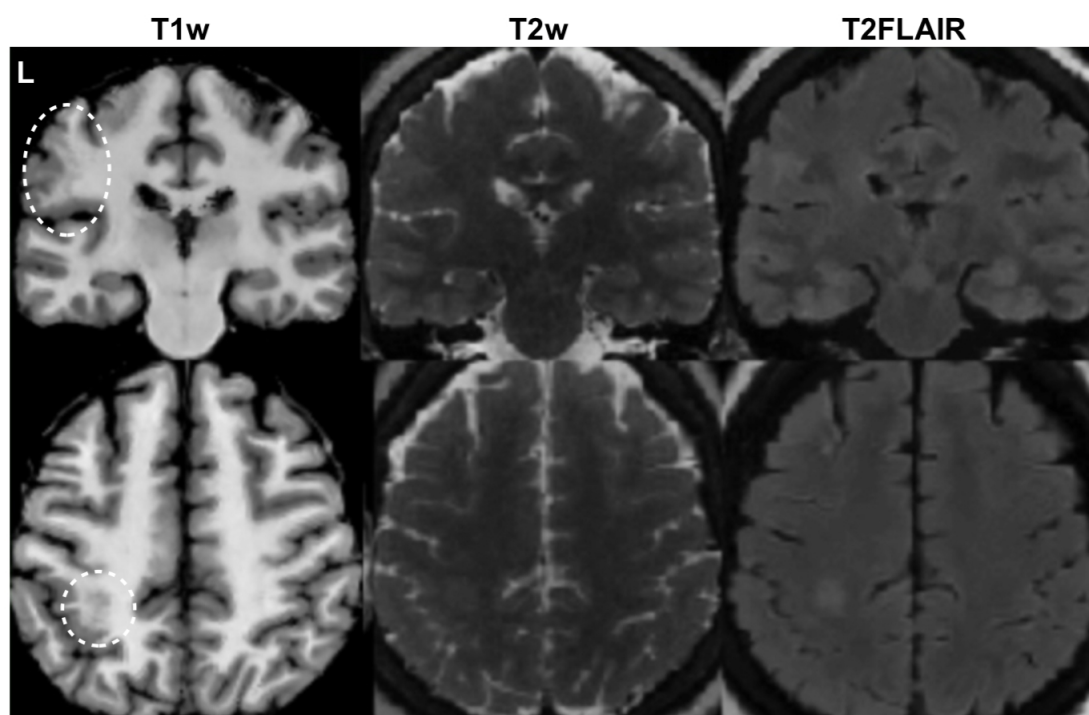


Figure 1.3. FCD in the left supramarginal gyrus (top) and superior parietal lobule (bottom). The related signal appears dark on T1w and bright on T2w/T2FLAIR 3D volume images. The WCFT neuroradiologist's report stated that the two dysplastic sites may be interconnected. L = left.

3D T1w and several imaging 2D coronal (T1FLAIR, T2FLAIR) sequences through the long axis of the hippocampus are particularly useful in suspected TLE (Duncan 1997). HS is identified by increased cerebrospinal fluid (CSF) space within the temporal horn of the lateral ventricles, loss of internal architecture (conspicuous on 2D T1FLAIR/T2FLAIR images), volume reduction of the hippocampus (conspicuous on 3D T1w) and local signal intensity increase as seen on coronal T2FLAIR images (Spencer 1994, Meiners et al. 1994, Mansouri et al. 2012). Images depicting this lesion are shown in Figure 1.4. The identification of HS on preoperative MRI is related to an improved post-surgical outcome in patients with TLE, particularly if electrophysiological, radiographic and semiological information

co-localize (Mansouri et al. 2012).

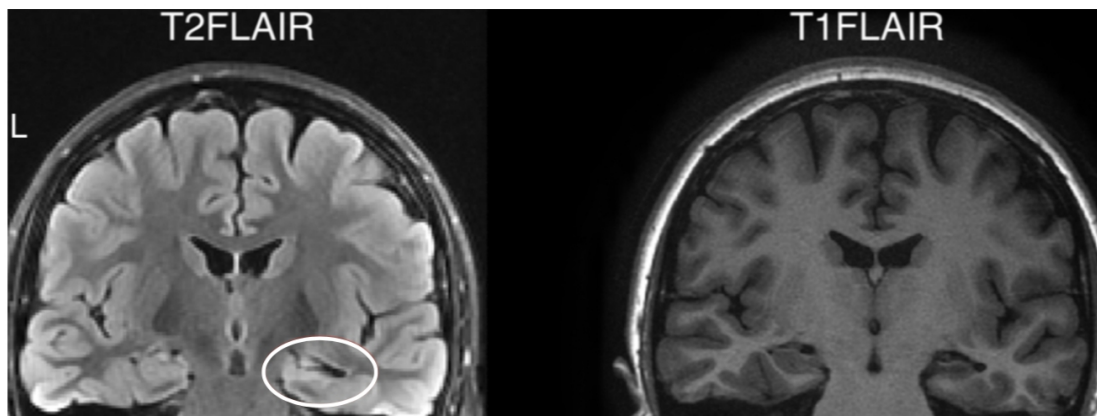


Figure 1.4. Right HS shown on T2FLAIR and T1FLAIR.

The T2FLAIR image shows hyperintense signal in the hippocampal region, while the T1FLAIR demonstrates hypointensity of the hippocampal formation with a marked volume loss. The loss of internal architecture in the right hippocampus is only marginally visible in both images. T1- and T2FLAIR both show blurring of the parahippocampal WM, which is a frequent finding co-occurring with HS. Images were acquired at WCFT. L = left.

1.5 Rationale for Advanced MRI of the Brain

In order to advance current standard diagnostic MRI for all patients and especially for those patients with subtle lesions that may have remained undetected on previous MRI, additional imaging and clinically informed neuroradiological assessment may be necessary. This section briefly describes additional sequences along with neuroradiological assessment and quantitative analysis techniques.

1.5.1 Additional Research Sequences

Functional magnetic resonance imaging (fMRI) sequences quantifying the blood oxygen level dependent signal have been applied in patients with epilepsy during rest (resting-state fMRI) and while performing a task (task-based fMRI). Task-based fMRI is traditionally used in clinical settings to localize important memory and language skills prior to surgery (Abou-Khalil 2007, Akanuma et al. 2003,

Aldenkamp et al. 2003). Patients are presented with a specific task, for example to memorize and recall words, while the blood oxygen level dependent signal is measured across the whole brain and correlated with the performed task so as to identify regions involved in task-related processing. The rationale for using research-based resting-state fMRI without the application of tasks in patients with epilepsy is to investigate possible regions of seizure onset and epileptogenic networks on an individual level (Bettus et al. 2010, Dansereau et al. 2014). Compared to healthy controls, regional altered blood flow and an altered network and functional connectivity between different brain regions may be found in patients when analyzing the data using whole-brain approaches. Another useful MR sequence is Arterial Spin Labelling, which can measure blood perfusion. The rationale for its application is that it is assumed that the epileptogenic region may have inter-ictal hypo-perfusion relative to other regions of the patient's brain (Galazzo et al. 2015).

Apart from measuring task-based functional connectivity clinically to investigate pre-surgical functions and to detect altered functional connectivity as compared to controls in scientific studies, research on structural connectivity has continuously gained interest. DTI is a technique, which enables researchers to quantify water diffusivity along the axis of axons and infer structural brain connections and tissue integrity between different brain areas. This became especially interesting since GM disruption in patients with epilepsy was thought to affect WM connections close to the seizure focus and in long-range connections between the seizure focus and other parts of the brain. For instance, multiple studies to date have shown that patients with left TLE seem to be more bilaterally affected than patients with right TLE when compared to controls and that diffusivity alterations are more severe and extensive ipsilateral to the side of seizure onset (Ahmadi et al. 2009, Yogarajah et al. 2008, Lin et al. 2008, Imamura et al. 2015). This technique also allows researchers to investigate correlations between clinical variables such as age of onset of epilepsy and seizure frequency and WM structural disruption. Manual tractography has been

the most widely applied technique to achieve mapping of structural connectivity (Metzler-Baddeley et al. 2011, Wakana et al. 2007). However, automated tractography is gaining increased recognition in scientific investigations as they require less time to implement and are reproducible and some of these automated tools also allow analysis of correlations between GM and WM structural disruption (Bonilha et al. 2010, Keller et al. 2017, Yeatman et al. 2012, Yendiki et al. 2011, Kreilkamp et al. 2017).

Although useful for assessing structural and functional connectivity, underlying pathobiological processes responsible for these alterations cannot be directly established through DTI or fMRI analysis. Advanced quantitative mapping of myelin in GM regions and WM tracts using T1w and T2w data (Van Essen et al. 2012) and the application of an iron mapping sequence could potentially reveal the underlying pathological process present in patients with epilepsy. Susceptibility-weighted imaging (SWI) is used to quantify iron in the brain and is particularly interesting in patients with epilepsy. Iron has been linked to febrile convulsions (Papageorgiou et al. 2015, Sharif et al. 2015) and epilepsy (Tombini et al. 2013) and may be associated with defects in the blood-brain-barrier and the deep GM nuclei that accumulate iron, leading to deleterious effects (Zhang et al. 2014).

1.5.2 Quantitative Techniques

Quantitative techniques allow comparisons against healthy controls and may complement traditional qualitative techniques employed by clinicians for first-hand evaluation. All sequences and derived images listed in 1.5.1 allow qualitative evaluation through visual assessment. This is a time-consuming process and diagnostic yield may vary with the quality of MRI and training (Von Oertzen et al. 2002). Additional techniques based on three-dimensional MRI that can quantify changes in the brain relative to healthy controls have important implications for studies aiming to characterize side of seizure onset and develop individual

diagnostics in a clinical setting (Martin et al. 2015).

Region of interest (ROI) analysis allows the a-priori investigation of brain regions thought to be involved in a disorder. It is a method whereby trained individuals with expert anatomical knowledge manually place the ROI on MRI of patients, this allows signal quantification and comparison to ROI values obtained from controls. Through statistical comparison, a decrease in structural volume or abnormally high/low signal can be detected. Many studies in epilepsy have successfully utilized the volume-based approach for the detection of HS (Jack 1994, Marsh et al. 1997, Matsufuji et al. 2012) and disruption of temporal lobe WM integrity as measured by diffusivity analysis (Ahmadi et al. 2009, Concha et al. 2005). Most frequently the relevant studies have focussed on manual delineation of tracts performed by a trained researcher based on a priori knowledge of neuroanatomy rather than using automated techniques (Kreilkamp et al. 2017). In patients with TLE, research has focussed on many temporal lobe tracts such as the cingulum angular bundle (CAB, otherwise referred to as the parahippocampal white matter bundle, PHWM) (Ahmadi et al. 2009, Yogarajah et al. 2008, Concha et al. 2007), which is the major connection of the hippocampus with other areas of the brain. The inferior and superior longitudinal fasciculus (ILF and SLF; Ahmadi et al. 2009, Imamura et al. 2015, Concha et al. 2012, Lin et al. 2008) connect the ventral and dorsoposterior aspects of the temporal lobe with the visual cortex and with the frontal lobe, respectively. The uncinate fasciculus (UF; Diehl et al. 2008, Ahmadi et al. 2009, Lin et al. 2008, Concha et al. 2012) forming connections from the temporal pole to the dorsomedial prefrontal cortex has also been studied. Finally, the fornix (Concha et al. 2007, Concha et al. 2010) has been investigated in patients with TLE as it belongs to the limbic system and connects the hippocampus with the hypothalamus. More details on these tracts and connections within the brain are presented in Chapter 3. However, manual methods are time-consuming and suffer from low reproducibility and reliability, which strongly justifies the development of newer automated methods that do not have these disadvantages.

Automated techniques have a lower time-demand as they circumvent the need for manual measurements by trained personnel (Leergaard et al. 2012). They are able to provide higher reliability through reproducible results generated by the same algorithm, whereas manual measurements may vary from one trained individual to another. For these reasons, the automated techniques may be readily implemented for the evaluation of patient MRI in clinical settings. Voxel-based morphometry (VBM) is a fully automated quantitative technique that allows exploratory analysis of the whole brain based on T1w data. The approach can be implemented to analyze various features of brain structure such as cortical thickness and subcortical atrophy. In patients with epilepsy, it has been successfully applied for the detection of HS (Bonilha et al. 2010) and FCD (Focke et al. 2008b, Huppertz et al. 2005) relative to healthy controls. Alternatively, rather than analyzing the whole brain, the ROI approach can be automated through the use of standard space templates and allows both regional GM and WM analysis. This requires normalization of the patient's MRI to a common template, this procedure is offered by many softwares and has been primarily used to detect WM tract diffusivity alterations (Liu et al. 2014, Scanlon et al. 2013). Atlas-based tractography works in a similar manner, however rather than extracting and investigating regions close to tracts, this method allows the more anatomically correct reconstruction of brain connections through voxel-by-voxel tractography (Hagler et al. 2009). Although useful for group analysis in research, these methods still need development before they can be applied to the analysis of individual patient MR images.

1.6 Motivation and Goals of this Thesis

The overall objective of this thesis was to develop and apply image analysis techniques in people with intractable focal epilepsy through advanced automated quantitative MR imaging and analysis. The work presented in this thesis uses data

collected from MRI-positive and MRI-negative patients to investigate the nature and significance of structural brain alterations in patients with epilepsy. Advanced post-processing image analysis techniques were applied to (I) characterize hippocampal atrophy (HA) and temporal lobe tract abnormalities in patients with refractory TLE and to investigate the relationship between these abnormalities and postoperative outcome and (II) to perform a series of quantitative MRI studies in patients with presumed MRI-negative refractory focal epilepsy to (IIa) implement a fully automated tool for the detection of lesions in individual patients based on T1w data and (IIb) to apply an automated tractography technique to DTI data of healthy controls and patients with non-lesional and lesional TLE and identify WM tract abnormalities between these groups.

1.6.1 Patients with TLE and Associated HS: Outcome Analysis

TLE is the most difficult type of epilepsy to treat medically, but considerably easier to treat surgically (Spencer 2002). Electrophysiological recordings indicating a temporal lobe seizure onset and the identification of HS during pre-surgical evaluation are the most important factors that allow clinicians to confidently identify an epileptogenic lesion, which may be amenable to surgery. The salient features that indicate HS are hippocampal volume loss, MRI signal intensity alterations, loss of digitations of the hippocampal head and disruption of internal architecture (due to neuronal loss). So far, however, it is not possible to identify different types of HS by expert neuroradiological assessment alone and clinicians are usually limited to the clinically available 1.5 and 3.0 Tesla MRI. Quantitative methods for hippocampal volume measurements can increase sensitivity in establishing the presence of HS (Duncan 1997, Woermann et al. 1998). Recently, more detailed automated quantitative hippocampal subfield mapping techniques based on multi-sequence MRI have been developed, such as HippocampalSubfields (Iglesias et al. 2015) provided within Freesurfer (Fischl 2012). It is unknown whether the multi-sequence automated hippocampal subfield volume analysis:

1. has any significance for seizure laterality,
2. reveals correlations between hippocampal subfield volume and any clinical variables such as age of onset, duration and seizure frequency,
3. reveals correlations with postoperative seizure outcomes.

No study to date has yet established whether this automated hippocampal subfield mapping is able to detect correlations with clinical variables or seizure laterality in large patient datasets (Sone et al. 2016). Different types of HS identified through histology have been shown to be related with post-surgical outcomes (Blümcke et al. 2007), however, it remains unclear whether in-vivo MRI analysis approaches can accomplish this in a similar way. Consequently, it is important to establish whether preoperative automated mapping of hippocampal subfields can determine the type of HS and could potentially predict surgical outcomes.

About 45% of patients undergoing resective surgery of the epileptogenic lesion often present with seizures again during a follow-up of five years (de Tisi et al. 2011). Recently, the importance of networks during seizure onset and propagation have been acknowledged (Berg and Scheffer 2011) and this has led to a paradigm shift in research and clinical practice. Epilepsy is no longer viewed as a sole GM disorder, but seen in the context of the brain as a dynamic network. DTI data is frequently used in clinics for neuroradiological assessment of gliomas (Inoue et al. 2005) and may be used during pre-surgical evaluation in order to avoid damage to WM tracts connecting eloquent cortex (Anastasopoulos et al. 2014, Bello et al. 2008), but DTI has not yet found application in the clinical assessment of TLE to determine disrupted WM connectivity. In order to achieve this, it is necessary to apply quantitative tractography techniques. This method has been applied in epilepsy research and requires a trained individual to make time-consuming measurements, while more recent techniques allow automated measurements. Additionally, rather than being limited to diffusion values extracted from whole tracts, this method allows

along-the-tract (waypoint) diffusivity measurements. It is unknown whether the automated tractography technique:

1. has any significance for seizure laterality,
2. could reveal correlations between diffusion values along temporal lobe tracts and the extent of gross hippocampal volume loss,
3. could reveal correlations between diffusion values extracted using whole / waypoint tract analysis and any clinical variables such as age of onset, duration and seizure frequency,
4. could reveal correlations between diffusion values extracted using waypoint tract analysis with postoperative seizure outcomes.

Given that automated tractography techniques provide substantial benefits for analyzing structural connectivity in a time-efficient, reproducible and reliable way over manual approaches, it is important to implement automated analysis approaches. Once their usefulness has been established through scientific research, these techniques may also be potentially readily implemented in clinical settings. Although it is important to assess the underlying dynamic pathobiological process underlying TLE with associated HS, the relationship between HA and WM tract alterations has not yet been established (Rodriguez-Cruces and Concha 2015). For these reasons, a study reported in this thesis was used to investigate this.

The above research questions were investigated in this thesis in an archival study, which involved data collected on patients with TLE and associated HS and healthy controls. The data for these studies had been acquired at a specialized epilepsy center in Bonn, Germany and featured an extensive dataset where clinical variables and post-surgical outcome were also documented. This allowed the characterization of HA and temporal lobe tract abnormalities in patients with refractory TLE and to investigate the relationship between these abnormalities, clinical variables and postoperative outcome. Based on this data, multiple quantitative MRI studies were

performed by the use of automated hippocampal subfield segmentation (Chapter 5) and WM tractography analyses (Chapter 6).

1.6.2 Patients with MRI-negative Focal Epilepsy

Patients who do not present with an underlying lesion on MRI (non-lesional), are less likely to achieve seizure freedom after epilepsy surgery: only 50% achieve short-term seizure freedom (Cohen-Gadol et al. 2005, Khan et al. 2014). In these patients with non-lesional epilepsy as determined by MRI, pre-surgical evaluation may only rely on other clinical assessments such as semiology, (invasive) inter-ictal EEG and video-telemetry. It is therefore important to utilize the most advanced MRI protocols and expert neuroradiological assessments during the diagnostic process (see Chapter 7) in order to identify potentially epileptogenic lesions (Von Oertzen et al. 2002). In patients with presumed MRI-negative refractory focal epilepsy, it is important to establish whether subtle lesions may be detectable on advanced MRI using quantitative methods, so that the best surgical seizure outcomes can be attained after surgery. FCD is a common lesion associated with medically refractory epilepsy (Sisodiya 2004, Fauser et al. 2004) and often epileptogenic (Fauser and Schulze-Bonhage 2006). Many automated quantitative whole-brain analysis approaches have been employed to identify potentially epileptogenic lesions such as FCDs. However, so far it remains unclear:

1. whether previously neuroradiologically diagnosed FCDs could also be identified by a fully automated integrated testing tool based on statistical significant differences of individual patients as compared to healthy controls (only T1w data),
2. how a newly developed automated multi-modal quantitative lesion detection technique compares to expert neuroradiological evaluation.

Although previous studies have promoted the use of automated voxel-based lesion detection approaches, clinical usefulness remains limited due to the necessity for

expert neuroradiologists to re-evaluate the identified sites for true presence of FCDs (Huppertz 2013). Therefore, this thesis presents the results of a study conducted with the aim of applying statistical significance testing in order to identify sites of FCD and implement multi-modal statistical testing through the use of the novel automated approach.

However, for the reasons presented in Section 1.6.1 it is important to extend studies in epilepsy from GM to WM analysis through structural connectivity analysis using DTI tractography. Automated DTI tractography provides substantial benefits over manual tractography techniques (see Section 1.6.1 and Chapter 6), while the manual approach is considered gold-standard in the absence of neuroanatomical data (Wakana et al. 2007). Automated tractography techniques are being increasingly employed in research as they are readily available for efficient use. However, previous studies have failed to complete extended validation of these methods and it is therefore important to establish:

1. whether the automated WM tract analysis provides similar whole tract diffusion characteristics to manual tractography in patients with TLE,
2. whether manual and automated tractography reveal similar correlations between diffusion values of whole tracts and any clinical variables such as age of onset, duration and seizure frequency,
3. whether the automated tractography technique can reveal additional information through along-the-tract analysis,
4. whether differences between patients with lesional and non-lesional TLE can be detected using automated tractography.

Previous research has only investigated correlations of FA values extracted from manual versus automated approaches (Yeatman et al. 2012). To date, no information has been provided with respect to comparisons between automated and manual tractography with relation to whole tract location and shape. Additionally, a study

comparing diffusion characteristics of WM tracts in healthy controls and patients with non-lesional and lesional TLE based on automated tractography techniques has not yet been performed.

The above research questions on patients with non-lesional and lesional epilepsy were investigated in this thesis through the use of prospectively collected data. The data for these studies was acquired at the WCFT in Liverpool, United Kingdom and involved healthy controls and patients with focal refractory epilepsy whose previous MRI did not indicate any lesions. Based on this data, multiple quantitative MRI studies were performed in order to implement a fully automated tool for the detection of lesions in individual patients (Chapter 8) and to apply an automated tractography technique to DTI data of healthy controls and patients with non-lesional and lesional TLE in order to identify WM tract abnormalities between these groups (Chapter 9).

Chapter 2: Materials and Objectives

Chapter 2: Materials and Objectives.....	30
2.1 Organization of Chapter 2.....	30
2.2 Refractory Temporal Lobe Epilepsy with Hippocampal Sclerosis.....	31
2.2.1 Introduction.....	31
2.2.2 Methodology.....	32
2.2.2.1 Materials and Participants.....	32
2.2.2.2 Applied MR Sequences.....	33
2.2.2.3 Quantitative MRI Analysis.....	34
2.2.3 Objectives and Hypotheses.....	34
2.2.3.1 Automated Quantitative MRI of the Hippocampus: Study 1.....	34
2.2.3.2 Automated Quantitative MRI of Temporal Lobe Tracts: Study 2.....	36
2.3 Focal 'Non-lesional' and Lesional Epilepsy.....	37
2.3.1 Introduction.....	37
2.3.2 Methodology.....	38
2.3.2.1 Materials and Participants.....	38
2.3.2.2 Applied MR Sequences.....	38
2.3.2.3 Quantitative MRI Analysis.....	40
2.3.3 Objectives and Hypotheses.....	41
2.3.3.1 Neuroradiological Assessment and Clinical Findings: Study 3.....	41
2.3.3.2 Automated Epileptogenic Lesion Detection: Study 4.....	42
2.3.3.3 Automated Tract Reconstruction: Study 5.....	42

2.1 Organization of Chapter 2

The aims of this thesis can be classified into two different general categories: (i) the investigation of neuroimaging correlates of persistent postoperative seizures in patients with TLE and associated HS undergoing amygdalahippocampectomy to alleviate seizures and (ii) the application of a dedicated MRI epilepsy research protocol and quantitative analysis in patients with 'non-lesional' intractable focal epilepsy in order to increase the number of patients with MRI-visible lesions. For both categories, novel automated tools have been implemented on two separate datasets in order to allow time-efficient and reproducible group- and individual-based analyses that are potentially adaptable to clinical settings. Wherever possible, quantitative comparisons were made between automated and manual techniques.

This chapter details the aims, materials, participants, methodology and objectives of all individual studies. As there are two different datasets, the first subsections of sections 2.2 and 2.3 introduce the relevant research questions and present the associated demographic and clinical information. The participant characteristics and details pertaining to MR sequences presented in Section 2.2 include information from these publications: Keller et al. (2015a), Kreilkamp et al. (2017), Elkommos et al. (2016). Sections 2.2.2.3 and 2.3.2.3 detail the methodology common to all quantitative MRI studies. The final subsections of 2.2 and 2.3 present the study objectives and hypotheses for the analysis specific to each individual study. The objective of Chapter 2 is to provide an overview of all studies conducted within this thesis and how they relate. More detailed information about MR sequences, MR analysis methods, their development and context within the clinical and scientific literature can be found in Chapter 4.

2.2 Refractory Temporal Lobe Epilepsy with Hippocampal Sclerosis

2.2.1 Introduction

The objective of this study was to investigate the relationship between quantitative preoperative MR imaging markers, clinical data and post-surgical outcomes in order to assess whether preoperative imaging of the hippocampal formation can predict surgical outcomes (Study 1) and whether WM tract disruption is related to HS, clinical characteristics of the disorder and postoperative outcome (Study 2). These investigations were performed using T1w and T2 Short TI Inversion Recovery (T2STIR) data for hippocampal structural analysis and diffusion tensor imaging (DTI) data was analyzed to reveal any disruption of diffusion metrics in WM tracts.

2.2.2 Methodology

2.2.2.1 Materials and Participants

Imaging data was acquired between July 2006 and January 2013 at the Life and Brain Center and the University Hospital Bonn, Germany using a 3T Magnetom Trio MR system (Siemens, Erlangen, Germany) with an eight-channel head coil. The study was approved by the local ethical board. All participants provided written informed consent (Keller et al. 2015b). Demographic and clinical data is presented in Table 2.1.

Variable	Patients with left TLE	Patients with right TLE	Controls
N	73	40	58
Mean age (SD), years	40.6 (12.9)	41.4 (14.4)	39.6 (13.4)
Sex (female/male)	46/27	16/24	34/24
Mean age at diagnosis (SD), years	17.1 (12.1)	17.3 (12.5)	N/A
Mean duration of epilepsy (SD), years	23.4 (13.6)	23.7 (16.1)	N/A
History of FC (no/yes)	36/21	22/10	N/A
History of SGTCS (no/yes)	31/28	20/9	N/A
Seizure frequency (SD), months	9.2 (15.7)	7.5 (16.8)	N/A
ILAE I / ILAE II-VI	26/29	20/8	N/A
T1w	73	40	58
T2STIR	70	36	N/A
DTI	41	23	44
Postoperative T1w	34	18	N/A

Table 2.1. Demographic, clinical and MR imaging information for all participants of Studies 1 & 2.

Details of individual patients/controls can be found in Table 2.A (Appendix: Raw Data). TLE = temporal lobe epilepsy; SD = standard deviation; SGTCS = secondary-generalized tonic-clonic seizure; FC = febrile convulsions.

The study comprised 113 patients with well-characterized mesial TLE and radiological evidence of HS (mean age 40.9 years (SD 13.3); 62 female; 73 with left

TLE, 40 with right TLE) who were being evaluated for suitability for neurosurgery at University Hospital Bonn, Germany.

Each patient underwent a detailed pre-surgical program, including comprehensive seizure semiology assessment, MRI, neuropsychological assessment, interictal electroencephalography and if clinically necessary, additional invasive electrophysiological recordings, as reported recently (Keller et al. 2015a, Kral et al. 2002). All patients showed evidence of a unilateral temporal lobe seizure onset with concomitant ipsilateral HS. Conventional indicators of HS were diagnosed by an experienced neuroradiologist (Keller et al. 2015a). No patient had bilateral HS, or evidence of a potential secondary epileptogenic lesion. Age of patient, age at diagnosis of epilepsy, duration of epilepsy, history of childhood febrile convulsions (FC) and incidence of secondary-generalized tonic-clonic seizures (SGTCS) were recorded for all patients. Patients who underwent temporal lobe surgery (standardized amygdalohippocampectomy) received postoperative follow up for a period of up to two years after surgery and outcome assessment using the ILAE outcome classification system (Wieser et al. 2001). 58 age- and sex-matched controls without any neurologic or psychiatric history (mean age 39.6 (SD 13.4); 34 female) were also recruited into the study.

2.2.2.2 Applied MR Sequences

T1w magnetization-prepared rapid acquisition gradient echo (MPRAGE) images were acquired (160 slices, repetition time [TR]=1,300 ms, inversion time [TI]=650 ms, echo time [TE]=3.97 ms, resolution=1.0 x 1.0 x 1.0 mm, flip angle=10°, acquisition time = 7:00 mins) for all controls and patients prior to surgery. A high in-plane resolution T2STIR sequence in the coronal plane angulated perpendicular to the long axis of the hippocampus (40 slices, TR = 5600 ms, TI = 100 ms, TE = 18 ms, resolution 0.45 x 0.45 x 2.0 mm, flip angle 0°, acquisition time = 3:40 min) was acquired for all patients (Elkommos et al. 2016). Postoperative T1w MPRAGE

images were also acquired for 52 patients. Furthermore, diffusion-weighted images (DWI, single shot spin-echo planar imaging sequence, TR=1,200 ms, TE=100 ms, 72 axial slices, resolution=1.726 x 1.726 x 1.7mm, no cardiac gating, GRAPPA acceleration factor=2.0; acquisition time = 9:30 min) were acquired for 64 patients (preoperatively) and 44 controls within the same scanning session. Diffusion gradients were equally distributed along 60 directions (b-value=1000 s/mm²). Additionally, seven datasets with no diffusion weighting (b-value=0 s/mm²) were acquired initially and interleaved after each block of ten DWI.

2.2.2.3 Quantitative MRI Analysis

All image pre-processing and analysis was performed on an iMAC running OSX Yosemite 10.10.5. Freesurfer version 5.3 was used for initial T1w-based brain segmentation (Fischl 2012) and Freesurfer version 6.0 (<https://surfer.nmr.mgh.harvard.edu/fswiki/HippocampalSubfields>, Iglesias et al. 2015) subsequently allowed the extraction of high-resolution hippocampal subfield volumes based on T2STIR (Study 1). DTI pre-processing was achieved by following the ENIGMA pre-processing steps (<http://enigma.ini.usc.edu/protocols/dti-protocols/>) with FSL (Smith et al. 2004) and was used as an input to TRACULA version 1.56 (Yendiki et al. 2011) within Freesurfer version 5.3 for probabilistic tract reconstruction (Study 2). Hippocampal volumes corrected for intracranial volume (ICV) extracted through Freesurfer version 5.3 were also used in this study for clinical correlations. Statistical analysis for both studies was performed using MATLAB 2015b.

2.2.3 Objectives and Hypotheses

2.2.3.1 Automated Quantitative MRI of the Hippocampus: Study 1

The aim of this study was to investigate the relationship between the preoperative volumes of hippocampal subfields volumes and postoperative seizure outcome in patients with refractory TLE using a novel automated MRI multi-sequence

segmentation technique based on T1w and T2STIR data. The automated hippocampal segmentation algorithm was used to identify 12 subfields in each hippocampus and to investigate whether volumes of subfields were related to the side of seizure onset and postoperative outcomes. The detailed methodology and all results of this study are presented in Chapter 5.

Objective 5.1

To investigate the relationship between preoperative hippocampal subfield volumes and clinical and surgical outcomes in patients with refractory TLE using a new MRI multi-sequence segmentation technique. It was hypothesized that post-surgical outcome was related to preoperative hippocampal subfield volume. For example, as ILAE HS type 1 is manifest as predominant loss of neurons and gliosis in CA1 and CA4 subfields and has been associated with an early seizure onset and improved seizure outcome after temporal lobe surgery (Blümcke et al. 2013), it was hypothesized that atrophy in these regions would be related to favorable post-surgical outcomes. Furthermore, as HS is the result of an initial precipitating injury (Pitkänen and Lukasiuk 2011, Blume 2006, Goldberg and Coulter 2013), it was assumed that clinical features such as age of onset, duration of epilepsy and seizure frequency would not be related with the degree of atrophy of gross hippocampal volume or of any subfields.

Objective 5.2

To determine the relationship between hippocampal subfield volumes and semi-quantitative hippocampal internal architecture (HIA) ratings. It was hypothesized that the semi-quantitative HIA ratings (visual scoring assessments representing a marker for loss of internal hippocampal architecture, an important feature of HS (Elkommos et al. 2016)) would correlate with whole hippocampal and subfield volumes.

2.2.3.2 Automated Quantitative MRI of Temporal Lobe Tracts: Study 2

A detailed understanding of WM tract alterations in patients with TLE is important as it may provide useful information for likely side of seizure onset, cognitive impairment and postoperative prognosis. Importantly, WM tract analysis can provide quantitative information not visible to the human eye from raw (diffusion) MRI as an addition to conventional structural MRI (e.g. T1w). Most frequently, quantitative DTI studies have relied on manual reconstruction of tract bundles. In the present study, an automated WM tractography analysis approach to quantify temporal lobe WM tract alterations in TLE was used to determine the relationships between tract alterations, the extent of HA and clinical characteristics of the disorder. Alterations of DTI scalar metrics along WM tracts were investigated with respect to hippocampal volume. The relationships between WM tract alterations and duration of epilepsy, age of onset of epilepsy, seizure burden (defined as a function of seizure frequency and duration of epilepsy) and post-surgical outcomes were also explored. The detailed methodology and all results of this study are presented in Chapter 6.

Objective 6.1

To investigate diffusion alterations of whole temporal lobe WM tracts in patients with left and right TLE relative to healthy controls using an automated probabilistic tractography approach. It was hypothesized that the automated method can identify diffusivity changes (in FA and MD values of temporal lobe WM tracts) relative to controls and among the two patient groups.

Objective 6.2

To investigate alterations along WM tracts using waypoint comparisons for ipsilateral and contralateral tracts between patient groups based on side of seizure onset and other clinical factors (e.g. history of febrile seizures). It was hypothesized that WM tract diffusivity measures in patients are more extensively affected ipsilaterally and in the presence of unfavorable clinical factors such as

greater seizure frequency, longer epilepsy duration, history of SGTC/febrile seizures, and earlier age of onset.

Objective 6.3

To determine the relationship between regional WM tract diffusivity and the degree of hippocampal (subfield) atrophy in patients with TLE. As HS is seen as an initial precipitating injury (Pitkänen and Lukasiuk 2011), it was hypothesized that no relationship between hippocampal volume and WM tract diffusion characteristics would be found, but rather that regional WM tract diffusivity is mediated by unfavorable clinical factors of the disorder such as epilepsy duration and age of onset.

Objective 6.4

To investigate whether patients with postoperative seizures and those who were rendered seizure free after surgery could be differentiated based on preoperative WM tract diffusivity measures. It was hypothesized that patients with persistent postoperative seizures would have more extensive abnormal diffusivity measures in ipsi- and contralateral temporal lobe tracts (such as the uncinate fasciculus (UF) and cingulum angular bundle (CAB)) than patients who were rendered seizure free.

2.3 Focal 'Non-lesional' and Lesional Epilepsy

2.3.1 Introduction

The overall aim of this study was to identify possible epileptogenic lesions by virtue of expert neuroradiological reassessment of an epilepsy research dedicated MRI protocol (Study 3) and automated quantitative analysis (Studies 4 and 5). T1w, T2w, T2FLAIR and DTI data were used to automatically quantify structural changes in individual patients relative to healthy controls, which were validated against

neuroradiological assessment (Study 4). An automated tractography approach was used to determine WM tract diffusivity abnormalities in patients with TLE on a group level (Study 5), which was compared to a manual tractography technique.

2.3.2 Methodology

2.3.2.1 Materials and Participants

The study was conducted at the WCFT, Liverpool, UK between November 2014 and April 2016. A 3.0 Tesla General Electric Discovery MR750 scanner (Waukesha, WI, USA) with a 32-channel head coil was used for acquisition of MR images. The study was approved by the ethical board of the University of Liverpool (Liverpool Central REC, 14/NW/0332, University of Liverpool sponsorship, UoL001021) and National Health Service R&D with a National Institute of Health Research adoption (The Walton Centre NHS Foundation Trust, RG127-14) for the application of MRI scanning and collection of previous clinical data in patients with refractory focal epilepsy. All participants provided written informed consent.

43 patients were recruited on the basis of having a focal onset of seizures, being refractory to medical treatment and showing no lesion on previous clinical MR imaging. The mean age of patients was 31.6 (SD=11) years and 26 of these were female (Table 2.2). Most patients had either a unilateral temporal (N=24) or unilateral frontal lobe (N=13) onset. Two participants had a bilateral (one with a temporal and the other with a frontal onset), two had a temporal-parietal, one patient had a frontotemporal and another had an unknown localization of seizure onset. 42 controls were recruited on the basis of having no neurological or psychiatric disorders. Mean age of controls was 32.3 (SD=8.7) years (Table 2.2).

2.3.2.2 Applied MR Sequences

Acquisition comprised a 3D axial T1w fast-spin-gradient (FSPGR) image with Phased Array Uniformity Enhancement (PURE) signal inhomogeneity correction

(140 slices, TR=8.2 ms, TI=450 ms, TE=3.22 ms, flip angle=12, with 1mm isotropic voxel size, acquisition time: 3:48 mins) for all participants. Axial 3D T2w CUBE images (with PURE correction, 312 slices, TR=2500 ms, TI = N/A, TE=71.2 ms, flip angle=90, with 0.5 mm isotropic voxel size) and 3D sagittal CUBE T2 fluid-attenuated inversion recovery (T2FLAIR) with PURE (312 slices, TR=6000 ms, TI=50 ms, TE=127.1 ms, flip angle=90 with 0.5mm isotropic voxel size) were also acquired.

Variable	Patients with left TLE	Patients with right TLE	Patients with other foci	Controls
N	16	8	19	42
Mean age (SD), years	32.1 (11.4)	31.8 (12.3)	31.1 (10.7)	32.3 (8.7)
Sex (female/male)	10/6	5/3	11/8	25/17
Mean age at diagnosis (SD), years	15.8 (11.4)	18.1 (11.6)	14.2 (9.3)	N/A
Mean duration of epilepsy (SD), years	16.4 (10.7)	13.7 (15.5)	16.9 (10.3)	N/A
History of febrile convulsions (no/yes)	12/4	7/1	18/1	N/A
History of SGTCS (no/yes)	5/11	3/5	3/16	N/A
History of brain infection (no/yes)	16/0	4/4	17/2	N/A
Complications at birth (no/yes)	16/0	6/2	17/2	N/A
Seizure frequency (SD), months	4.9 (8.9)	3.4 (4.7)	7.3 (12.1)	N/A

Table 2.2. Demographic and clinical information for all participants of Studies 3-5.

Patients with other onsets included (14 patients with a frontal lobe onset and five patients with other onsets: see text). All participants underwent the same imaging protocol. Details of individual patients/controls can be found in Table 2.B (Appendix: Raw Data). TLE = temporal lobe epilepsy; SD = standard deviation; SGTCS = secondary-generalized tonic-clonic seizure.

It took 3:18 minutes to acquire the T2w image and 7:27 minutes to acquire the T2FLAIR CUBE image. DTI data were acquired using a 60-direction spin echo pulse sequence (66 slices, TR = 8000ms, TI = N/A, TE = 82 ms, flip angle = 90, voxel

size = 1x1x2 mm, no cardiac gating, with ASSET, b-value = 1000 s/mm²; FOV = 256 mm) with six b0 images without diffusion weighting. The acquisition time was 8:56 minutes. Additionally, a T1FLAIR coronal image (52 slices, TR = N/A, TI = 920 ms, TE = 9.94 ms, flip angle = 111, voxel size = 0.4x0.4x3mm) and a T2FLAIR coronal image (40 slices, TR = 12000 ms, TI = 2713 ms, TE = 98.7 ms, flip angle = 160, voxel size = 0.86x0.86x4 mm) were acquired for patients (diagnostic purposes) and controls. Acquisition times for these coronal images were four minutes for T1FLAIR and 3:24 minutes for T2FLAIR. Every MR image acquired within this study was obtained for all participants (patients and controls) and assessed by a consultant neuroradiologist at the WCFT (Study 3). One participant (control) had to be excluded from further analysis due to a structural lesion (meningioma) and another dataset had to be excluded as this control had received a different T1w sequence (rather than the T1w FSPGR). Resting-state functional MRI, Arterial-Spin-Labeling and Susceptibility-weighted Angiography imaging were also acquired within this study but not analyzed within this thesis.

2.3.2.3 Quantitative MRI Analysis

For Study 4, image pre-processing and statistical analysis was performed on an iMAC running OSX Yosemite 10.10.5 and Human Connectome Project (HCP) workbench software (Glasser and Van Essen 2011) was used to automatically set the origin of the T1w image to the anterior commissure. DTI data was pre-processed using the ENIGMA preprocessing steps to mitigate effects of image artifacts (<http://enigma.ini.usc.edu/protocols/dti-protocols/>) using FSL (Smith et al. 2004). Finally, image pre-processing and statistical testing was achieved through the computational anatomy toolbox (CAT12) within Statistical Parametric Mapping (SPM12; Wellcome Department of Cognitive Neurology, www.fil.ion.ucl.ac.uk) using an automated in-house MATLAB 2015b script.

For Study 5, image pre-processing and statistical analysis was performed on a

MacBookPro laptop running OSX Yosemite 10.10.5. Diffusion Toolkit version 0.6.3 (<http://www.trackvis.org>) was used for manual tractography and AFQ (Yeatman et al. 2012) was used for automatic deterministic tractography on the previously pre-processed DTI data from Study 4. Statistical analysis was performed using MATLAB 2015b.

2.3.3 Objectives and Hypotheses

2.3.3.1 Neuroradiological Assessment and Clinical Findings: Study 3

Patients with epilepsy who were deemed to be MRI-negative by virtue of earlier non-specialist MRI assessment were included in the study. Localization of seizure onset had been evaluated using seizure semiology and EEG. These patient cases were re-evaluated with the present protocol using diagnostic assessment of multiple MRI sequences by an experienced neuroradiologist with specialist experience in detecting epileptogenic lesions. Wherever possible, findings were related to the etiology and history of the patient and possible correlations were discussed. Clinical reports were gathered throughout the whole duration of the study and the relevant information was updated accordingly. The detailed methodology and all results of this study are presented in Chapter 7.

Objective 7.1

The ultimate aim of this study was to evaluate whether a dedicated epilepsy research protocol with expert image re-evaluation can increase identification of patients with lesions. The earlier MRI was included in an evaluation of lesion conspicuity to qualitatively re-evaluate factors likely to have contributed to the new presentation of a lesion. It was hypothesized that multiple factors such as image quality, lesion conspicuity on standard MRI (not specialized in depicting epilepsy-related lesions) and neuroradiologists' expertise in identifying epilepsy-related lesions contribute to varying results of MRI reports.

2.3.3.2 Automated Epileptogenic Lesion Detection: Study 4

The objective of this study was similar to the preceding study, however rather than assessing images by expert visual assessment, an automated quantitative voxel-based lesion detection technique was used. Voxel-based parametric testing was used to determine individual differences in feature maps between individual patients and the cohort controls. Detailed methodology and results are presented in Chapter 8.

Objective 8.1

The objective of this study was to implement and automatize a previously developed lesion detection technique and to apply this to T1w images of patients with cryptogenic focal epilepsy. It was hypothesized that neuroradiologically identified lesions by virtue of the dedicated epilepsy research MRI could also be detected using the automated voxel-based approach based on T1w images.

Objective 8.2

A further objective was to incorporate other MR images into the automated voxel-based approach in order to improve sensitivity and specificity of the approach. It was hypothesized that the automated tool in conjunction with multimodality testing (with the incorporation of T2w/T2FLAIR/DTI data) can identify previously undetected epileptogenic lesions while reducing the false positive rate based on multimodal testing.

2.3.3.3 Automated Tract Reconstruction: Study 5

The aim of this study was to identify diffusion alterations in WM tracts such as the fimbria-fornix (FF), uncinate fasciculus (UF) and parahippocampal white-matter bundle (PHWM) in patients with cryptogenic focal epilepsy using an automated technique, which could be potentially implemented in a clinical setting. The automated tractography technique was employed in controls, patients with TLE and HS (as established by the neuroradiological assessment based on the epilepsy

dedicated research MRI) and patients with TLE without HS to explore group differences between controls and patient groups. It was investigated whether WM diffusivity changes were related to clinical variables including age of onset of epilepsy, duration of epilepsy, seizure frequency and presence of SGTCS. Furthermore, a comparison of the automated tractography approach and a manual tract reconstruction technique was performed. Methodological details and results of this study are presented in Chapter 9.

Objective 9.1

The first objective was to investigate the agreement between manually and automatically generated tracts in patients with TLE. Furthermore, consistency between the automated and manual approaches with respect to whole tract diffusivity metrics (FA/MD), detection of diffusivity abnormalities in tracts of patients with TLE and clinical correlations with diffusion metrics were investigated. It was hypothesized that manual and automated methods produce tracts of the same shape, volume and at similar locations and in order to assess this, the Dice coefficient was computed. Moreover, it was hypothesized that DTI-metrics extracted from WM tracts using the two different approaches are consistent (high correlations of FA/MD values across approaches) and that significant group-wise results of whole-tract diffusion measures arising of comparisons between the two patient groups and controls were also comparable. It was hypothesized that AFQ would identify the same number of group-wise differences and correlations.

Objective 9.2

The second objective of this chapter was to investigate whether along-the-tract diffusivity analysis of FF, UF and PHWM within the automated tractography approach can reveal correlations with clinical variables and group differences between patients with left/right TLE, those with HS, those without and controls and provide more detailed information than the manual approach. It was

hypothesized that the along-the-tract analysis offered within the automated tractography approach would confirm previous group-wise findings, detect correlations with clinical variables and that it could reveal more detail in diffusivity alterations regarding correlations with clinical variables such as age of onset of epilepsy and epilepsy duration and when investigating diffusivity alterations in patients with HS, those without and controls.

Chapter 3: Neuroanatomy

Chapter 3: Neuroanatomy.....	45
3.1 Organization of Chapter 3.....	45
3.2 Neuroanatomy of the Cerebrum.....	46
3.2.1 Divisions.....	46
3.2.2 Brain Development.....	50
3.2.3 Malformations of Cortical Development.....	52
3.3 Temporal Lobe.....	57
3.3.1 Hippocampus.....	57
3.3.2 Hippocampal Internal Architecture.....	58
3.3.3 Hippocampal Functions and Projections.....	60
3.4 Temporal Lobe Connectivity.....	65
3.4.1 Fimbria and Fornix.....	66
3.4.2 Parahippocampal Cingulum.....	68
3.4.3 Inferior Longitudinal Fasciculus.....	68
3.4.4 Superior Longitudinal Fasciculus.....	69
3.4.5 Uncinate Fasciculus.....	69

3.1 Organization of Chapter 3

The two most frequent causes of medically refractory focal epilepsy are HS and malformations of cortical development such as FCD, which forms the largest subgroup of these type of lesions (Martin et al. 2015). Together, HS and FCD constitute about 50% of all surgical pathology in patients affected by epilepsy (Miyata et al. 2013). In order to understand the underlying structural and functional brain alterations in patients with epilepsy presenting with HS and/or FCD, the present chapter seeks to present background information on healthy brain structure, function and development. Chapter 3 provides an overview of the gross cerebral neuroanatomy, the basics of brain development with a special focus on neuronal migration, the temporal lobe and the major structural connections of the temporal lobe with other areas of the brain. Particular emphasis is given to the temporal lobe and hippocampus as most patients investigated in this thesis have TLE with associated HS. Another subset of investigated patients presented with FCD. The

presence of subtle dysplastic lesions in patients with focal epilepsy and previous unremarkable MRI and an initial precipitating injury (e.g. HS) in patients with TLE may facilitate the development of epileptogenic brain structures or networks. The background of neurodevelopment, neuroanatomy and cytoarchitecture relevant for understanding the primary pathologies in intractable focal epilepsy (i.e. HS and FCD) is presented within this chapter as an understanding of healthy structure and function may facilitate the investigation of underlying pathological mechanisms found in focal epilepsy.

3.2 Neuroanatomy of the Cerebrum

3.2.1 Divisions

The nervous system is composed of the central and peripheral nervous system. While brain and spinal cord form the central nervous system, the peripheral nervous system is formed by all remaining nerves and nerve cell clusters (ganglia). The brain is composed by the cerebrum consisting of the two hemispheres with cerebral cortex and respective underlying WM, the diencephalon (formed by the thalamus and hypothalamus), and the cerebellum and brain stem. The downward continuation of the brain stem constitutes the spinal cord. There are four major divisions of the cerebrum: the frontal, temporal, parietal and occipital lobes. Major cortical sulci appearing as furrows in the cortical surface separate these lobes: ventrally, the frontal lobe is separated from the temporal lobe by the Sylvian fissure, while the central sulcus separates the frontal lobe at the more anterior position from the parietal lobe at the posterior aspect of the brain and caudally the parietal-occipital sulcus denotes the limits between the parietal, temporal and occipital lobe (Figure 3.1).

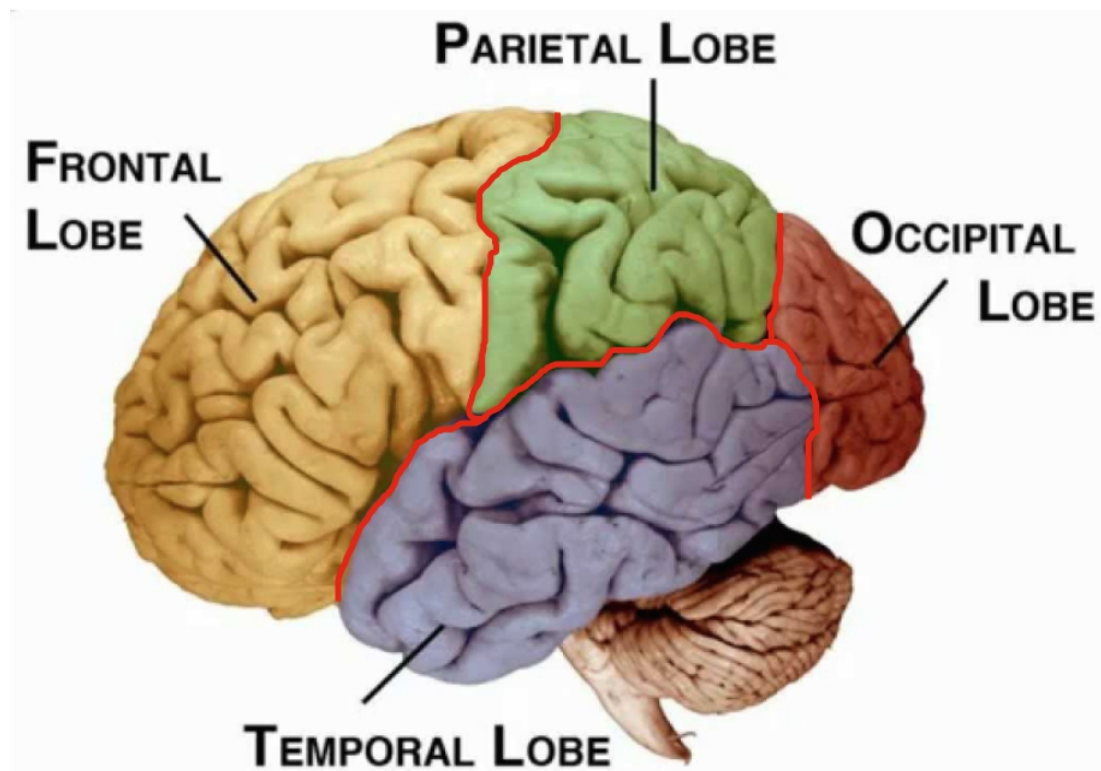


Figure 3.1. Left lateral view of the brain showing the four lobes of the left cortical hemisphere of the cerebrum, brain stem (light brown) and cerebellum (brown) (from Human Anatomy Wiki 2017).

Ventrally, the Sylvian fissure separates the frontal lobe (orange) from the temporal lobe (blue), while caudally this most anterior lobe (frontal lobe) is separated from the parietal lobe (green) by the central sulcus. The occipital lobe is situated at the very posterior end of the brain (red area), caudal to the temporal and parietal lobes and separated via the parietal-occipital sulcus. Separations between lobes are also indicated with the red lines.

Medially, an additional lobe is often described: the limbic lobe (Duvernoy 2005), which includes the thalamic nuclei and temporal and frontal lobe structures (Figure 3.2).

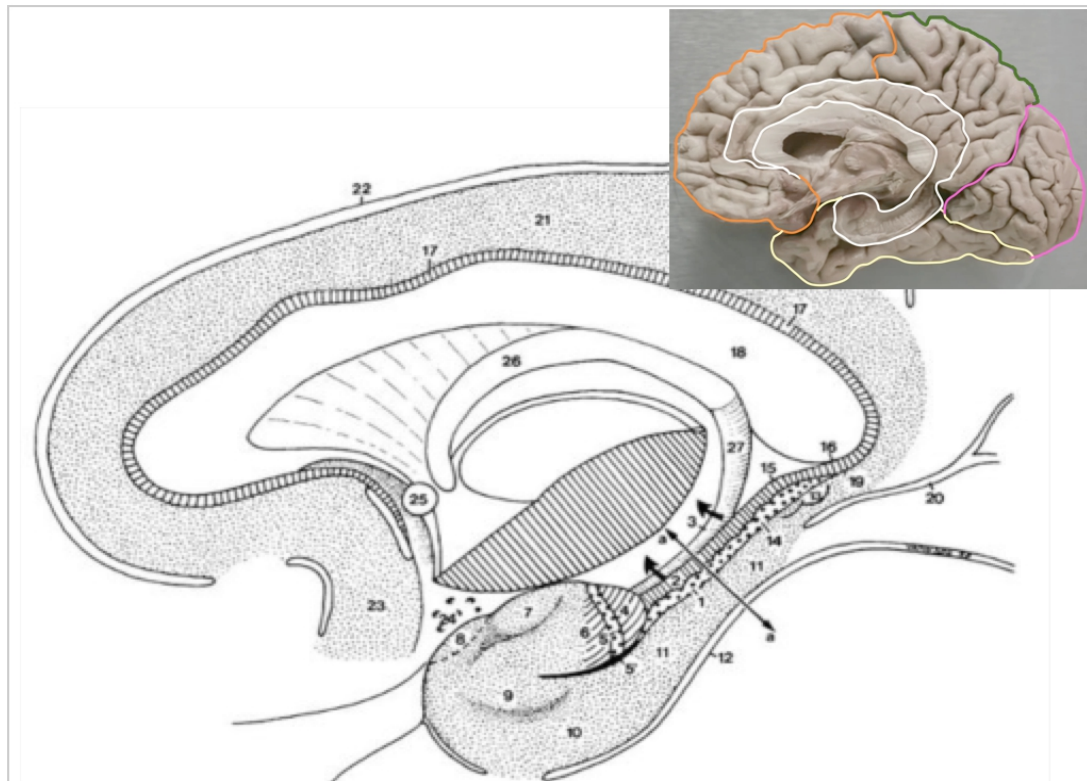


Figure 3.2. Medial aspect of right limbic lobe with the hippocampus (from Duvernoy 2005). The inset (modified from Krebs et al. 2014) shows the limbic lobe (white) with relation to frontal (orange), temporal (yellow), parietal (green) and occipital (pink) lobes.

Hippocampal body:

1. Dentate gyrus (margo denticulatus)
2. Cornu ammonis
3. Fimbria placed upwards (arrows) to show cornu ammonis

Hippocampal head (uncal part):

4. Apex of the uncus
5. Band of Giacomini (uncal extension of margo denticulatus (1))
- 5' Uncal sulcus
6. Gyrus uncinatus

The anterior part of the uncus, belonging to the parahippocampal gyrus (piriform lobe) is composed of:

7. Semilunar gyrus
8. Prepiriform cortex
9. Gyrus ambiens
10. Entorhinal area
11. Parahippocampal gyrus
12. Collateral sulcus

Hippocampal tail:

13. Gyri of Andreas Retzius (intralimbic gyrus)
14. Fasciola cinerea prolonging the dentate gyrus
15. Gyrus fasciolaris, extension of the cornu ammonis
16. The gyrus subsplenialis prolongs the gyrus fasciolaris and is itself continued by the indusium griseum (17) on the dorsum of the corpus callosum (18)
19. Isthmus
20. Anterior calcarine sulcus
21. Cingulate gyrus
22. Cingulate sulcus
23. Subcallosal area
24. Anterior perforated substance
25. Anterior commissure
26. Fornix
27. Crus of the fornix

The dotted area indicates the *limbic lobe*. The a-a line indicates the plane of the section of Figure 3.8.

Specifically, the limbic system comprises the hippocampus, fornix, mammillary bodies (situated at the anterior end of the fornix), anterior thalamus (an almond-shaped structure situated immediately below the fornix), cingulum and the parahippocampal gyrus (Mark et al. 1993, Duvernoy 2005, Friedman and Chou 2007).

All lobes have different functions, which have been investigated in fMRI and lesion studies. The frontal lobe is responsible for higher executive functions (e.g. critical thinking/judgement, attention and planning). Evidence for some of these functions has been found most spectacularly by the investigation of Phineas Gage, a railway worker who suffered a severe injury to his frontal lobe after an accident where an iron tamping rod pierced his face, skull and brain. Shortly after the accident and his recovery, Gage's contractors found that “the equilibrium or balance ... between his intellectual faculties and animal propensities, seems to have been destroyed. He is fitful, irreverent, indulging at times in the grossest profanity ..., devising many plans of future operation, which are no sooner arranged than they are abandoned in turn for others appearing more feasible” (Harlow 1868). The case of Phineas Gage illustrated to the doctors at the time that damage to the frontal lobe may cause dramatic changes in personality and behavior, while sensation, movement and consciousness remain intact (Mesulam 2002). The frontal lobe is the last lobe to mature in children and WM development in this lobe lags behind other cortical areas (Huttenlocher 1990, Mrzljak et al. 1990). Fuster (2002) has stated that the intellectual maturation depends on the ability to organize behavior and cognition into goal-directed structures of action and attention, language, and creativity are all dependent on these organizational skills. Various fMRI studies have confirmed that regions within the frontal lobe play a pivotal role in emotional processing (Quarto et al. 2016), planning (Novais-Santos et al. 2007, Boghi et al. 2006), critical thinking (Cao et al. 2016) and attention (Fazio et al. 2016). Among other things, the temporal lobe processes auditory input (Squire et al. 2001), with one of its major functions being language

comprehension (Jackson et al. 2005) and memory (Squire et al. 2004, Squire et al. 2001). The functions of the hippocampus, one of the most important structures of the brain, which lies within the temporal lobe, are discussed in more detail in subsection 3.3. While the parietal lobe concerns itself with tactile, motor functions and sensory input (Fogassi and Luppino 2005, Penfield and Rasmussen 1950, Culham and Valyear 2006), the occipital lobe integrates visual information received through the optic nerves (Toosy et al. 2004) and structures of the limbic lobe are activated during processing of emotions (Lee et al. 2016), identification of danger (Surguladze et al. 2003) and formation of new memories (Friedman and Chou 2007). Proper anatomical development of the lobes with their complex structures is critical for their correct functioning.

3.2.2 Brain Development

According to Barkovich (2005), the development of the cerebral cortex is a stepwise process and includes both sequential and simultaneous steps. The individual steps necessary for brain development are regulated by genes and their respective expression. Many malformations of cortical development are caused by genetic defects, map to certain chromosomes (Dobyns et al. 1996, Piao et al. 2002, Guerrini and Marini 2006) and may cause epilepsy (Kuzniecky 2015, Barkovich et al. 2012, Barkovic et al. 1997).

Brain development begins with neurulation, the process during which the neural plate develops into the neural tube. At about 20 days of gestation, the three major developmental divisions of the brain (fore-, mid- and hindbrain) can be distinguished (Barkovich 2005). Eventually the forebrain develops into the telencephalon (containing the two cerebral hemispheres) and diencephalon (containing thalamus, hypothalamus, epithalamus and subthalamus). The midbrain develops into the cerebral peduncle and superior and inferior colliculus situated within the brain stem while the hindbrain later develops into the medulla oblongata, pons and cerebellum. After neurulation and after four weeks of gestation, neuronal proliferation of

precursor cells occurs. These will constitute the cytoarchitecture of the cerebral cortex once proliferation and subsequent migration of these new neurons has completed (see Figure 3.3 for a timeline and Figure 3.4 for a summary on these cell stages). During migration, programmed neuronal cell death commences (apoptosis), primarily affecting proliferating precursor cells (Lossi and Merighi 2003, Blaschke et al. 1996). The density of synapses grows and the process of synaptogenesis begins in the 19th week of gestation. Finally, in the 29th week of gestation, while migration, apoptosis and synaptogenesis are still in progress, myelination begins and continues into early adulthood (Tau and Peterson 2010).

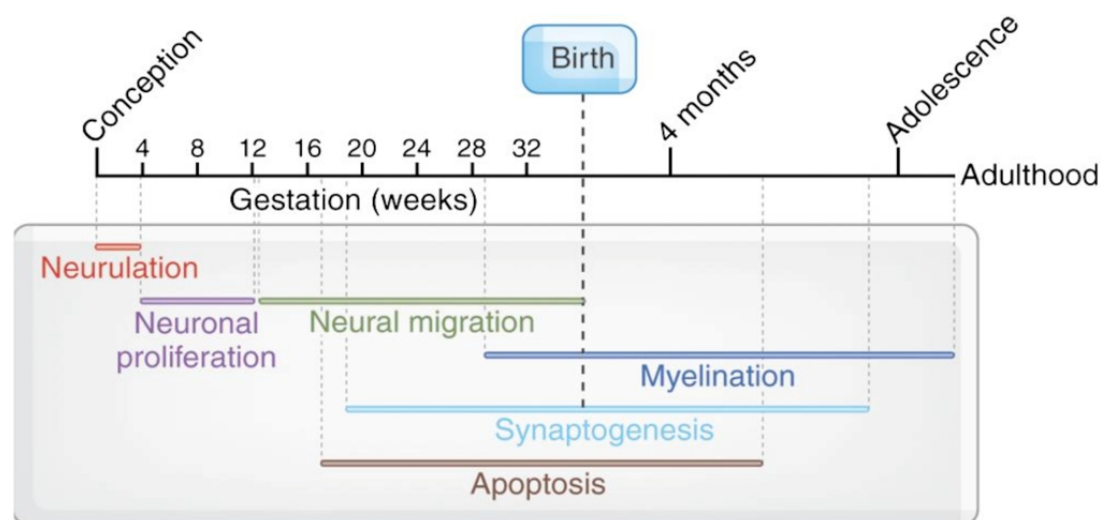


Figure 3.3. Stages of brain development (from Tau and Peterson 2010).
A timeline of major developmental events occurring in the development of the human brain. Six stages are shown.

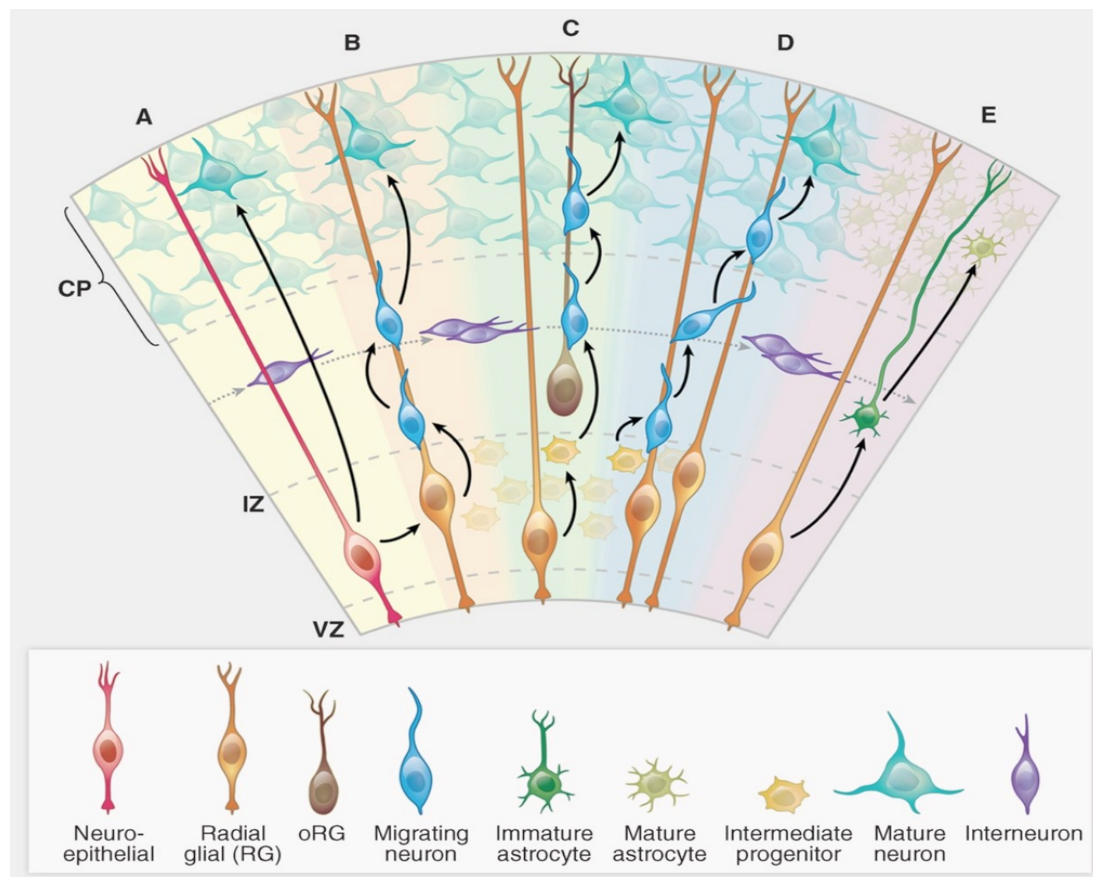


Figure 3.4. Cortical development (from Poduri et al. 2013)

(A) A neuroepithelial cell (red) at the VZ serves as progenitor for both a pyramidal neuron (green-blue) as well as a radial glial cell (gold). (B) A newly differentiated neuron (blue) migrates along a radial glial fiber. (C) Neurons (blue) continue to migrate along the outer radial glial cells' process (brown) as intermediate progenitor cells (small yellow) form. (D) Intermediate progenitor cells begin to generate neurons (blue). (E) The progenitor cells in the ventricular zone begin to give rise to astrocytes (dark green). Interneurons (purple) generated elsewhere migrate tangentially. CP = cortical plate; IZ = intermediate zone; VZ = ventricular zone; oRG = outer radial glial (outside of VZ).

3.2.3 Malformations of Cortical Development

Some epilepsies may be due to failed neuronal migration causing malformations of cortical development, which presents as abnormal neuronal position and differentiation from GM (Barkovich et al. 2005). This can result in FCDs (Barkovich et al. 2012), which were initially described by Taylor et al. (1971) and have later

been linked to abnormal stem cell development (Barkovich et al. 1997). According to Barkovich et al. (2012) certain FCDs can be classified as ‘malformations secondary to abnormal post-migrational development’ since some evidence suggests that injury to the cortex during cortical development may cause FCDs. Correct development of the cerebral cortex's laminar structure is essential for healthy brain development, meaning that any failure may cause malformations, which in turn may lead to mental impairment and/or epilepsy. The neurons of the neuronal tube are called precursor cells or neural stem cells and these undifferentiated cells undergo symmetric mitotic divisions (Ronan et al. 2013), generating new stem cells or neuroblasts that will eventually differentiate into neurons and glial cells (Guerrini and Marini 2006, Poduri et al. 2013, Fernandez et al. 2016). After the continued division of many precursor cells, called the proliferation stage (Guerrini and Marini 2006, Tau and Peterson 2010), the ventricular zone is established. Apical radial glial cells, serving as primary progenitor cells, generate neurons through asymmetric division directly and indirectly through secondary intermediate progenitor cells and basal radial glial cells (Fernandez et al. 2016, Barry et al. 2014). During the following migration stage some neurons leave this zone to build the marginal zone at the pial surface, while the intermediate neurons differentiate into different types of neurons, giving rise to the intermediate zone. The cortical layer is built in an inside-out fashion, where every successive generation of neurons surpasses another (Guerrini and Marini 2006). There are three modes of neuronal migration: radial (along the fibers of the radial glial cells) including somal translocation (only the soma of the neuron is moved), tangential (interneurons moving away from other parts of the brain), and multipolar migration (Cooper 2014). According to Nadarajah and Parnavelas (2002), somal translocation is the most common mode of migration during early cortical development, while radial migration occurs more often in the more mature cortex and multipolar migration is prevalent when neurons enter the intermediate zone (Cooper 2014). Cortical organization within the six cortical layers is achieved through apoptosis and synaptogenesis, until each layer contains different types of

neurons with distinct connections and functions (Guerrini and Marini 2006). At the earliest stages, the cortical plate only consists of two to three cell bodies ($\sim 15\ \mu\text{m}$), however, eventually the mature cerebral cortex spans two to four mm in thickness (Poduri et al. 2013). Genetic mutations can cause disorders of neuronal migration and cerebral cortical organization through the abnormal neuronal and glial cell differentiation (Barkovich et al. 1997, Guerrini and Marini 2006, Barkovich et al. 2005). Thus neurons of abnormal size and morphology are generated during the proliferation stage (Guerrini and Marini 2006, Figure 3.5).

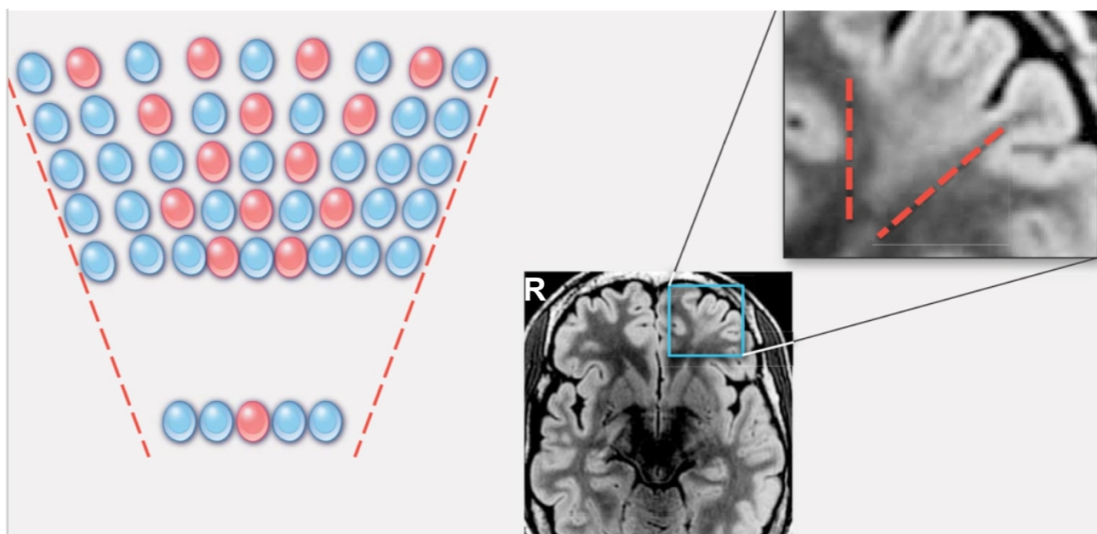


Figure 3.5. FCD as a result of suspected somatic mutation in a progenitor cell (from Poduri et al. 2013).

Healthy progenitor cells (bottom row, blue) give rise to healthy neurons and glial cells (top five layers, blue), while a progenitor cell with a somatic mutation (red) generates unhealthy cells (top five layers, red), thus mutated cells are interspersed with healthy neurons and glial cells. The respective produced funnel-shaped lesion in the adult brain can be detected in the left frontal lobe on the axial T2w MRI as a FCD characterized by GM thickening, GM/WM blurring and a transmantle sign reflecting the funnel shape of the developmental process. However, the right frontal lobe and other regions of the brain present a sharp GM/WM boundary, healthy GM thickness and no transmantle sign. R = right.

Barkovich et al. (2005) have classified malformations of cortical development into three categories based on the developmental stage at which the malformation occurred: (1) cortical dysplasia (FCD, as shown in Figure 3.5) during neuronal and

glial proliferation or apoptosis, (2) heterotopia (presence of GM within WM) as a result of abnormal neuronal migration, and (3) polymicrogyria (multiplication of small gyri in certain areas) occurring after late cortical migration and organization. Examples of these malformations with the two subtypes of heterotopia can be found in Figure 3.6. Other malformations of cortical development not shown here include schizencephaly, characterized by a cleft in the brain, literally “split brain” and lissencephaly, “smooth brain”. Each of these malformations arise from interferences with these three developmental stages and may display varying degrees of epileptogenicity (Palmini 2011).

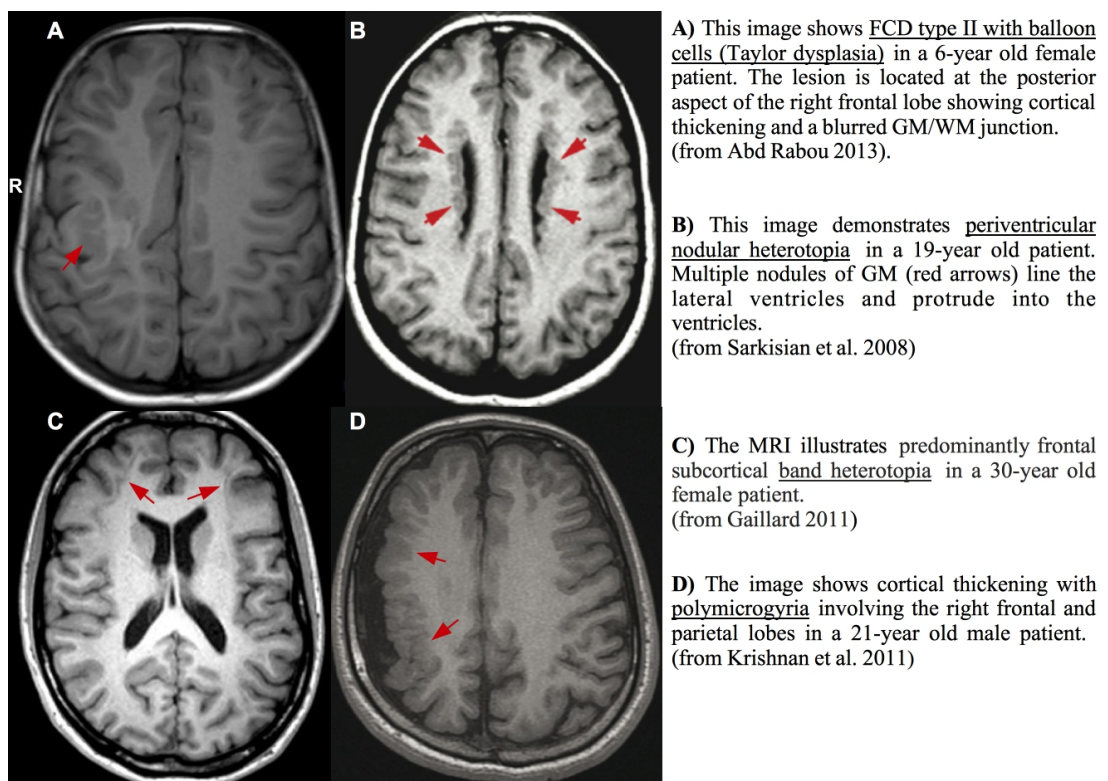


Figure 3.6. Various types of malformations of cortical development shown on conventional axial T1w MR images in four different patients. A detailed description of the images can be found in the right panel. R = right.

The first widely accepted uniform terminology regarding pathological classification

of FCDs was described by Palmini et al. (2004). However, this has now been revised by an ILAE task force (Blümcke et al. 2011): Microscopically identifiable FCDs may present either as radial (FCD type Ia) or tangential (FCD type Ib) dyslamination of the neocortex in one or multiple lobes. According to the authors, FCD type II is an isolated lesion characterized by cortical dyslamination and dysmorphic neurons without (type IIa) or with balloon cells (type IIb). Additionally, Blümcke et al. (2011) have included a novel description of FCD type III, which co-occur with another lesion. Following this new terminology, FCDs can occur with HS (type IIIa), with epilepsy-associated tumors (type IIIb), adjacent to vascular malformations (type IIIc) or epileptogenic lesions acquired in early life such as glio-mesodermal scarring resulting from perinatal hemorrhagic brain injury (type IIId). Some FCDs present with GM/WM junction blurring, GM thickening and abnormal signal intensities on MRI (Palmini 2011, Barkovich et al. 1997, Lerner et al. 2009). Other FCDs may be even more subtle and present with atrophy of GM/WM and are not necessarily visible on MRI (Tassi et al. 2002, Lerner et al. 2009) such as type IIa (Blümcke et al. 2011). Cells of the transcortical FCD type IIb (Blümcke et al. 2011, first described by Taylor et al. (1971) as Taylor dysplasia) have been frequently described in patients with epilepsy and may stem from mutated radial glial progenitors (Lamparello et al. 2007). This type of FCD appears with a transmantle sign extending to the ventricles on MRI (Bronen et al. 1997, Tassi et al. 2002). Even though MRI can often contribute to the detection of FCDs, there are no highly sensitive imaging parameters available that can reliably differentiate among FCD subtypes (Blümcke et al. 2011). Less frequently, patients with TLE without HS may present with encephalocele arising from neural tube defect or trauma (Vargas et al. 2008). Amygdala enlargement has also been linked to TLE and may be the result of a chronic neuroinflammatory process or related to FCDs (Lv et al. 2014, Kim et al. 2012). The MRI of patients with focal epilepsy may show presence of gliosis (Cendes et al. 2016), which is caused by proliferation and hypertrophy of astrocytes (Bernasconi et al. 2011). Postoperatively, gliosis may be found in the sclerotic

hippocampus (Spencer 2002) or the FCD (Blümcke et al. 2011) in histopathological examinations.

3.3 Temporal Lobe

3.3.1 Hippocampus

The human hippocampus is present in the left and right medial temporal lobes and appears as an arc-shaped cortical fold (Figure 3.7). It has a rostro-caudal extent of approximately 5 cm (Insausti and Amaral 2012). Functionally it is classified as being part of the limbic lobe (Figure 3.2). The relevance of this structure to epilepsy is summarized in Table 3.1 at the end of this chapter. The hippocampus is situated at the caudal aspect from the amygdala and borders dorsally on the parahippocampal gyrus, laterally on the temporal horn of the lateral ventricle and caudally on the splenium (Duvernoy 2005). The hippocampus has three parts: the head (anterior), body (middle) and tail (posterior) and is formed by the dentate gyrus and CA. These two laminar structures belong to the older of the two evolutionary developmental cortices, the archeocortex (instead of neocortex). The dentate gyrus and the CA are embedded into each other (Duvernoy 2005, Duvernoy et al. 2013) and are described in more detail within the following section.

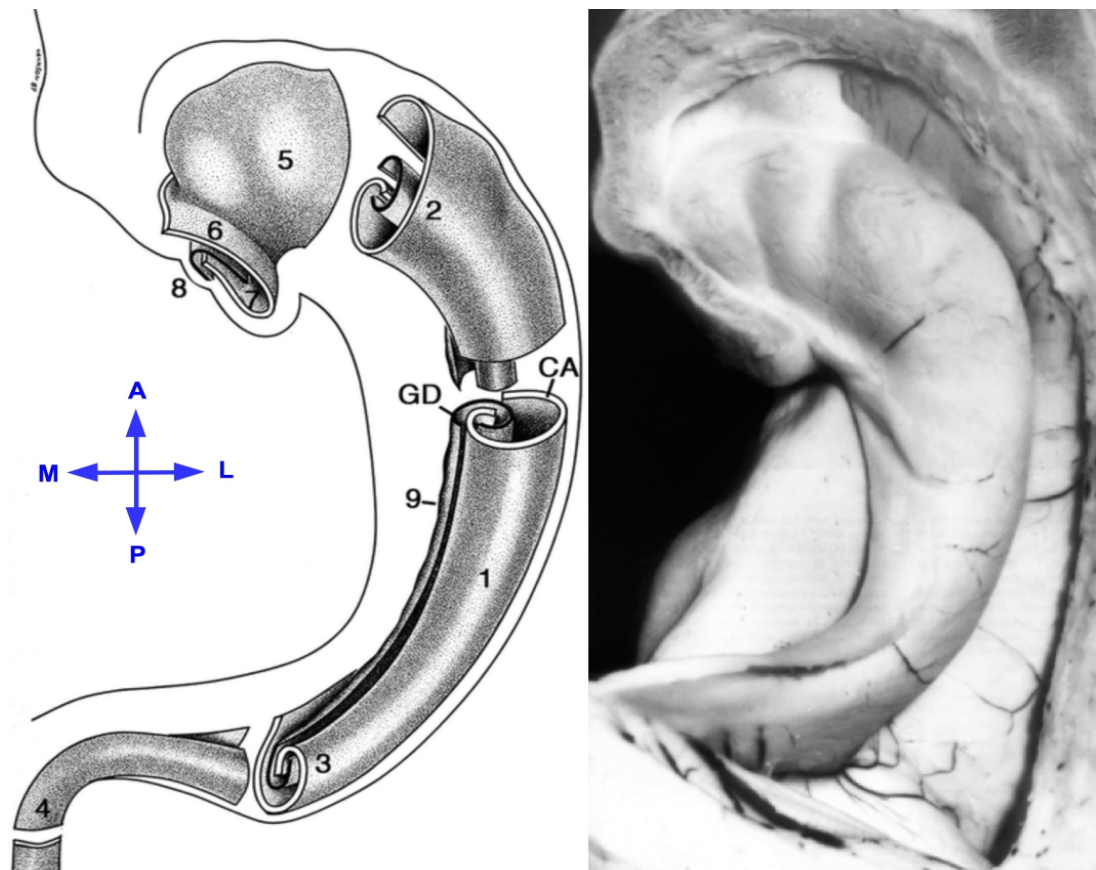


Figure 3.7. Illustration of the internal structure of the hippocampus (left, from Duvernoy et al. 2013) and a corresponding post-mortem view of the hippocampus after opening of the temporal horn of the lateral ventricle (right, from Duvernoy 1998).

The CA and dentate gyrus (GD) form two interlocking U-shaped laminae. 1 hippocampal body, 2 hippocampal head, 3 hippocampal tail, 4 terminal segment of the tail, 5 hippocampal digitations, 6 vertical digitations, 7 CA and GD in the medial surface of the uncus, 8 band of Giacomini, 9 margo denticulatus. A = anterior; L = lateral; M = medial; P = posterior.

3.3.2 Hippocampal Internal Architecture

The CA can be divided into three cytoarchitectonic layers including the stratum oriens, stratum pyramidale and the molecular zone (composed of the stratum radiatum, stratum lacunosum and stratum moleculare; Lorente de No 1934), while the dentate gyrus is composed of the strata moleculare, strata granulosum and polymorphic layer (Duvernoy et al. 2013). Instead of having six neuronal layers like neocortex, both of these hippocampal structures have only three cytoarchitectonic

layers, which is characteristic for archeocortex (Figure 3.8).

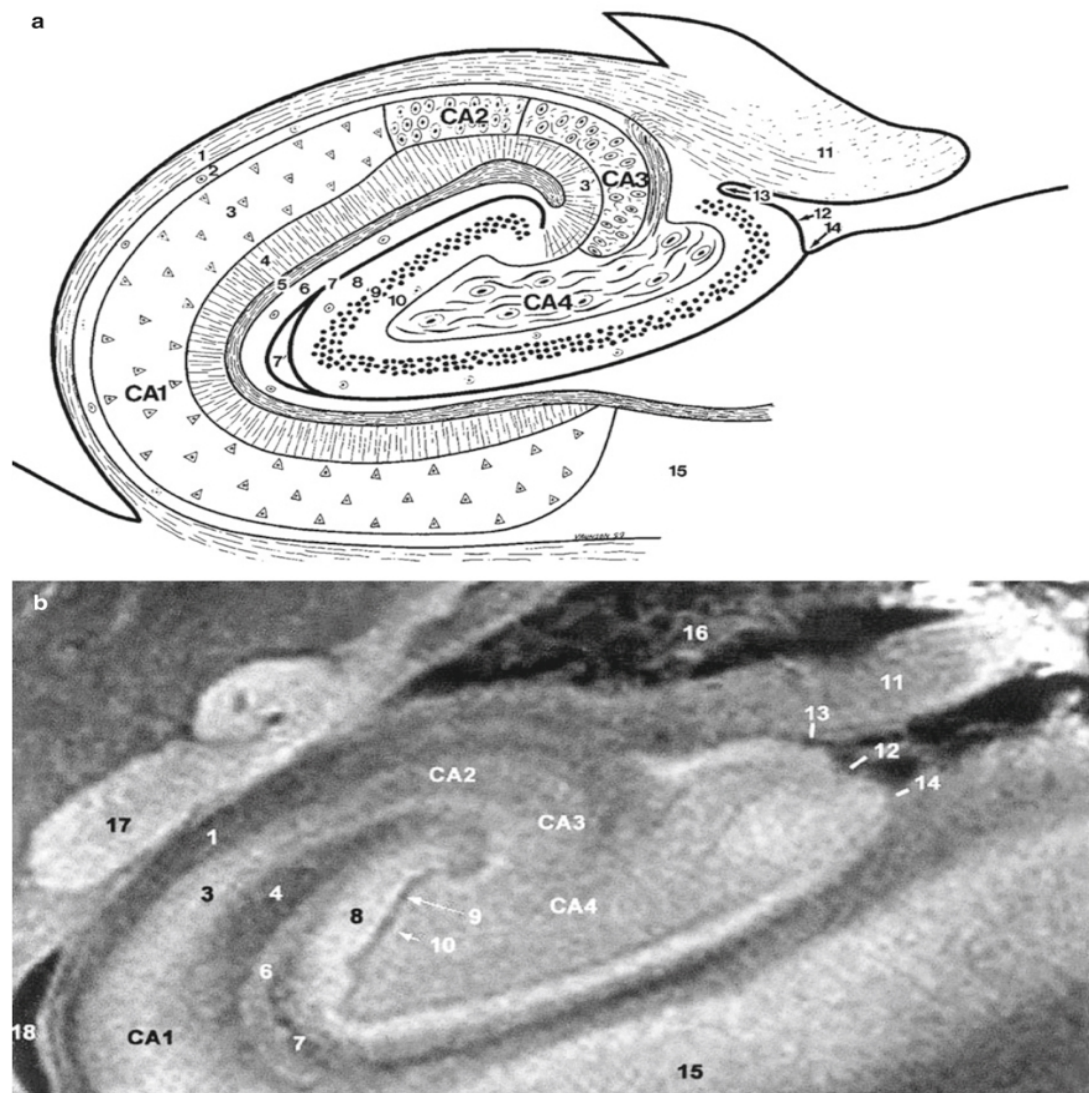


Figure 3.8. Cross-sectional diagram (a) and 9.4T MRI (b) of the right human hippocampus (from Duvernoy et al. 2013).

The right side of the image is the medial, while the left side is the lateral aspect of the hippocampus. CA1–CA4, fields of the cornu ammonis with pyramidal cells. Cornu ammonis: 1 alveus, 2 stratum oriens, 3 stratum pyramidale, 3' stratum lucidum, 4 stratum radiatum, 5 stratum lacunosum, 6 stratum moleculare, 7 vestigial hippocampal sulcus (note a residual cavity, 7'); dentate gyrus (with granule cells) with 8 stratum moleculare, 9 stratum granulosum and 10 polymorphic layer; 11 fimbria, 12 margo denticulatus, 13 fimbriodentate sulcus, 14 superficial hippocampal sulcus, 15 subiculum (transition area of hippocampus and parahippocampal gyrus), 16 choroid plexuses, 17 tail of caudate nucleus, 18 temporal (inferior) horn of the lateral ventricle.

The stratum pyramidale of the CA has four different cytoarchitectonic subfields, CA1-4, which are defined by different characteristics of the neurons found in these areas (Lorente de No 1934). CA1 is the continuation of the subiculum and neurons in this large region have a triangular shape and are less densely packed than the oval-shaped neurons found in CA2, a region that is dense and narrow in comparison (Duvernoy et al. 2013, Braak 1980). CA3 is situated at the genu (bend) of the CA. The dentate gyrus envelops the CA4 region of the CA, which consists of few sizeable ovoid neurons among the large mossy myelinated fibers of CA4 (Duvernoy et al. 2013).

The dentate gyrus and CA1-3 regions are separated from one another via the hippocampal sulcus and some residual cavities (Duvernoy et al. 2013, Insausti and Amaral 2012). The stratum granulosum is the main layer of the dentate gyrus, consisting of small round densely packed granular neurons with mossy fibers traversing the polymorphic layer and reaching into CA3-4 (Duvernoy et al. 2013). Dendrites from the basal poles of granular neurons extend into the stratum moleculare, which is a thick region separated from the CA by the vestigial hippocampal sulcus (Duvernoy et al. 2013). The polymorphic and molecular layers have only few interneurons and the polymorphic layer unites the stratum granulosum with CA4 (Duvernoy et al. 2013, Lim et al. 1997).

3.3.3 Hippocampal Functions and Projections

Functions of the hippocampus include early memory storage, formation of long-term memory (learning) and spatial navigation and according to Duvernoy et al. (2013), regulation of emotional behavior, certain aspects of motor control and regulation of hypothalamic functions are also part of hippocampal functions. A most notable primary contribution to the knowledge on memory functions of the hippocampus is the study of H.M., a patient treated for mesial temporal epilepsy with epilepsy surgery including bilateral hippocampal resections. This resulted in H.M. becoming

seizure-free, however, postoperatively he had been severely impaired in his ability to form new semantic knowledge (Schmolck et al. 2002) or learn new words, while being able to retain preoperatively acquired knowledge on correct grammatical and lexical usage (Kensinger et al. 2001). Maguire et al. (2006) conducted a virtual reality study on a London taxi driver with bilateral hippocampal lesions and found that he was impaired in novel navigational tasks compared to colleagues not affected by hippocampal damage, but performed equally when asked to choose routes learned 40 years ago. Draganski et al. (2006) conducted a longitudinal study on students of medicine preparing for their preliminary medical examination. The authors were able to show that the hippocampal volume increases during the participant's continued studies relative to those of sex-, age- and education-matched controls. They therefore concluded that the hippocampus as structural component contributes crucially during learning of new information and formation and consolidation of memories, which has also been shown by animal model and human lesion studies (Insausti et al. 2013, Mishkin 1978, Squire 1992, Squire et al. 1990, Squire and Wixted 2011). Amnesia may be caused by circumscribed lesions to the hippocampus (Kesner and Goodrich-Hunsaker 2010, Zola-Morgan et al. 1989, 1986, Insausti et al. 2013). Recent studies have shown that the hippocampus is involved in the formation of both types of declarative memory: episodic (relating to events and their relations, autobiographical) and semantic (relating to facts and concepts) memory (Burgess et al. 2002, Schmolck et al. 2002, Sormaz et al. 2017, Kaneda et al. 2017). This has also been shown by various fMRI studies (Strange et al. 1999, Cohen et al. 1999, Schacter et al. 1999). The anterior hippocampus has been linked to episodic memory and imagination, while the posterior hippocampus seems to be involved in navigation and both regions serve visual scene perception (Zeidman and Maguire 2016). However, these functions cannot be understood as completely segregated hippocampal functions, for example other studies have shown involvement of the posterior hippocampus in the other substructure's functions such as episodic memory (Bonnici et al. 2012) and imagination (Gaesser et al. 2013). Some studies have also

suggested that the hippocampi of each of the two hemispheres subserve different tasks (Golby et al. 2001) with the left aiding verbal functions (Sepeta et al. 2016) and the right being involved in spatial encoding (Wei et al. 2016). Research in patients with TLE has confirmed these findings (Bonelli et al. 2013), as patients with left TLE and associated ipsilateral hippocampal dysfunction are more likely to have verbal memory impairments (Helmstaedter et al. 1997, Gleissner et al. 2004, Bonelli et al. 2010), while patients with right TLE and HS have been found to have spatial and visual memory impairments (Barr 1997, Bonelli et al. 2010, Lee et al. 2002). Nevertheless, in some patients compensatory mechanisms may come into effect even prior to surgery that allow recruitment of extra-temporal regions for specific memory-related tasks (Sidhu et al. 2013) and some post-surgical memory impairments may be temporary (Gleissner et al. 2004). Furthermore, animal studies have revealed that the hippocampus may be involved in emotional processing (Yang and Liang 2014, Yamamuro et al. 2010, Kaneda et al. 2017, Bannerman et al. 2003) and many of these studies have related these processes to effects on memory performance. These studies not only demonstrate the crucial role of the hippocampus in neuroplasticity (Eriksson et al. 1998), short-term information storage, memory, learning and spatial navigation, but also that the hippocampus is a constant assessor and distributor of information to many other parts of the brain for long-term storage. This is shown by the fact that long-term knowledge storage does not depend on the hippocampus as shown in the case of the taxi driver with bilateral hippocampal damage and patient H.M. Indeed, the hippocampal projections are more complex than those of the rest of the cortex. While neocortical connections mostly allow bi-directional communication between different brain areas, hippocampal connections are specialized for uni-directional afferent and efferent (in- and outward) projections.

Despite its relatively small size, the entorhinal area, which is located at the ventromedial aspect of the hippocampus within the parahippocampal gyrus, forms the principal input (Szirmai et al. 2012, Duvernoy et al. 2013, Insausti and Amaral 2012). The polysynaptic intrahippocampal pathway, also called the perforant path, is

composed of a long neuronal chain connecting the entorhinal cortex with the dentate gyrus, CA3, CA1 and the subiculum (Duvernoy et al. 2013, Figure 3.9). The fibers, originating from the entorhinal cortex, merge in the angular bundle, travel caudally and perforate through the subiculum (Insausti and Amaral 2012). Some of these fibers project to CA3/CA1 first before reaching the dentate gyrus while others directly terminate in the stratum moleculare of the dentate gyrus (Insausti and Amaral 2012). The excitatory neurotransmitter in the perforant path is glutamate (White et al. 1977), which may be enhanced in patients with epilepsy (Scimemi et al. 2006). The mossy fibers, which are fine and non-myelinated, form connections between neurons of the dentate gyrus with the oval-shaped neurons of the less densely packed CA3 region (Lim et al. 1997, Buhl and Whittington 2006, Duvernoy et al. 2013, Lorente de No 1934) and CA4 regions of the hippocampus (Duvernoy et al. 2013, Insausti and Amaral 2012). The connections of pyramidal cells between CA3 and CA1 are called Schaffer collaterals (Schaffer 1892, Szirmai et al. 2012).

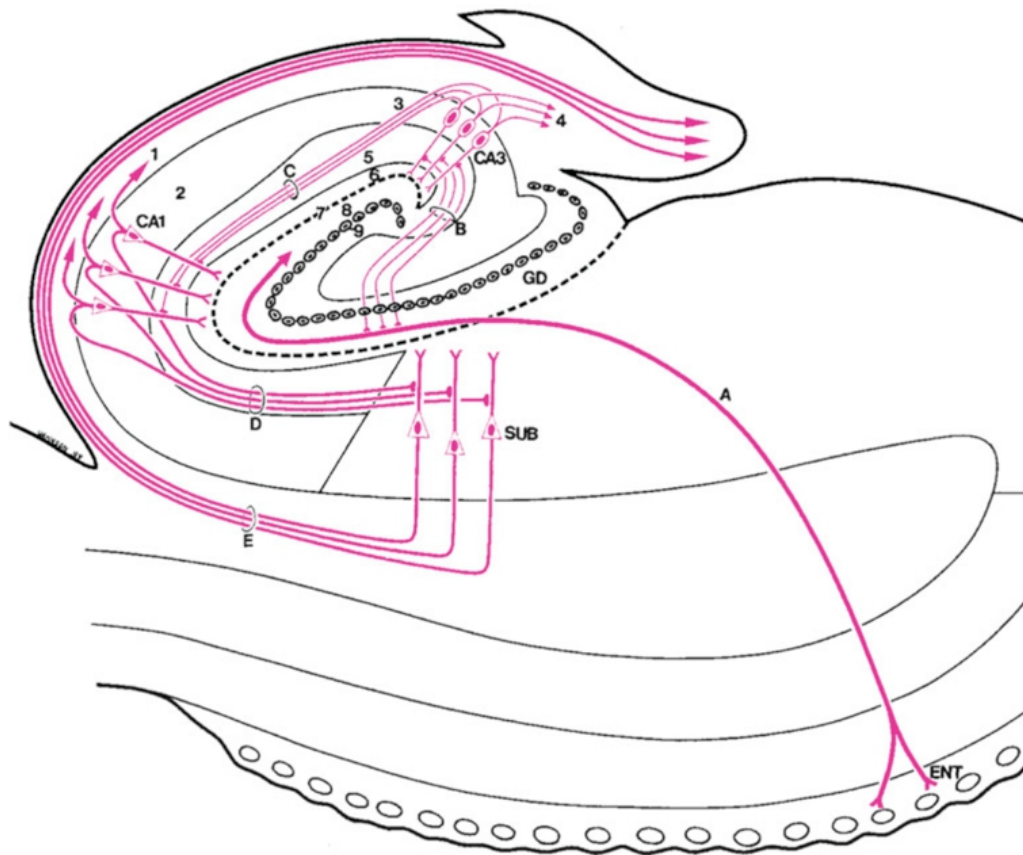


Figure 3.9. Projections of the hippocampal and parahippocampal regions (from Duvernoy et al. 2013).

A-E are parts of the neural chain forming the polysynaptic intrahippocampal pathway. Cornu ammonis: 1 alveus, 2 stratum pyramidale, 3 Schaffer collaterals, 4 axons of pyramidal neurons (mainly to septal nuclei), 5 strata lacunosum and radiatum, 6 stratum moleculare, 7 vestigial hippocampal sulcus. Dentate gyrus (GD): 8 stratum moleculare, 9 stratum granulosum. CA1, CA3 fields of the cornu ammonis, SUB subiculum. ENT (Layer II of the entorhinal area) is the origin of this chain; its large pyramidal neurons are grouped in clusters, giving a granular aspect at the entorhinal surface.

Ramon y Cajal (1893) and Lorente de No (1934) both mention commissural connections between both the left and right hippocampus, these belong to the external regulatory circuit (Duvernoy et al. 2013, Insausti and Amaral 2012) and provide input to CA1 and CA3 (Traub and Miles 1991a). The commissural fibers enter and exit the hippocampus via the fimbria. The hippocampus has been found to

have both excitatory and inhibitory circuitry (Lim et al. 1997, Traub and Miles 1991a, Duvernoy et al. 2013), which have been extensively studied in living rodents and primates. According to Traub and Miles (1991b), the two types of circuits can be split into the recurrent excitatory connections between CA3 (Miles and Wong 1986, Le Duigou et al. 2014) and CA1 pyramidal cells (Christian and Dudek 1988) and inhibitory cells activated by collateral and afferent fibers (Newberry and Nicoll, 1984, Andersen et al. 1963, Traub and Miles 1991b). The complex multi-synaptic hippocampal communication depends on intact hippocampal subfields (i.e. CA1-4) and may be disturbed in patients with HS (Falconer 1974, Liu et al. 2012, Deyo and Lytton 1997). For a detailed review of hippocampal connectivity the reader is referred to Insausti and Amaral (2012).

3.4 Temporal Lobe Connectivity

Three distinct GM regions can be identified within the temporal lobe as cortical ridges between the clefts on the brain surface (Figure 3.1). These are the superior, middle and inferior gyri as seen from top to bottom on the lateral aspect of the temporal lobe surface. The medial aspect of this lobe consists of the parahippocampal (ventrally) and intralimbic gyrus (dorsally, mainly formed by hippocampus, Figure 3.2) (Duvernoy 2005). All of these gyri are connected with other GM regions of the brain through WM tracts such as the FF, CAB (PHWM), ILF, SLF and the UF (Figure 3.10). Details on the individual trajectories of these temporal lobe tracts are described in the following subsections and their relevance to epilepsy is summarized in Table 3.1 at the end of this chapter.

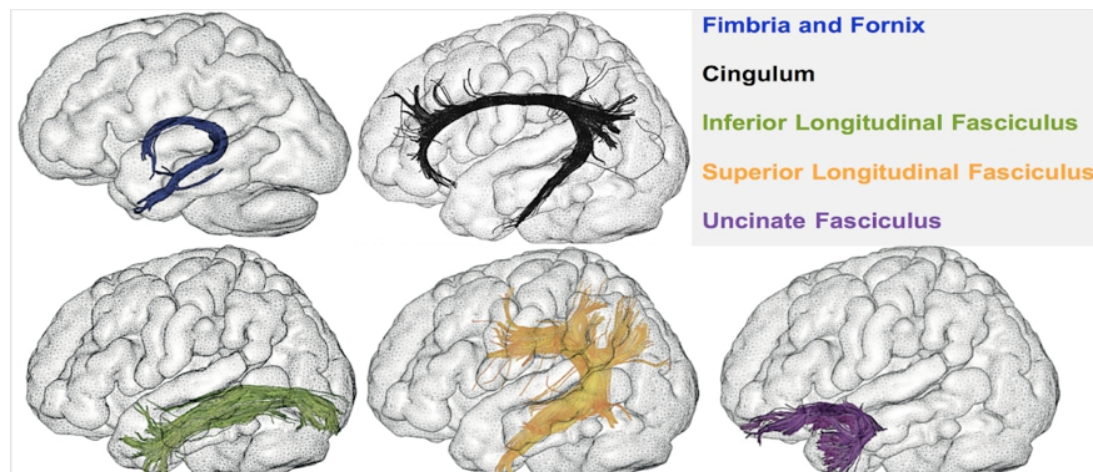


Figure 3.10. Left lateral views of major temporal lobe connections with the rest of the brain (modified from Catani and de Schotten 2008, visualized through tractography).

3.4.1 Fimbria and Fornix

The fimbria forms the continuation of the alveus situated within the CA. It is a prominent WM connection travelling dorsomedially along the hippocampus (Figure 3.8, Figure 3.10 (blue tract) and Figure 3.11). This WM tract connects the hippocampus with the fornix (Figure 3.2) and allows long-range connections to other structures such as the mammillary bodies and hypothalamus (Figure 3.11). The fimbria and fornix are both part of the limbic system. The associative pathways within the alveus and fimbria connect areas of the same hemisphere, are mostly efferent and originate from CA1 pyramidal cells and the subiculum (Christian and Dudek 1988, Kiernan 2012). Furthermore, the hippocampal commissures form afferent connections between the left and right hippocampi, which form a bridge between the two hemispheres directly after neuronal projections pass the crus of the fornices (Figure 3.11).

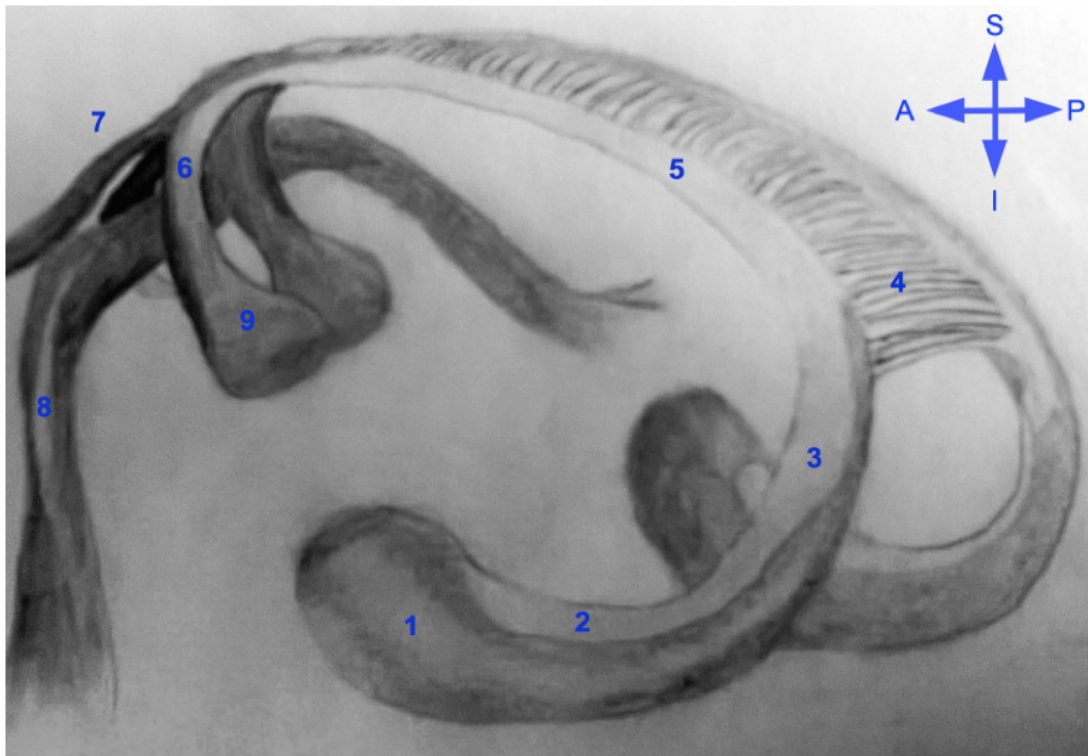


Figure 3.11. Hippocampus with Fimbria and Fornix (from RANZCRPart1 2015)

1: hippocampus, 2: fimbria, originating from the alveus within cornu ammonis; 3: crus of the fornix; 4: hippocampal commissures; 5: body of the fornix; 6: column of the fornix, post-commissural fornix; 7: pre-commissural fornix; 8: anterior commissure; 9: mammillary body; S: superior; I = inferior; P = posterior; A = anterior.

The columns of the fornix connect with the mammillary bodies, which in turn project to the hypothalamus. Several of the subcortical afferents, e.g. amygdala and thalamus, enter the hippocampal formation through the fornix (Insausti and Amaral 2012). The precommissural fornix connects hippocampal fibers arising from the CA, subiculum and entorhinal cortex with the ventral striatum (nucleus accumbens) with innervation of the lateral septal nucleus (Duvernoy et al. 2013, Insausti and Amaral 2012). Fornical connections have been shown to be involved in memory networks (Hescham et al. 2017).

3.4.2 Parahippocampal Cingulum

The parahippocampal cingulum is located adjacent to the ventral aspect of the hippocampal head and body within the parahippocampal gyrus (Figure 3.10, black tract). It is part of the cingulum, a long C-shaped WM association pathway belonging to the limbic system within the cingulate gyrus (Figure 3.2). It is situated immediately dorsal to the corpus callosum and reaches from below the rostrum of the corpus callosum in the frontal lobe (subcallosal gyrus), bends around the splenium of the corpus callosum, continuing into the area immediately below the hippocampus and terminating in the entorhinal cortex of the medial temporal lobe (Hagler et al. 2009). Largely, the cingulum is composed of fibers originating in the anterior thalamic nucleus and the hippocampus (Brodal 1981, Duvernoy et al. 2013) that project to the parahippocampal gyrus. The GM areas connected via the cingulum have been shown to be involved in the modulation of behavior (Alexander and Brown 2011), sensory and cognitive processes such as spatial navigation and memory (Vogt et al. 1992) and emotions (Vogt 2005). The parahippocampal cingulum is in close correspondence with the amygdaloid region, which also constitutes an important involvement in affective behavior (Vogt et al. 1992).

3.4.3 Inferior Longitudinal Fasciculus

The ILF connects the temporal lobe with the occipital lobe and travels along the ventral aspect of the lateral ventricles (Figure 3.10, green tract). The ILF is an associative fiber bundle lying in the central portions of temporal and occipital lobes (Jellison et al. 2004, Catani and Thiebaut de Schotten 2008). It has short and long fibers that connect visual areas to the hippocampus and amygdala (Catani and Thiebaut de Schotten 2008, Catani et al. 2003). It can be easily identified by following the WM of the anterior temporal lobe posteriorly, traveling past the junction of frontal and temporal branches of the anterior floor of the external capsule, while excluding the most posterior temporal lobe WM, before arriving at the tip of the occipital horn (Catani and Thiebaut de Schotten 2008). The ILF has been shown

to be connected to GM areas associated with functions such as face recognition (Grossi et al. 2014, Fischer et al. 2016), visual perception (Shinoura et al. 2010, Ffytche and Catani 2005, Catani and Thiebaut de Schotten 2008), reading (Epelbaum et al. 2008, Sarubbo et al. 2015), visual memory (Shinoura et al. 2007) and functions related to language (Mandonnet et al. 2007, Catani and Thiebaut de Schotten 2008).

3.4.4 Superior Longitudinal Fasciculus

The SLF can be found in both brain hemispheres and can be divided into the parietal segment and the arc-shaped arcuate fasciculus also termed superior longitudinal fasciculus temporal segment (SLFt, Figure 3.10, yellow tract). The SLF forms a connection of the temporal, parietal and the frontal lobe (Hagler et al. 2009, Kiernan 2012, Catani and Thiebaut de Schotten 2008). The SLFt is an association pathway composed of long and short WM fibers and the fibers at the frontal region run perpendicularly to the projection fibers of the corona radiata, arch around the Sylvian fissure before ending in the temporal lobe. Specifically, one of its most important links is the left-hemispheric interconnection of Wernicke's area within the posterior part of the superior temporal gyrus and Broca's area within the inferior frontal gyrus (Kiernan 2012, Catani et al. 2005). The WM bundle has been associated with phonological language (Shinoura et al. 2013) and reading (Travis et al. 2016, Thiebaut de Schotten et al. 2014) functions in humans and is the largest association bundle in humans (Jellison et al. 2004). The functions of the SLFt have been related to unilateral neglect (Thiebaut de Schotten et al. 2008), prosody (Cattaneo 2013) and semantics (Catani and Thiebaut de Schotten 2008). A direct and indirect connectivity pathway (Catani and Mesulam 2008) has been established in the SLFt through research on aphasia and using DTI studies.

3.4.5 Uncinate Fasciculus

The UF is an associative pathway that connects the ipsilateral anterior temporal lobe with the ventral aspect of the prefrontal cortex and is considered to be part of the

limbic system (Figure 3.10, purple tract). The more anteriorly placed temporal fibers of the UF run medially to the fibers of the ILF, enter the external capsule, arch forward around the Sylvian fissure and medially into the orbitofrontal cortex, and eventually merge with fibers from the inferior frontal occipital fasciculus (Catani and Thiebaut de Schotten 2008). Language (Agosta et al. 2010, Catani and Mesulam 2008), memory (Diehl et al. 2008, Papagno et al. 2016) and functions related to emotion processing have been associated with connectivity mediated by the UF (Von der Heide et al. 2013).

Structure	Relation to Epilepsy	Selected References
Hippocampus	Structure within the limbic system and part of the temporal lobe; may be epileptogenic in patients with TLE constituting HS; patients may have verbal/visual memory impairments based on side of HS (left/right, respectively)	Duvernoy et al. 2013, Bonelli et al. 2010, Helmstaedter et al. 1997
Fimbria-Fornix	Structure within the limbic system and part of the temporal lobe; hippocampal commissures form afferent connections between the left and right hippocampi; may play a part in propagation of seizures and may be able to stratify patients with TLE with and without HS	Duvernoy et al. 2013, Insausti & Amaral 2012, Concha et al. 2009
Parahippocampal Cingulum	Structure within the limbic system and part of the temporal lobe; connects the hippocampus with the amygdala and frontal lobe; may play a part in propagation of seizures; may be directly linked with the epileptogenic network and resection of the parahippocampal area may be related to post-surgical outcomes.	Vogt et al. 1992, Liu et al. 2012, Thivard et al. 2005, Bonilha et al. 2007,
Inferior Longitudinal Fasciculus	Part of the temporal lobe; connection of visual areas (occipital lobe) with hippocampus (temporal lobe); may play a part in propagation of seizures and its diffusion values may be useful for seizure focus lateralization	Catani & Thiebaut de Schotten 2008, Catani et al. 2003, Concha et al. 2012
Superior Longitudinal Fasciculus (temporal segment)	Connects the temporal lobe with the frontal lobe; strongly involved in language skills; may play a part in propagation of seizures, especially in temporal plus epilepsies	Shinoura et al. 2013, Catani & Mesulam 2008, Ahmadi et al. 2009, Liu et al. 2012, Barba et al. 2017
Uncinate Fasciculus	Structure within the limbic system and part of the temporal lobe; connects the temporal lobe with the frontal lobe; may play a part in propagation of seizures; may be able to stratify patients and controls; larger resections of the uncinate have been related to better postoperative seizure outcomes	Catani & Thiebaut de Schotten 2008, Concha et al. 2012, Keller et al. 2016

Table 3.1. Brain Structures and Their Relation to Epilepsy.

Chapter 4: Review on MR Physics

Chapter 4: Review on MR Physics.....	72
4.1 Introduction.....	72
4.2 Basic Principles of MR Image Acquisition.....	73
4.3 3D Volume T1-weighted Imaging.....	76
4.3.1 Principles.....	76
4.3.2 Applications.....	78
4.4 3D Volume T2-weighted Imaging.....	78
4.4.1 Principles.....	78
4.4.2 Applications.....	80
4.5 3D Volume T2FLAIR.....	81
4.5.1 Principles.....	81
4.5.2 Applications.....	83
4.6 High-resolution Coronal FLAIR Sequences.....	83
4.6.1 Principles.....	83
4.6.2 Applications.....	84
4.7 Diffusion Tensor Imaging.....	85
4.7.1 Principles.....	85
4.7.2 Analysis Approaches.....	89
4.7.2.1 Manual Methods.....	89
4.7.2.2 Automated Methods.....	90

4.1 Introduction

This chapter gives an overview providing sufficient background for the MR sequences acquired and analyzed. It is not intended to be a detailed description of principles underlying MRI acquisition as this would go beyond the scope of this thesis. All structural brain imaging sequences used within the studies are described in the subsections along with the rationale and context of applying them to patients with epilepsy. For instance, the 3D T1w image is used clinically to assess gross brain structure and scientifically for mapping the hippocampal volume and other GM structures in quantitative analysis. For preoperative evaluation, most epilepsy centers include either a 2D or 3D T2w sequence and a T2FLAIR sequence and these sequences have been especially useful for the detection of FCDs clinically (Lerner et al. 2009) and have also been used in quantitative MRI studies (Focke et al. 2008b,

Focke et al. 2009, Martin et al. 2015). Coronal sequences are used during pre-surgical evaluation in order to assess the presence of HS (Wieshmann et al. 1996). It has become increasingly important to assess WM abnormalities in patients with epilepsy to investigate the whole scope of underlying pathobiological processes in epilepsy. This is discussed in section 4.7 of this chapter, which includes information from Kreilkamp et al. (2017). A summary of all used MR sequences with respective rationale and context of applications in patients with epilepsy can be found at the end of this Chapter in Table 4.1. From an imaging perspective, the aforementioned sequences have an acquisition time of approximately four to ten minutes, whereas another “fast” MR imaging technique, called Echo Planar Imaging (EPI), is able to provide full spatial encoding within a single radio-frequency excitation, thus allowing to image time-dependent physiological processes that occur in seconds and even milliseconds (MacIntosh and Graham 2013). Diffusion imaging using EPI makes use of the fact that water (i.e. hydrogen protons) moves along WM tracts of the brain and the imaging-derived metrics allow researchers and clinicians to infer the state of WM integrity (Section 4.7). Fast imaging comes at a cost of lower signal-to-noise ratio (SNR) and geometric distortions, which makes extensive image post-processing necessary. For these reasons, DTI is not commonly used in the first MRI assessment of patients with epilepsy. However, it has found a broad application in scientific research and has been clinically used at later stages, e.g. for preoperative evaluation in order to avoid damage to important WM tracts connecting areas of eloquent cortex (Duncan et al. 2016; see Chapter 1).

4.2 Basic Principles of MR Image Acquisition

The phenomenon of nuclear magnetic resonance was first discovered in the first half of the 20th century (Bloch 1946, Purcell et al. 1946) and started to revolutionize diagnostic procedures from the 70s since brain structure could be visualized in high detail without exposure to radiation. The discoveries of Paul Lauterbur and Peter

Mansfield in the 70s allowed scientists to advance imaging from a single (temporal) to a second (spatial) dimension and to mathematically analyze MRI signals that had been acquired through fast imaging techniques, respectively (Geva 2006). In 1970, Raymond Damadian started probing the use of MRI as a medical diagnostic tool by imaging different animal tissue types and was able to detect cancerous tissue as its MRI signal had a longer relaxation time than non-cancerous tissue (Damadian 1971, Geva 2006). By 1974, he received the first ever patent in the field of MRI for his scanner and method for detecting cancer (Damadian 1974). The discovery soon spread within the field of medicine with scanners being available from the beginning of the 1980s and rapidly found applications in various disorders and diseases.

Instead of relying on X-rays, the MRI scanner uses magnetism in conjunction with radio wave transmission to produce images of human or animal anatomy. MR utilizes inherent physical properties of nuclear particles found in tissue, namely the fact that the electrically charged atomic protons precess (spin around their own axis). The imaging sample is placed in a strong magnetic field while a radio-frequency wave is transmitted and subsequently the protons' response to this wave can be measured (Figure 4.1). Human tissue mostly contains hydrogen atoms (the hydrogen atomic nucleus is a single proton) and since different tissues have a different nuclear density and have different relaxation times this accounts for varying contrasts across tissues. Gradients have to be applied so that the signals can be localized. In particular, for a single plane a linearly increasing frequency-encoding gradient is applied.

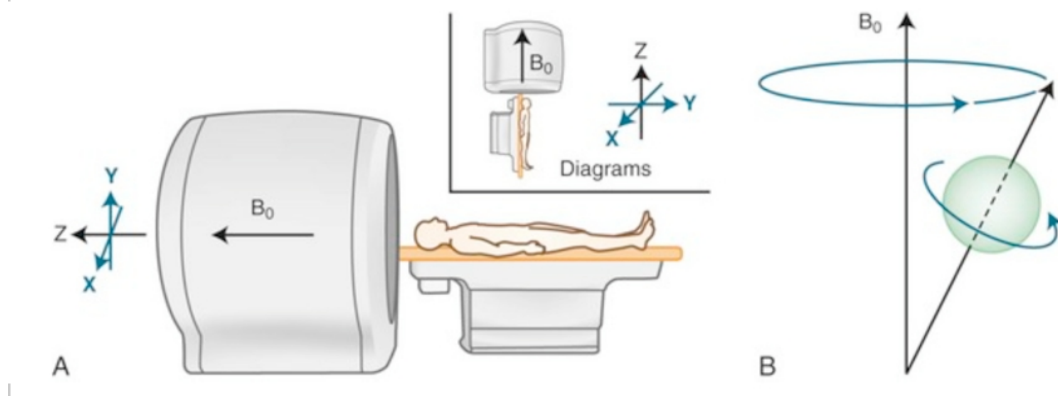


Figure 4.1. MR Scanner (A) and the Spinning Proton (B) (from Ajtai et al. 2015).

As the person is lying in the scanner, a magnetic field is applied parallel to the person's body (Z-axis), while a radio-frequency wave is applied, which deflects the proton from the main magnetic field. This makes it possible to encode the proton's phase (perpendicular Y-axis) while spinning about the axis of B_0 (B) and to determine the proton spin frequency (X-axis) (B, lower arrow) during precession. Gradually the proton returns to only rotating about its own axis along B_0 (steady state). The diagram in panel B and MR images in general have a different frame of reference than depicted in panel A (see inset 'diagrams').

Slight variations of the proton spins' frequencies and phase makes it possible to assign the emitted signal to one location in the 2D image plane. 3D images of human tissue are acquired by slice-selection. This is made feasible by using a magnetic field gradient: rather than having the same field strength in the entire tissue, a gradient is applied. This causes slight variations in the resonant frequencies. All of these slight variations in magnetic field strength, frequency and phase influence the protons' precession and an emitted signal can be captured and assigned to a specific location in 3D space. All MR sequences follow this principle and are described in the following sections along with their indication in patients with epilepsy. The Spin-Echo pulse sequence is the conventional way of acquiring MR signal (Figure 4.2) and yet another radio-frequency pulse can be added to this sequence, which has effects on image contrast and appearance (i.e. by using an inversion recovery sequence).

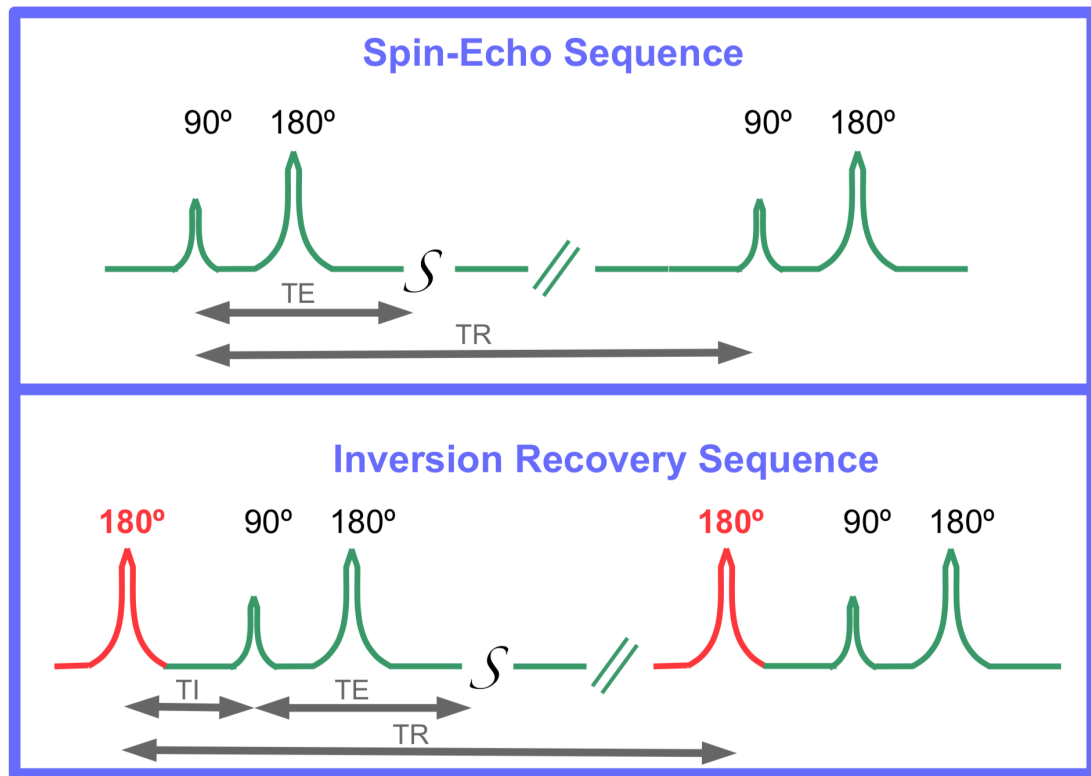


Figure 4.2. Conventional MRI sequences with radio-frequency pulses (from Elster 2017). In order to acquire the MR signal within a spin-echo sequence, a 90° radio pulse is applied. The echo (S) is caused by the 180° radio pulse, which acts like a magnetic barrier and reflects the echo of the first 90° decay signal. For an inversion recovery sequence another 180° radio pulse is added before the 90° and 180° pulses. The time between the added 180° pulse and the 90° pulse is called TI. Apart from nulling the signal from fat and water, the added 180° pulse also flips the sign of the magnetization vector from z to -z. In both sequences, the time between the two 90° excitation pulses is termed TR. S = Signal-readout/echo, TE = echo time, TR = repetition time, TI = inversion time.

4.3 3D Volume T1-weighted Imaging

4.3.1 Principles

The design of a T1w sequence is based on the so-called spin-lattice (longitudinal, measured on z-axis) relaxation emitted by the hydrogen protons (Johnson et al. 2005). The energy is emitted to the lattice (surroundings) of the protons. Hydrogen protons are projected into the transverse plane by the application of a radio-

frequency pulse and as the effect wears off, the spins return to equilibrium and align again with the static magnetic field (Johnson et al. 2005). The T1 relaxation is defined as the time when the protons in the tissue have reached 63% of their equilibrium value, i.e. the original magnetization (Figure 4.3). As such, the T1 relaxation times are associated with the magnetic field strength. T1 relaxation times differs across different tissue types: Fat appears brightest (shortest T1), WM is bright at a short relaxation rate, while GM and CSF emit the least signal and have a longer T1 relaxation rate (MacIntosh and Graham 2013).

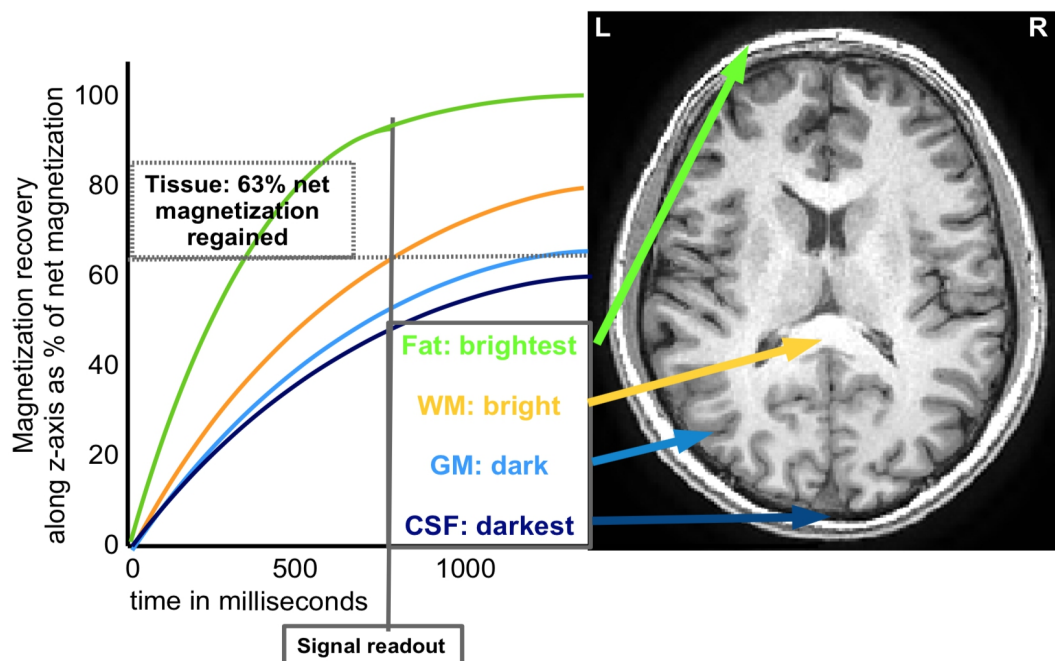


Figure 4.3. T1 relaxation time at 3T and derived T1w grayscale image (from Farrall 2015). T1 relaxation times, defined as the time where 63% of net magnetization has been regained (dashed line): Fat = 370 ms; WM = 830 ms; GM = 1330 ms; CSF = 3600 ms (Gold et al. 2004, Wansapura et al. 1999). A signal readout time at 800 ms reveals optimal contrast with the tissue-dependent T1 relaxation curves having an optimal distance between each other (distinct signal differences across tissue types). MRI was acquired at the WCFT. Figure used and modified with permission of Professor Andrew Farrall at the Edinburgh Imaging Academy (www.ed.ac.uk/edinburgh-imaging/academy). L = left; R = right.

A 3 Tesla T1w image may be acquired using an inversion recovery sequence or

using a spin-echo sequence with a short repetition time (TR, the time between repetitions of the pulse sequence) and a short time to echo (TE, the time at which sampling of the magnetization signal occurs), at about <750 ms (Figure 4.3) and 40 ms respectively.

4.3.2 Applications

The application of T1w sequences has become standard procedure in medicine and science as its high contrast between tissues allows a multitude of scientific and clinical investigations on anatomical images (Figure 4.3). The medical use of T1w images allows diagnostic assessment of abnormal brain structure and any lesions such as tumors and cysts. For research purposes the T1w sequence can be used to segment GM, WM and CSF in order to restrict analysis to certain tissue classes (Kurth et al. 2015a) or brain structures of interest (Fischl et al. 2002). T1w images can also further be used to analyze cortical thickness (Hutton et al. 2009) and related brain atrophy (Ashburner and Friston 2000), all of which can contribute to a deeper understanding of pathologic mechanisms in neurological conditions (Giorgio and De Stefano 2013) and are especially relevant for patients with epilepsy (Sisodiya et al. 1995a, Sisodiya et al. 1995b).

4.4 3D Volume T2-weighted Imaging

4.4.1 Principles

The functionality of the T2-weighted (T2w) sequence is based on the spin-spin relaxation time along the transverse plane (X- and Y-axis). As protons are projected into the transverse plane they initially all spin in the same phase. However, related field inhomogeneities and intrinsic T2 effects present in different tissue types cause the protons to spin differently (e.g. slower) and loose phase coherence with other protons (Johnson et al. 2005) resulting in a loss of magnetization. T2 relaxation time is defined as the time when transverse magnetization has lost 37% of its initial value

due to incoherence of hydrogen proton spins (Figure 4.4).

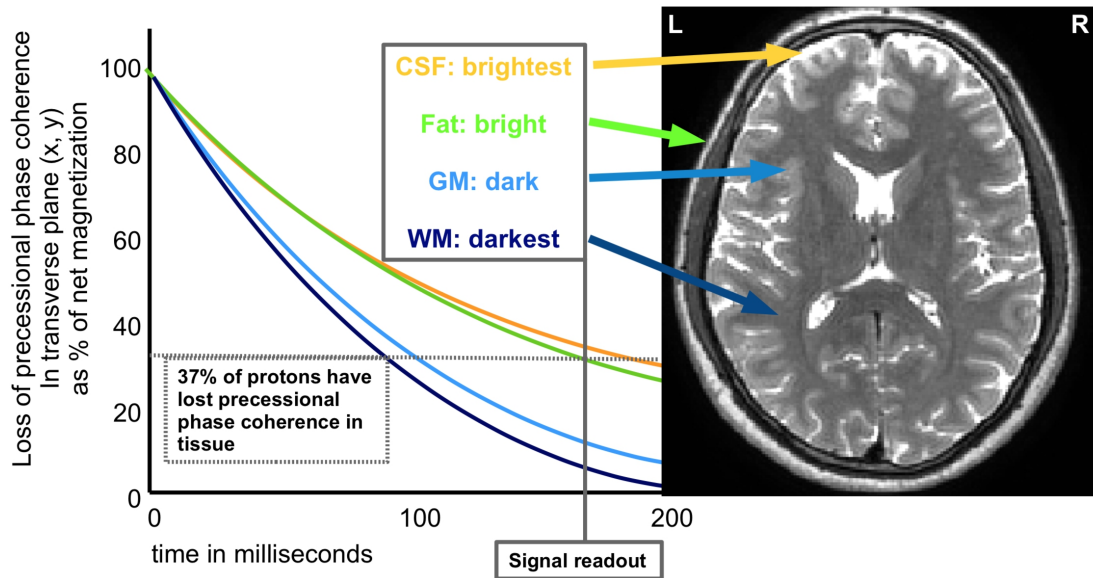


Figure 4.4. T2 relaxation times at 3T and derived grayscale T2w image (from Farrall 2015). T2 relaxation times, defined as the time where 37% of all protons in the tissue have lost precessional phase coherence: WM = 90 ms; GM = 100 ms; Fat = 180 ms; CSF = 190 ms. A signal readout time at 180 ms reveals contrast with T2 relaxation curves having an optimal distance between each other (distinct signal differences across tissue types). MRI was acquired at the WCFT. Figure used and modified with permission of Professor Andrew Farrall at the Edinburgh Imaging Academy (www.ed.ac.uk/edinburgh-imaging/academy). L = left; R = right.

Similarly as for T1 relaxation, different tissue types will show different relaxation times, where fat appears dark (short relaxation time), with GM having short T2 and WM even shorter relaxation times while liquid appears light (longest relaxation rate as there is almost no field inhomogeneity). A 3 Tesla T2w sequence requires a long TR (typically at >2000 ms) and long TE (approximately 100 ms) and may also be acquired using an inversion recovery sequence (e.g. Short TI Inversion Recovery, STIR).

4.4.2 Applications

In many epilepsy centers, along with the T1w image, often also either a 2D or 3D T2w image is acquired for patients for anatomical imaging. A 3D T2w sequence may prove especially useful for some cases (e.g. encephalocele, edema, atrophy or Rasmussen's encephalitis (Kuzniecky and Jackson 2005)), in pre-surgical evaluation and for various research purposes as it provides a whole-brain image with high SNR without distortions. According to Mansouri et al. (2012), the imaging protocol for patients with suspected neocortical epilepsy should include a whole head thin sectioned 3D T1w and T2w sequence. The 2D T2w sequence can be acquired so that a resulting image can depict a higher in-plane resolution than a 3D sequence (i.e. <0.5 mm in two dimensions). Often however, a 2D sequence does not cover the entire brain, but is set up to depict parts of the brain that are especially important for clinicians to evaluate. The T2w image shows a similar contrast to diffusion images sampled using EPI, however as T2w is sampled without an EPI sequence and diffusion-sensitizing gradient, it does not suffer from susceptibility effects. Consequently, the T2w image may be used to correct for geometric distortions within diffusion images (Ardekani and Sinha 2005). As the signal of T1w and T2w images complement each other they may be used to visualize myelin in the brain and can be used to account for field inhomogeneities (Glasser and Van Essen 2011). On T2w images, WM appears dark only after full myelination, at about two years of age (Figure 4.5). Before then, the appearance of WM on T2w images is much brighter. In T1w images, the reverse is true as WM gradually changes from hypointense to hyperintense signal relative to GM. GM signal intensities largely stay very similar, whereas WM signal changes during brain development. WM is mostly unmyelinated at birth, which is reflected by T1 and T2 relaxation times that are distinctly different compared to those of older children and adults (Figure 4.5). Not surprisingly, the MRI techniques typically used for myelin assessment in infants are T1w and T2w sequences (Welker and Patton 2012). It is likely that patients with early onsets of epilepsy show altered patterns of myelination during neurodevelopment due to an

early insult. Changed diffusivity values (Section 4.7) may indicate altered myelin content in WM tracts (Yeatman et al. 2012) and the evidence of changed diffusivity in patients with TLE is abundant (Section 4.7.2). These changes may be directly detectable using T1w/T2w based myelin mapping (Glasser and Van Essen 2011).

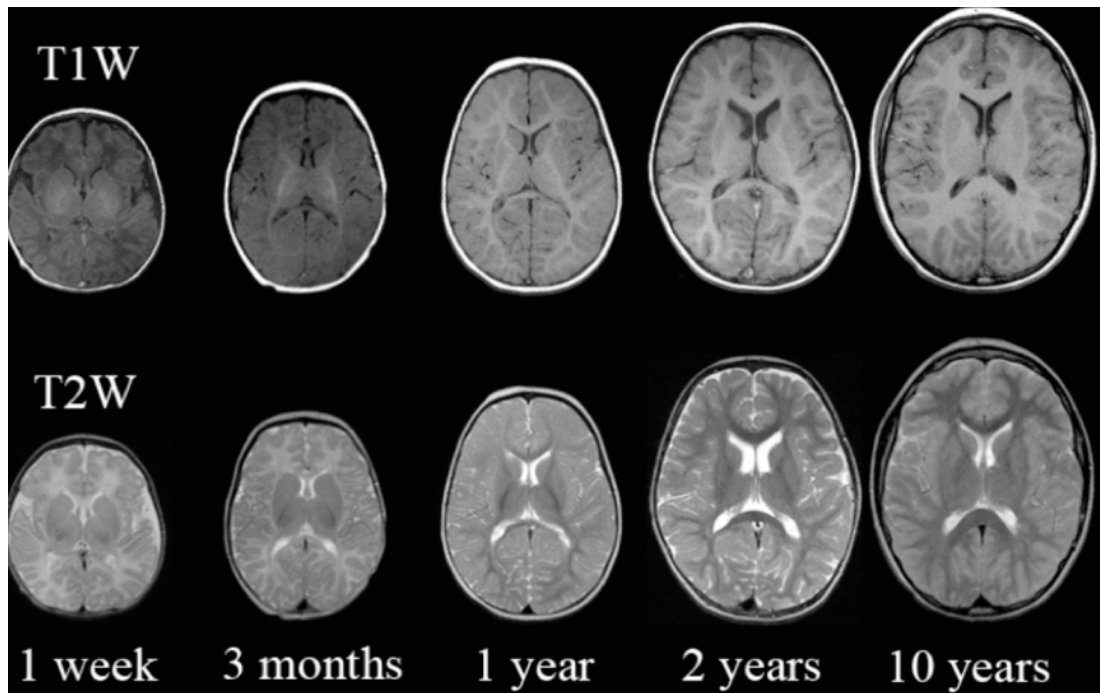


Figure 4.5. T1w and T2w signal patterns at different time points during brain development (from National Institutes of Health 2012)

The GM/WM T1w and T2w signal patterns at an age of one week is the reverse of the pattern seen at an age of one year and older. Information on side of MRI was not provided in source.

4.5 3D Volume T2FLAIR

4.5.1 Principles

The principles pertaining to the acquisition of a 3D T2w image are also relevant for the 3D T2FLAIR, which is a pulse sequence that can image brain tissue while suppressing signal from fluids. The T2FLAIR image is acquired using an inversion

recovery sequence (Figure 4.2). Furthermore, a long TR is used, giving rise to a heavily T2w image (Okuda et al. 1999, Figure 4.4). However, at this point the fluid has neither longitudinal nor transverse net magnetization and its signal is suppressed (Bitar et al. 2006). This is achieved by the initial 180° radio-frequency pulse followed by a long inversion time to allow fluid to attain equilibrium so that no net magnetization remains (Figure 4.6, bottom row).

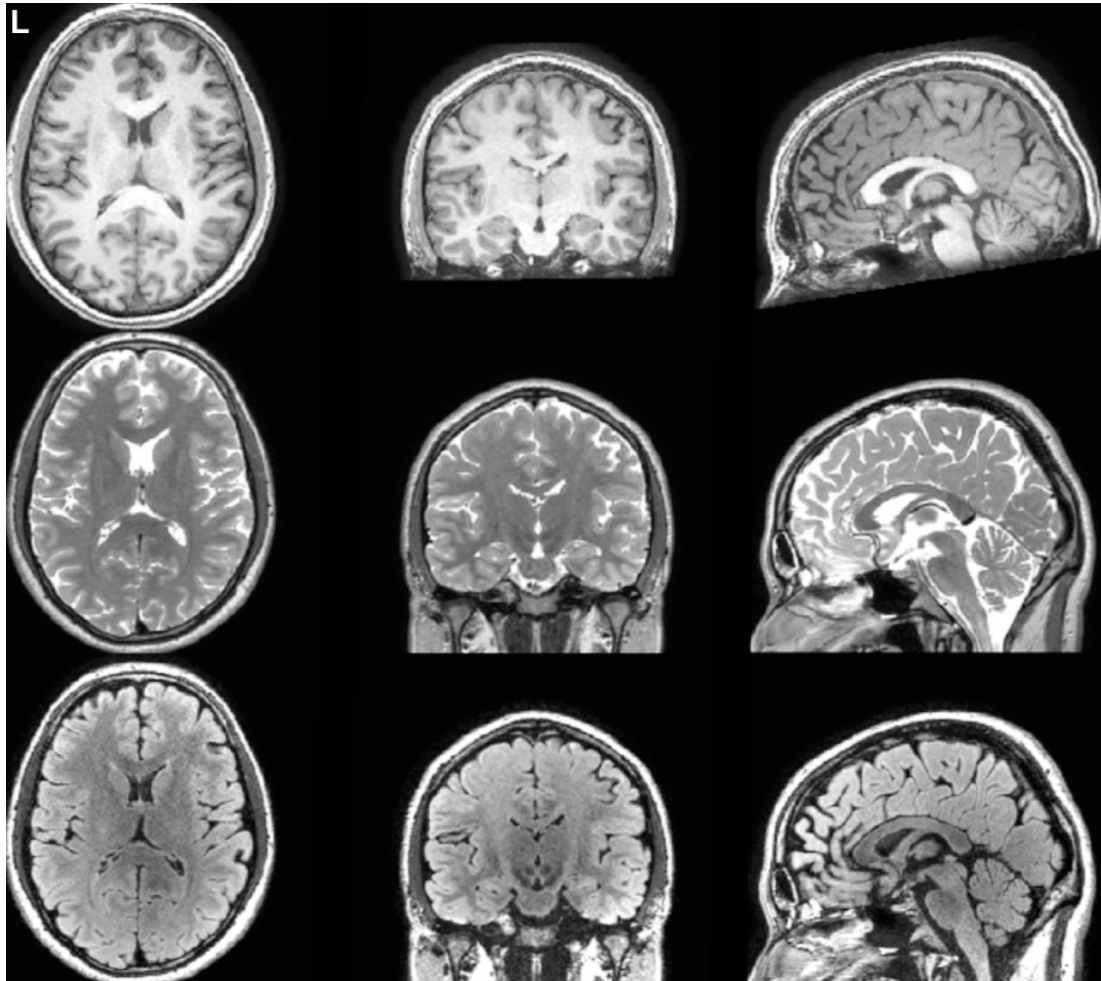


Figure 4.6. Anatomical T1w (top row), T2w (middle row) and T2FLAIR (bottom row) images in axial, coronal and sagittal views (left to right). The images were acquired at the WCFT as part of the epilepsy research dedicated protocol. L = left.

The nulling of liquid signal is useful when the periphery of cortex and periventricular regions close to CSF have to be investigated. In the following section also other clinical and scientific applications are discussed.

4.5.2 Applications

The 3D volume T2FLAIR has proved to be very useful for a wide range of neurological conditions. These include the detection of FCD (Focke et al. 2008b, Rugg-Gunn et al. 2005), which largely has been based on scientific quantitative approaches, and further clinical applications such as in patients with infarction (Shiono et al. 1996, Tsuchiya et al. 1997, Jain et al. 2016), increased blood–brain-barrier permeability and plasma leakage (Haller et al. 2013), tumor-related infiltration/metastatic lesions (Bitar et al. 2006), lesions related to multiple sclerosis (Hittmair et al. 1996, Hashemi et al. 1995), subarachnoid hemorrhage (Noguchi et al. 1995) and meningitis (Vaswani et al. 2014).

4.6 High-resolution Coronal FLAIR Sequences

4.6.1 Principles

Another clinical application of the FLAIR sequence is shown by the use of 2D high-resolution coronal images typically acquired at smaller voxel sizes (e.g. 0.5x0.5x3 mm) compared to 3D sequences. 2D coronal T1- and T2FLAIR images are acquired using an inversion-recovery sequence (Figure 4.2) and provide high anatomical detail within the temporal lobes, as they are aligned with the long axis of the hippocampus (Kuzniecky 2002) and have small in-plane voxel sizes (Figure 4.7).

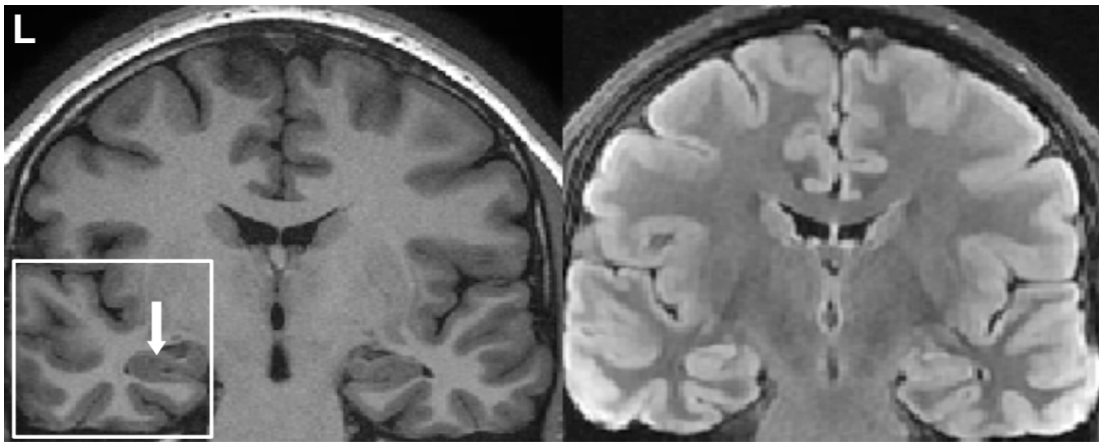


Figure 4.7. Coronal T1- and T2FLAIR images.

These images allow a very accurate depiction of brain tissue within the coronal plane due to the high in-plane resolution. Note the level of detail within the temporal lobe (box) and hippocampus (arrow). Images were acquired at the WCFT. L = left.

SNR and contrast-to-noise ratio (CNR) of in-plane voxels are critically and positively influenced by increasing the through-plane slice thickness and reducing the number of total slices (reducing the imaging matrix size). The rationale for acquiring these images is to be able to depict smaller structures within the temporal lobes and gross anatomy of this region to ultimately increase the diagnostic yield in patients with epilepsy. These images permit the visualization of HS, amygdala enlargement and GM/WM blurring (presence of dysplasia) within the area of the temporal lobes.

4.6.2 Applications

These images have become a clinical standard in evaluating brain structures like the hippocampus, amygdala and other structures of the temporal lobes in patients with mesial TLE owing to the high in-plane resolution (Howe et al. 2010, Duncan 1997). Aligning the images along the hippocampal axis allows for visualization of hippocampal volume, intensity and subfields, which is crucial when diagnosing HS.

The volume of the hippocampus and integrity of hippocampal subfields can be visually determined on the 2D coronal T1FLAIR image, while the T2FLAIR image is useful for determining hyperintense signal from within the hippocampus and atrophy, both of these are features indicating HS (Dinner et al. 1998, Spencer 1994, Mansouri et al. 2012). In HS, neuronal cell death is followed by replacement with gliotic tissue in affected subfields of the hippocampus and this effect can be measured using semi-quantitative hippocampal internal architecture (HIA) ratings (Ver Hoef et al. 2013a). Coronal images without the application of a FLAIR sequence, which have been perpendicularly aligned with the long axis of the hippocampus, have been investigated using HIA ratings (Elkommos et al. 2016) and other quantitative studies based on data collected on patients with TLE, which are performed on the entire hippocampal structure by manually measuring the volume via stereology and associated point counting (Mackay et al. 2000, Roberts et al. 1994). However, automated analysis techniques such as voxel-based volume estimation (Keller et al. 2002a) are not dependent on image alignment with the long axis of the hippocampus and are typically not performed on FLAIR but on T1w images. Furthermore, subfield and entorhinal volumes have been investigated with automated subfield quantification tools (Sone et al. 2016, Schoene-Bake et al. 2014). Manually and automatically obtained volume measures can be quantitatively compared to volumes acquired in healthy controls to determine the extent of gliosis/atrophy and correlate these measures with clinical variables (duration of epilepsy, age of onset, seizure frequency, etc.) and outcome. Specifically, the identification of HS on preoperative MRI has been shown to correlate with good postoperative seizure outcomes (Spencer et al. 2005, Chapter 1), this is discussed in more detail in Chapters 5 and 6.

4.7 Diffusion Tensor Imaging

4.7.1 Principles

DTI aims to visualize WM tracts in the whole human brain through quantifying microscopic motion of hydrogen protons. DTI makes use of the fact that this motion can be restricted along WM tracts (anisotropic), while hydrogen protons that are located elsewhere in the brain (e.g. in CSF) will move freely (isotropic). The EPI sequence is the most common way of acquiring DTI data as it allows fast imaging of the whole brain to determine diffusion within WM structures. Instead of acquiring just a single line of imaging data as is the case with the spin-echo imaging sequence, EPI allows the acquisition of multiple lines within each TR period after a single radio-frequency excitation (Poustchi-Amin et al. 2001). There are many ways to acquire EPI data. For example, this may be achieved by fast oscillation of the frequency-encoding (readout) gradient. The detailed principles governing acquisition and physics of diffusion weighted imaging are described in Figure 4.8. Acquisition involves multiple 3D images of the brain with the application of different diffusion gradients in order to determine motion of the hydrogen protons in certain directions. From this information the principle direction of diffusion for all hydrogen protons can be determined. WM tracts can be modeled using the most commonly employed method, which is also the oldest, the tensor estimation model (Basser et al. 1994). In order to achieve this, a minimum of six DWI are required, while it is also necessary to acquire an image without diffusion weighting (equivalent to a T2w image) (Figure 4.9).

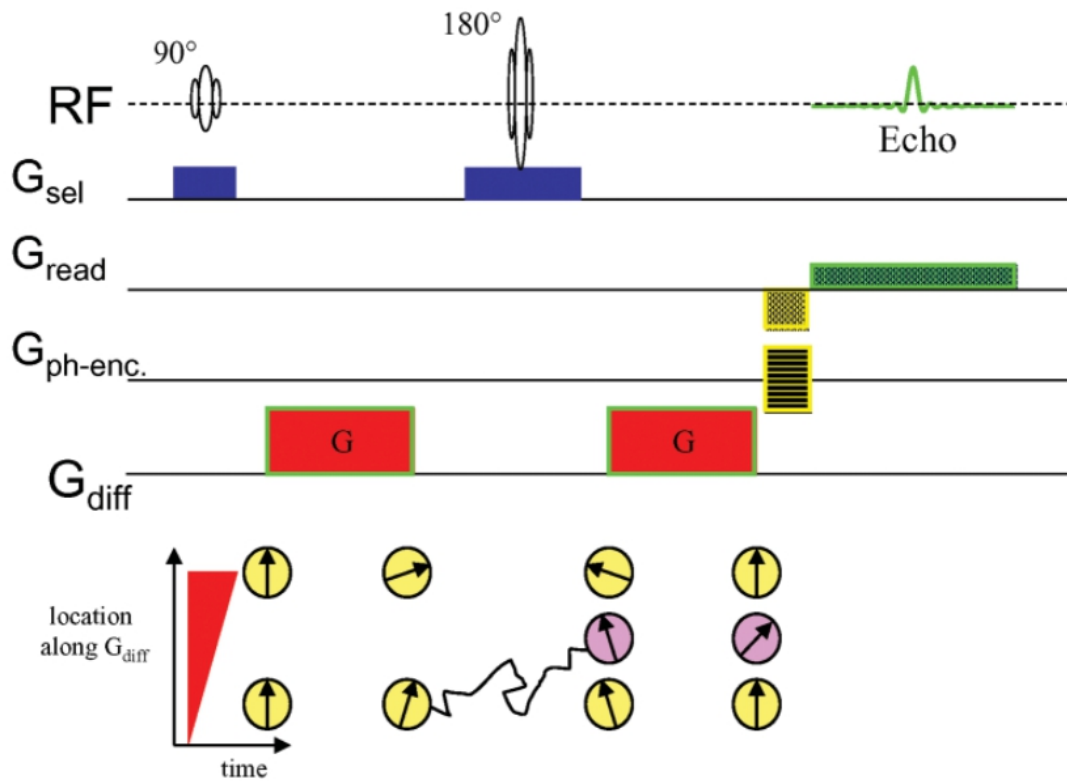


Figure 4.8. Diffusion Weighted Imaging Sequence (from Le Bihan et al. 2006).

A gradient pulse pair (G_{diff}) is used to cause spin phase shifts along their locations. As in a conventional spin-echo sequence, a 90° pulse is applied and during the application of another 180° pulse diffusing spins remain out of phase (pink circles) as they are at a different location with respect to the diffusion-sensitizing gradient. All other proton spins are brought to their initial phase (yellow circles) and emit higher signals than spins that are out of phase because these respective protons have moved. The signals of the spinning protons are measured by the readout gradient. G_{sl} = slice selection gradient, G_{read} = readout gradient, G_{ph-enc} = phase-encoding gradient, G_{diff} = diffusion gradient, RF= radio-frequency pulse.

High signal within b_0 images reflects the random Brownian motion of water molecules (i.e. protons), which occurs in all directions (isotropic diffusion) in CSF in the ventricles of the brain and between the pial surface and skull. In contrast to this, the low b_0 image signal found in brain tissue indicates restricted diffusion and in the case of WM tracts, the diffusion is highly anisotropic meaning that the water molecules can only move in the direction of the particular tracts. To probe different directions of hydrogen proton motion, diffusion-sensitizing gradients are applied in diffusion-weighted images. As proton motion is random in CSF (and not directed in

any one particular direction), liquid appears dark on all diffusion-weighted images, while water protons that follow the trajectory of tracts are restricted in certain directions only. These protons do not emit a high signal, as they are out of phase and have moved to a different location (along the tract) relative to the diffusion-sensitizing gradient during acquisition. Diffusion of hydrogen protons present in GM are restricted in all directions, this is why the signal in this tissue class always appears brighter than in areas with WM tracts, regardless of which diffusion direction was applied.

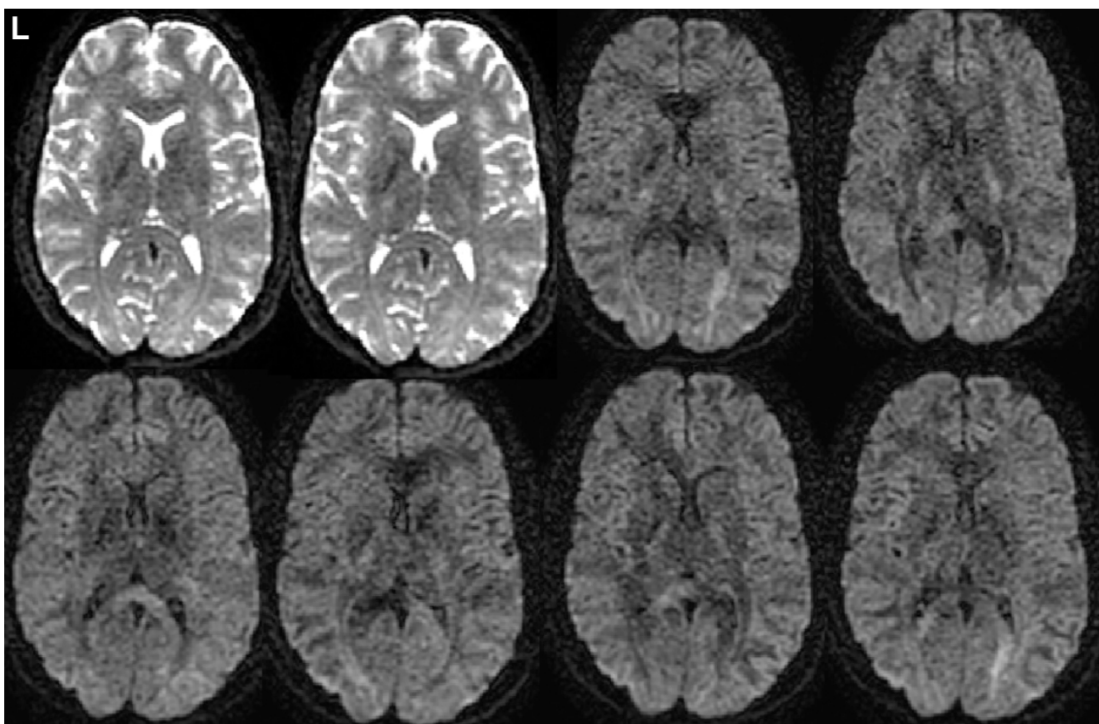


Figure 4.9. Axial sections of whole brain diffusion data.

The first two images on the left of the first row show b0 images (no diffusion weighting), while the remaining six pertain to volume imaging acquired with different diffusion gradients (diffusion-weighted images). Note how voxel intensities across b0 images are the same for the corresponding voxels in the other b0 image (both b0 images look the same). This is not the case in diffusion-weighted images, since the proton spins vary according to different diffusion gradients giving rise to different intensities in these volumes when compared to each other. This is a necessary feature for tensor estimation. Images were acquired at the WCFT (a subset of 2 out of 6 b0 and 6 out of 60 diffusion-weighted volumes is presented). L = left.

However, before the diffusion tensor can be computed, images have to be post-processed to account for distortion and motion. This can be performed on the console of the scanner but also by using tools developed by the scientific community such as FSL (Smith et al. 2004), TRACULA (Yendiki et al. 2011) or AFQ (Yeatman et al. 2012). Most frequently, the tensor-derived scalar metrics apparent diffusion coefficient, fractional anisotropy (FA) and mean diffusivity (MD) are analyzed in scientific studies. Axial and radial diffusivity also provide additional information on WM tract integrity. For a detailed description of how to compute the diffusion tensor and derived metrics, the reader is referred to Soares et al. (2013) and Jellison et al. (2004). The apparent diffusion coefficient has proved useful for assessment of stroke and cancer (Le Bihan 2014), while in patients with epilepsy, FA and MD are most frequently assessed to provide a measure on integrity of individual WM tracts connecting different brain areas (Otte et al. 2012, Chapter 3). Within this thesis, the analysis was restricted to FA and MD values in order to provide a straightforward presentation and explanation of results.

4.7.2 Analysis Approaches

4.7.2.1 Manual Methods

DTI has received a lot of attention clinically and scientifically since its development in the 80s. In 1984, Denis Le Bihan started to perform studies on the development of DTI to differentiate gliomas from liver tumors (Le Bihan 2014). However, he quickly decided to probe tissue within the brain instead as the first images suffered from motion artifacts (due to breathing) and found a way to image diffusion properties of tissues when working with Peter Basser (Basser et al. 1994). Apparent diffusion coefficient maps are used to achieve mapping of glioma appearing as hyperintense imaging signal and each voxel represents microscopic hydrogen proton motion in the order of mm^2/s . Additionally, computing the diffusion tensor from DWI, which allows subsequent tractography, has facilitated visualization of WM tracts and quantification of associated diffusion metrics along the tracts (Le Bihan et

al. 2006, Le Bihan 2014, Basser et al. 1994). This method has provided clinicians with important information about location of tracts that connect eloquent cortex, which must not be damaged during resective surgery (James et al. 2015, Sivakanthan et al. 2016, Duncan et al. 2016). There are a variety of ways to reconstruct WM tracts from DTI data. The most frequently applied have been manual tractography techniques that require a trained researcher to segment individual tract bundles based on known anatomical features. Using these approaches, previous studies have reported significant alterations in DTI scalar metrics, such as FA and MD, of the parahippocampal fibers (Ahmadi et al. 2009, Yogarajah et al. 2008, Concha et al. 2007), ILF (Ahmadi et al. 2009, Imamura et al. 2015, Concha et al. 2012), SLF (Ahmadi et al. 2009, Concha et al. 2012, Lin et al. 2008), UF (Ahmadi et al. 2009, Rodrigo et al. 2007, Diehl et al. 2008, Lin et al. 2008, Concha et al. 2012) and FF (Concha et al. 2005, Concha et al. 2007, Concha et al. 2010). However, manual tractography suffers from low reproducibility and is very time-consuming as ROIs have to be drawn in GM and surrounding WM where tracts are thought to originate or end (Leergaard et al. 2012). So that a significant practical limitation of manual tractography methods is the availability of trained personnel and the time consuming nature of making measurements. Similar to advantages associated with the evolution of automated morphometric techniques from manual volumetric approaches based on T1w data (Bonilha and Keller 2015), a technique that automatically reconstructs probabilistic WM tract bundles could circumnavigate some of the shortcomings of manual tractography approaches.

4.7.2.2 Automated Methods

Many software developers have continued to provide automated tractography tools together with pre-defined ROIs in WM tract atlases (Yendiki et al. 2011, Yeatman et al. 2012, Hagler et al. 2009), thus contributing to the scientific endeavor of circumventing drawbacks inherent in manual techniques. Automated tools will facilitate studies with large sample sizes, which will be essential for establishing a

connectome for the human brain (Marcus et al. 2011) and decrypting network disorders such as epilepsy (Hagler et al. 2009, Richardson 2012, Imamura et al. 2015). In order to investigate WM diffusivity, automated methods can allow whole-brain analysis, rather than being restricted to pre-chosen ROIs. Similarly, automated tractography allows visualization and quantification of WM tracts of the entire brain, as a reference tractography atlas is used. This method can be performed in native patient space or in standard space and both allow group comparisons. Additionally, automated tools such as TRACULA enable researchers to investigate tissue characteristics of WM tracts in relation to morphometric analyses of subcortical and cortical structures (Storsve et al. 2016, Søsnes et al. 2016) and along tracts, which can resolve subtle intra-tract microstructural changes and relationships with morphometric abnormalities. There is only limited anatomical specificity provided in conventional tractography studies in TLE, as techniques are typically restricted to the analysis of whole-tract diffusion alterations. Information obtained from whole-tract analyses are limited because there may be significant variations in diffusion characteristics along the length of WM tracts (Johnson et al. 2013), and it is likely that some pathological tract alterations occur in circumscribed regions within tracts and not along entire tracts in patients with TLE. Therefore it is important to develop methods that permit analysis of within-tract tissue characteristics in patients with TLE (Concha et al. 2012, Glenn et al. 2016). These features are particularly interesting for individual patient comparisons against a healthy control cohort (Martin et al. 2015).

Image	Rationale	Applications
3D T1w	whole brain imaging: SNR and CNR are optimal to depict brain structure	clinical: myelination during development, anatomy, lesions and malformations; scientific: segmentation of WM/GM/CSF; analysis of atrophy and malformations
3D T2w	whole brain imaging: SNR and CNR allow depiction of brain structure	clinical: myelination during development, lesions (encephalocoele, edema) and malformations (atrophy or Rasmussen's encephalitis); scientific: image alignment (for DTI), may aid in T1w-based GM pial segmentation
3D T2FLAIR	whole brain imaging: simultaneous suppression of CSF	clinical and scientific: lesions at peripheral areas of cortex and periventricular regions (e.g. dysplasia)
2D Coronal T1FLAIR	detailed imaging: temporal lobe structures; SNR and CNR are optimal in the imaged 2D plane	clinical: lesions within temporal lobes (e.g. volume of hippocampi)
2D Coronal T2FLAIR	detailed imaging: temporal lobe structures; SNR optimal in imaged 2D plane	clinical: lesions within temporal lobes (e.g. hyperintense signal in HS)
DTI	whole brain imaging: WM tract structure/integrity	clinical: trajectory of WM tracts (pre-surgical evaluation) scientific: brain network disorders (e.g. epilepsy)

Table 4.1. Summary of MRI sequences used within this study of patients with focal epilepsy. SNR = signal-to-noise ratio; CNR = contrast-to-noise ratio; CSF = cerebrospinal fluid; HS = hippocampal sclerosis.

Chapter 5: Automated Multi-sequence Hippocampal Subfield Segmentation in Refractory Temporal Lobe Epilepsy: Relation to Clinical Outcomes

Chapter 5: Automated Multi-sequence Hippocampal Subfield Segmentation in Refractory Temporal Lobe Epilepsy: Relation to Clinical Outcomes.....	93
5.1 Introduction.....	93
5.2 Methods.....	97
5.2.1 Participants.....	97
5.2.2 MRI Acquisition.....	97
5.2.3 MRI Analysis.....	98
5.2.4 Statistical Analysis.....	100
5.3 Results.....	101
5.3.1 Volumes and Clinical Correlations.....	101
5.3.2 Outcome.....	103
5.4 Summary.....	107

5.1 Introduction

Quantitative MRI techniques provide sensitive surrogate markers of HS (Cascino et al. 1991, Jackson et al. 1990). Global HA is most frequently quantified on T1w MRI in patients with TLE, and has been correlated with various clinical features of the disorder in some studies, including age of onset of intractable seizures, duration of epilepsy, a history of childhood febrile seizures, and postoperative seizure outcome (Fuerst et al. 2001, Salmenpera et al. 1998, Tasch et al. 1999, Jack et al. 1992, Wieshmann et al. 2008). However, other studies have failed to report these associations (Cendes et al. 1993, Keller et al. 2015b, Mueller et al. 2012). A potential reason for these discrepancies could be the fact that hippocampal volume alone is not a reliable predictor of post-surgical outcome (Bonilha and Keller 2015, Quigg et al. 1997, Goh et al. 2014, Mueller et al. 2012) or even of the presence or absence of HS (Jackson et al. 1990 and Jackson et al. 1994 respectively). Indeed, hippocampal volume asymmetry has also been demonstrated in age-matched healthy controls regardless of image presentation (radiological versus neurological) during manual measurements (Rogers et al. 2012). Apart from hippocampal volume also the

hippocampal internal architecture (HIA) and variations in signal intensities should be taken into account when assessing a patient's MRI clinically (Wieshmann et al. 2008). Signal intensity assessment and semi-quantitative HIA ratings are made based on high-resolution coronal MRI, which allow the detailed slice-wise assessment of gross temporal lobe and GM structures due to their high SNR and CNR. The HIA ratings can indicate severity and type of HS and may even reliably show correlations with various clinical features of the disorder (Ver Hoef et al. 2013a, Ver Hoef et al. 2013b). Consequently, identifying relationships between clinical features and quantitative characteristics of the hippocampus in TLE is important as they may offer insights into the pathophysiology of the disorder, inter-individual patient heterogeneity, and may provide the basis for imaging prognostic markers of treatment outcome.

The ILAE Commission on Diagnostic Methods have reported three principle patterns of HS based on histopathological analysis (Blümcke et al. 2013). The most common pattern of cell loss, ILAE HS type 1, is manifest as predominant loss of neurons and gliosis in CA1 and CA4 subfields (Blümcke et al. 2013, Blümcke et al. 2007, Thom et al. 2010). ILAE HS type 2 and 3 are less common patterns of HS, manifest as pathological changes predominantly in CA1 or CA4, respectively (Blümcke et al. 2013, Blümcke et al. 2007, Thom et al. 2010). Importantly, these patterns of HS appear to be related to various clinical aspects of TLE and may have significance for postoperative prognosis. ILAE HS type 1 is more frequently associated with a history of initial precipitating injuries in early childhood, an early seizure onset and improved seizure outcome after temporal lobe surgery (Blümcke et al. 2013, Blümcke et al. 2007, Thom et al. 2010, Giulioni et al. 2013, Na et al. 2015). ILAE HS type 2 and 3 appear to be associated with a later age of onset and a less favorable postoperative outcome (Blümcke et al. 2013, Blümcke et al. 2007, Thom et al. 2010, Giulioni et al. 2013, Na et al. 2015), although there are some inconsistencies in these relationships (Deleo et al. 2016). Given the clinical relevance of regional

hippocampal subfield pathology in TLE, it is important to develop and apply MRI approaches that permit assessment of hippocampal subfield structure and volume in this patient group, particularly if such non-invasive imaging measures can be used to predict treatment outcome.

There have been significant advances in the development of MRI techniques for the segmentation and volume estimation of hippocampal subfields. Manual delineation techniques applied to high-field (i.e. ≥ 4 Tesla) MRI are the most reliable approaches to identify the approximate location of subfields in individual subjects (Prudent et al. 2010, Kerchner et al. 2010, Wisse et al. 2012, Huang et al. 2013, Malykhin et al. 2010, Mueller et al. 2011, Mueller et al. 2009, Mueller et al. 2007, Mueller and Weiner 2009). Automated hippocampal subfield approaches applied to high-field MRI have also been described (Wisse et al. 2016). However, applications of these approaches are constrained by the necessity of non-clinical high-field MRI scanners and the time-inefficient manner of manual tracing. There have therefore been developments of automated hippocampal subfield techniques that can be applied to clinically acquired (i.e. ≤ 3 Tesla) MRI data (Van Leemput et al. 2009, Pipitone et al. 2014, Yushkevich et al. 2015a, Winston et al. 2013a). The approach described by Van Leemput et al. (2009) has proved to be particularly popular, given this method's release in context of the freely available Freesurfer software (<http://freesurfer.net>, Fischl 2012). This technique was previously applied to investigate hippocampal subfield alterations in patients with TLE (Schoene-Bake et al. 2014). However, there have been concerns raised with this approach, including reliance on low-resolution T1w images and an imprecise parcellation scheme (Wisse et al. 2014). Recently, a revised automated hippocampal subfield technique has been introduced that has improved anatomical delineation of the constituent parts of the hippocampus based on multi-sequence ex-vivo 7T MRI, including standard resolution T1w images and high in-plane resolution T2w images (Iglesias et al. 2015). In a large sample of patients with refractory TLE and HS who underwent conventional T1w and high-

Chapter 5: Multi-sequence Hippocampal Subfield Segmentation

resolution T2STIR MRI, this latest approach was applied to investigate whether preoperative in-vivo hippocampal subfield analysis had significance for laterality, postoperative seizure control, semi-quantitative HIA ratings and other clinical features of TLE.

The aim of this study was to investigate the clinical and surgical outcome correlates of preoperative hippocampal subfield volumes in patients with refractory TLE using a novel automated MRI multi-sequence segmentation technique. An automated hippocampal segmentation algorithm was used to identify 12 subfields in each hippocampus and relate these to epilepsy laterality and postoperative outcomes.

Objective 5.1

To investigate the relationship between preoperative hippocampal subfield volumes and clinical and surgical outcomes in patients with refractory TLE using a new MRI multi-sequence segmentation technique.

It was hypothesized that post-surgical outcome was related to preoperative hippocampal subfield volume. For example, as ILAE HS type 1, is manifest as predominant loss of neurons and gliosis in CA1 and CA4 subfields and has been associated with an early seizure onset and improved seizure outcome after temporal lobe surgery (Blümcke et al. 2013), it was hypothesized that atrophy in these regions would be related to favorable post-surgical outcomes. Furthermore, as HS is an initial precipitating injury (Pitkänen and Lukasiuk 2011, Blume 2006, Goldberg and Coulter 2013), it was assumed that clinical features such as age of onset, duration of epilepsy and seizure frequency would not be related with the degree of atrophy of gross hippocampal volume or of any subfields.

Objective 5.2

To determine the relationship between hippocampal subfield volumes and semi-

quantitative hippocampal internal architecture (HIA) ratings.

It was hypothesized that the semi-quantitative HIA ratings (visual scoring assessments representing a marker for loss of internal hippocampal architecture, an important feature of HS (Elkommos et al. 2016)) would correlate with whole hippocampal and subfield volumes.

5.2 Methods

5.2.1 Participants

106 patients with well-characterized mesial TLE and radiological evidence of HS (mean age = 40.3 years (SD 13.6); 58 female; 70 with left TLE, 36 with right TLE) who were being evaluated for suitability for neurosurgery at University Hospital Bonn, Germany were studied. Each patient underwent a detailed pre-surgical program, including comprehensive seizure semiology assessment, MRI, neuropsychological assessment, interictal electroencephalography and if clinically necessary, additional invasive electrophysiological recordings, as reported recently (Keller et al. 2015a). All patients showed evidence of a unilateral temporal lobe seizure onset with concomitant ipsilateral HS. Conventional indicators of HS were diagnosed by an experienced neuroradiologist (Keller et al. 2015a). No patient had bilateral HS or evidence of a potential secondary epileptogenic lesion. Age of patient, age at diagnosis of epilepsy, duration of epilepsy, history of childhood FC and incidence of SGTCS were recorded for all patients. Patients who underwent temporal lobe surgery (standardized amygdalohippocampectomy) received postoperative follow up for a period of up to two years after surgery and outcome assessment using the ILAE outcome classification system (Wieser et al. 2001).

5.2.2 MRI Acquisition

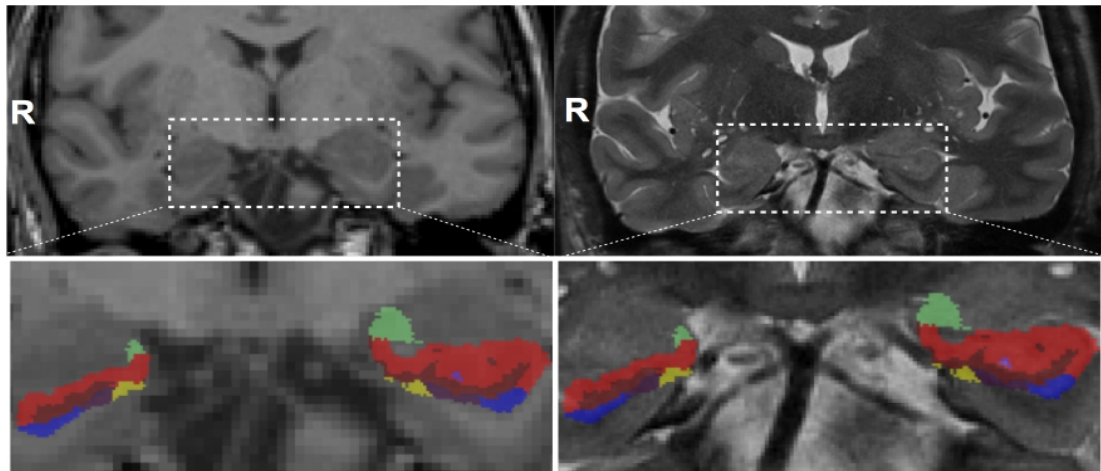
All patients underwent MRI at the Life & Brain Center in Bonn on a 3 Tesla scanner (Magnetom Trio, Siemens, Erlangen, Germany) using an eight-channel head coil. For the purposes of the present study, two MRI sequences, including a 3D T1w

MPRAGE image (160 slices, TR = 1300 ms, TI = 650 ms, TE = 3.97 ms, resolution $1.0 \times 1.0 \times 1.0$ mm, flip angle 10°) and a high in-plane resolution T2STIR sequence in the coronal plane angulated perpendicular to the long axis of the hippocampus (40 slices, TR = 5600 ms, TI = 100 ms, TE = 18 ms, resolution $0.45 \times 0.45 \times 2.0$ mm, flip angle = 0°) were acquired.

5.2.3 MRI Analysis

For each patient quantitative automated segmentation and cortical parcellation of T1w data were performed using Freesurfer 5.3.0 (Fischl 2012). The standard Freesurfer “recon-all” processing stream was used, which provides surfaces and morphometry data for each subject in addition to GM/WM segmentations. Automatic labelling and volume estimation of hippocampal subfields was guided by the segmentation of the whole hippocampus (previous step) and performed using the adaptive segmentation technique described by Iglesias et al. (2015) in context of Freesurfer 6 (<https://surfer.nmr.mgh.harvard.edu/fswiki/HippocampalSubfields>). Figure 5.1 shows the anatomical locations of the hippocampal subfields on T1w and T2STIR images in a patient with right TLE after the use of this software module.

A. Hippocampal Head



B. Hippocampal Body

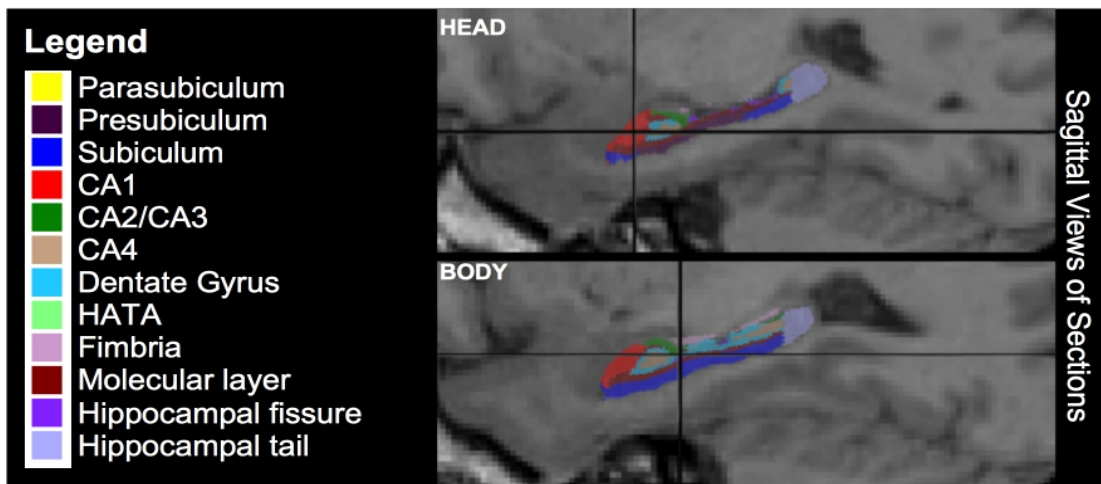
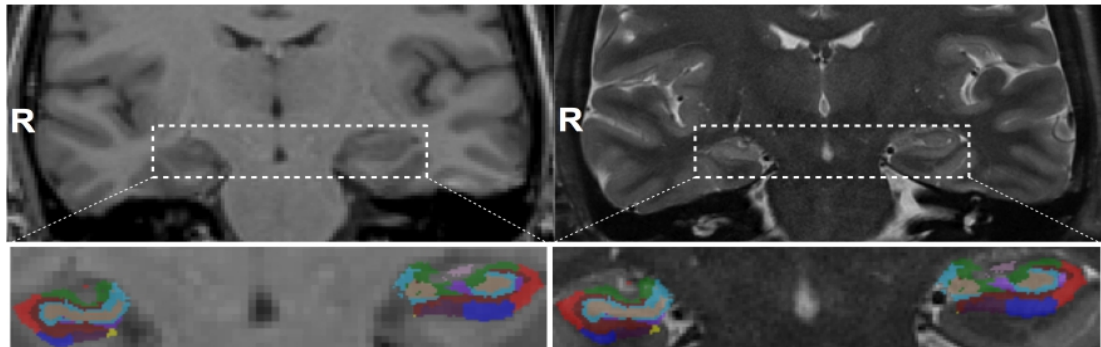


Figure 5.1. Anatomical locations of segmented subfields on T1w (left) and T2STIR images (right) in a patient with right TLE. The same slices are shown for both images in the hippocampal head (A) and hippocampal body (B). R = Right; CA = Cornu Ammonis; HATA = Hippocampus-Amygdala Transition Area.

Chapter 5: Multi-sequence Hippocampal Subfield Segmentation

The protocol co-registered T1w and T2STIR data and used these images simultaneously to generate labels and volumes for the whole hippocampus and 12 hippocampal subfields:

1. Parasubiculum
2. Presubiculum
3. Subiculum
4. CA1
5. CA2/CA3
6. CA4
7. Granule cell layer of the dentate gyrus (GC-DG)
8. Hippocampus-amygdala transition area (HATA)
9. Fimbria
10. Molecular Layer
11. Hippocampal fissure
12. Hippocampal tail

Semi-quantitative HIA ratings have been shown to be a significant predictor of the laterality of seizure onset in TLE (Ver Hoef et al. 2013a, Elkommos et al. 2016) and were integrated into image analysis in order to determine whether HIA correlated with gross hippocampal and subfield volumes as estimated by Freesurfer. Each T2STIR image slice that depicted the hippocampus was graded with a score of ‘1’ when no internal architecture was discernible to ‘4’ where excellent internal architecture differentiation could be appreciated (Elkommos et al. 2016). The rater (Dr Samia Elkommos) was blinded to patient clinical information such as outcome and laterality and the images were rated on consecutive coronal T2STIR sections in a rostral to caudal direction.

5.2.4 Statistical Analysis

All statistical analyses were performed using MATLAB 2015b. Group comparison analyses were performed using the unpaired Mann-Whitney U test (data non-

normally distributed, $p < 0.05$), and included analysis of effects of laterality of epilepsy and postoperative outcome on subfield volume. With respect to postoperative outcome, comparisons were made between patients who attained a postoperative outcome of ILAE I (complete seizure freedom) relative to ILAE II-VI (persistent postoperative seizures) (Keller et al. 2015a). Relationships between subfield volume and continuous clinical data, including age of onset of epilepsy, epilepsy duration, seizure frequency and estimated seizure burden, were investigated using Spearman correlation coefficients. Seizure burden was defined as equal to $\log_{10}(\text{frequency} \times \text{duration})$, with the logarithm being applied to accommodate patients with very high seizure frequency. Correlations were performed corrected for patient age. Relationships between categorical relationships, including postoperative outcome and sex, side of TLE, history of childhood FC and presence of SGTCS was investigated using Chi-Squared tests of independence. Furthermore, the relationships between HIA ratings and automatically extracted Freesurfer subfield volumes were investigated. Gross hippocampal and subfield volumes were corrected for ICV and statistical tests were corrected for multiple comparisons using the False-Discovery-Rate (FDR) procedure (Benjamini and Hochberg 1995).

5.3 Results

The accuracy of the hippocampal subfield labels was visually checked for all patients. The subfields of one hippocampus in three patients could not be successfully generated due to motion artifacts. Therefore analyses were restricted to the 103 with successful reconstructions.

5.3.1 Volumes and Clinical Correlations

Table 5.1 shows the comparison of ipsilateral and contralateral subfield volumes between patients with left and right TLE. There were no significant differences in subfield volumes of the ipsilateral hippocampi between patients with left and right TLE.

Chapter 5: Multi-sequence Hippocampal Subfield Segmentation

Side	Region	TLE	Mean	SD	Z	p-value (FDR-corr.)
Ipsilateral	Hippocampal Tail	Left	0.025	0.007	0.15	0.96
		Right	0.025	0.005		
	Subiculum	Left	0.022	0.005	1.89	0.37
		Right	0.020	0.003		
	CA1	Left	0.032	0.009	-0.72	0.76
		Right	0.032	0.007		
	Hippocampal Fissure	Left	0.008	0.002	1.3	0.53
		Right	0.008	0.002		
	Presubiculum	Left	0.015	0.004	2.6	0.11
		Right	0.014	0.003		
	Parasubiculum	Left	0.003	0.001	1.3	0.53
		Right	0.003	0.001		
	Molecular Layer HP	Left	0.029	0.006	0.32	0.96
		Right	0.028	0.005		
	GC-ML-DG	Left	0.015	0.004	0.21	0.96
		Right	0.015	0.003		
	CA2/3	Left	0.010	0.003	-0.85	0.74
		Right	0.010	0.003		
	CA4	Left	0.013	0.003	0.05	0.96
		Right	0.012	0.003		
	Fimbria	Left	0.004	0.001	1.48	0.53
		Right	0.004	0.001		
	HATA	Left	0.004	0.001	1.16	0.53
		Right	0.004	0.001		
	Whole Hippocampus	Left	0.170	0.040	0.46	0.93
		Right	0.166	0.030		
Contralateral	Hippocampal Tail	Left	0.036	0.006	3.3	0.01
		Right	0.032	0.005		
	Subiculum	Left	0.028	0.005	-1.02	0.52
		Right	0.028	0.004		
	CA1	Left	0.045	0.008	-1.7	0.32
		Right	0.043	0.006		
	Hippocampal Fissure	Left	0.088	0.002	0.74	0.55
		Right	0.084	0.002		
	Presubiculum	Left	0.018	0.003	-2.4	0.08
		Right	0.019	0.003		
	Parasubiculum	Left	0.004	0.001	-1.23	0.52
		Right	0.004	0.001		
	Molecular layer HP	Left	0.038	0.007	1.14	0.52
		Right	0.036	0.005		
	GC-ML-DG	Left	0.021	0.004	0.43	0.67
		Right	0.021	0.003		
	CA2/3	Left	0.015	0.003	0.58	0.61
		Right	0.015	0.003		
	CA4	Left	0.018	0.003	0.82	0.54
		Right	0.017	0.002		
	Fimbria	Left	0.005	0.001	-0.88	0.54
		Right	0.005	0.002		
	HATA	Left	0.0045	0.001	-2.66	0.05
		Right	0.005	0.001		
	Whole Hippocampus	Left	0.230	0.036	0.99	0.52
		Right	0.225	0.028		

Table 5.1. Comparison of Subfield Volumes Corrected for ICV in Patients with Left/Right TLE.

Patients with right TLE had reduced ICV corrected volumes of the contralateral

hippocampal tail ($Z=3.3$, $p_{(FDR-corr)}=0.01$), and patients with left TLE had lower contralateral presubiculum ($Z=-2.4$, $p_{(FDR-corr)}=0.08$) and HATA ($Z=-2.66$, $p_{(FDR-corr)}=0.05$) volumes relative to the corresponding patient group (Table 5.1; Figure 5.2). For patients as a whole group, and patients with left and right TLE separately, there were no significant relationships between age of onset, duration of epilepsy corrected for age, seizure frequency/burden, incidence of SGTCS/febrile convulsions and hippocampal subfield volumes ($p_{(FDR-corr)}>0.05$).

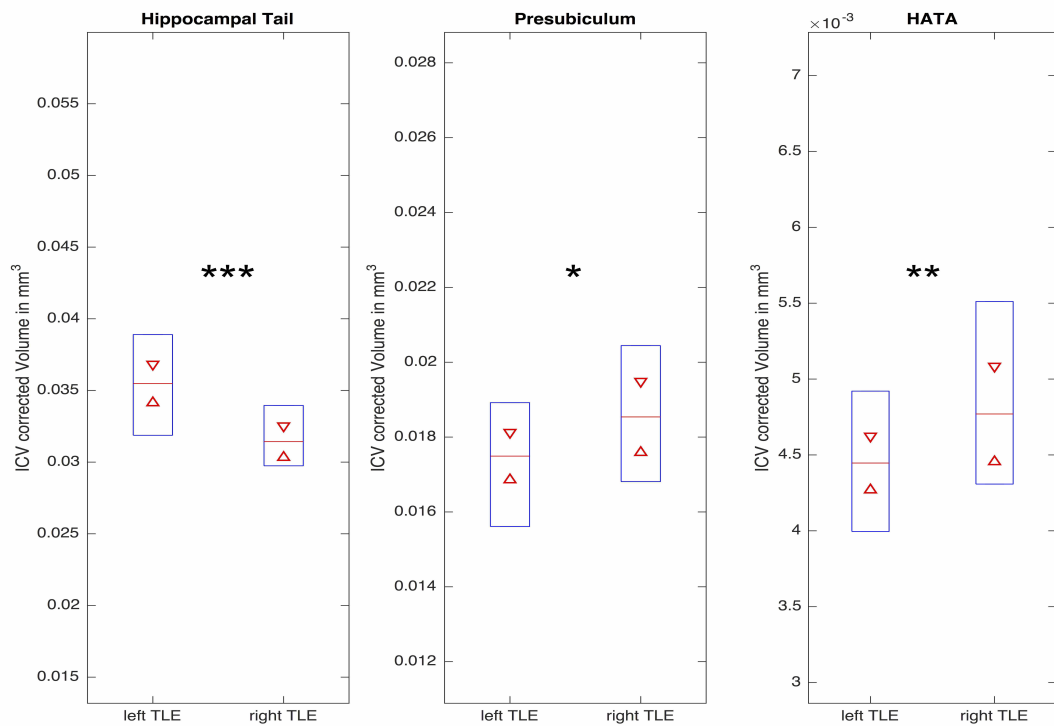


Figure 5.2. Decreased contralateral hippocampal volumes in patients with right TLE compared to patients with left TLE (hippocampal tail) and vice versa (presubiculum/HATA). Blue boxplots indicate data distribution, with the median (red line) and 95% confidence intervals (red triangles). * $p_{(FDR-corr)}<0.1$; ** $p_{(FDR-corr)}<0.05$; *** $p_{(FDR-corr)}<0.01$.

5.3.2 Outcome

Of the 103 with successful reconstructions, 76 patients had received amygdalohippocampectomy and postoperative outcome assessment. Of these

Chapter 5: Multi-sequence Hippocampal Subfield Segmentation

patients, 41 (54%) patients had an excellent postoperative seizure outcome (ILAE I) and 35 (46%) had a suboptimal outcome (ILAE II-VI) (minimum 12 months follow up, mean 23 months). A breakdown of clinical variables according to outcome is provided in Table 5.2. An increased number of males had an excellent outcome compared to females ($\chi^2=4.5$, $p<0.05$), and right-sided patients had fewer suboptimal outcomes ($\chi^2=3.7$ $p=0.05$). There were no significant differences between outcome groups in incidence of febrile/SGTC seizures, age, age at onset of epilepsy, duration of epilepsy, seizure frequency or seizure burden.

Variable	ILAE I	ILAE II-VI	Statistics
N	41 (54%)	35 (46%)	-
Outcomes	I = 41	II = 7 III = 14 IV = 11 V = 3 VI = 0	-
left / right TLE	23/18	27/8	$\chi^2=3.7$, $p=0.05$
female / male	17/24	23/12	$\chi^2=4.5$, $p=0.04$
Febrile Seizures, no / yes	28/13	21/14	$\chi^2=0.6$, $p=0.45$
SGTCS, no / yes	25/16	21/14	$\chi^2=0.01$, $p=0.93$
Age	38.3 (12.4)	39.1 (14.2)	$Z=-0.08$, $p=0.94$
Onset	15.9 (11.94)	14.9 (11.5)	$Z=0.27$, $p=0.79$
Duration Corrected for Age	0.58 (0.29)	0.59 (0.3)	$Z=-0.06$, $p=0.95$
Seizure Frequency	8.8 (16.5)	8.4 (15.6)	$Z=-0.75$, $p=0.45$
Seizure Burden	1.87 (0.52)	1.89 (0.52)	$Z=-0.14$, $p=0.89$

Table 5.2. Clinical Variables According to Surgery Outcome.

TLE = Temporal Lobe Epilepsy; SGTCS = Secondary-Generalized Tonic-Clonic Seizures.

When all patients were considered together, there were no significant differences in the volume of ipsilateral or contralateral hippocampal subfields between those with excellent and suboptimal outcomes ($p_{(\text{FDR-corr})}>0.05$; Table 5.3).

Chapter 5: Multi-sequence Hippocampal Subfield Segmentation

Side	Region	Outcome	Mean	SD	Z	p-value (FDR-corr.)
Ipsilateral	Hippocampal Tail	ILAE I	0.026	0.006	-0.570	0.690
		ILAE II-VI	0.026	0.007		
	Subiculum	ILAE I	0.022	0.005	-0.830	0.690
		ILAE II-VI	0.022	0.005		
	CA1	ILAE I	0.033	0.009	-0.780	0.690
		ILAE II-VI	0.033	0.008		
	Hippocampal Fissure	ILAE I	0.008	0.002	0.323	0.750
		ILAE II-VI	0.008	0.002		
	Presubiculum	ILAE I	0.015	0.004	-1.271	0.690
		ILAE II-VI	0.015	0.003		
	Parasubiculum	ILAE I	0.003	0.001	-2.011	0.580
		ILAE II-VI	0.004	0.001		
	Molecular Layer HP	ILAE I	0.029	0.006	-0.552	0.690
		ILAE II-VI	0.029	0.006		
	GC-ML-DG	ILAE I	0.015	0.004	-0.667	0.690
		ILAE II-VI	0.015	0.004		
	CA2/3	ILAE I	0.011	0.003	-0.323	0.750
		ILAE II-VI	0.011	0.003		
	CA4	ILAE I	0.013	0.004	-0.552	0.690
		ILAE II-VI	0.013	0.003		
	Fimbria	ILAE I	0.004	0.001	-0.761	0.690
		ILAE II-VI	0.004	0.001		
	HATA	ILAE I	0.004	0.001	-0.866	0.690
		ILAE II-VI	0.004	0.001		
	Whole Hippocampus	ILAE I	0.174	0.042	-0.865	0.690
		ILAE II-VI	0.177	0.039		
Contralateral	Hippocampal Tail	ILAE I	0.034	0.005	-0.020	0.980
		ILAE II-VI	0.035	0.008		
	Subiculum	ILAE I	0.028	0.004	0.560	0.980
		ILAE II-VI	0.028	0.005		
	CA1	ILAE I	0.044	0.007	-0.410	0.980
		ILAE II-VI	0.045	0.009		
	Hippocampal Fissure	ILAE I	0.087	0.002	-0.230	0.980
		ILAE II-VI	0.089	0.002		
	Presubiculum	ILAE I	0.018	0.002	0.150	0.980
		ILAE II-VI	0.018	0.004		
	Parasubiculum	ILAE I	0.004	0.001	-1.060	0.980
		ILAE II-VI	0.004	0.001		
	Molecular layer HP	ILAE I	0.037	0.006	-0.220	0.980
		ILAE II-VI	0.038	0.007		
	GC-ML-DG	ILAE I	0.021	0.004	-0.896	0.980
		ILAE II-VI	0.021	0.004		
	CA2/3	ILAE I	0.015	0.003	-0.125	0.980
		ILAE II-VI	0.015	0.003		
	CA4	ILAE I	0.017	0.003	-0.750	0.980
		ILAE II-VI	0.018	0.003		
	Fimbria	ILAE I	0.005	0.001	0.042	0.980
		ILAE II-VI	0.005	0.001		
	HATA	ILAE I	0.005	0.001	-0.021	0.980
		ILAE II-VI	0.005	0.001		
	Whole Hippocampus	ILAE I	0.229	0.032	-0.240	0.980
		ILAE II-VI	0.231	0.039		

Table 5.3. Comparison of Subfield Volumes Corrected for ICV in Patients with Outcomes ILAE I versus ILAE II-VI.

No significant differences were observed between outcome groups when patients

with left or right TLE were considered separately. Significant correlations were observed between semi-quantitative ipsilateral HIA ratings and ipsilateral hippocampal tail ($\rho=0.31$; $p_{(\text{FDR-corr})}<0.05$), subiculum ($\rho=0.25$; $p_{(\text{FDR-corr})}<0.05$), CA1 ($\rho=0.35$; $p_{(\text{FDR-corr})}<0.05$), parasubiculum ($\rho=0.25$; $p_{(\text{FDR-corr})}<0.05$), molecular layer ($\rho=0.33$; $p_{(\text{FDR-corr})}<0.05$), CA2/3 ($\rho=0.32$; $p_{(\text{FDR-corr})}<0.05$), CA4 ($\rho=0.26$; $p_{(\text{FDR-corr})}<0.05$) and the whole hippocampal volume ($\rho=0.3$; $p_{(\text{FDR-corr})}<0.05$). All of these significant relationships are shown in Figure 5.3.

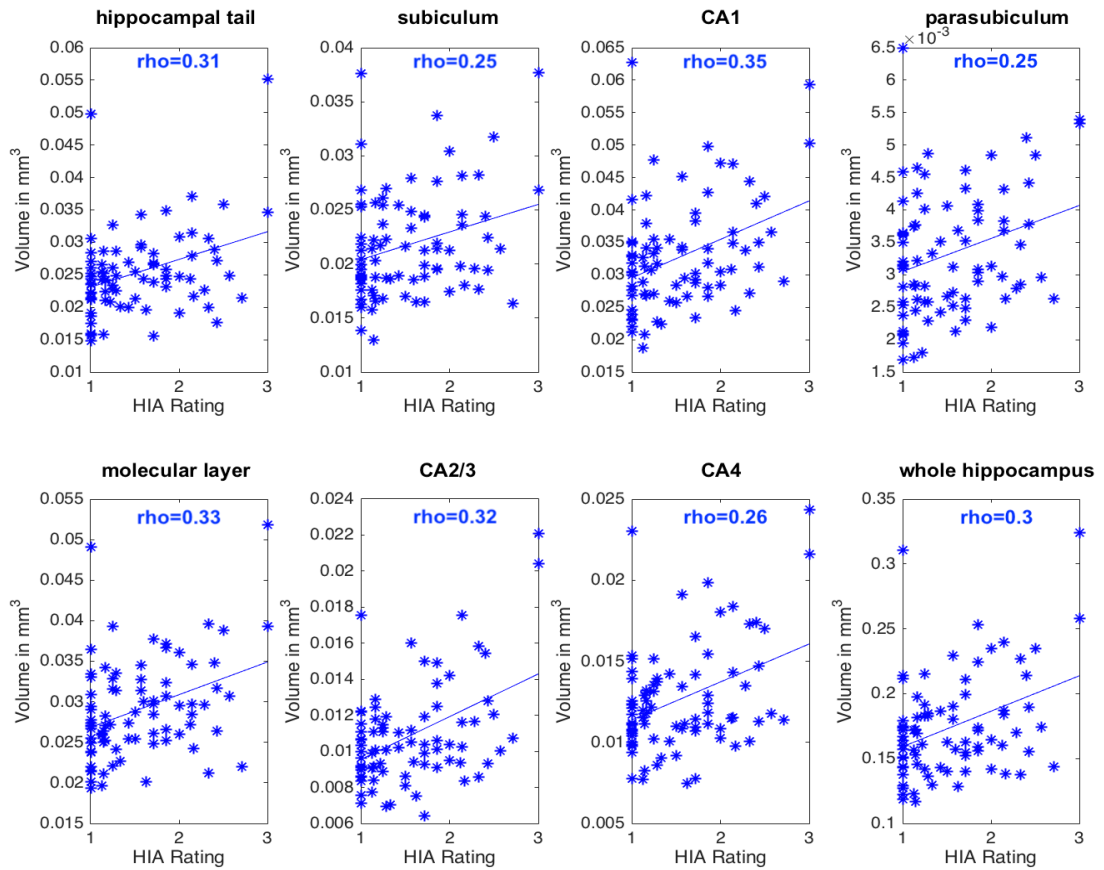


Figure 5.3. Significant correlations of ipsilateral hippocampal internal architecture (HIA) ratings and ipsilateral subfield volumes extracted via Freesurfer. Linear least-square lines were fitted to the data.

There were no correlations between contralateral HIA ratings and contralateral hippocampal or subfield volumes ($p_{(\text{FDR-corr})} > 0.05$).

5.4 Summary

Objective 5.1:

Preoperative hippocampal subfield volumes and clinical and surgical outcomes

Firstly, patients with left TLE had significantly decreased volume of the contralateral presubiculum and HATA regions relative to patients with right TLE. Conversely, patients with right TLE had significantly smaller contralateral hippocampal tail volumes relative to patients with left TLE. Contrary to the initial hypothesis, it was found that the high-resolution hippocampal subfield segmentation technique cannot establish a link between hippocampal subfield volume loss and post-surgical outcome.

Objective 5.2

Hippocampal subfield volumes and semi-quantitative HIA ratings

Ipsilateral and contralateral hippocampal subfield volumes did not correlate with duration of epilepsy, age of onset of epilepsy, epilepsy burden, a history of febrile seizures or prevalence of SGTCS. Semi-quantitative HIA ratings were significantly related to several hippocampal subfield volumes.

Chapter 6: TRActs Constrained by UnderLying Anatomy (TRACULA) in Patients with Refractory Epilepsy: Relation to Post-surgical Outcome

Chapter 6: TRActs Constrained by UnderLying Anatomy (TRACULA) in Patients with Refractory Epilepsy: Relation to Post-surgical Outcome.....	108
6.1 Introduction.....	108
6.1.1 Objectives and Hypotheses.....	111
6.1.2 Organization of Chapter.....	112
6.2 Methods.....	113
6.2.1 Participants.....	113
6.2.2 MR Acquisition.....	114
6.2.3 Data Pre-processing.....	114
6.2.4 Quality Assessment after Pre-processing.....	115
6.2.5 Extraction of Volumes and Tracts.....	116
6.2.6 Statistical Analysis.....	117
6.3 Results.....	120
6.3.1 Data Quality Assessment.....	120
6.3.2 Patients vs Controls	121
6.3.2.1 Volumes.....	121
6.3.2.2 Whole-tract Diffusion Metric Analysis.....	121
6.3.2.3 Waypoint Diffusion Metric Analysis.....	124
6.4 Summary.....	128

6.1 Introduction

Extrahippocampal abnormalities have been frequently described in TLE, including cortical and subcortical GM alterations demonstrated using morphometric techniques (see reviews by Bernhardt et al. 2013, Keller and Roberts 2008, Richardson 2012, Bonilha and Keller 2015) and WM tract alterations using DTI and tractography (see reviews by Rodríguez-Cruces and Concha 2015, Gross 2011). Tractography approaches have proved to be particularly interesting as they can provide quantitative information regarding neuroanatomical structure and pathology that exist beyond conventional visual analysis of MRI, and may yet provide important information on cognitive deficits and treatment prognosis in people with epilepsy. Furthermore, the

recent revision of seizure disorder definitions to acknowledge the importance of networks for the onset of focal seizures (Berg and Scheffer 2011) has encouraged a new direction of imaging research to model neuroimaging data in context of structural and functional networks and connectivity (Richardson 2012). Reconstruction of WM tracts from DTI data represent the most frequently applied technique of generating structural connectivity in the human brain (Jellison et al. 2004, Mori et al. 2009).

There are a variety of ways to reconstruct WM tracts from DTI data. The most frequently applied have been manual tractography techniques that require a trained researcher to segment individual tract bundles based on known anatomical features. Using these approaches, previous studies have reported significant alterations in DTI scalar metrics, such as FA and MD of the parahippocampal fibers (Ahmadi et al. 2009, Yogarajah et al. 2008, Concha et al. 2007), ILF (Ahmadi et al. 2009, Imamura et al. 2015, Concha et al. 2012) and SLF (Ahmadi et al. 2009, Concha et al. 2012, Lin et al. 2008), UF (Ahmadi et al. 2009, Rodrigo et al. 2007, Diehl et al. 2008, Lin et al. 2008, Concha et al. 2012) and FF (Concha et al. 2005, Concha et al. 2007, Concha et al. 2010). However, a significant practical limitation of manual tractography methods is the availability of trained personnel and the time consuming nature of making measurements. Similar to advantages associated with the evolution of automated morphometric techniques from manual volumetric approaches based on T1w MRI data (Bonilha and Keller 2015), a technique that automatically reconstructs probabilistic WM tract bundles could circumnavigate some of the shortcomings of manual tractography approaches.

Freesurfer software (Fischl 2012) has continued to develop and provide freely available tools along with community support for morphometric and tractographic analyses. In context of this software, Tracts Constrained by Underlying Anatomy (TRACULA, Yendiki et al. 2011) offers the opportunity to automatically reconstruct

major WM bundles. A significant advantage of this approach is that the automated reconstruction of tracts is performed in each subject's native space without warping to standard space and tissue characteristics of WM tracts can be investigated in relation to morphometric analyses of subcortical and cortical structures (Storsve et al. 2016, Sølsnes et al. 2016). This is particularly interesting in TLE with associated HS as relationships between extent of damage to the epileptogenic hippocampus and tract tissue characteristics can be investigated. HS may occur in response to an initial precipitating injury prior to a period of epileptogenesis that later gives rise to the onset of recurrent spontaneous seizures (Pitkänen and Lukasiuk 2011, Blume 2006, Goldberg and Coulter 2013). However, the etiology of extrahippocampal brain alterations in TLE remains unknown. Some morphometric MRI studies have suggested that the extent of HA is correlated with the degree of extrahippocampal temporal lobe atrophy (Moran et al. 2001, Bonilha et al. 2010, Mueller et al. 2010, McMillan et al. 2004), suggesting that a common process of gross atrophy may occur. However, less is known about the relationship between HA and WM tract alterations (Rodriguez-Cruces and Concha 2015). One study revealed a correlation between the extent of HA and WM tract alterations (Scanlon et al. 2013) but another study reported no relationship (Concha et al. 2012). In the present study, the relationships between extent of HA, as quantified using Freesurfer morphometric tools, temporal lobe WM tract alterations, and various clinical aspects of TLE were computed.

There is only limited anatomical specificity provided in conventional tractography studies in TLE, as techniques are typically restricted to the analysis of whole-tract diffusion alterations. Information obtained from whole-tract analyses are limited because there may be significant variations in diffusion characteristics along the length of WM tracts (Johnson et al. 2013), and it is likely that some pathological tract alterations occur in circumscribed regions within tracts and not along entire tracts in patients with TLE. Therefore it is important to develop methods that permit analysis

of within-tract tissue characteristics in patients with TLE (Concha et al. 2012, Glenn et al. 2016). In the present study, TRACULA methods were applied in order to investigate within-tract alterations in TLE, and to determine whether these regional alterations are influenced by the extent of HA and clinical variables. Unlike other methods frequently used that are limited to confined WM structural diffusivity analysis via ROI analysis (Keller et al. 2012) or tract-based spatial statistics (Smith et al. 2006) based on diffusion metric maps in the standard International Consortium for Brain Mapping (ICBM) template space, TRACULA allows whole-brain tractography. Despite the potential advantages of utilizing automated tractography approaches, TRACULA has only recently been used in an increased number of clinical studies, including schizophrenia (Yendiki et al. 2011), bipolar disorder (Sprooten et al. 2016), myotonic dystrophy (Wozniak et al. 2014) and Alzheimer's disease (Lee et al. 2015a). Even though neuroscientists are paying more attention to tract analysis techniques such as TRACULA, there have been no applications to date in epilepsy, which is characterized by regional GM and WM pathology.

6.1.1 Objectives and Hypotheses

The overall goal of the present study was to apply an automated probabilistic tractography approach and to determine the extent of pre-surgical diffusion alterations in patients with TLE and whether these would be correlated with clinical variables or degree of HA. There were four study objectives:

Objective 6.1

To investigate diffusion alterations of whole temporal lobe WM tracts in patients with left and right TLE relative to healthy controls using an automated probabilistic tractography approach. It was hypothesized that the automated method can identify diffusivity changes (in FA and MD values of temporal lobe WM tracts) relative to controls and among the two patient groups.

Objective 6.2

To investigate alterations along WM tracts using waypoint comparisons for ipsilateral and contralateral tracts between patient groups based on side of seizure onset and other clinical factors (e.g. history of febrile seizures). It was hypothesized that WM tract diffusivity measures in patients are more extensively affected ipsilaterally and in the presence of unfavorable clinical factors such as greater seizure frequency, longer epilepsy duration, history of SGTC/febrile seizures, and earlier age of onset.

Objective 6.3

To determine the relationship between regional WM tract diffusivity and the degree of hippocampal (subfield) atrophy in patients with TLE. As HS is seen as an initial precipitating injury (Pitkänen and Lukasiuk 2011), it was hypothesized that no relationship between hippocampal volume and WM tract diffusion characteristics would be found, but rather that regional WM tract diffusivity is mediated by unfavorable clinical factors of the disorder such as epilepsy duration and age of onset.

Objective 6.4

To investigate whether patients with postoperative seizures and those who were rendered seizure free after surgery could be differentiated based on preoperative WM tract diffusivity measures. It was hypothesized that patients with persistent postoperative seizures would have more extensive abnormal diffusivity measures in ipsi- and contralateral temporal lobe tracts (such as the UF and CAB) than patients who were rendered seizure free.

6.1.2 Organization of Chapter

Demographic and clinical details of all study participants, the methods of diffusion imaging processing, tractography and statistical analyses are presented in Section

6.2. Results from group-wise statistical testing and correlation analysis are presented in Section 6.3. Within Section 6.4 the significant findings from this study are briefly presented in relation to the objectives.

6.2 Methods

6.2.1 Participants

64 patients with well-characterized TLE and associated ipsilateral HS (41 patients with left TLE, 23 patients with right TLE) and 44 age- and sex-matched controls were studied. Age and sex did not differ significantly between patients and controls and no significant difference in any of the clinical variables ($p>0.05$) between patients with left and right TLE were found (Table 6.1).

Radiological evidence of HS was assessed by an experienced neuroradiologist using standard criteria, including hippocampal volume loss and internal structural disruption on T1w MRI and/or hyperintensities on T2w/FLAIR images (Keller et al. 2015a, 2015b). There was no evidence of bilateral HS in any patient or of a secondary extrahippocampal lesion that may have contributed to seizures (Keller et al. 2015a). All patients underwent comprehensive pre-surgical evaluation, and all had a confident diagnosis of mesial TLE based on semiological, electrophysiological and imaging investigations (Kral et al. 2002). All patients underwent amygdalahippocampectomy and HS was confirmed histologically using standard criteria (Blümcke et al. 2013). Post-surgical seizure outcome was assessed using the ILAE outcome classification system (Wieser et al. 2001). All patients had a minimum of 1 year and an average of 2 years of postoperative follow-up. All patients and controls provided written informed consent and the local ethics committee approved this study (Keller et al. 2015b).

Variable	Group			Statistics	
	Left TLE	Right TLE	Controls	Statistic	p-value
N	41 (38%)	23 (21%)	44 (41%)	-	-
Sex (female / male)	26 / 15	10 / 13	29 / 15	$\chi^2 (2) = 3.5$	0.2
Febrile seizures (no / yes)	20 / 8	10 / 5	-	$\chi^2 (1) = 0.1$	0.8
SGTCS (no / yes)	15 / 13	9 / 6	-	$\chi^2 (1) = 0.2$	0.7
Outcome (ILAE I / ILAE II-VI)	9 / 16	10 / 5	-	$X^2 (1) = 3.5$	0.06
Variables with Mean (SD)					
Age (years)	43.8 (13)	41.3 (14.9)	43.2 (14.2)	$F (2, 107) = 0.24$	0.8
Age at onset in years	18 (12.3)	14.3 (11.5)	-	$T (62) = 1.2$	0.3
Duration in years	22.7 (13.1)	22 (17.5)	-	$T (62) = 0.17$	0.9
Seizure frequency, months	5.4 (3.9)	9.4 (22.4)	-	$T (41) = -0.9$	0.4
Seizure burden	1.9 (0.45)	1.8 (0.44)	-	$T (41) = 0.9$	0.4

Table 6.1. Demographic and Clinical Variables According to Seizure Laterality.

Abbreviation: TLE = Temporal Lobe Epilepsy. The conducted statistical tests were Chi-Squared tests of independence for the first three variables; one-way ANOVA for age and unpaired two-tailed t-tests for all remaining clinical variables.

6.2.2 MR Acquisition

Each participant underwent MRI at the Life & Brain Center in Bonn on a 3 Tesla scanner. 3D T1w and DTI were acquired for all participants. All scanning and imaging parameters are detailed in Chapter 2, Section 2.2.

6.2.3 Data Pre-processing

For each participant automated segmentation and cortical parcellation of T1w data was performed using Freesurfer version 5.3.0. The standard Freesurfer “recon-all” processing stream was used, which provides surfaces and morphometry data for each subject (Keller et al. 2012) in addition to GM/WM segmentations. This information was also subsequently used to restrict tractography analysis to WM. However, before tensor fitting and tractography were performed within Freesurfer (TRACULA

version 1.56), DTI data was processed using the ENIGMA DTI-preprocessing steps (<http://enigma.ini.usc.edu/protocols/dti-protocols/>). In particular, the first b0 image was used as a reference for co-registration of subsequent b0 images (FSL FLIRT, Smith et al. 2004). The resulting co-registered b0 images were averaged and served as a reference image during motion correction on the diffusion-weighted images. The gradient table information was adjusted accordingly (Leemans and Jones 2009). Subsequently the data was processed in order to account for geometric distortions, this was performed on the mean b0 image via the T1w image. In order to achieve distortion correction, the T1w image was rigidly aligned with the mean b0 image (Smith et al. 2004) and the mean b0 image was nonlinearly registered to this T1w image in diffusion space using Advanced Normalization Tools (<http://stnava.github.io/ANTs/>). The resulting nonlinear registration information was used to unwarp subsequent diffusion-weighted images in native diffusion space. TRACULA's default tensor fitting and tract reconstruction pipelines using the ball-and-stick model were applied to the pre-processed data.

6.2.4 Quality Assessment after Pre-processing

The DTI data, T1w Freesurfer segmentations and anatomical alignment of the co-registered b0/T1 images were assessed visually. TRACULA's performance in tract reconstruction was then visually appraised so that any failed reconstructions could be re-initialized in order to recover the tracts.

As DTI-derived scalar metrics have been shown to vary with SNR (Farrell et al. 2007), the SNR for every diffusion-weighted image was calculated through TRACULA using the mean of the signal intensity of the whole brain WM divided by the standard deviation of the same area. All SNR values were averaged for each participant for further statistical analysis. As all SNR values are derived from whole-brain images acquired on the same scanner, variability is expected to be low and normally distributed. The data was tested for normality and for differences in mean

SNR of all three groups using a One-Way ANOVA (data normally distributed, Lilliefors $p > 0.05$).

Diffusion metrics have been shown to be vulnerable to differences in motion across patient-control cohorts. Therefore any differences in the total motion index (TMI) between patients with left and right TLE and controls were assessed. The TMI has been previously defined as a summary value, which takes average translation/rotation, slice dropout and dropout severity into account and may reduce the number of false positives when used as a nuisance regressor during analysis of data collected on study participants who have moved differently (Yendiki et al. 2013). The data was tested for normality and for differences in mean TMI of all three groups using a Kruskal-Wallis ANOVA (data non-normally distributed, Lilliefors < 0.05). Multiple comparison correction was performed using the Dunn-Sidak approach (Dunn 1964).

6.2.5 Extraction of Volumes and Tracts

For patients and controls ICV, left and right hippocampal volumes were extracted from Freesurfer's recon-all segmentation step (Table 6.2). Subsequently, tract DTI-derived scalar metrics (FA and MD) were extracted for those tracts previously reported to be affected in patients with TLE using manual tractography techniques. The following temporal lobe tracts were analyzed: the SLFt, ILF, UF and CAB (otherwise referred to as PHWM) (Figure 6.1). Unfortunately, TRACULA does not provide tract reconstruction of the fornix, therefore it was not possible to investigate this structure in the present study. TRACULA directly provides tract mean DTI-derived metric values. Value extraction was confined to the center of the tract for all tracts investigated (the average over the highest-probability path) as extraction from a larger tract region with a lower pathway probability may potentially occlude any localized effects as more voxels not showing any effects would be included.

Variable	Side	M (SD) in mm ³			Comparisons (corrected p-values)			Statistics	
		ITLE	C	rTLE	LTLE	ITLE	C	X ² - statistic	p- value
					vs C	vs rTLE	vs rTLE		
Intracranial volume (ICV)	whole brain	1504800 (261470)	1645200 (122970)	1568100 (23783)	<0.05	0.79	0.47	6.6	<0.05
Hippocampal volume	left	0.2 (0.06)	0.27 (0.02)	0.27 (0.03)	<0.001	<0.001	0.9	35.2	<0.001
corrected for ICV (%)	right	0.3 (0.05)	0.27 (0.02)	0.2 (0.04)	0.9	<0.001	<0.001	40.5	<0.001

Table 6.2. Kruskal-Wallis ANOVA Comparing Volumes across all groups.

M = Mean; SD = Standard Deviation; TLE = Temporal Lobe Epilepsy; C = Control; r = right; l = left.

6.2.6 Statistical Analysis

Results were considered significant at $p < 0.05$. Statistical testing was performed using a Macintosh Laptop OSX 10.9.2 running MATLAB R2015b. As native space volumes and tracts cannot be assumed to be normally distributed due to inter-subject variability the normality of the data was tested. Given that the data pertaining to hippocampal/intracranial volumes and DTI-derived metric values were non-normally distributed (Lilliefors $p < 0.05$), non-parametric tests were used for analysis. Patient-control group comparisons on hippocampal volumes and ICV were performed using a Kruskal-Wallis ANOVA, with a Dunn-Sidak correction for multiple comparisons (Dunn 1964). Patient-control group comparisons on mean tract diffusion metrics were performed using a non-parametric ANCOVA with a single regression model accounting for both multiple comparisons and TMI (Conover and Iman 1982).

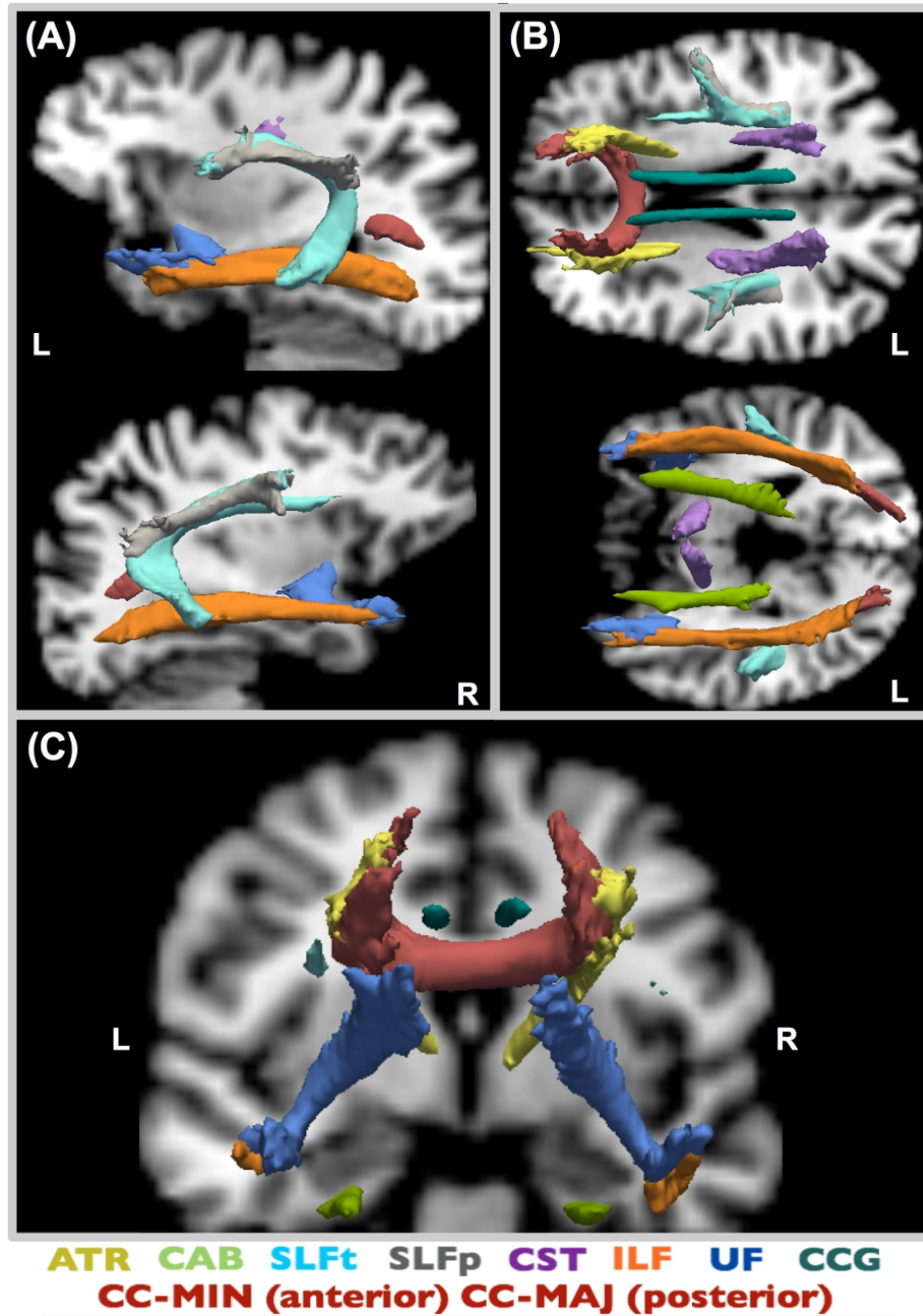


Figure 6.1. All reconstructed TRACULA tracts.

Estimated probability tracts from TRACULA are overlaid on T1w (native space, control) and shown in sagittal (A), axial (B) and coronal (C) views at 20% of maximum probability. TRACULA tracts analyzed: CAB, SLFt, ILF and UF. R=Right; L=Left; CC-MIN=corpus callosum (forceps minor); CC-MAJ=corpus callosum (forceps major); ATR=anterior thalamic radiations; UF=uncinate fasciculus; ILF=inferior longitudinal fasciculus; CAB=cingulum angular bundle; SLFt=superior longitudinal fasciculus (temporal segment); SLFp=superior longitudinal fasciculus (parietal segment); CST=corticospinal tract; CCG=cingulum–cingulate gyrus bundle.

Additionally the patients were dichotomously grouped according to presence of childhood FC and SGTCS and differences in DTI-metrics using the unpaired Wilcoxon-rank-sum test were investigated. TRACULA offers a DTI-metric value along the trajectory of a pathway through generating a weighted average of the respective values over all sampled paths for a particular tract. As native space tracts had a slightly different length for each data set and the endings did not always correspond, shorter tracts contained some NaN ('not a number') waypoints, which were ignored in statistical testing. This comparison was based solely on native space tract values and did not represent a voxel-based approach, where each voxel represents the same type of region of tissue after normalization to standard space. However, in order to visualize differences between patients and controls along the different tracts, mean tract paths in MNI space were generated. Waypoint average FA/MD values along the native space tracts were separately compared between patients with left/right TLE and controls using a non-parametric ANCOVA and a single regression model, which accounted for both multiple comparisons and TMI. The unpaired Wilcoxon-Rank-Sum test was performed on patients with and without history of childhood FC and presence of SGTCS. As multiple locations along a tract were analyzed, significance levels were corrected with the FDR procedure by Benjamini and Hochberg (1995) and considered significant at $p < 0.05$.

Correlations between whole-tract and waypoint DTI-metrics with extent of HA and clinical information were investigated using Pearson product-moment linear correlation coefficients. Clinical information included age, age at onset of epilepsy, duration of epilepsy and seizure burden. Hippocampal volume was corrected for ICV and duration was corrected for patient age to control for the effects of normal brain maturation. Seizure burden was defined as $\log_{10}(\text{frequency} \times \text{duration})$. The logarithm was applied in order to accommodate patients with very high seizure frequency. Significance levels were corrected with the FDR procedure and considered significant at $p < 0.05$.

Finally, waypoint tract diffusion metrics of patients with optimal (ILAE I) and suboptimal (ILAE II-VI) post-surgical outcomes were compared to those of the controls. In order to achieve this, the data collected on patients with right TLE (N=23) was side-flipped to allow ipsilateral/contralateral analysis. The same proportion (36%) of controls (N=16) was also side-flipped to avoid any left-right bias (Keller et al. 2015a). Correlations between waypoint DTI-metrics and outcome were investigated using the Pearson product-moment linear correlation coefficients.

6.3 Results

6.3.1 Data Quality Assessment

Visual assessment revealed satisfactory T1w Freesurfer segmentations and excellent anatomical agreement between b0 and T1w images after co-registration. Using the conventional image processing stream for TRACULA, at least one tract was only partially reconstructed in 50 participants (46%). However, all tracts were successfully reconstructed after reinitialization.

No significant difference between groups were found for SNR (left TLE: Mean=4.02, SD=0.22; right TLE: Mean=4.03, SD=0.21; controls: Mean=3.94, SD=0.19); $F(2,107)=2.15$ $p=0.12$. However, the study did show that the TMI was significantly different between patients with left TLE (mean TMI = -0.6, SD = 0.95), right TLE (mean TMI = -0.7, SD = 0.99) and controls (mean TMI = 1.2, SD = 0.99) ($\chi^2(2,107)=52.1$ $p=4.9*10^{-12}$). Post hoc testing revealed that controls had a higher TMI than either patient group ($p<0.001$), whereas the two patient groups did not differ significantly among each other ($p=0.9$). The TMI value was entered as a nuisance regressor into the non-parametric ANCOVA in order to mitigate confounding effects on patient-control comparisons (Yendiki et al. 2013).

6.3.2 Patients vs Controls

6.3.2.1 Volumes

There were no differences in ICV between patient groups. However, ICV was significantly smaller for patients with left TLE relative to controls (Table 6.2). Patients with left TLE and right TLE had significantly smaller ipsilateral hippocampal volumes (corrected for ICV) than controls. There was no evidence of contralateral HA in patients relative to controls. None of the demographic (age) or clinical variables (age at onset, duration corrected for age and seizure burden) correlated with ipsilateral hippocampal volumes (corrected for ICV).

6.3.2.2 Whole-tract Diffusion Metric Analysis

Whole-tract FA values are presented in Figure 6.2 and Table 6.3. Patients with left TLE had a significant decrease in FA of all tracts (except ipsilateral SLFT) in both hemispheres compared to controls. Relative to controls, patients with right TLE had a significant decrease in FA in all ipsilateral tracts, and a decrease in FA in contralateral UF and CAB.

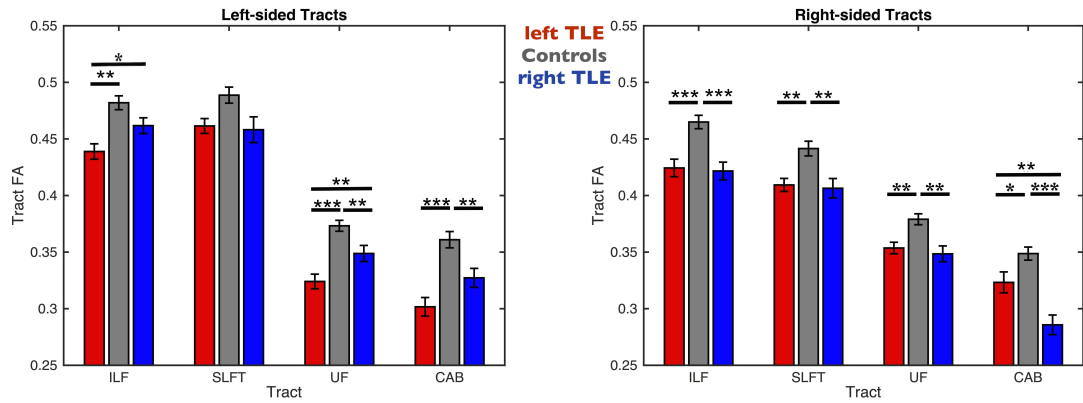


Figure 6.2. FA Values from TRACULA Tracts ILF, SLFT, UF and CAB.

The plot shows mean center tract FA distributions along with error bars for left and right tracts of patients with left TLE (red bars), controls (gray bars) and patients with right TLE (blue bars). Asterisks and bars show significantly reduced FA values for patients when comparing to controls and between the two patient groups. $*p < 0.05$; $**p < 0.01$; $***p < 0.001$, corrected for multiple comparisons.

Tract	Side	M (SD)			p-values from regression model			Statistics	
		ITLE	C	rTLE	ITLE	ITLE	C	F-statistic	p-value
					vs C	vs rTLE	vs rTLE		
SLFt	left	0.46 (0.04)	0.49 (0.05)	0.46 (0.05)	0.2	0.9	0.33	4	<0.05
	right	0.41 (0.04)	0.44 (0.04)	0.41 (0.04)	<0.01	0.69	<0.01	7.05	<0.01
ILF	left	0.44 (0.04)	0.48 (0.04)	0.46 (0.03)	<0.01	<0.05	0.29	4.06	<0.05
	right	0.42 (0.05)	0.46 (0.04)	0.42 (0.04)	<0.001	0.59	<0.001	11.78	<0.001
UF	left	0.32 (0.04)	0.37 (0.03)	0.35 (0.03)	<0.001	<0.01	<0.01	16.5	<0.001
	right	0.35 (0.03)	0.38 (0.03)	0.35 (0.03)	<0.01	0.68	<0.01	7.01	<0.01
CAB	left	0.3 (0.05)	0.36 (0.05)	0.33 (0.04)	<0.001	0.09	<0.01	6.2	<0.01
	right	0.32 (0.06)	0.35 (0.04)	0.29 (0.04)	<0.05	<0.01	<0.001	15.2	<0.001

Table 6.3. Non-parametric ANCOVA Comparing FA across all groups.

M = Mean; SD = Standard Deviation; TLE = Temporal Lobe Epilepsy; C = Control; l = left; r = right; FA = fractional anisotropy; SLFt = superior longitudinal fasciculus (temporal segment); ILF = inferior longitudinal fasciculus; UF = uncinate fasciculus; CAB = cingulum angular bundle. Corrected p-values.

Additionally, a significant decrease in FA in the left UF and ILF in patients with left TLE relative to patients with right TLE and a significant decrease in FA in patients with right TLE in the right CAB relative to patients with left TLE were detected. Across all patients, whole-tract FA values did not correlate with ipsilateral hippocampal volumes. There were significant correlations between patient age and FA in the ipsilateral ($\rho=-0.4$, $p<0.01$) and contralateral ($\rho=-0.26$, $p<0.05$) UF and the contralateral SLFt ($\rho=-0.36$, $p<0.01$). Duration of epilepsy (corrected for age) was significantly correlated with FA in the contralateral UF ($\rho=-0.27$, $p<0.05$). Seizure burden was significantly correlated with FA values in the ipsilateral ($\rho=-0.33$, $p<0.05$) and contralateral ($\rho=-0.32$, $p<0.05$) UF. Age at onset of epilepsy and seizure frequency did not correlate with FA in any tract. Whole-tract MD values are presented in Figure 6.3 and Table 6.4. Larger patient-control differences were observed in MD relative to FA. Patients with left and right TLE had bilateral increase in MD of all tracts (except for left SLFT in patients with right TLE) relative to

controls. Additionally, increased MD in the left CAB in patients with left TLE relative to patients with right TLE and increased MD in the right UF in patients with right TLE relative to patients with left TLE were found. Whole-tract MD values did not correlate with ipsilateral hippocampal volume.

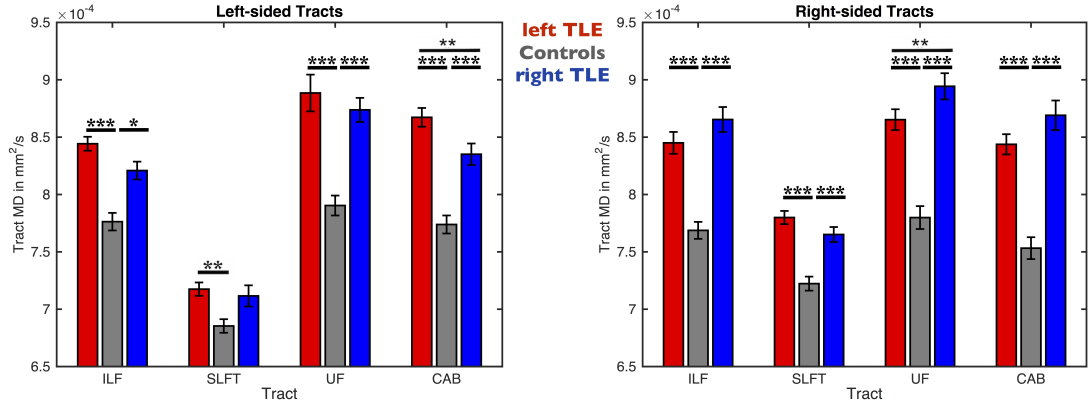


Figure 6.3. MD Values from TRACULA Tracts ILF, SLFt, UF and CAB.

The plot shows mean center tract MD distributions along with error bars for left and right tracts of patients with left TLE (red bars), controls (gray bars) and patients with right TLE (blue bars). Asterisks and bars show significantly reduced MD values for patients when comparing to controls. * $p < 0.05$; ** $p < 0.01$; *** $p < 0.001$, corrected for multiple comparisons.

Age correlated with the MD of the ipsilateral SLFt ($\rho = 0.35$, $p < 0.01$). Duration of epilepsy (corrected for age) was significantly correlated with MD in the ipsilateral ($\rho = 0.3$, $p < 0.05$) and contralateral ($\rho = 0.46$, $p < 0.001$) UF and with the contralateral ILF ($\rho = 0.3$, $p < 0.05$). Seizure burden was significantly correlated with MD in the contralateral UF ($\rho = 0.31$, $p < 0.05$). Age at onset of epilepsy was significantly correlated with MD of the contralateral UF ($\rho = -0.35$, $p < 0.01$). Seizure frequency did not correlate with any diffusion measure. There were no significant differences in FA or MD of any tract between patients with / without a history of childhood FC, or between those with / without secondary seizure generalization ($p > 0.05$).

Tract	Side	M (SD) (in 10^{-4} mm ² /s)			p-values from regression model			Statistics	
		ITLE	C	rTLE	ITLE	ITLE	C	F-statistic	p-value
					vs	vs	vs		
					C	rTLE	rTLE		
SLFt	left	7.2 (0.4)	6.9 (0.4)	7.1 (0.4)	<0.01	0.5	0.07	6.5	<0.01
	right	7.8 (0.4)	7.2 (0.4)	7.7 (0.3)	<0.001	0.17	<0.001	20.5	<0.001
ILF	left	8.4 (0.4)	7.8 (0.5)	8.2 (0.4)	<0.001	0.28	<0.05	17.24	<0.001
	right	8.4 (0.6)	7.7 (0.5)	8.7 (0.5)	<0.001	0.06	<0.001	41.8	<0.001
UF	left	8.9 (1)	7.9 (0.6)	8.7 (0.5)	<0.001	0.74	<0.001	18.9	<0.001
	right	8.7 (0.6)	7.8 (0.7)	8.9 (0.5)	<0.001	<0.05	<0.001	33.02	<0.001
CAB	left	8.7 (0.5)	7.7 (0.5)	8.4 (0.4)	<0.001	<0.05	<0.001	26.8	<0.001
	right	8.4 (0.6)	7.5 (0.6)	8.7 (0.6)	<0.001	0.14	<0.001	38.2	<0.001

Table 6.4. Non-parametric ANCOVA Comparing MD across all groups.

M = Mean; SD = Standard Deviation; TLE = Temporal Lobe Epilepsy; C = Control; l = left; r = right; FA = fractional anisotropy; SLFt = superior longitudinal fasciculus (temporal segment); ILF = inferior longitudinal fasciculus; UF = uncinate fasciculus; CAB = cingulum angular bundle. Corrected p-values.

6.3.2.3 Waypoint Diffusion Metric Analysis

Waypoint comparisons along the native tracts are shown in Figure 6.4 and revealed regionally reduced FA within the UF, ILF and CAB, predominantly ipsilateral to seizure onset, with fewer widespread changes in contralateral tracts. For both patient groups, tract alterations were more widespread in analysis of MD and affected ipsi- and contralateral tracts.

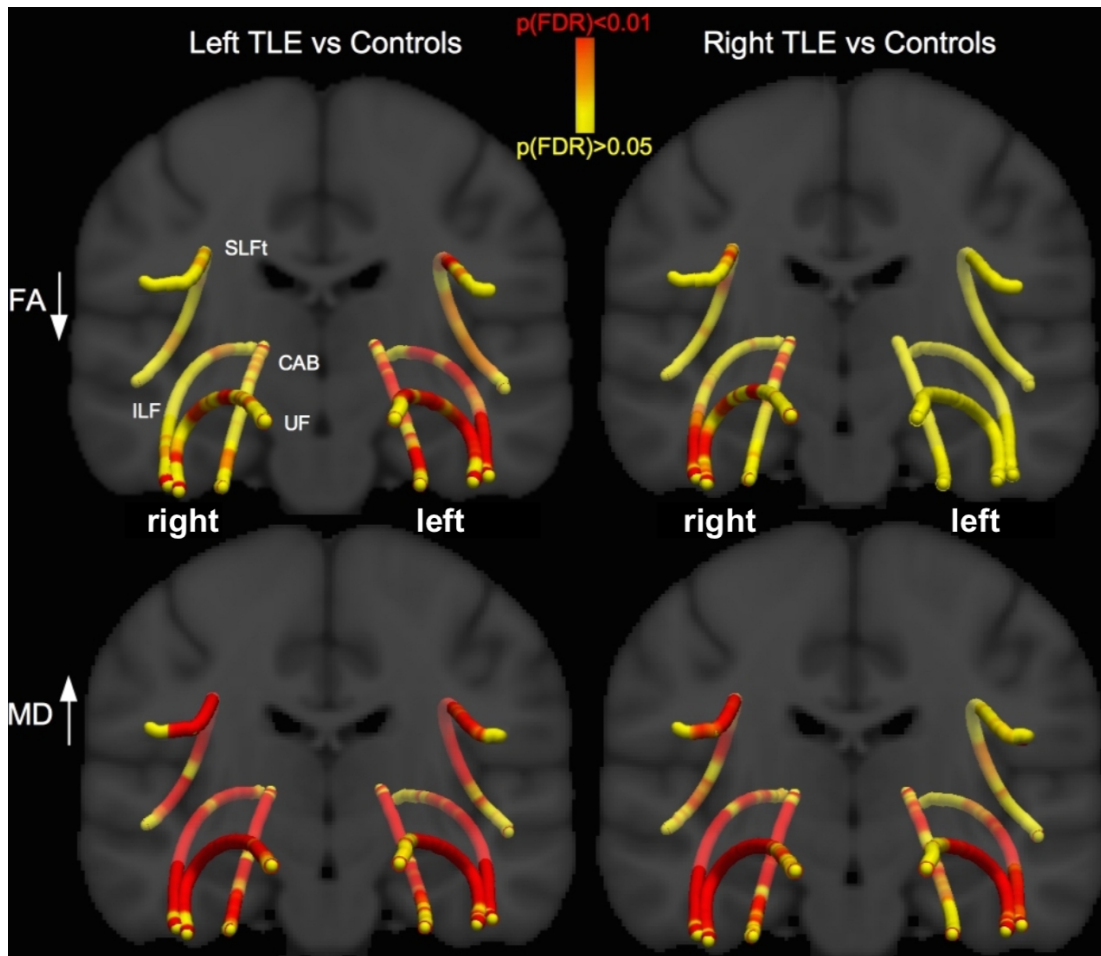


Figure 6.4. Waypoint comparison p-values along the tracts.

Differences between the patient groups and controls are shown projected onto a T1w template. Red regions show significantly reduced FA (first row) and increased MD (second row) relative to controls. Changes are more pronounced in MD than in FA and patients with left TLE are more bilaterally affected than patients with right TLE. TLE = Temporal Lobe Epilepsy; FA = fractional anisotropy; MD = mean diffusivity; SLFt = superior longitudinal fasciculus - temporal segment; CAB = cingulum angular bundle; ILF = inferior longitudinal fasciculus; UF = uncinate fasciculus.

For both FA and MD, patients with left TLE showed more extensive bilateral changes (FA of contralateral ILF/UF, MD of SLFt) than patients with right TLE (only a small region affected in FA of contralateral ILF, MD abnormalities were not observed in at least a third of the length of contralateral tracts). Along-the-tract DTI-metrics and extent of ipsilateral HA were not correlated. There were significant

correlations between patient age and FA of the bilateral UF/SLFt and MD contralaterally. Correlations between FA/MD and clinical variables are shown in Figure 6.5. Duration of epilepsy was significantly correlated with FA and MD in anterior temporal sections of UF and ILF. Younger age at onset of TLE did not correlate with FA, but there was a significant correlation with MD in the anterior temporal lobe portions of the ipsilateral UF and ILF. Seizure burden was significantly correlated with FA in anterior regions of the ipsilateral UF. Seizure frequency did not correlate with any diffusion measure.

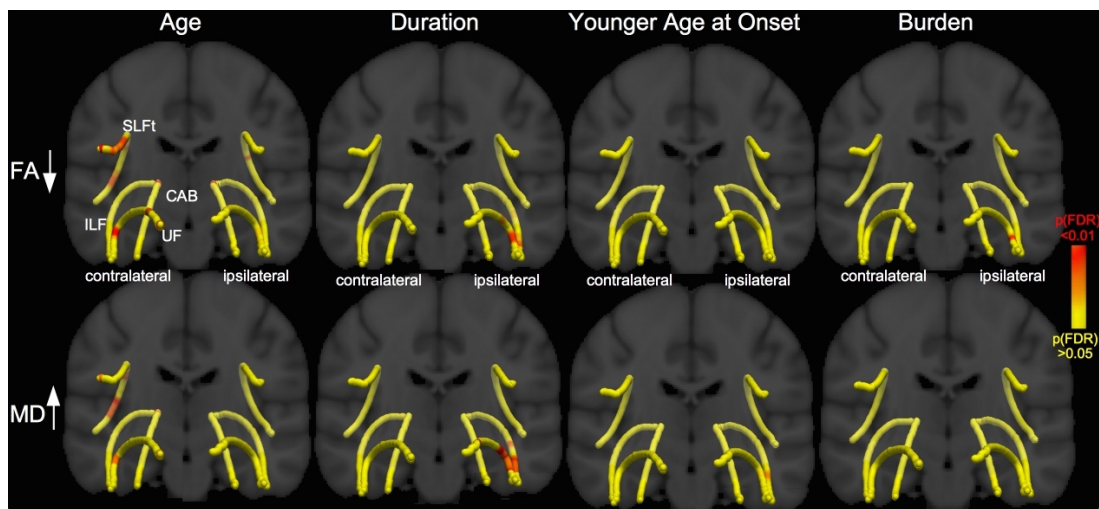


Figure 6.5. Waypoint correlation p-values along the tracts according to side of seizure onset. Relationships between the DTI-metrics and clinical variables are shown projected onto a T1w template and mean tract pathways. Red regions show significant correlations with reduced FA (first row) and increased MD (second row). Relationships between duration (corrected for age) and FA/MD of ipsilateral anterior UF and ILF regions and correlations between age at onset (MD of UF/ILF) and seizure burden (FA of UF) were found. FA = fractional anisotropy; MD = mean diffusivity; SLFt = superior longitudinal fasciculus - temporal segment; CAB = cingulum angular bundle; ILF = inferior longitudinal fasciculus; UF = uncinate fasciculus.

There were no significant differences in FA or MD along any tract between patients with / without a history of childhood FC, or between those with / without secondary seizure generalization ($p > 0.05$). Results obtained from comparing FA and MD values of patients with excellent outcomes (ILAE I) and suboptimal outcomes (ILAE II-VI)

against controls are presented in Figure 6.6.

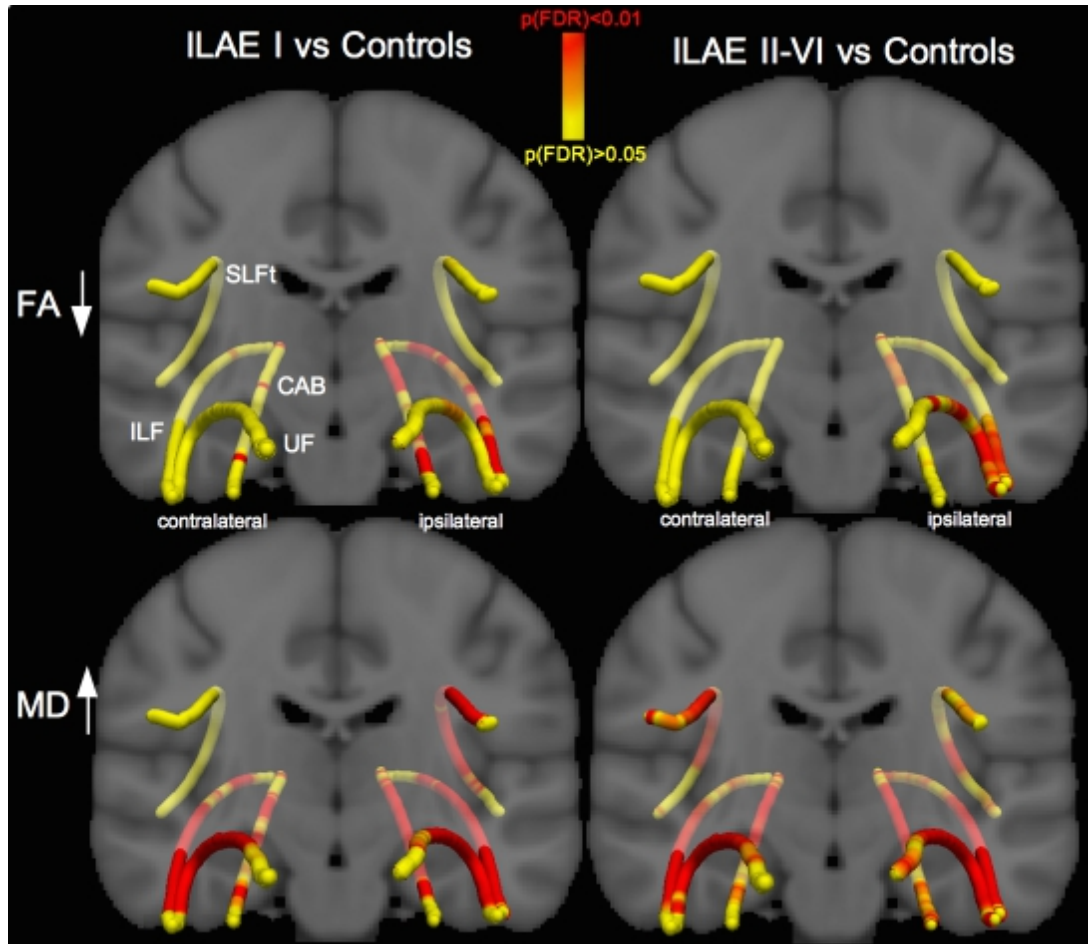


Figure 6.6. Waypoint comparison p-values along the tracts according to outcome. Differences between the patient groups and controls are shown projected onto a T1w template. Red regions show significantly reduced FA (first row) and increased MD (second row) relative to controls. Changes are more pronounced in MD than in FA and patients with ILAE II-IV are affected in the contralateral SLFt (increase of MD relative to controls) whereas patients with ILAE I did not show this change. TLE = Temporal Lobe Epilepsy; FA = fractional anisotropy; MD = mean diffusivity; SLFt = superior longitudinal fasciculus - temporal segment; CAB = cingulum angular bundle; ILF = inferior longitudinal fasciculus; UF = uncinate fasciculus.

When comparing patients with ILAE I outcomes against controls, a decrease in FA in anterior and posterior sections of the ipsilateral CAB and along the entire length of

the ipsilateral ILF with relative sparing of the ipsilateral UF could be noted. Contralaterally, only two (CAB) and one (ILF) small region within those tracts showed a decrease in FA relative to controls survived FDR correction. Ipsilaterally, the FA values of the UF, anterior ILF and posterior CAB were decreased in patients with ILAE II-VI relative to controls. Within this patient group, an increase in MD values of the contralateral SLF was found relative to controls, which was not seen in patients with excellent outcomes. In summary, diffusion alterations are more pronounced in MD than in FA measures and patients with ILAE I showed ipsilateral diffusion alterations when compared to controls, while patients with suboptimal outcomes (ILAE II-VI) also showed contralateral diffusion alterations when compared to controls. Waypoint diffusion metrics did not show any correlation with outcome.

6.4 Summary

The overall aim of this study was to apply a novel automated WM tractography approach to patients with TLE and established HS and healthy controls. There were four primary objectives of the present study.

Objective 6.1

Diffusion alterations of whole temporal lobe WM tracts in patients relative to healthy controls

Whole-tract FA/MD abnormalities were observed in nearly all temporal lobe tracts investigated (except left SLFt), the effects being observed bilaterally, but most strongly ipsilaterally. Tract diffusion alterations were more strongly bilaterally distributed in patients with left TLE.

Objective 6.2

Diffusion alterations along ipsi- and contralateral temporal lobe WM tracts

This investigation confirmed that in patients with right/left TLE ipsilateral tracts were more extensively affected than contralateral tracts. Additionally, specific regions within tracts that demonstrate these alterations in diffusion characteristics could be identified. For example, patients with right TLE mainly showed decreased FA in the temporepolar regions of the UF and ILF, while patients with left TLE were affected throughout the length of the temporal tracts. No alterations were found between patients with SGTCS/FC and those without.

Objective 6.3

Regional WM tract diffusivity and degree of hippocampal (subfield) atrophy

The extent of HA was not related to (i) the degree of FA and MD alterations of temporal lobe tracts or (ii) the clinical characteristics of patients, whereas diffusion alterations of ipsilateral temporal lobe tracts were significantly related to age at onset of epilepsy, duration of epilepsy and epilepsy burden but not frequency of seizures.

Objective 6.4

Preoperative WM tract diffusivity measures in patients with and without postoperative seizure symptoms

Although not statistically significant ($p=0.06$), this study showed a trend that patients with right-sided TLE were more likely to be seizure-free after surgery, than those with left-sided TLE. Patients with excellent outcomes had more ipsilaterally distributed WM tract diffusion alterations than patients with persistent postoperative seizures, who were affected more extensively and bilaterally.

Chapter 7: Neuroradiological Findings in Patients with 'non-lesional' Focal Epilepsy Revealed by Research Protocol

Chapter 7: Neuroradiological Findings in Patients with 'non-lesional' Focal Epilepsy Revealed by Research Protocol.....	130
7.1 Introduction.....	130
7.2 Materials and Methods.....	132
7.3 Results.....	133
7.4 Discussion.....	143

7.1 Introduction

The detection of a brain abnormality on MRI (Téllez-Zenteno et al. 2010, Lerner et al. 2009, Mosewich et al. 2000, Jehi et al. 2007) in addition to concordant focal EEG spike discharges (Siegel et al. 2004, Janszky et al. 2000, Berg et al. 2003) has been related to good surgical outcomes, while patients with no remarkable MRI findings are rendered seizure free less often (Berg et al. 2003, Holmes et al. 2000, Scott et al. 1999). Unfortunately, it is not uncommon for patients with severe seizure activity to present with an unremarkable MRI. However, it is likely that (subtle) epileptogenic lesions are not detected on routine clinical MRI and contribute to ongoing seizure activity. It is important that (i) the MRI protocol and (ii) subsequent qualitative and quantitative assessment of the images is specifically tailored for patients with epilepsy so that potentially small lesions causing debilitating seizures can be detected and treated. Several publications so far have discussed the factors that can increase accuracy of lesion detection through MRI in clinical practice (ILAE 1997, von Oertzen et al. 2002, Duncan et al. 2016, Friedman 2014). In one study, outcome after surgery improved significantly with the introduction of an epilepsy dedicated MRI protocol, which allowed depiction of epilepsy related lesions (e.g. HS) rather than applying a standardized MRI protocol not suitable for identifying these lesions (von Oertzen et al. 2002). Nevertheless, the authors state that even with a dedicated

protocol, optimization of acquisition parameters (e.g. angulation according to the presumed seizure onset zone) may be necessary for individual patients (von Oertzen et al. 2002). Overall, when correlating radiological findings with histopathology, neuropathological diagnoses were predicted correctly in 89% of epilepsy dedicated MRI reports but only by 22% of 'non-expert' reports (MRI assessed by radiologists not attached to epilepsy centers) based on standard MRI (von Oertzen et al. 2002). Consequently, an early referral to a specialist epilepsy center may increase the lesion detection rate. Hardware may also play a role: Phal et al. (2008) and Winston et al. (2013b) reported an up to 30% increase in diagnostic yield of 3 Tesla images versus 1.5 Tesla, which is mainly due to a higher SNR facilitating detection of focal epileptogenic lesions.

The goal of this study of patients with focal refractory epilepsy was to apply a dedicated epilepsy research protocol for patients with 'non-lesional' epilepsy. This required the recruited patients to have received previous clinical MRI (no dedicated epilepsy research protocol) with no discernible brain abnormality. Patients with imaging performed on 1.5 Tesla and 3 Tesla scanners, with and without dedicated clinical epilepsy protocols were included. Considering the previous reports of increased diagnostic yield using 3T as opposed to 1.5 Tesla MRI (Phal et al. 2008, Winston et al. 2013b) and the application of epilepsy dedicated MRI protocols (von Oertzen et al. 2002), the objective of the present chapter was to determine whether the use of a dedicated epilepsy research protocol in a specialist hospital of neurology and neurosurgery would benefit lesion conspicuity and identification.

Importantly, a subset of MRI could be assessed to illustrate if MR hardware, image signal decay due to artifacts (e.g. head motion), radiological expertise or the protocol had an influence on the individual diagnosis at the time. Failure to identify lesions earlier may have multiple reasons and may be directly linked to lesion conspicuity. The work conducted in this chapter may provide important clinical information on the number of patients who have epileptogenic lesions but have unremarkable MRI by virtue of previous imaging protocols not dedicated to highlight epileptogenic

lesions. Identification of an underlying brain abnormality can potentially afford important implications for treatment consequences, such as earlier referral for epilepsy surgery for patients with focal medically refractory epilepsies. According to Wiebe and Jette (2012b) surgery has been shown to be cost-effective (Wiebe et al. 1996), to save lives (Bell et al. 2010) and improve quality of life through seizure frequency reduction (Seiam et al. 2011). Consequently, epilepsy surgery may afford many advantages over the continued use of AEDs for the individual patient.

Objective 7.1

The ultimate aim of this study was to evaluate whether a dedicated epilepsy research protocol with expert image re-evaluation can increase identification of patients with lesions. The earlier MRI was included in an evaluation of lesion conspicuity to qualitatively re-evaluate factors likely to have contributed to the new presentation of a lesion. It was hypothesized that multiple factors such as image quality, lesion conspicuity on standard MRI (not specialized in depicting epilepsy-related lesions) and neuroradiologists' expertise in identifying epilepsy-related lesions contribute to varying results of MRI reports.

7.2 Materials and Methods

43 patients (26 female; mean age \pm std = 31.6 \pm 11, range 19-61) with focal refractory epilepsy who had failed at least two trials of AED treatments were studied. Patients were prospectively recruited into the study if previous clinical MRI was deemed to be 'non-lesional' by the clinicians involved in the initial assessment (this included general radiologists at other trusts and neuroradiologists at the WCFT). Localization of seizure onset had been thoroughly evaluated using seizure semiology and scalp EEG investigations at the WCFT in Liverpool, UK. All technical details pertaining to hard- and software are detailed in Chapter 2. Each participant received 3D T1w, T2w, T2FLAIR sequences and two coronal images (2D T1FLAIR and T2FLAIR) aligned with the long axis of the hippocampus and these were assessed by a neuroradiologist. In those patients, who had a lesion identified on the most recent

dedicated epilepsy research MRI, the previous clinical MRI was included. The previous clinical MRI of individual patients was re-evaluated through neuroradiological reassessment (performed by Dr Kumar Das and Dr Shubhabrata Biswas) in order to determine the factors influencing the accuracy and confidence of visual lesion detection. The details of the scanner hardware (e.g. 3T and 32-channel head coil) and sequence acquisition parameters are described in Chapter 4. Demographic and clinical information for all patients are summarized in Chapter 2 and detailed in Appendix I: Raw Data.

7.3 Results

Scanning with the dedicated epilepsy-dedicated protocol, 29/43 (67%) patients remained MRI-negative after investigation by a consultant neuroradiologist. However, 14/43 (33%) patients were found to have potentially epileptogenic brain lesions. Diagnostic information for these patients is presented in Table 7.1.

All available images are presented in the results sections along with clinically relevant information for each patient. 11/14 (79%) previously 'non-lesional' patients had EEG-imaging concordant localization features (except for patients with IDs 59/65/84) rendering them potential candidates for resective surgery. This had been assessed during the multidisciplinary team meetings considering results from MRI, neurophysiological and neuropsychological testing. For eight of the 14 patients (57%) previous MRI was available for retrospective evaluation (from WCFT and one other trust). The other images could not be retrieved as they had been acquired at other trusts. This section initially presents the eight cases with a new identifiable lesion for whom previous MRIs were available. Subsequently, the remaining six cases for whom previous MRI was not obtainable are presented.

ID	Sex	Age	Infection/ febrile convulsion	Onset	Duration	EEG	Type	Frequency (per week)	Finding
22	f	54	no/no	5	50	right TL	SPS, SGTCS, CPS	2	right HS & Small-vessel-disease
24	f	39	yes/yes	36	2.5	right TL	SGTCS	0.5	right HS & right cerebello-pontine angle cystic lesion - epidermoid
25	m	47	no/no	34	13	bilateral TL	A, SGTCS, CPS	2	bilateral HS
27	f	38	no/yes	7	31	left TL	CPS, SGTCS	0.5	left HS
38	f	30	no/no	15	15	left TL	SGTCS	1	left HS
51	f	43	no/yes	6	37	left TL	SGTCS, CPS	2	left HS & left TL pole FCD & Small-vessel-disease/Rasmussen's/Encephalitis
56	f	23	yes/no	6	17	right TL	A, CPS	2.5	right HS and right parahippocampal FCD
59	f	27	no/no	6	21	bilateral FL	CPS, SGTCS	7	FCD in left supramarginal gyrus & left parietal lobule
61	f	36	no/yes	30	6	left TL	SGTCS	2 per year	left temporal encephalocele
65	m	22	no/no	5	17	left TL	A, CPS, SPS, SGTCS	6	FCD/gliosis in right superior frontal gyrus
66	m	18	no/no	10	8	left TL	CPS, SPS, SGTCS	1	left HS
69	m	29	no/no	10	19	right TP	CPS, SGTCS	7	right cortical gliosis
81	f	40	no/yes	7	33	left TL	A	2	left HS
84	f	19	no/no	18	1	left FT	CPS, SGTCS	35	left amygdala enlargement

Table 7.1. Patient Demographic and Clinical Information and Recent MRI-findings. Bold patient IDs indicate that the previous MRI was available for assessment (N=8). f=female, m=male, SPS=Simple Partial Seizures, SGTCS=Secondary-Generalized Tonic-Clonic Seizures, A=Absence Seizures, CPS=Complex Partial Seizures, TL=Temporal Lobe, FL=Frontal Lobe, TP=temporoparietal, FT=frontotemporal.

ID	22	24	25	38	66	56	61	65
Lesion	right HS & Small-vessel-disease	right HS & right cerebello-pontine angle cystic lesion - epidermoid	bilateral HS	left HS	left HS	right HS and right para-hippocampal FCD	left temporal encephalocele	FCD/ gliosis in right superior frontal gyrus
MRI	epilepsy protocol at WCFT	epilepsy protocol at WCFT	epilepsy protocol at WCFT	epilepsy protocol at WCFT	epilepsy protocol at WCFT	standard protocol at other trust	epilepsy protocol at WCFT	epilepsy protocol at WCFT
Reason	<i>Low SNR</i>	<i>motion artifacts and human factor: documentation</i>	human factor: documentation	human factor: not reported	human factor: not reported	<i>angulation not orthogonal to the long axis of the hippocampus</i>	<i>2D MRI only (large slice thickness, ~5 mm)</i>	<i>2D MRI only (large slice thickness, ~5 mm)</i>
Figure	7.1	7.2	7.3	7.4	7.5	7.6	7.7	7.8

Table 7.2. Lesions found in the most recent MRI and retrospective comparison to previous MRI and reports. Epilepsy dedicated research protocol: 2D coronal FLAIR MRI with high in-plane resolution (~0.5 mm), 3D T1w/T2w/T2FLAIR imaging. Technical reasons for previous MRI-negative report in italics.

The reasons for lesions not being reported in this dataset were multifactorial and were due to the following factors (Table 7.2):

- General technical issues affecting image quality and lesion conspicuity:
 - Low SNR (Figure 7.1) and movement artifacts (Figure 7.2) have contributed to loss of lesion conspicuity on the T2FLAIR images. Consequently, the lesion was not identified as HS (Figure 7.1, Figure 7.2).
 - The previous MRI was not part of a dedicated epilepsy (research) protocol, revealed some technical issues and therefore did not clearly show the lesion (poor angulation along the long axis of the hippocampus: Figure 7.6; large slice thickness: Figure 7.7 & Figure 7.8).
- Human factors leading to lesions not being identified:
 - Clinical team previously evaluating the patient cases does not document lesion (Figure 7.4, Figure 7.5).

- The standard MRI was reviewed and reported as 'non-lesional' by a general radiologist, although the lesion was visible (Figure 7.6).
- Loss of information during communication: Neuroradiologist referred to the abnormality without stating “hippocampal sclerosis” and subsequently the information was inappropriately documented (Figure 7.2 & Figure 7.3) and did not reach the consultant neurologist. Rather, the hippocampi for these patients were referred to as “small”, e.g.: “small appearance of the left hippocampus” (patient with ID 24) and “bilateral small hippocampi” (patient with ID 25).

In-vivo MRI is the most reliable and frequent imaging method used to provide information on macroscopic brain structure, and in the presence of varying data quality it is often impossible for neuroradiologists to evaluate the definite presence of lesions. Indeed, in one case where the quality of the image was not sufficient (Figure 7.2), the neuroradiologist preferred to make use of the wording “small hippocampus”. High lesion conspicuity on good quality MRI is the core characteristic for neuroradiologist to be able to confidently report an abnormality. The lesion that most frequently escaped the attention of clinicians was HS (nine cases, of which two had an additional FCD), followed by FCDs (two cases), and others including gliosis, encephalocele and amygdala enlargement (one case each).

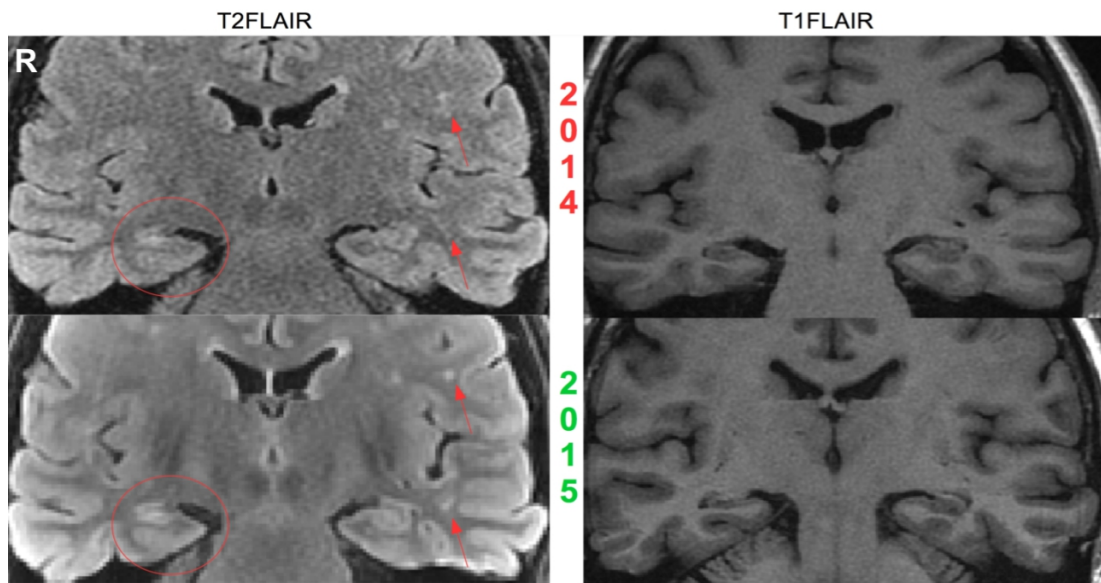


Figure 7.1. Patient 22: right HS and Small-Vessel Disease. In 2014 this patient received a dedicated epilepsy protocol at WCFT. Although the T1FLAIR coronal sequence shows a comparable quality relative to the most recent 2015 T1FLAIR, Small Vessel Disease and right HS were not detected by the neuroradiologist. HS and WM lesions related to small vessel disease are increasingly conspicuous on the most recent T2FLAIR image relative to the 2014 T2FLAIR image, the latter of which suffers from lower SNR. R = right.

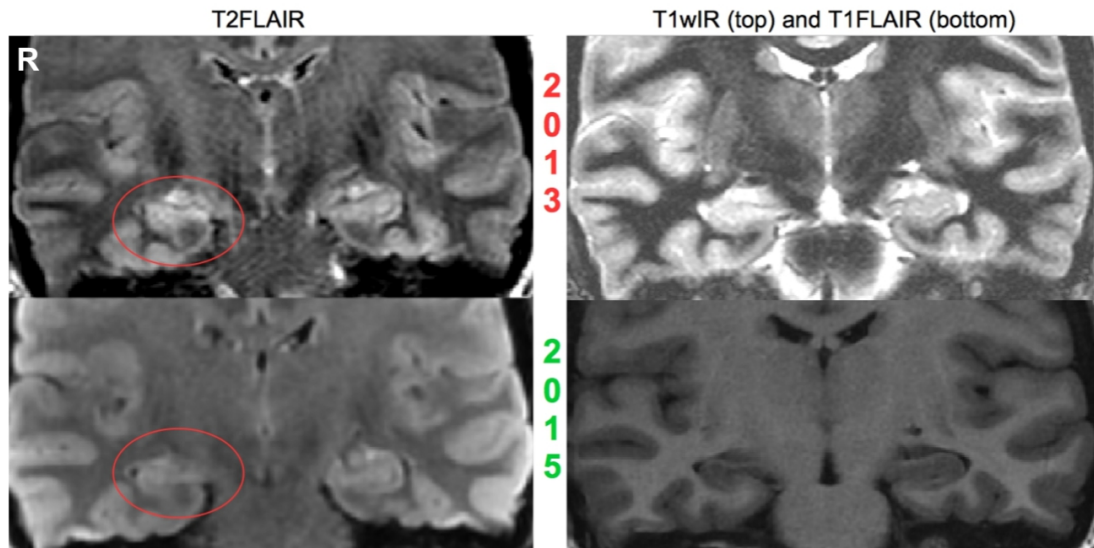


Figure 7.2. Patient 24: right HS. While early images do not show clear evidence of HS, the expert neuroradiologist termed this as “small right hippocampus” without explicitly diagnosing HS. This was inappropriately documented and this information did not reach the consultant neurologist. In the later image right HS was re-diagnosed. R = right.

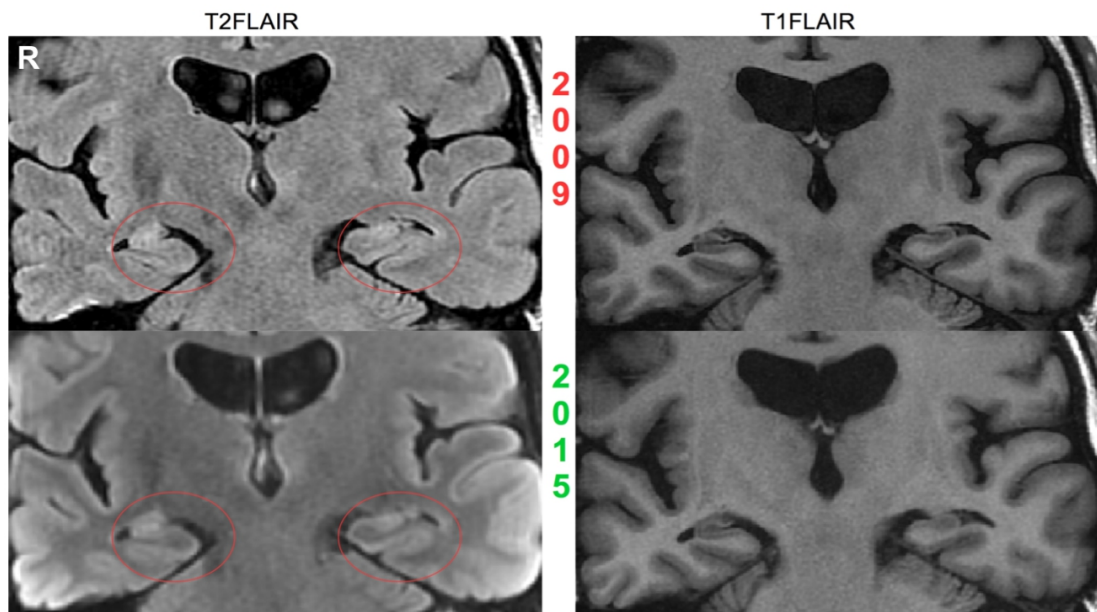


Figure 7.3. Patient 25: bilateral HS. The images from 2009 show bilateral HS as demonstrated by hyperintensity on T2FLAIR and volume loss on T1FLAIR; this was referred to as “bilateral small hippocampi” by the expert neuroradiologist. This was inappropriately documented and the information did not reach the consultant neurologist. In 2015 the patient was diagnosed with bilateral HS. R = right.

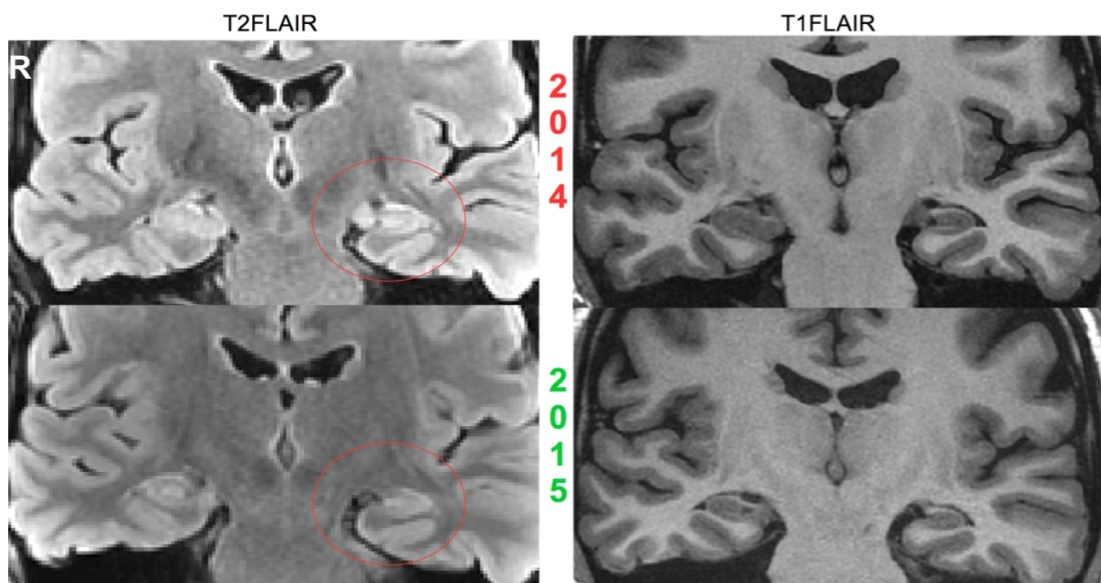


Figure 7.4. Patient 38: left HS. Despite signal hyperintensity on T2FLAIR and volume loss on T1FLAIR, HS was only diagnosed in 2015. Lesion conspicuity was similar for both MRI sessions. R = right.

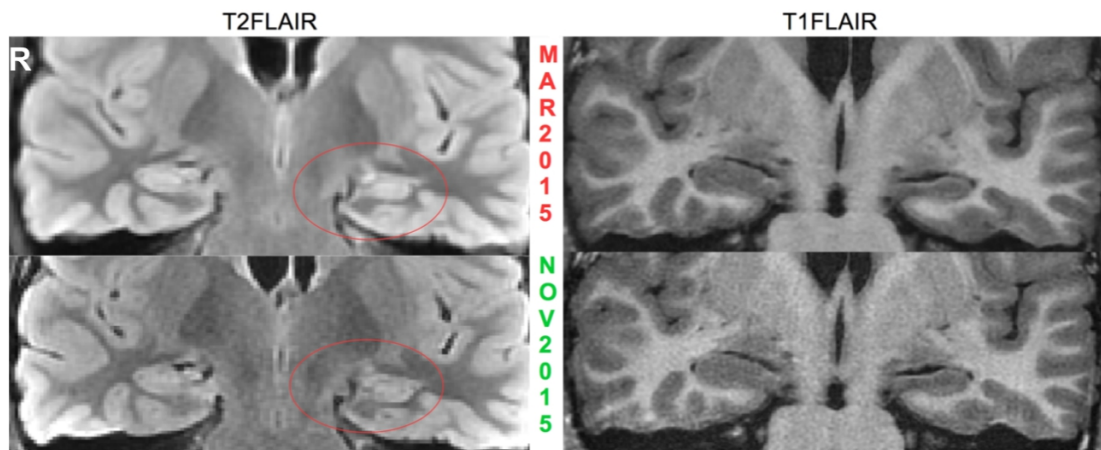


Figure 7.5. Patient 66: left HS. This patient received comparable quality of epilepsy-dedicated imaging in March and November 2015. However, HS was only diagnosed on the later images, which show hyperintensity on T1FLAIR and HA on T1FLAIR. Lesion conspicuity was similar for both MRI sessions. R = right.

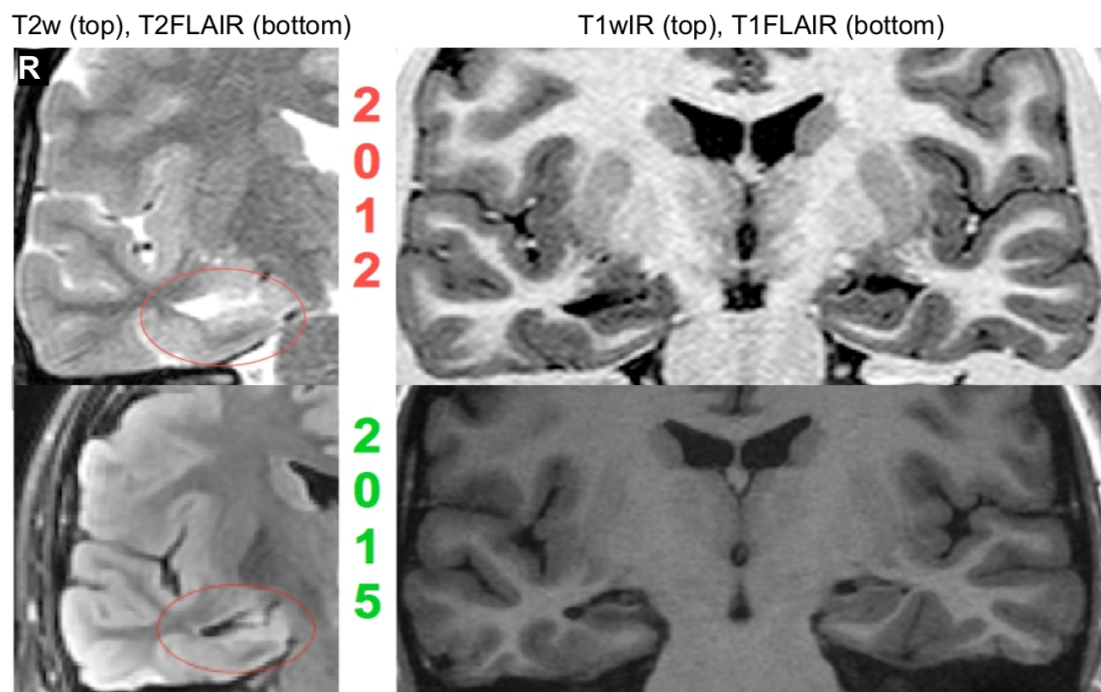


Figure 7.6. Patient 56: right HS with parahippocampal WM blurring. In 2012 this patient received imaging at a general hospital (left: T2w; right: T1w Inversion Recovery) with an angulation not orthogonal to the long axis of the hippocampus. HS and parahippocampal WM blurring are more conspicuous on the epilepsy research image of 2015 (left: T2FLAIR; right: T1FLAIR), particularly relative to the contralateral hemisphere. R = right.

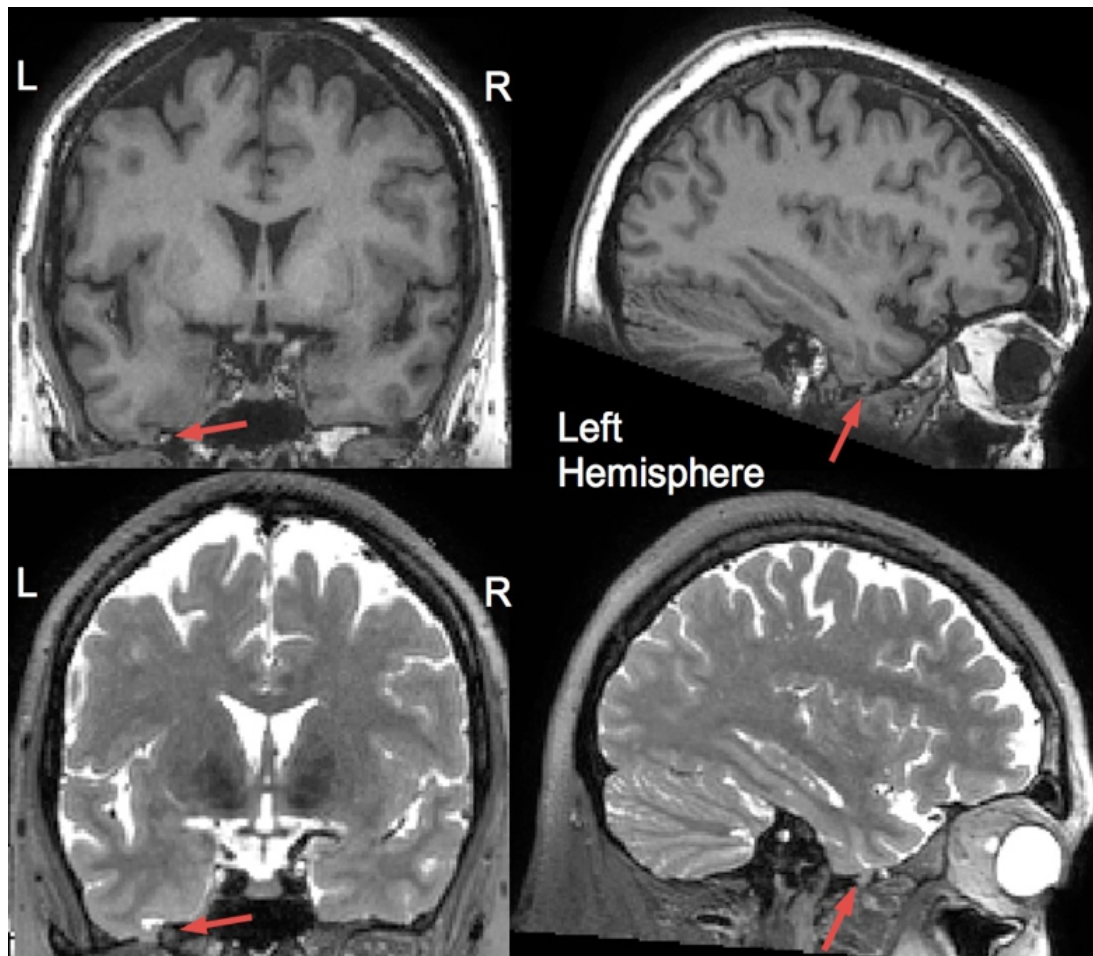


Figure 7.7. Patient 61: left temporal encephalocele. Left temporal encephalocele was diagnosed based on a 3D volume T2w acquisition, which is not routinely acquired in the evaluation of patients with epilepsy at the WCFT but was part of the study's dedicated epilepsy research protocol. Note how the lesion is more conspicuous on the T2w image (below) compared to the T1w (top). Diagnosis was later confirmed with computed tomography imaging. Older MRIs (all 2D) with large slice thickness (~5 mm) from 2009 failed to reveal this abnormality. L = left; R = right.

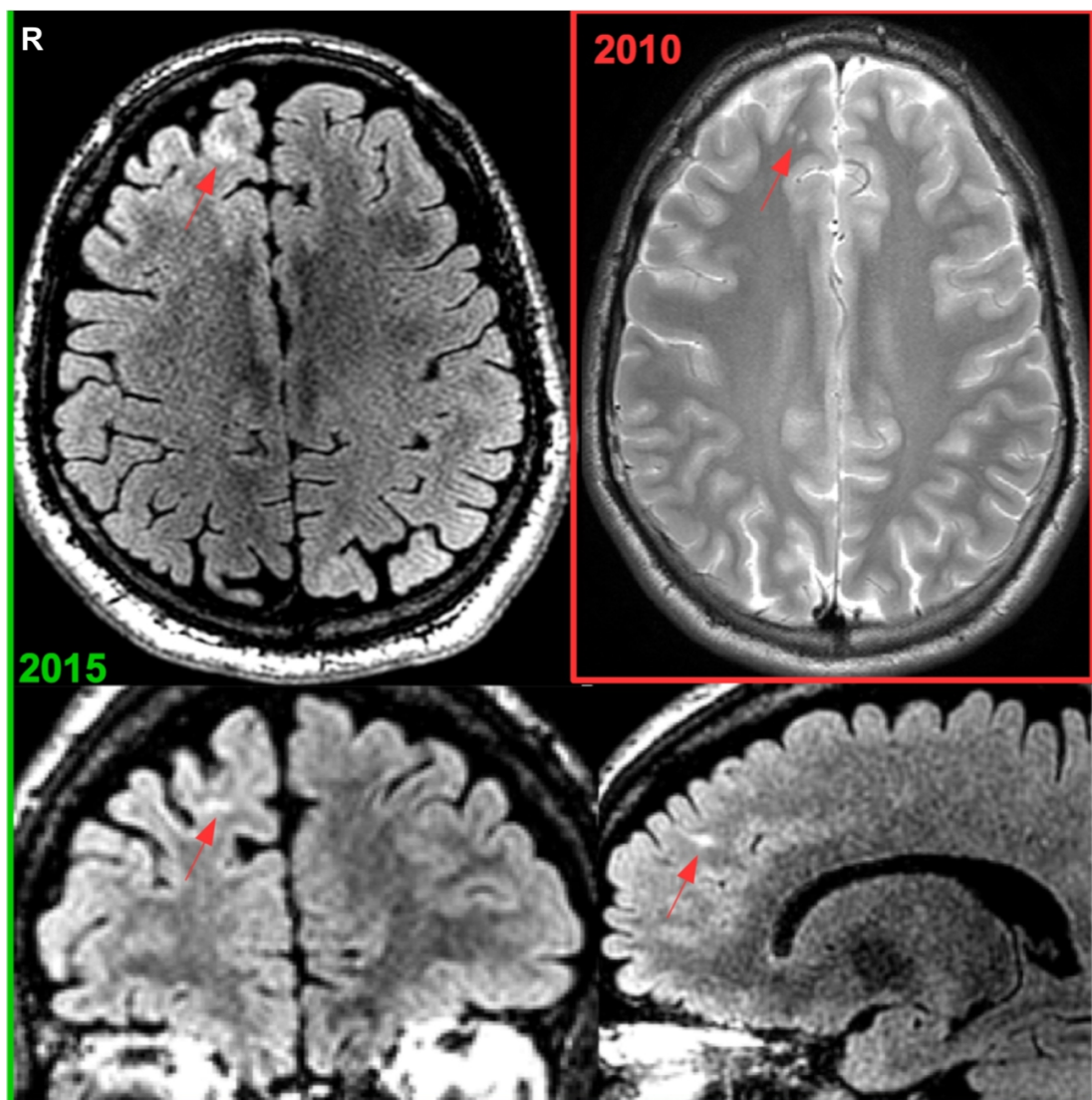


Figure 7.8. Patient 65: FCD / gliosis in right superior frontal gyrus. Diagnosis was made based on the 3D T2FLAIR image of 2015 (green image borders). The abnormality was not reported on the previous 2D axial T2w image (red image borders) where only one slice showed the small abnormality. R = right.

The previous images for patients 27, 51, 59, 69, 81 and 84 could not be retrieved. All lesions reported for these patients were conspicuous on the most recent images acquired using the dedicated epilepsy research protocol (Figure 7.9).

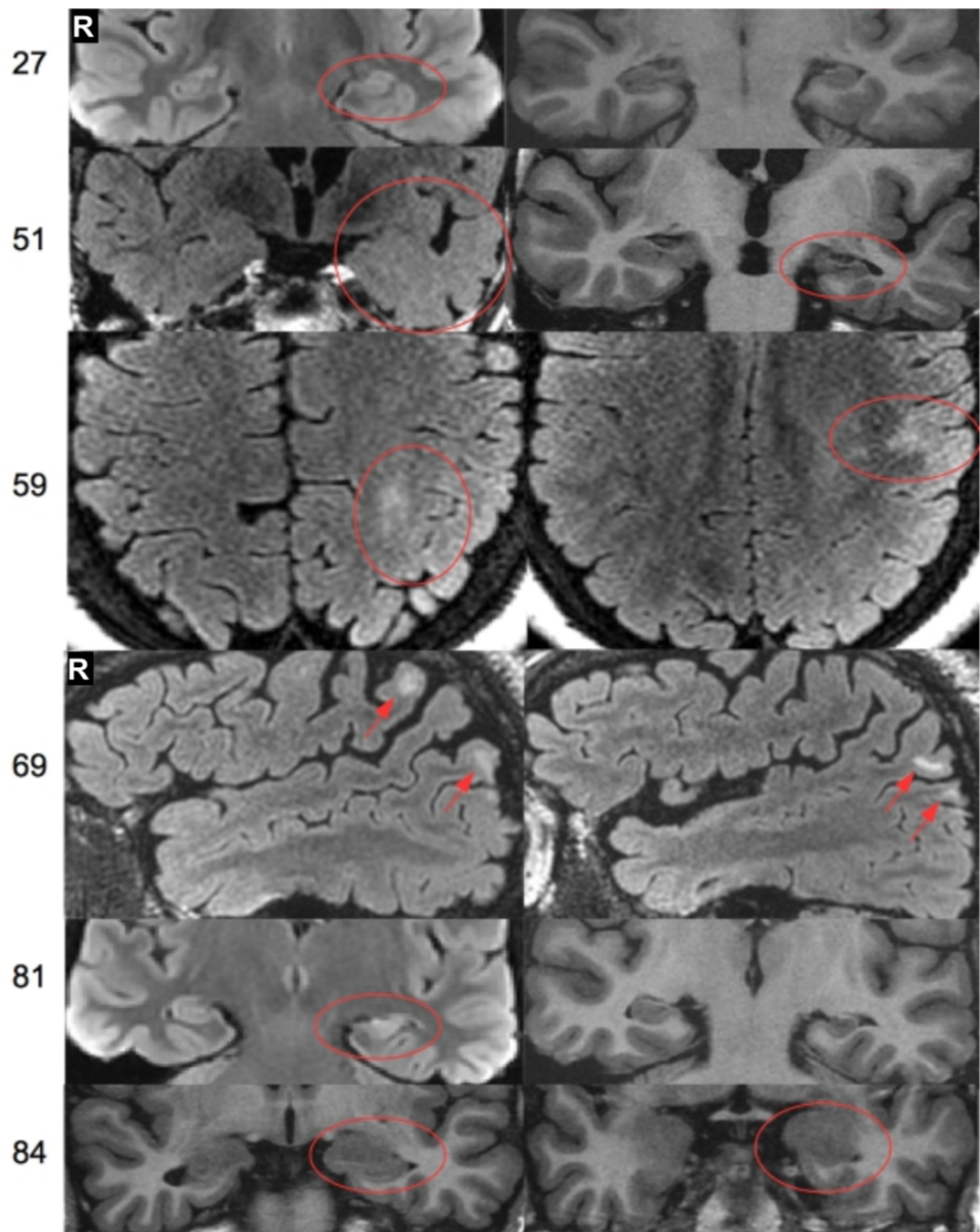


Figure 7.9. Formerly 'non-lesional' cases showing lesions using the epilepsy dedicated research protocol. Numbers refer to patient IDs. Please refer to Table 7.1 for details on each lesion identified. R = right.

7.4 Discussion

The objective of this chapter was to review new MRI presentations of brain lesions using an epilepsy-dedicated MRI protocol in a cohort of patients with refractory focal epilepsy who were previously deemed to be non-lesional and to attempt to ascertain the potential reasons for why lesions were previously not identified. 33% of all patients recruited had a newly identified brain lesion. The primary factors explaining the newly identified lesions were the choice of MRI sequences, imaging parameters (in particular: no previous use of a dedicated epilepsy (research) protocol, including the lack of angulation orthogonal to the long axis of the hippocampus and large slice thickness), data quality (motion artifacts and low SNR), lesion not reported (human factor) and loss of information through incomplete documentation (wording: “small hippocampus” versus “hippocampal sclerosis”).

The results presented here indicate that one important factor for why lesions had previously escaped the attention of the reporting neuroradiologist may be the choice of sequence with lesions being more conspicuous on dedicated epilepsy protocols (ILAE 1997, von Oertzen et al. 2002, Duncan et al. 2016, Friedman 2014). According to Duncan et al. (2016), Duncan (1997) and ILAE (1997), 3D whole-brain T1w and T2w and 2D FLAIR imaging should be included in an effective epilepsy dedicated protocol. Additional, apart from the specific choice of the sequence itself, lesion conspicuity may be influenced by data quality, slice thickness, angulation and resolution. Expert neuroradiologist reassessment using epilepsy dedicated MRI can detect HS with sensitivity and specificity of over 90% (von Oertzen et al. 2002, Oppenheim et al. 1998). Two images not routinely acquired in the evaluation of patients with epilepsy at the WCFT proved useful for the detection of FCDs/gliosis (3D T2FLAIR) and encephalocele (3D T2w). Tschampa et al. (2015) have previously indicated that 2D/3D T2FLAIR sequences are equally useful for detecting FCDs visually, while Friedman (2014) stated that the whole-brain coronal 3D T2w sequence can be helpful in detecting encephalocele and may be superior over T1w (Toledano et al. 2016). Encephaloceles may be an under-appreciated etiology of TLE

(Saavalainen et al. 2015). Additionally, an isotropic voxel size may increase the diagnostic yield as it can cover multiple locations within the brain and may identify small lesions, such as encephalocoele or gliosis. It has been previously reported that image artifacts such as subject motion can affect lesion conspicuity (Phal et al. 2008). As a rule, when patients moved excessively during the recently applied epilepsy research dedicated protocol, MRI was reacquired in order to avoid motion artifacts. Regarding human factors, the lesion most frequently left unreported was HS (nine cases), which was also reported in a previous study (von Oertzen et al. 2002). These authors reported that HS was overlooked in 86% of cases when the MRI was read by general radiologists relative to expert neuroradiologists. In this sample, FCDs accounted for the second most frequent lesions left unreported (four cases). Multiple sites of gliosis and unilateral amygdala enlargement were identified in two different patients on their most recent epilepsy dedicated research MRI conducted in the context of this study. Unfortunately, the previous MRI was not available in these cases. The review presented here has shown several patients with multiple lesion sites, therefore it is important that neuroradiologists are aware of the satisfaction-of-search effect (Berbaum et al. 1990) and continue radiological assessment even when epilepsy-related lesions have already been identified. Another important point relates to the communication between neuroradiologists and clinicians. A recent study on patients with frontotemporal dementia has found that diagnostic information may be inappropriately reported (limited factual description with incomplete misleading interpretation of MRI) unless MRIs are jointly reviewed and discussed by neurologists and neuroradiologists (Dewer et al. 2016). In the present study, the apparent hesitation in officially diagnosing hippocampal volume loss on MRI as HS has resulted in two patients being misclassified as non-lesional. Therefore, neuroradiologists and clinicians may benefit from an equidistant rating scale where it is possible for the consultant neuroradiologist to indicate how confident they are in reporting an abnormality and to state reasons for why their confidence is very high/high/medium/low or very low (e.g. due to slice angulation/motion artifacts). A similar rating scale has been used by some centers to record the degree of atrophy in patients (Dewer et al. 2016, Kipps et al. 2007, Scheltens et al. 1995), the likelihood

of presence of FCD (Wang et al. 2015) and artifacts (Phal et al. 2008). A confidence rating scale may facilitate reacquisition with appropriate and individualized sequence parameters if necessary, but certainly this should be subject to further research.

Even though the true positive rate of 33% within this investigation of a realistic clinical setting is large and potentially clinically significant for individual patients, one limitation remains the fact that results are based on a small sample size. It is striking however, that the true positive rate of 33% also reflects the commonly reported number of patients with medically refractory focal epilepsy who do not benefit from epilepsy surgery. This may possibly indicate that remaining (additional) lesional tissue has indeed not been appreciated on MRI before surgery. Another limitation of this dataset is that it does not allow the direct comparison of individual sequence acquisition parameters or of MR hardware. The type of MR sequences and the data quality varied for all initial clinical MR studies, which were not part of the more recently applied epilepsy dedicated protocol and acquired at different time points. As in the example of an initial negative report based on MRI with poor quality and lesion conspicuity, the lesion may not have been appreciated due to artifacts, human factors or both (i.e. retrospectively the lesion is discernible on the initial MRI even when taking the artifacts into account). This also reflected the opinion of the consultant neurologist and neuroradiologists who retrospectively re-evaluated the initial MRI: in almost all cases the reasons for leaving an abnormality unreported remain multifactorial. Consequently this made it difficult to attribute a single reason to leaving a lesion unreported. A prospective study where MRI is evaluated by an expert neuroradiologist in a blinded fashion (e.g. one with motion artifacts, one without in the same patient etc.) may resolve some of these open questions. Nevertheless, this retrospective study of previous MRI in a realistic clinical setting was capable of shedding light onto the factors that may influence everyday clinical practice. An acknowledgement of these being multifactorial may facilitate a deeper understanding and reevaluation of current MR protocols, neuroradiological assessment and communication between clinicians.

In conclusion, it is important for all clinicians to continuously proceed in the detailed assessment of lesions on in-vivo MRI and discuss difficult patient cases in MDT meetings. Only this way it is possible to identify (multiple) lesions in one patient. Most importantly, a dedicated epilepsy protocol for the sake of conspicuity and confidence in reporting lesions should be followed. In some cases, where technical issues such as movement or wrong angulation may compromise diagnostic evaluation, it may be worth re-acquiring the data. For patients who remain 'non-lesional' it may be apt to also acquire 3D T2FLAIR and 3D T2w data as this can increase the lesion pick-up-rate, is easily implemented and can be performed at low costs concerning acquisition times. As a direct result of this translational study using research dedicated MRI, clinicians at the WCFT members of the MDT have now started to request 3D T2FLAIR images for patients with refractory focal epilepsy and previous inconclusive MRI. This study showed that if abnormalities are not reported by the particular term for the lesion (e.g. "hippocampal sclerosis"), the information is likely to be inappropriately documented and may not reach the consultant neurologist. Ultimately, consideration of all the interdependent factors mentioned in this review have important implications for (i) treatment options for the individual patient, especially regarding epilepsy surgery performed on newly identified epileptogenic lesions and (ii) study populations that may have been confounded by undetected lesions in patient samples if sequences are not dedicated to depicting epilepsy lesions and MRI is not reassessed through an expert neuroradiologist. These factors may influence everyday clinical practice and research in lesional epilepsy, which emphasize the need to follow a general discussion on this topic for the ultimate benefit of the current and future patients on a clinical and scientific basis. As some lesions may be too subtle to appreciate on MRI, even through expert neuroradiological assessment, it is important to develop automated lesion analysis tools, which allow reliable whole-brain quantitative comparison of a single patient's MRI with those acquired from healthy controls. Therefore, this thesis chapter is followed by the introduction of a novel automated and reproducible quantitative detection tool for FCDs (Chapter 8), which may assist in human reassessment of MRI.

Chapter 8: Automated Multimodal MRI Analysis for Diagnostic Purposes in Patients with MRI-negative Epilepsy

Chapter 8: Automated Multimodal MRI Analysis for Diagnostic Purposes in Patients with MRI-negative Epilepsy	147
8.1 Introduction.....	147
8.2 Methods.....	152
8.2.1 Participants.....	152
8.2.2 MRI Acquisition.....	152
8.2.3 Data Pre-processing.....	152
8.2.4 Generation of Feature Maps	153
8.2.5 Statistical Analysis.....	156
8.3 Results.....	158
8.3.1 Data Quality Assessment.....	158
8.3.2 Neurological Assessment and Statistical Analysis of Feature Maps.....	158
8.3.3 Multi-modal Analysis Based on MAP Clusters.....	160
8.4 Summary.....	164

8.1 Introduction

The high anatomic specificity of MRI may depict focal lesions and can be expertly assessed by visual analysis through neuroradiologists (Von Oertzen et al. 2002). It is important to find ways to improve the diagnostic yield from MRI through optimized MRI protocols (see Chapter 7), expert neuroradiological assessment (also Chapter 7) and quantitative analysis of post-processed volumetric MRI (this chapter; Sisodiya et al. 1995a).

This chapter focuses on quantitative analysis to improve detection of FCD, which is a common lesion associated with medically refractory epilepsy (Sisodiya 2004, Fauser et al. 2004) and often epileptogenic (Fauser and Schulze-Bonhage 2006). It is the most common lesion in children (Bast et al. 2006, Woermann and Vollmar 2009) and is the third most common lesion after HS and tumors in adult patients (Lerner et al. 2009, Becker et al. 2006, Von Oertzen 2014). Within this study, a dedicated epilepsy research protocol was performed on patients with medically refractory focal epilepsy, who were deemed to be non-lesional based on previous MRI. The most

recent MRIs conducted in context of this study allowed (i) a clinical diagnostic assessment by an experienced neuroradiologist at the WCFT (Chapter 7) and (ii) the application of an automated quantitative voxel-based lesion detection technique on patients' MRIs in order to find potentially epileptogenic lesions such as FCDs (this chapter).

FCD is a type of cortical malformation that is neuroradiologically characterized by cortical thickening, GM/WM blurring and transmantle signs, which are abnormal extensions of GM towards the ventricles (Barkovich et al. 1997, Huppertz et al. 2005). FCDs may show increased signal on T2w or T2FLAIR images, cortical thinning, localized brain atrophy but others may not be discernible on structural MRI (Blümcke et al. 2011). FCDs are the result of genetic defects or environmental insult during the stages of brain development that lead to disruptions of neuronal proliferation, migration and organization (Tassi et al. 2002, Barkovich et al. 2005, Palmini et al. 2004, Sisodiya 2004, Sarkisian et al. 2008). The different types of FCDs and MRI presentations are described in Chapter 3 (neuroanatomy and brain development).

Many efforts have been made to automatically identify lesions in patients with epilepsy using quantitative MRI analysis. The approaches used involve voxel-based analysis (Kassubek et al. 2002, Merschhemke et al. 2003, Bonilha et al. 2006, Focke et al. 2008b, Focke et al. 2009, Colliot et al. 2006, Rugg-Gunn et al. 2005), cortical surface mapping (Besson et al. 2008, Huppertz et al. 2008, Bastos et al. 1999) and texture analysis (Antel et al. 2003, Bernasconi et al. 2001). All of the lesions found in these studies have been defined either neuroradiologically (Rugg-Gunn et al. 2005, Antel et al. 2003), neurophysiologically (Kassubek et al. 2002, Focke et al. 2009) or histopathologically (Huppertz et al. 2005, Wang et al. 2015, Focke et al. 2008b, Colliot et al. 2006, Bastos et al. 1999, Huppertz et al. 2008, Bernasconi et al. 2001, Bonilha et al. 2006). Huppertz et al. (2005) have published a method on FCD detection using 3D T1w images and the Morphometric Analysis Program (MAP) developed by these authors is used by a dozen clinical centers worldwide (Huppertz

2013). Approaches allowing the extraction of certain MRI features not easily accessible by visual analysis may provide supplementary information (Martin et al. 2015, Huppertz et al. 2005). These types of individualized quantitative methods highlighting features of FCDs demonstrated high sensitivity in lesion detection accuracy with significant histopathological correlations (Huppertz et al. 2005, Colliot et al. 2006). Wang et al. (2015) have applied MAP and were able to show that neuroradiological assessment of results provided by the automated lesion detection tool can identify subtle FCDs in patients. The patients undergoing resective surgery attained postoperative seizure freedom and the areas deemed to be dysplastic by MAP could be confirmed through histological examination (Wang et al. 2015).

However, despite the recent addition of cortical thickness analysis to MAP (Huppertz 2013), no further development towards an integrated multi-contrast approach has been implemented into this tool. Rather, MAP results have been retrospectively evaluated by neuroradiologists and marked manually as being either a true or false positive finding (Huppertz 2013, Wang et al. 2015). Other significant drawbacks of the MAP software include the fact that it is not freely available despite the use of reproducible segmentation and normalization algorithms submitted in context of Statistical Parametric Mapping (SPM; Wellcome Department of Imaging Neuroscience Group, London, UK; <http://www.fl.ion.ucl.ac.uk>) and that it has not been adapted to most recent SPM versions. However, these offer significant improvements in image segmentation and spatial normalization (co-registration of individual T1w to standard space, which allows group comparisons) compared to older versions (Ashburner and Friston 2005, Ashburner 2007, Dahnke et al. 2012, Malone et al. 2015, Farokhian et al. 2017). The improvements to image processing may affect MAP results, since MAP heavily relies on anatomical accuracy of co-registrations and tissue segmentation. Furthermore, the MAP tool has not been extensively tested on control cohorts without FCDs and so information on false positives is still lacking. Few studies have investigated false-positive generation through similar analysis using T2FLAIR imaging in patients with FCDs (Focke et al. 2008b, Focke et al. 2009, Martin et al. 2017). Similar to the work performed by

Wang et al. (2015), which is the only publication to date reviewing MAP in light of false positives, it is important to perform appraisal of control-control comparisons when using the MAP tool and to address the issue of false positive findings. False positive rates have been shown to decrease when reevaluation of suspicious MAP regions was performed by a trained neuroradiologist (Wang et al. 2015). However, a tool which integrates high sensitivity and specificity would be most beneficial to clinical practice as time-consuming reevaluation of many false positive findings in patients and controls could be avoided, providing more resources for patients with true positive findings. False positive findings could potentially be mitigated by the introduction of another sensitive measure like T2w (House et al. 2013, Wang et al. 2015, Rugg-Gunn et al. 2005) and T2FLAIR intensities (Focke et al. 2009). For the detection of FCDs it can be essential to study suspicious areas on all these images (Colombo et al. 2009, Bernasconi et al. 2011). Furthermore, since the present study involved DTI, it was possible to investigate the sensitive measures (FA and MD) in context of FCD. In order to achieve this, FA/MD values were compared between patients and controls. DTI has proved useful in the analysis of WM disruption in epilepsy (Keller et al. 2013, Rugg-Gunn et al. 2001, Bonilha et al. 2010), while MD has been shown to be especially sensitive (Concha et al. 2012, Glenn et al. 2016, Keller et al. 2017). It is likely that abnormal cortical development influences WM integrity and anatomy during brain development (Rakic and Schwaab 1988, Lee et al. 2004, Widjaja et al. 2009, Widjaja et al. 2007) and that these changes persist through adulthood.

Two issues were addressed within the present study in order to evaluate whether diagnosis may be facilitated by: (i) an automated lesion detection procedure combined with continued integration of novel improved software tools and (ii) the reduction of false positives using a novel automated approach on multi-modal images. The MAP algorithm was implemented into the most recent version of SPM. As the MAP tool alone does not provide statistics with its results but is based on visual assessment only, in this study MAP is extended to include individualized statistics aiming to facilitate quantitative lesion detection. It was evaluated whether

previously reported lesions could be automatically identified using the automated voxel-based method and whether additional lesions could be identified in the cohort of patients with MRI-negative epilepsy. In an attempt to reduce the number of false positives and provide reliable automated information for the detection of legitimate epileptogenic lesions, the diffusion characteristics of clusters deemed to be structurally different in individual patients relative to controls were mapped. All study results are obtained with the use of the latest segmentation algorithms and appropriate statistical testing on multi-modal images accounting for age, sex and ICV. Thereby, in contrast to recent studies applying MAP, all current methodological standards have been followed in order to develop an automated lesion detection tool. This approach is particularly promising for patients with MRI-occult FCDs as this is the most common histopathological finding in patients with refractory cryptogenic epilepsy (Bernasconi et al. 2011, Taylor et al. 1971, Sisodiya 2004). It is therefore especially important to continue the development of an automated, time-efficient and reproducible lesion detection tool in patients with 'non-lesional' epilepsy.

Objective 8.1

The objective of this study was to implement and automatize a previously developed lesion detection technique and to apply this to T1w images of patients with cryptogenic focal epilepsy. It was hypothesized that neuroradiologically identified lesions by virtue of the dedicated epilepsy research MRI could also be detected using the automated voxel-based approach based on T1w images.

Objective 8.2

A further objective was to incorporate other MR images into the automated voxel-based approach in order to improve sensitivity and specificity of the approach. It was hypothesized that the automated tool in conjunction with multimodality testing (with the incorporation of T2w/T2FLAIR/DTI data) can identify previously undetected epileptogenic lesions while reducing the false positive rate based on multimodal testing.

8.2 Methods

8.2.1 Participants

40 healthy controls (23 female) and 43 patients (26 female) with focal refractory epilepsy were prospectively recruited on the basis of failing multiple AED treatments and showing no lesion on previous MRI (see Chapter 2). Localization of seizure onset had been thoroughly evaluated using seizure semiology and surface EEG investigations. All relevant demographic and clinical information can be viewed in Chapter 2 and Appendix I: Raw Data.

8.2.2 MRI Acquisition

Each participant received 3D T1w, T2w, T2FLAIR, DTI and two coronal sequences (2D T1FLAIR and T2FLAIR) aligned with the long axis of the hippocampus. The latter two sequences were acquired for diagnostic purposes only. For details on image acquisition see Chapter 2. A specialist neuroradiologist with long-term clinical experience in evaluating MRI for patients with epilepsy performed diagnostic assessment of the images for structural lesions.

8.2.3 Data Pre-processing

A modified version of the automated FCD detection procedure was applied to the T1w images (Huppertz et al. 2005). Specifically, Human Connectome Project (HCP) workbench software (Glasser and Van Essen 2011) was used to set the origin of the T1w image to the anterior commissioner and T2w and T2FLAIR images were linearly co-registered to this T1w image using SPM12. Before co-registration to native T1w image space, DTI data was processed using the ENIGMA DTI preprocessing steps to mitigate effects of image artifacts (<http://enigma.ini.usc.edu/protocols/dti-protocols/>). In particular, the first b0 image was used as a reference for co-registration of the five subsequent b0 images (FSL FLIRT, Smith et al. 2004). The resulting co-registered b0 images were averaged and served as a reference image during motion and distortion correction performed on the DWIs. In order to achieve distortion correction, the T2w image was rigidly aligned

with the mean b0 image (Smith et al. 2004). The mean b0 image and the T2w image in diffusion space were thus combined to a pair of images with the first image representing geometric distortions while the T2w image served as the reference. From this pair the susceptibility-induced off-resonance field was estimated (Andersson et al. 2003) and the two images were combined into a single corrected one, which was then brain-extracted. The DWIs were corrected for motion and the resulting nonlinear registration information from the distortion correction step was used to unwarp subsequent DWIs in native diffusion space (Andersson and Sotiropoulos 2016). The gradient table information was adjusted according to the rigid body motion parameters (Leemans and Jones 2009). FA and MD maps were calculated within FSL (Smith et al. 2004) and co-registered to the T1w image.

8.2.4 Generation of Feature Maps

Automated GM/WM segmentation of T1w data was performed using the Computational Anatomy Toolbox (CAT12) in SPM12 while simultaneously applying registration to ICBM template space through DARTEL (Ashburner 2007). After segmentation, the homogeneity of normalized and intensity corrected T1w images were separately evaluated for patients and controls using the CAT12 tool. The total intracranial volume (TIV) was also estimated in order to correct for different head volume. The warp field resulting from the registration to template space was applied to the co-registered intensity-corrected T2w, T2FLAIR and FA/MD images so that these would be in the same space as the normalized T1w image. T1w junction (providing information of blurred GM/WM area through voxel intensities that are neither clear GM nor WM tissue) and extension (providing information of GM thickness) images were generated using the previously published procedures based on T1w segmentations (Huppertz et al. 2005, Kassubek et al. 2002) and subsequently smoothed with a 6mm Gaussian kernel (Kassubek et al. 2002, Wilke et al. 2003) (Figure 8.1). For this procedure, unmodulated images with non-linear registration and default normalization were used (Wilke et al. 2003). Using the T1w segmentations, T2w images were also processed to acquire T2w junction maps (House et al. 2013) and T2FLAIR junction maps were also computed. In order to

achieve this, the same procedure as described in Huppertz et al. (2005) was used on T2w images (House et al. 2013) and T2FLAIR images. As a novel addition, T2w extension maps using the Kassubek et al. (2002) technique were also computed. This was performed using the binary T1w GM segment mask, which was multiplied with the T2w image in order to obtain T2w image intensities. This resulted in the T2w extension map, which provided information on T2w signal within GM areas. The same approach was performed on the T2FLAIR images. For the T2FLAIR maximum (MAX) map, the T2FLAIR image had been thresholded to show the voxels with intensities higher than two SD above the mean intensity of GM (which has higher intensities in T2FLAIR image compared to WM). All images were smoothed with a 6 mm Gaussian kernel.

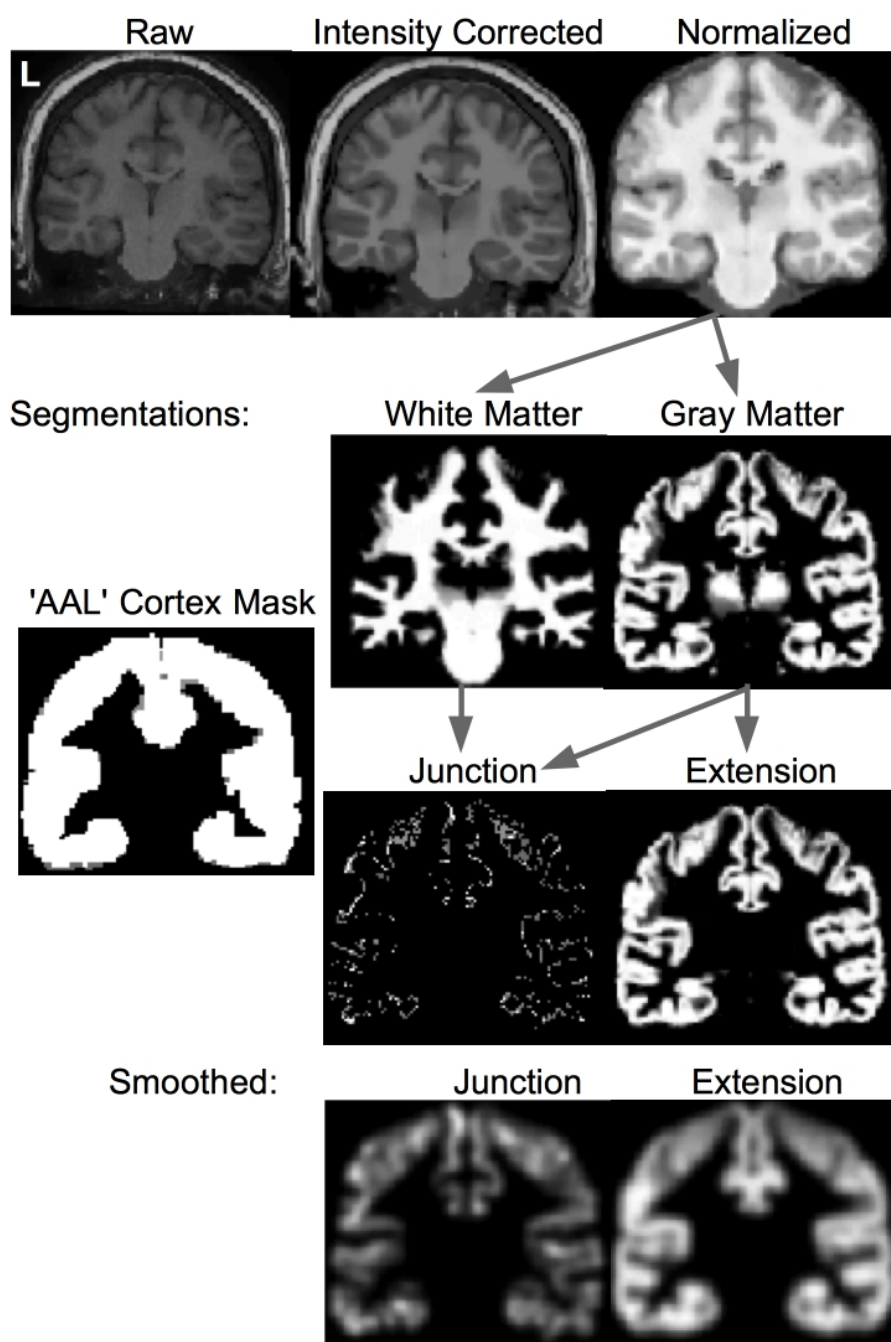


Figure 8.1. Procedure for obtaining T1w junction and extension images (Huppertz et al. 2005).

Raw T1w images were intensity corrected, normalized and segmented into WM/GM maps. These were used to obtain GM/WM voxel intensity thresholds. Any voxels with intensities of half a standard deviation higher/lower than the mean GM/WM intensities were saved to a binarized junction image, which was cortex-masked ('AAL' in SPM12). The GM segment was also masked and served as the extension image. Both resulting images were smoothed with a 6mm FWHM smoothing kernel. The data of patient 59 is featured here. L =left.

8.2.5 Statistical Analysis

The smoothed T1w junction (JCT) and extension (EXT) images of all controls were averaged. These mean JCT/EXT images were each thresholded at their average whole-brain signal intensity, binarized and used as a mask during statistical analysis. Separate two-sample t-tests (Focke et al. 2008b) with assumptions of equal variance and non-independence were used to determine individual patient-control group and individual control-control group differences (Salmond et al. 2002, Colliot et al. 2006) within smoothed T1w JCT/EXT maps. TIV, sex and age were considered as covariates. A general workflow of the applied statistical tests can be viewed in Figure 8.2. Statistical thresholds were an uncorrected $p < 0.01$ (voxel-level) and $p < 0.05$ FWE-cluster corrected (Focke et al. 2009). This liberal threshold was used in order to facilitate the detection of lesions, even at the cost of an increasing number of false positives, which has been recently discussed (Scarpazza et al. 2013). Sensitivity for lesion detection is important for an automated tool used in clinical settings and specificity should be improved for the sake of time-efficiency. Therefore, all significant clusters of more than 3.5 cm^3 (3500 voxels) gained through the individual statistical testing on T1w JCT/EXT maps served as masks. The threshold of a 3.5 cm^3 cluster was defined based on the size of every true positive cluster, i.e. all lesions suggestive of an FCD as reported by the consultant neuroradiologist at the start of the study.

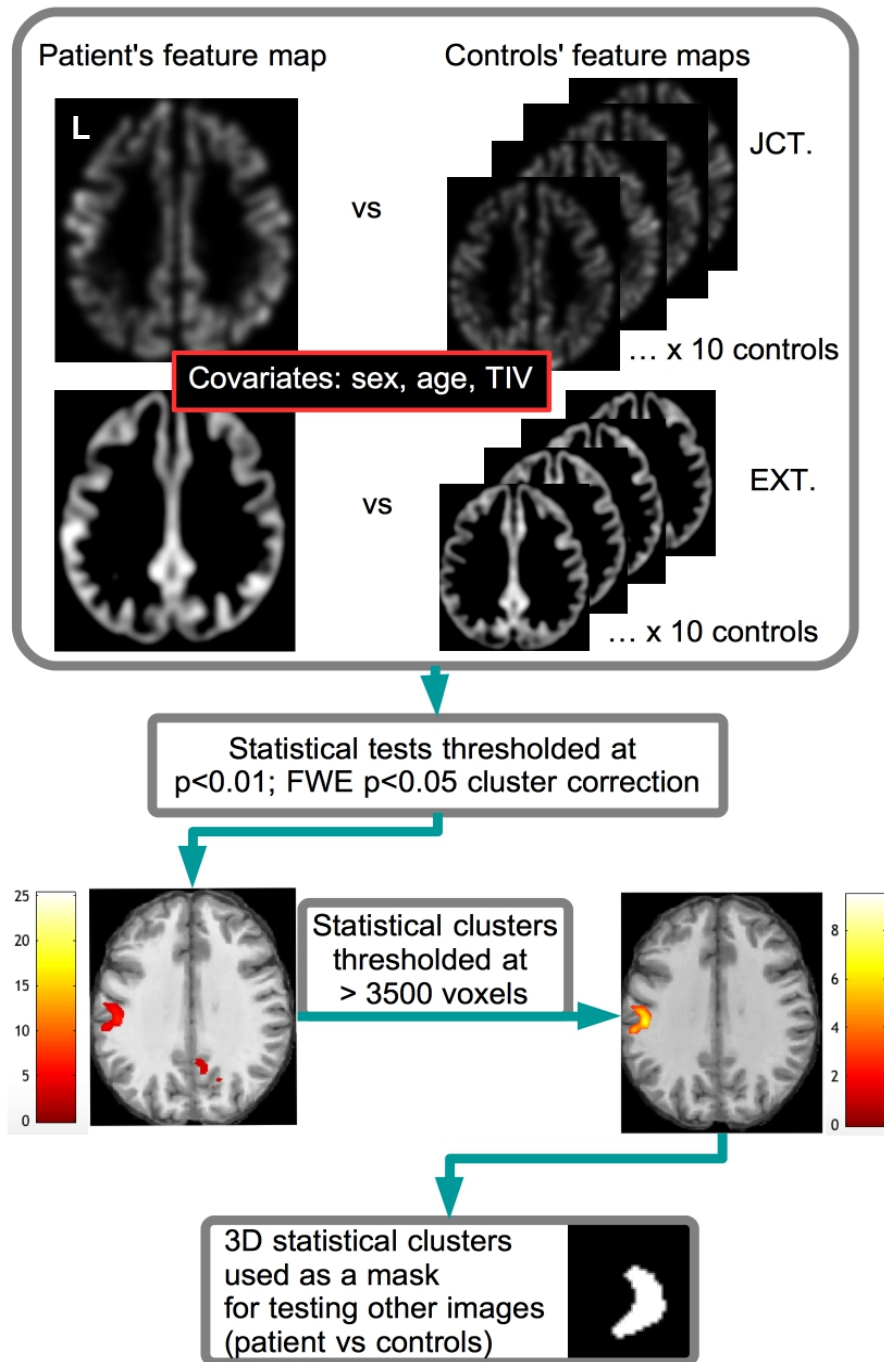


Figure 8.2. General workflow of the applied statistical tests in T1w JCT and EXT maps. This graph shows the generation of the binarized cluster masks based on T1w used to restrict statistical testing for all other imaging modalities to regions that are potentially dysplastic. Patient 59 is given as an example (cluster in the JCT map). In the case that any one of the remaining imaging modalities showed a significant effect, the site was again reviewed by a neuroradiologist. TIV = total intracranial volume; JCT = T1w junction image; EXT = T1w extension image. FWE = family-wise error. T-scores: yellow/red bars. L = left.

The resulting $>3.5 \text{ cm}^3$ cluster masks were used in individual patient-control comparisons based on normalized and 6mm-smoothed T2w JCT/EXT images, T2FLAIR JCT/EXT/MAX images and GM/WM FA and MD images during voxel-based analysis in SPM12. The initial clinical diagnostic report was used as a reference for determining the presence of FCD and classifying the T1w JCT/EXT clusters as true positives.

8.3 Results

8.3.1 Data Quality Assessment

The Wilcoxon Sign-Rank test revealed that there were no significant age differences between controls (mean age \pm std = 32.4 \pm 8.8) and patients (mean age \pm std = 31.6 \pm 11); $z=0.45$, $p=0.7$, data non-normally distributed (Lilliefors, $p<0.05$). The sample homogeneity of the normalized and intensity corrected T1w images was in an acceptable range of correlations ranging from 0.96 to 0.98.

8.3.2 Neurological Assessment and Statistical Analysis of Feature Maps

29 patients remained MRI-negative after diagnostic reassessment of the epilepsy research dedicated MR protocol. However, 14 patients (33%) were found to have at least one epileptogenic lesion. Of these, seven had HS, two had dual pathology (HS & FCD), two had dysplasia, one patient had amygdala enlargement, another had encephalocele and one patient had gliosis (see Chapter 7). Of the 14 patients with lesions, eleven had lesions concordant with the likely epileptogenic region as identified by EEG. Five of six and four of six sites of dysplasia were separately detected by T1w JCT/EXT images respectively, while both images together detected all sites of dysplasia (100%). Two sites that the tool found could be confirmed by the neuroradiologist as FCDs that had been previously missed. These sites can be appreciated in Figure 8.3, in the second row (left PHWM GM/WM blurring, patient 51) and in the third row (right FCD in temporal pole, patient 56). All true positives originating from the T1w image analysis are shown in Figure 8.3.

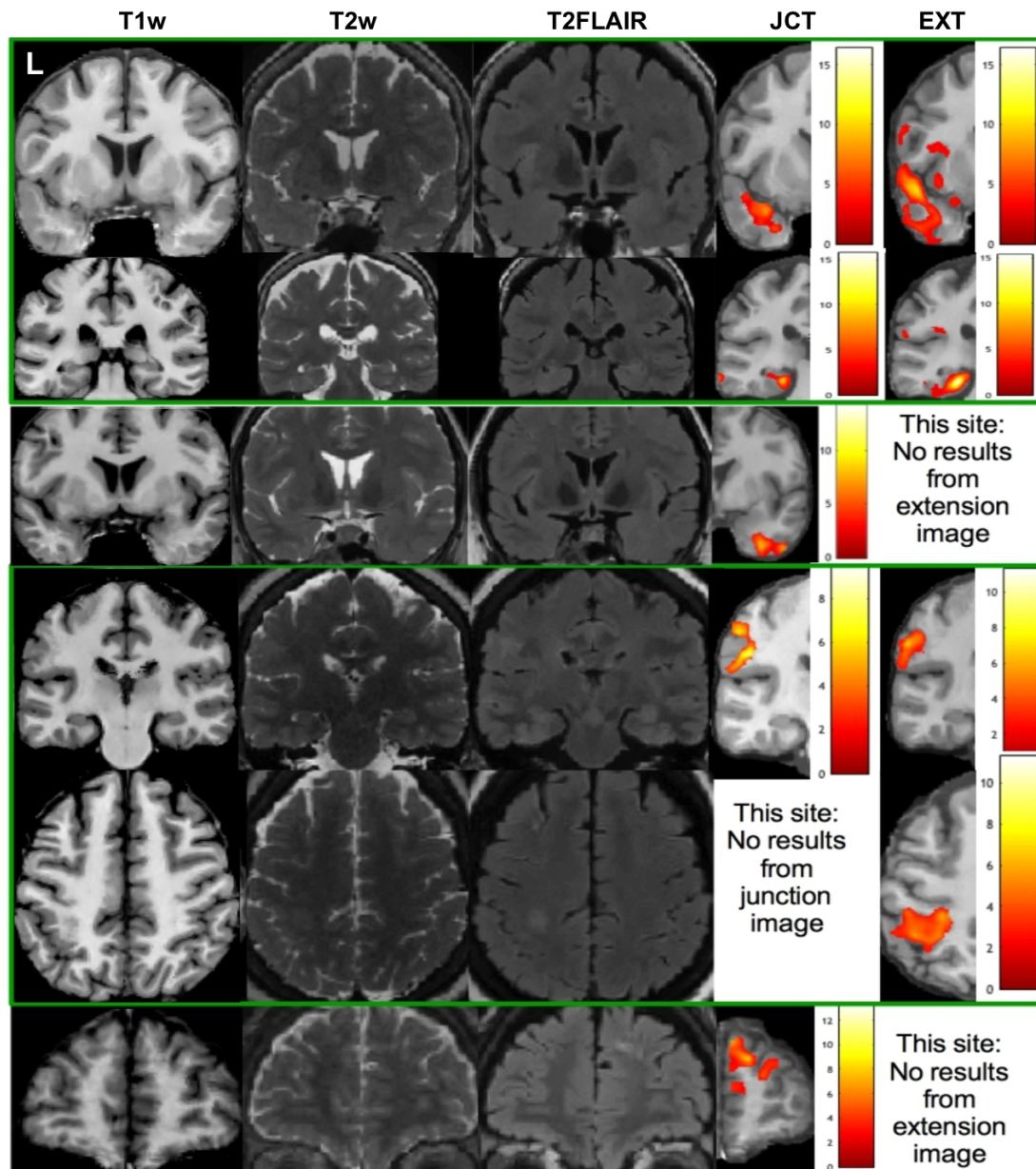


Figure 8.3. Four patients with dysplasia and true positive findings: results from individual statistical testing against 40 controls using T1w JCT and EXT maps. Green bars indicate single patients with two sites of dysplasia. T-scores are represented for JCT and EXT results. From top to bottom: patients with IDs 51, 56, 59 and 65. JCT = T1w junction image; EXT = T1w extension image. L = left.

The true and false positive rates for significant clusters of the respective feature maps can be viewed in Table 8.1.

	Patients			Controls		
	T1w Junction	T1w Extension	Combination JCT + EXT	T1w Junction	T1w Extension	Combination JCT + EXT
True Positive Sites	83% (5/6)	67% (4/6)	100% (6/6)	N/A	N/A	N/A
False Positives	53% (23/43)	30% (13/43)	53% (23/43)	35% (14/40)	18% (7/40)	50% (20/40)

Table 8.1 Results of statistical testing on T1w JCT/EXT images after application of $p < 0.01$ and $p < 0.05$ FWE cluster correction.

The results show that the false positive rate lies between 18% and 53%, while the true positive rate is high. It was at 100% for the combined JCT and EXT image analysis. JCT = junction image; EXT = extension image.

Overall the candidate regions evaluated with the statistical test for both T1w JCT/EXT images were 29/43 (67%) patients (including true positives). For 20/40 (50%) controls, statistical testing on the T1w JCT/EXT images revealed at least one false positive per control. Since these were found in the controls, they were deemed to be non-dysplastic sites, i.e. false positives, and did not form the basis for any further testing.

8.3.3 Multi-modal Analysis Based on MAP Clusters

23 patients showed no true positives at all, however false positives in at least one area of the brain in either a T1w JCT or EXT cluster were found. Clusters were thresholded at the true positive lesion cluster size of 3.5 cm^3 (eliminating eight patients with false positives). The resulting masks of potential lesion sites in 15 patients and the four patients with true positive dysplastic lesions served as ROIs for testing of FA/MD/T2FLAIR/T2w images. In the case that any of these image modalities were significantly different from controls, those clusters served as basis for re-review by a consultant neuroradiologist. Three patients showed suspicious JCT/EXT images but testing on the clusters remained statistically insignificant in any of the other image modalities (FA/MD (both GM/WM) and T2w JCT/EXT, T2FLAIR JCT/EXT/MAX) and were thus deemed to be false positives. The original

false positive number was reduced from 23 (these had only been counted if the patient showed only false positives) to twelve, where eight had been eliminated based on the $>3.5 \text{ cm}^3$ cluster threshold and another three based on the multi-modality test (Figure 8.4). These twelve patients showing abnormalities in also the other image modalities were re-evaluated once more by the consultant neuroradiologist on the basis of the location of the JCT/EXT map clusters. These patients are shown in Figure 8.5 and resulting multimodal ROI testing is shown in Table 8.2.

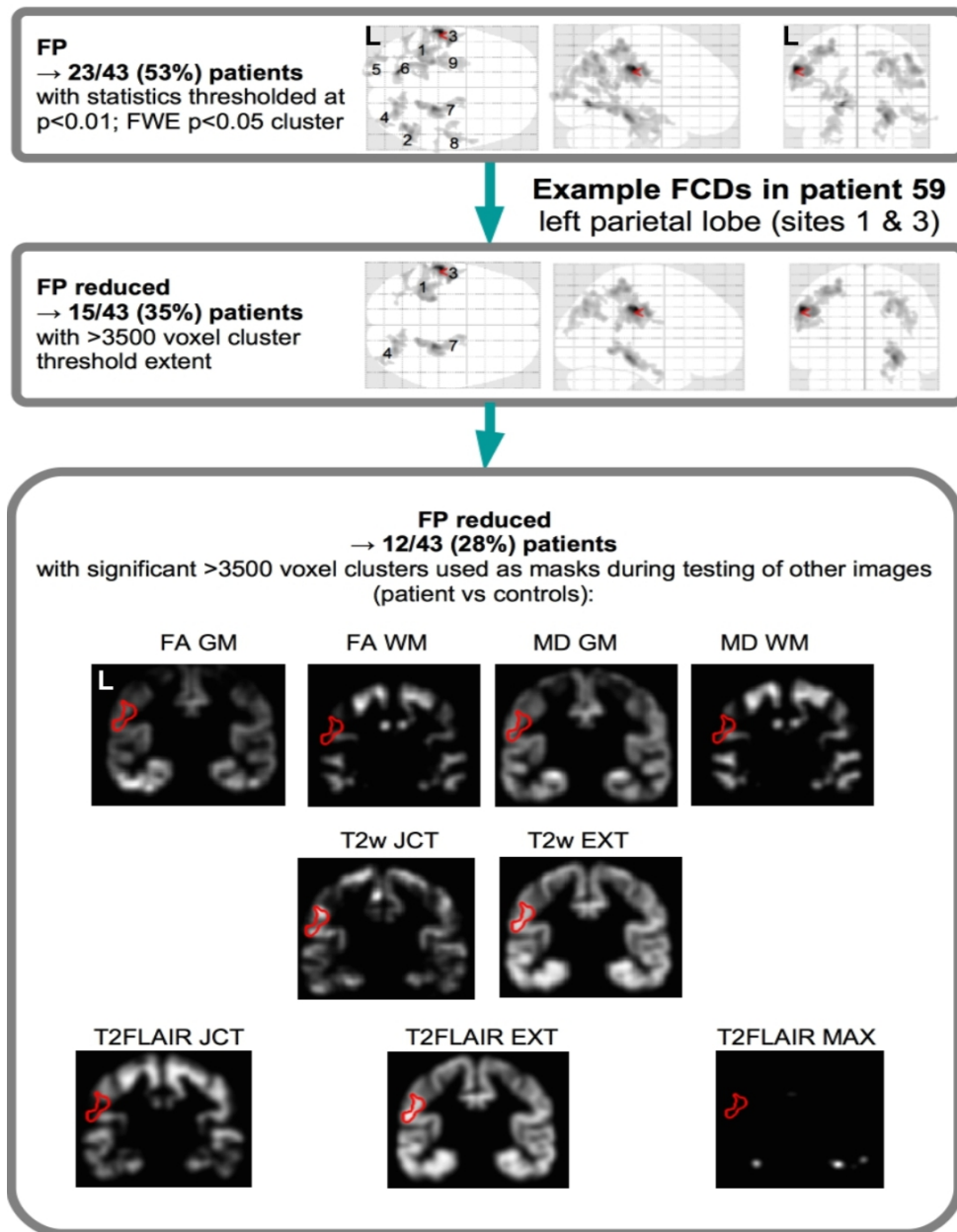


Figure 8.4 Reduction of the false positive rate within the patient sample.

An example patient (59) is featured with all clusters found in EXT and these have been numbered (dorsal → ventral). Based on the statistical test with $p < 0.01$, FWE-cluster correction at $p < 0.05$, 23 patients presented with false positives (first box). Cluster extent thresholding at > 3500 ($> 3.5 \text{ cm}^3$) voxels reduced this number by eight patients (second box). Note the reduction of false positives within a single patient. Using the cluster masks derived from single patients, statistical testing was performed on other imaging modalities. Three patients had insignificant findings in all other imaging modalities and were deemed to be non-dysplastic sites (third box). Overall, the false positive rate was reduced from 53% to 28%. The sites found by the automated tool in these remaining twelve patients were re-reviewed by a neuroradiologist. EXT = extension; JCT = junction; FP = false positive; FA = fractional anisotropy; MD = mean diffusivity; GM/WM = gray/white matter; L = left.

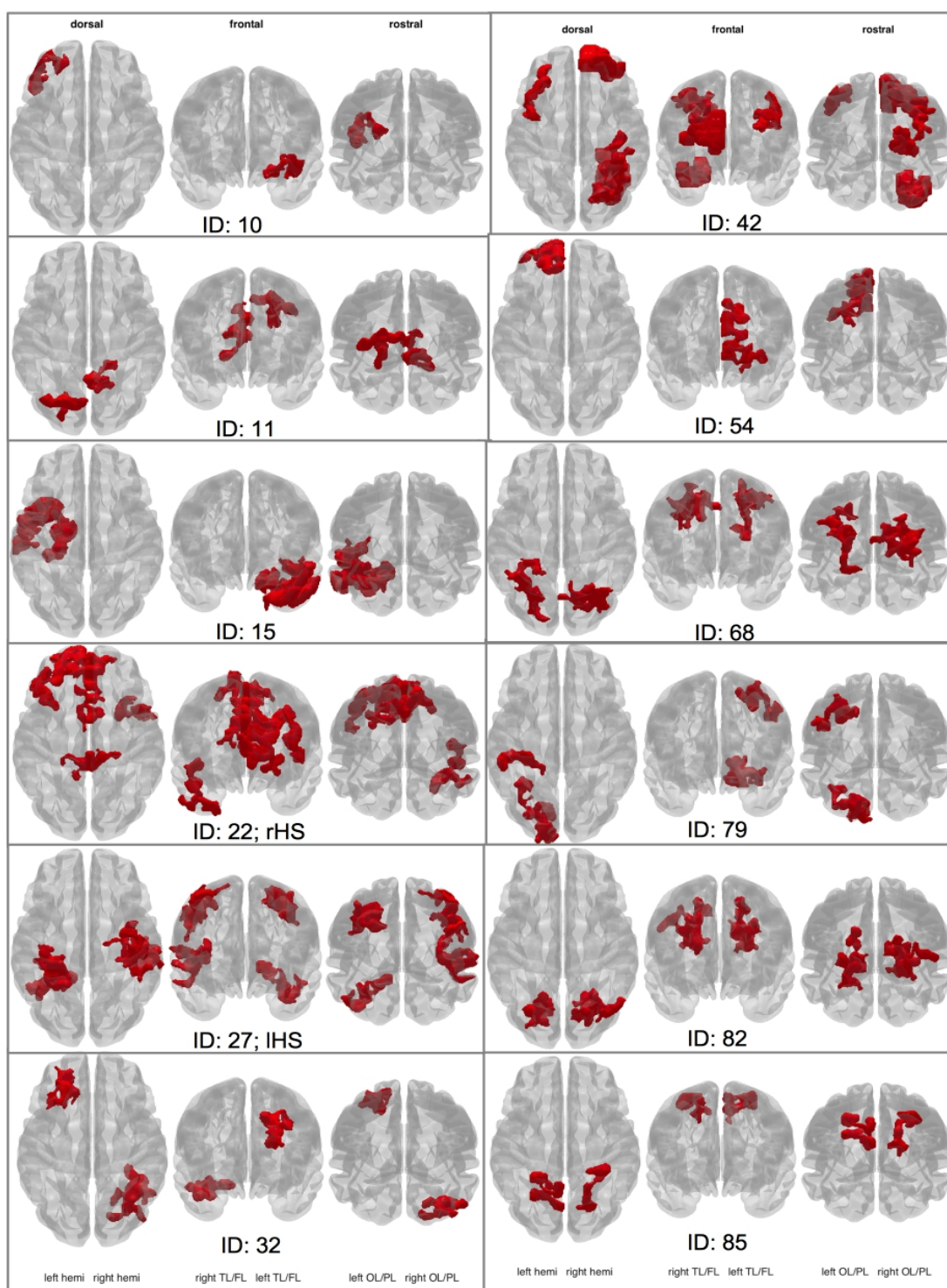


Figure 8.5. Results of combined $>3.5 \text{ cm}^3$ cluster masks based on T1w JCT/EXT analysis. All clusters of the twelve patients are shown. The corresponding sites in T1w/T2w/T2FLAIR images were re-reviewed by a consultant neuroradiologist and clusters (in red) were used as masks in multimodal analysis. HS = hippocampal sclerosis; l = left; r = right; OL/PL/TL/FL = occipital/parietal/temporal/frontal lobe; JCT = junction; EXT = extension.

ID	FA GM	FA WM	MD GM	MD WM	T2w JCT	T2w EXT	T2FLAIR JCT	T2FLAIR EXT	T2FLAIR MAX	Neuro- radiologist
51		<	>	<			<			lesion
56			>							lesion
59	>	<	>	<			<		>	lesion
65									>	lesion
10									>	no lesion
11			>						>	no lesion
15		<		<			<			no lesion
22	>		>				>			rHS, no FCD
27	>		>						>	lHS, no FCD
32			>							no lesion
42	>		>							no lesion
54									>	no lesion
68									>	no lesion
79									>	no lesion
82	>	<	>	<					>	no lesion
85									>	no lesion

Table 8.2. Summary of multimodal statistical testing based on $>3.5 \text{ cm}^3$ cluster masks of T1w JCT/EXT testing.

Patients with neuroradiologically determined FCDs (first four rows) and all twelve patients with no previously identified FCDs with at least one significant result (at $p < 0.01$ and $p < 0.05$ FWE corrected) in one modality are presented. The arrowheads indicate an increased ($>$) and decreased ($<$) signal in the respective patients' image compared to controls. These were also the patients that were re-reviewed by a consultant neuroradiologist. For three patients (34/49/86), none of the images tested in the multimodal approach with their respective $>3.5 \text{ cm}^3$ cluster masks reached significance.

8.4 Summary

The overall aim of this study was to apply a dedicated epilepsy protocol in order to increase the reliable diagnostic yield of MRI in patients with refractory focal epilepsy who were previously reported to be non-lesional. There were two objectives of this study.

Objective 8.1

Automatization of a lesion detection technique and application to MRI of patients with cryptogenic focal epilepsy

CAT12 in SPM12 permitted the implementation of the previously published method by Huppertz et al. (2005) using a fully automated approach. This identified 100% of dysplastic lesions through statistical testing on T1w JCT/EXT images, when results were combined. This means that all sites of dysplasia reported at the start of the study were detected using this technique. Two additional sites in two different patients (left parahippocampal FCD in patient 51 and right temporal pole FCD in patient 56), which had previously escaped neuroradiological assessment, could be identified and were neuroradiologically confirmed.

Objective 8.2

Incorporation of other MRI modalities and effects on sensitivity and specificity

The number of false positives generated through EXT/JCT images (which were 1.5 to 2 times higher than the size of the false positive rate reported in Wang et al. (2015) due to the very low statistical threshold applied in this study) could be reduced by using a cluster threshold ($>3.5 \text{ cm}^3$) on EXT/JCT images and voxel-based analysis of all significant clusters in FA/MD/T2FLAIR and T2w images from 23 patients to twelve. Of the twelve remaining patients with suspicious areas according to the individualized statistical test, none were reported to have an abnormality suggestive of FCD based on time-efficient neuroradiological reassessment guided by the detection tool.

Chapter 9: Manual and Automated Tractography Approaches in Patients with 'non-lesional' and lesional Temporal Lobe Epilepsy

Chapter 9: Manual and Automated Tractography Approaches in Patients with 'non-lesional' and lesional Temporal Lobe Epilepsy.....	166
9.1 Introduction.....	166
9.1.1 Objectives.....	169
9.1.2 Organization of Chapter	170
9.2 Materials and Methods.....	170
9.2.1 Participants.....	170
9.2.2 Data Preprocessing and Quality Assurance.....	171
9.2.3 Manual and Automated Tractography.....	173
9.2.4 Statistical Analysis.....	175
9.3 Results.....	177
9.3.1 Statistics: Demographic and Clinical Information.....	177
9.3.2 Manual versus Automated Tractography.....	178
9.3.2.1 Quality Control.....	178
9.3.2.2 DTI-metrics.....	178
9.3.2.3 Consistency of Tracts.....	180
9.3.2.4 Correlations Between Whole-tract DTI Metrics and Clinical Variables.....	180
9.3.3 Tract Profile Analysis (AFQ)	181
9.4 Summary	185

9.1 Introduction

Quantitative analysis can extend conventional visual assessment of MRI and is especially useful when modeling network connections in the brain. This can be achieved by using tractography analysis approaches, which shed light on structural connectivity and neuroanatomical structure and may be particularly useful for investigating potentially epileptogenic networks. Typically this is performed using manual tractography, however, recently automated tools that automatically reconstruct WM pathways have been developed (see also Chapter 6). Automated approaches are more time and resource efficient compared to manual approaches as

they do not require time-consuming delineation of tracts by trained researchers (Hagler et al. 2009).

AFQ (<https://github.com/jyeatman/AFQ>) is a novel tool, which allows investigation of WM tract diffusion alterations in standard space (Yeatman et al. 2012). It has been predominantly used to assess WM changes along tracts, which is especially useful for the study of network disorders. Diffusion characteristics have been shown to vary along tracts in healthy individuals (Johnson et al. 2013), in preterm children and adolescents (Travis et al. 2015a, Travis et al. 2016, Søsnes et al. 2016), in patients with anorexia nervosa (Travis et al. 2015b), autism spectrum disorder (Libero et al. 2015), depression (Sacchet et al. 2014a, Sacchet et al. 2014b) and in patients with TLE (Keller et al. 2017, Glenn et al. 2016, Concha et al. 2012). In patients with TLE, these localized changes are possibly related to the severity and chronicity of the disorder rather than to an initial precipitating injury like HS (Kreilkamp et al. 2017). The recent interest in automated tractography using AFQ is promising for the study of neurological and psychological disorders, however evidence for significant correlations with manual tractography is still sparse. So far, Yeatman et al. (2012) have been the only authors to publish information comparing AFQ to manual tractography, which is considered to be the gold-standard (Wakana et al. 2007). However, this information is limited to correlations of FA, diffusion values obtained from manual versus automated tractography (Yeatman et al. 2012). To date, no information has been provided with respect to comparisons between AFQ and manual tractography with relation to whole tract shape, size and location (morphology), the estimation of diffusion measures and consistency of results pertaining to differences in diffusion characteristics between groups across these different approaches. However, these measures are necessary to contribute to a deeper understanding of how manual tractography techniques (typically assessing whole-tract diffusion characteristics based on manual tractography) relate to novel

automated tools and how reliable tractography using AFQ may be. This type of validation has already been performed in volumetric WM analysis in clinical settings (Zijdenbos et al. 1994) and can easily be implemented using the Dice coefficient (Dice 1945). While it is important to develop automated whole-tract and along-the-tract diffusion tractography methods (Concha et al. 2012, Glenn et al. 2016, Keller et al. 2017, Kreilkamp et al. 2017), it should not come at the cost of disregarding the large quantity of previous research using manual methods. Automated techniques provide substantial benefits as they circumvent the need for extensive training of researchers to perform manual measurements and provide reproducible algorithms that can be applied to multiple datasets in an efficient manner. Recent literature has relied on these novel automated methods even though they have not been extensively validated in healthy controls and patients with brain disorders apart from few exceptions (such as TRACULA (Yendiki et al. 2011), Chapter 6). In the absence of neuroanatomical data, manual techniques are considered to be closest to the ground truth and are regarded as the "gold standard" when performing tractography studies (Yeatman et al. 2012). For these reasons, AFQ and manual tractography approaches were applied in patients with TLE with and without HS and healthy controls (Mueller et al. 2006, Liu et al. 2012). These cited studies have shown more widespread WM alterations in patients with TLE and associated HS. Therefore, an aim of this study was to apply these comparisons using the manual and novel automated tractography approaches.

AFQ additionally offered the possibility to extract diffusion metrics along tracts (unlike the manual approach) and perform (i) comparisons across patient groups defined by seizure onset laterality and (ii) correlations of these values with clinical variables. The FF (Concha et al. 2005, Concha et al. 2009, Concha et al. 2010), PHWM (Ahmadi et al. 2009, Keller et al. 2012) and UF (Lin et al. 2008, Ahmadi et al. 2009) tracts were analyzed due to their central involvement in TLE. The FF was

also included in WM tract analysis for the automated approach as it is readily available, which is not the case for manual tractography. WM alterations within this tract have been shown to differentially affected in patients with excellent post-surgical outcomes and those without when compared to controls (Keller et al. 2017).

9.1.1 Objectives

There were two objectives for the study presented in this chapter.

Objective 9.1

The first objective was to investigate the agreement between manually and automatically generated tracts in patients with TLE. Furthermore, consistency between the automated and manual approaches with respect to whole tract diffusivity metrics (FA/MD), detection of diffusivity abnormalities in tracts of patients with TLE and clinical correlations with diffusion metrics were investigated.

It was hypothesized that manual and automated methods produce tracts of the same shape, volume and at similar locations and in order to assess this, the Dice coefficient was computed. Moreover, it was hypothesized that DTI-metrics extracted from WM tracts using the two different approaches are consistent (high correlations of FA/MD values across approaches) and that significant group-wise results of whole-tract diffusion measures arising of comparisons between the two patient groups and controls are also comparable. The number of significant group differences and correlations found by AFQ and manual tractography as the "gold standard" were directly compared. It was hypothesized that AFQ would identify the same number of group-wise differences and correlations.

Objective 9.2

The second objective of this chapter was to investigate whether along-the-tract diffusivity analysis of FF, UF and PHWM within the automated tractography approach can reveal correlations with clinical variables and group differences between patients with left/right TLE, with HS, those without and controls and provide more detailed information than the manual approach.

It was hypothesized that the along-the-tract analysis offered within the automated tractography approach would confirm previous group-wise findings, detect correlations with clinical variables and that it could reveal more detail in diffusivity alterations regarding correlations with clinical variables such as age of onset of epilepsy and epilepsy duration and when investigating diffusivity alterations in patients with HS, those without and controls.

9.1.2 Organization of Chapter

Demographic and clinical details of all the participants studied, methods relating to manual and automated tractography and statistical analysis are presented in Section 9.2. Results from comparisons between manual and automated tractography techniques and group comparison studies as well as correlation studies are separated and presented in Section 9.3. A summary of significant findings from this study is detailed in Section 9.4 together with the chapter objectives.

9.2 Materials and Methods

9.2.1 Participants

Demographic and clinical characteristics are detailed in Table 9.1. A history of brain infection was positive if the patient reported to have had meningitis or encephalitis.

Seizure burden was calculated as $\log(\text{duration of epilepsy} \times \text{seizure frequency per week})$. For all details regarding acquisition parameters for the used sequences the reader is referred to Chapter 2, Section 2.3.

Variable	Patients with left TLE	Patients with right TLE	Controls
N	16	8	40
Sex (female/male)	10/6	5/3	23/17
Mean age in years (SD)	32.1 (11.4)	31.8 (12.3)	32.4 (8.7)
History of infection (no/yes)	16/0	4/4	-
History of febrile seizures (no/yes)	12/4	7/1	-
SGTCS (no/yes)	5/11	3/5	-
Mean age of onset (SD)	15.8 (11.4)	18.1 (11.6)	-
Mean seizure burden (SD)	1.4 (0.5)	1.3 (0.7)	-
Mean duration corrected for age (SD)	0.5 (0.3)	0.4 (0.3)	-
Mean seizure frequency per week (SD)	4.9 (8.9)	3.4 (4.7)	-
Presence of HS (no/yes)	12/4	4/4	-

Table 9.1. Demographic and clinical information for all participants.

TLE = Temporal Lobe Epilepsy; SD = Standard Deviation; SGTCS = Secondary-Generalized Tonic-Clonic Seizure; HS = hippocampal sclerosis.

9.2.2 Data Preprocessing and Quality Assurance

Before tensor fitting and tractography were performed, DTI data was processed using FMRIB Software Library (FSL) version 5.0.9 (<http://fsl.fmrib.ox.ac.uk/fsl/fslwiki/FSL>) according to the ENIGMA DTI-preprocessing steps to mitigate effects of image artifacts (<http://enigma.ini.usc.edu/protocols/dti-protocols/>). In particular, the first b0 image was used as a reference for co-registration of the five subsequent b0 images (FSL FLIRT, Smith et al. 2004).

The resulting co-registered b0 images were averaged and served as a reference image

during motion and distortion correction on the diffusion-weighted images. In order to achieve distortion correction, the T2w image was rigidly aligned with the mean b0 image (Smith et al. 2004). The mean b0 image and the T2w image in diffusion space were thus combined to a pair of images with the first image representing geometric distortions while the T2w image served as an anatomically correct reference. From this pair the susceptibility-induced off-resonance field was estimated (Andersson et al. 2003) and the two images were combined into a single corrected one, which was then brain-extracted. The diffusion-weighted images were corrected for motion and the resulting nonlinear registration information from the distortion correction step was used to unwarp subsequent diffusion-weighted images in native diffusion space (Andersson and Sotiropoulos 2016). The gradient table information was adjusted according to the rigid body motion parameters (Leemans and Jones 2009).

A recent publication (Yendiki et al. 2013) has introduced a value to characterize gross motion: TMI, which serves as a summary value for magnitudes of translational and rotational motion. As DTI data aims to accurately assess microscopic motion in order to derive tissue diffusion metrics, it is important to consider macroscopic motion, which may otherwise have confounding effects on group-wise differences. Changes in TMI between patients with left TLE, right TLE and controls were assessed by using the Kruskal-Wallis ANOVA (data non-normally distributed, Lilliefors Test $p < 0.05$). Another possible confounding factor in DTI analysis are variations in SNR, which has been shown to alter diffusion metrics (Farrell et al. 2007). Any effects of SNR on FA/MD group comparisons were ruled out by performing a Kruskal-Wallis ANOVA on SNR values extracted from the motion corrected data (FSL eddy), which had subsequently been used during tensor estimation. Specifically, the AFQ WM segmentation map was used and thresholded at 0.9, it was then used to mask the motion corrected diffusion-weighted images and extract mean and standard deviations for WM intensities to compute the ratio of the

two (\rightarrow SNR), similarly proposed in TRACULA (Yendiki et al. 2011).

9.2.3 Manual and Automated Tractography

Manual tractography was performed in Diffusion Toolkit version 0.6.3 (<http://www.trackvis.org>) using the 2nd order Runge-Kutta tract propagation algorithm in native diffusion space [step size of 1mm, angle threshold of 35°]. After tensor estimation and whole-brain tractography the UF and PHWM were analyzed. To achieve this, these two temporal lobe tracts were extracted using ROI placement on the native diffusion space FA image. Specifically, ‘AND’ and ‘NOT’ ROIs were placed based on a previously published method to delineate fibers belonging to either UF or PHWM bundles (Metzler-Baddeley et al. 2011) (Figure 9.1). For conventional whole-ROI analysis of FA and MD, tract density images were saved for bilateral UF and PHWM tracts and binarized.

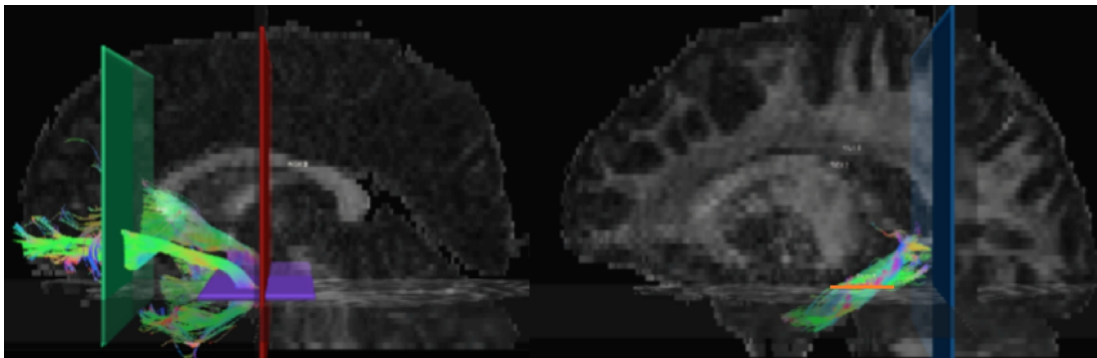


Figure 9.1. Manual delineation of UF (left) and PHWM (right) tracts.

Tracts were delineated using ROIs drawn on the subjects' FA image in native diffusion space. 'AND' ROIs (green, purple and orange) served as ROIs where tracts were allowed to pass through, while 'NOT' ROIs (red and blue) were used to define the end of tracts. Tract colors define the principle direction of diffusion for single fibers (red = left/right, blue = inferior/superior, green = anterior/posterior).

Automated whole-brain AFQ tractography was run using default parameters: 4th order Runge-Kutta approach (Yeatman et al. 2012) based on the Euler method (step

size of 1mm, angle threshold of 35°; Basser et al. 2000). However, before this, AFQ performed a series of preprocessing steps automatically, including T1w co-registration for each diffusion-weighted image, brain extraction (Smith 2002) and voxel-wise estimation of the diffusion tensor. After whole-brain tractography, AFQ non-linearly co-registered the mean b0 image to the ICBM template and the inverse transformation was used to map the normalized ICBM WM ROIs provided within AFQ to the individual subject space. The ends of AFQ fiber bundles were defined by these ROIs and tracts were subsequently clipped and classified as belonging to the respective tracts by AFQ (Figure 9.2). These steps were performed in individual T1w image space within AFQ.

For conventional whole-ROI analysis of FA and MD, tract density images were saved for bilateral UF and PHWM tracts and binarized. After tract segmentation, tract cores for UF, PHWM and FF (not available in manual tractography) were identified and FA/MD value profiles for each tract were calculated based on the weighted-mean approach, where FA/MD values of fibers close to the tract core contribute more to the along-the-tract measures than fibers distant to the core. This allowed tract profile group (Travis et al. 2015a, Yeatman et al. 2012, Keller et al. 2017) and correlation analysis within AFQ.

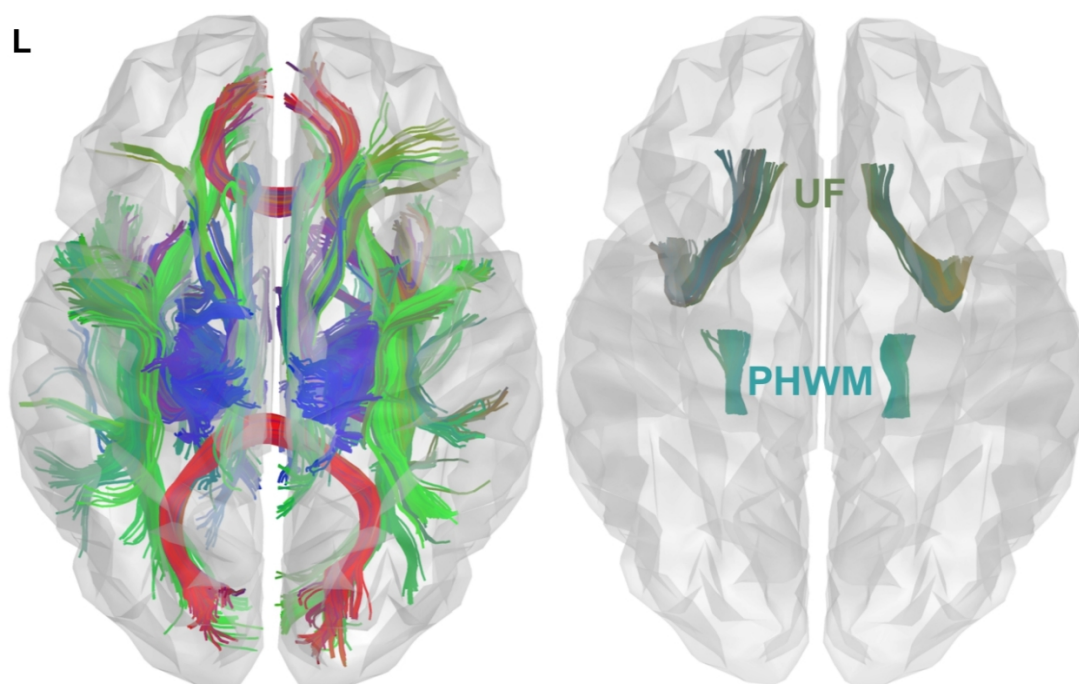


Figure 9.2. Dorsal views of the brain showing all bilateral cleaned (left) and clipped UF and PHWM AFQ tracts (right).

The colors of the tracts denote the principle direction of diffusion for the midpoint of the particular fiber (red = left/right, blue = inferior/superior, green = anterior/posterior). Image rendered in standard ICBM space with MRicroS tool, version 2015 (<https://www.nitrc.org/plugins/mwiki/index.php/mricros:MainPage>). L = left.

9.2.4 Statistical Analysis

Differences in demographic information between all three groups was assessed with a Kruskal-Wallis ANOVA (age) and chi-square test of independence (sex). An unpaired two-tailed Wilcoxon-Rank-Sum test was used to assess differences in continuous clinical variables (age of onset, seizure burden, epilepsy duration corrected for age and seizure frequency per week) of patient groups (right and left TLE & patients with and without HS) while a chi-square test of independence was used for dichotomous variables relating to history of infection, febrile seizures and SGTCs.

The number of significant group differences found between AFQ and manual tractography were directly compared. To achieve this, the manual tracts were clipped to the same length as the AFQ fibers using the AFQ ROI endings in all three dimensions (x/y/z) and whole-tract FA (thresholded at $FA > 0.2$) and MD values were extracted from both tractography approaches using FSL software (Smith et al. 2004). All data was non-normally distributed (Lilliefors, $p < 0.05$), and therefore a non-parametric Kruskal-Wallis ANOVA was used to investigate differences between participant groups (patients with left/right TLE and controls). Post-hoc analysis was conducted using the Bonferroni correction procedure. Furthermore, whole-tract FA/MD value correlations between approaches were assessed using the Spearman correlation coefficient with Bonferroni multiple comparison correction. Tract morphology of all clipped fibers generated either by AFQ or the manual method were assessed using the Dice coefficient (Dice 1945). The following results from Dice coefficient analysis indicated poor agreement (< 0.2), fair agreement (0.2-0.4), moderate agreement (0.4-0.6), good agreement (0.6-0.8) and excellent agreement (0.8-1.00) as previously discussed (Cicchetti 1994, Zijdenbos et al. 1994). Additionally, gross volumes of automatically and manually generated tracts were assessed using a paired Wilcoxon-Sign-Rank test. Correlations between whole-tract diffusion metrics and various clinical measures were also investigated using the Spearman Rank Correlation Coefficient. These included seizure burden ($\log(\text{duration of epilepsy} \times \text{seizure frequency per week})$), age of onset, duration of epilepsy corrected for age, seizure frequency per week, and age. After investigating correlations pertaining to the automated and manual approach, both sets of results were separately corrected for multiple comparisons according to the FDR procedure. For every tractography approach, the Wilcoxon-Rank-Sum test was used to assess any differences between diffusion metrics and sex, the presence of HS, febrile seizures and SGTCS. After testing this, results derived from both tractography

approaches were corrected using the FDR procedure separately.

AFQ additionally allowed the analysis of diffusion metrics along the tracts (tract profile analysis). Using this approach, comparisons were made between patients with left TLE, right TLE and controls. A comparison between patients with HS and those without and controls was also conducted. For this analysis, the patients with right TLE were side-flipped and a subset of controls was also side-flipped to account for inter-hemispheric differences (Keller et al. 2015a). The reason for performing this was to allow the investigation of ipsilateral and contralateral effects with a sufficient number of participants (N=8). Finally, demographic (age, sex) and clinical variables (age of onset, duration of epilepsy corrected for age, seizure burden and frequency, history of febrile and SGTC seizures) were correlated with diffusion characteristics as generated by AFQ tract profile analysis. Along-the-tract diffusion value and correlation analysis were corrected for multiple comparisons using the FDR procedure. Results were considered significant at $p < 0.05$.

9.3 Results

9.3.1 Statistics: Demographic and Clinical Information

All demographic/clinical information (Table 9.1) underwent statistical testing between patients with left/right TLE and controls. There were no differences between the three groups concerning age ($\chi^2(2,63)=0.3$, $p=0.9$) or sex ($\chi^2(2)=0.9$, $p=0.6$). Analysis of differences in age of onset ($Z=-0.46$, $p=0.7$), seizure frequency ($Z=0.22$, $p=0.8$), burden ($Z=0.28$, $p=0.8$) and duration corrected for age ($Z=0.89$, $p=0.4$) did not reveal any significant effect with respect to side of seizure onset. There were also no differences in clinical information between patients with left/right TLE: history of febrile seizures ($\chi^2(1)=0.03$, $p_{\text{(Yate)}}=0.9$), infection ($\chi^2(1)=3.8$,

$p_{(Yate)}=0.051$) and SGTCS ($\chi^2(1)=0.02$, $p_{(Yate)}=0.9$). However, as the chi-square test is inappropriate for data where any expected frequency is below 1 or if the expected frequency is less than 5 in more than 20% of subgroups (Preacher 2001), results could only be considered to be accurate when Yate's correction was performed on the statistics (Yates 1934). As this was the case for these variables, results were reported here only after Yate's correction had been employed ($p_{(Yate)}$).

9.3.2 Manual versus Automated Tractography

9.3.2.1 Quality Control

Before comparing any DTI-derived metrics motion differences between groups were assessed. However, no differences in TMI between controls (Mean = 0.3 ; SD = 1.6), patients with left TLE (Mean = 0.4; SD = 1.4) and patients with right TLE were found (Mean = 0.02; SD = 1.3); $\chi^2(2,63) = 0.3$, $p = 0.9$. The mean SNR for diffusion-weighted images did not differ among groups: controls (Mean = 2.9; SD = 0.1), patients with left TLE (Mean = 2.8; SD = 0.1) and patients with right TLE (Mean = 2.8; SD = 0.2); $\chi^2(2,63) = 4.1$, $p = 0.1$.

9.3.2.2 DTI-metrics

Significant results in whole WM tract FA/MD (ROI) values across patient and control groups are shown in Figure 9.3 and Table 9.A (Appendix II: Supplementary Material). For AFQ group analysis, patients with left TLE had significantly reduced FA in the right PHWM and increased MD in the right UF relative to controls. These changes were also identified by the manual method, however, additional changes were found for patients with left TLE when compared to controls: decreased FA in the left UF, increased MD in the left UF and in the right PHWM and patients with right TLE had increased MD in the left PHWM.

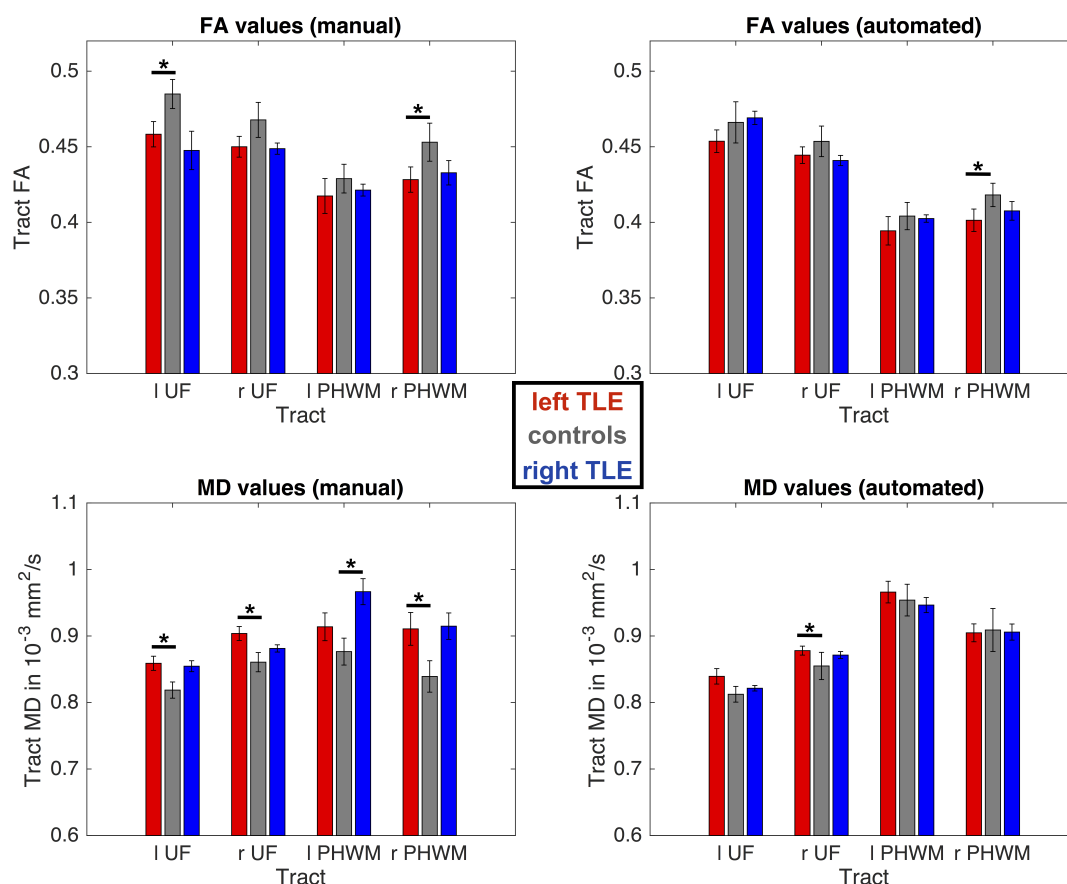


Figure 9.3. Whole-tract diffusion measures for manual (left) versus AFQ (right) tractography.

For each group and tract median FA/MD values are presented along with respective standard errors. Using manual tractography, patients with left TLE had significantly reduced FA values in the left UF and right PHWM and increased MD values in left and right UF and PHWM, while patients with right TLE had an increase in MD in the left PHWM compared to controls (top left and bottom left). AFQ was only able to identify the FA decrease in the right PHWM and MD increase in the right UF for patients with left TLE (bottom right). FA = fractional anisotropy; MD = mean diffusivity; UF = uncinate fasciculus; PHWM = parahippocampal white matter bundle; l = left; r = right. * $p < 0.05$, corrected for multiple comparisons.

FA values extracted from the two different approaches were significantly correlated for each tract: left UF ($R = 0.6$, $p < 0.001$), right UF ($R = 0.8$, $p < 0.001$), left PHWM ($R = 0.7$, $p < 0.001$), right PHWM ($R = 0.7$, $p < 0.001$). The agreement between MD

values extracted from AFQ and from the manual measurements also correlated well for left UF ($R = 0.8$, $p < 0.001$) and right UF ($R = 0.8$, $p < 0.001$), whereas left PHWM ($R = 0.4$, $p < 0.01$) and right PHWM ($R = 0.3$; $p < 0.05$) could not be considered significant after performing Bonferroni correction; $p(\text{corr}) = \alpha/n = 0.05/8 = 0.006$.

9.3.2.3 Consistency of Tracts

The automatically reconstructed fiber tracts had increased volume (Mean = 1457; SD = 630) when compared to manual tracts (Mean = 1018; SD = 566); paired Wilcoxon-Sign-Rank test ($Z = 12.3$; $p < 0.001$). Tract morphology between automated and manual tractography approaches were assessed using the dice coefficients. The respective results for tract ROIs were 0.54 (± 0.12) for the left UF, 0.57 (± 0.14) for the right UF, 0.6 (± 0.12) for the right PHWM and 0.6 (± 0.08) for the left PHWM. Based on the framework proposed by Cicchetti (1994), the agreement between the two methods was moderate for UF (bilateral) and good for PHWM (bilateral). A visual assessment also revealed that shape and location of the tracts matched each other across tractography methods and the same tract center voxels were identified with excellent overlap (Dice Coefficients), however, the automated tractography approach yielded slightly larger tract estimates (see above).

9.3.2.4 Correlations Between Whole-tract DTI Metrics and Clinical Variables

No correlations between clinical variables and DTI-metrics extracted through manual tractography (Table 9.2) were found. However, for data extracted from AFQ, there were significant correlations between age of onset and ipsilateral PHWM FA ($R = 0.6$; $p_{(\text{FDR})} < 0.05$) and MD ($R = -0.6$; $p_{(\text{FDR})} < 0.05$), duration of epilepsy and ipsilateral PHWM MD ($R = 0.8$; $p_{(\text{FDR})} < 0.01$), which survived correction for age ($R = 0.7$; $p_{(\text{FDR})} < 0.01$). For dichotomous variables (sex, HS, SGTCS, history of febrile seizures) no significant effects were observed using both tractography approaches and are presented in Table 9.B (Appendix II: Supplementary Material).

Manual Tractography								Automated Tractography					
Tract Metric	Side	Age	Age of Onset	Burden	Duration	Duration (corr. Age)	Frequency	Age	Age of Onset	Burden	Duration	Duration (corr. Age)	Frequency
UF	ipsi	R=-0.6 p=0.1	R=0.01 p=1	R=-0.4 p=0.3	R=-0.4 p=0.2	R=-0.3 p=0.6	R=-0.2 p=0.7	R=-0.4 p=0.3	R=0.01 p=1	R=-0.1 p=1	R=-0.2 p=0.6	R=-0.1 p=0.8	R=-0.1 p=0.8
	contra	R=0.1 p=0.8	R=0.5 p=0.2	R=-0.1 p=1	R=-0.3 p=0.4	R=-0.4 p=0.2	R=0.2 p=0.7	R=-0.2 p=0.5	R=0.3 p=0.4	R=-0.3 p=0.5	R=-0.5 p=0.1	R=-0.4 p=0.2	R=0.1 p=1
MD	ipsi	R=0.3 p=0.4	R=-0.1 p=0.9	R=-0.1 p=1	R=0.3 p=0.5	R=0.2 p=0.7	R=-0.2 p=0.6	R=0.1 p=0.8	R=-0.3 p=0.5	R=-0.1 p=0.9	R=0.2 p=0.5	R=0.3 p=0.5	R=-0.2 p=0.5
	contra	R=0.01 p=1	R=-0.5 p=0.1	R=0.2 p=0.7	R=0.5 p=0.1	R=0.6 p=0.1	R=0.01 p=1	R=0.1 p=0.9	R=-0.4 p=0.3	R=0.3 p=0.4	R=0.5 p=0.1	R=0.5 p=0.1	R=0.1 p=0.8
PHWM	ipsi	R=-0.03 p=1	R=0.6 p=0.1	R=-0.2 p=0.7	R=-0.4 p=0.2	R=-0.5 p=0.1	R=0.02 p=1	R=-0.1 p=0.8	R=0.6 p=0.02	R=-0.2 p=0.5	R=-0.5 p=0.1	R=-0.6 p=0.1	R=-0.02 p=1
	contra	R=-0.1 p=1	R=0.4 p=0.2	R=-0.01 p=1	R=-0.3 p=0.4	R=-0.3 p=0.4	R=0.02 p=1	R=-0.02 p=1	R=0.4 p=0.2	R=0.01 p=1	R=-0.4 p=0.3	R=-0.4 p=0.3	R=0.1 p=0.9
PHWM	ipsi	R=0.4 p=0.2	R=-0.3 p=0.5	R=0.1 p=1	R=0.5 p=0.2	R=0.4 p=0.2	R=-0.2 p=0.6	R=0.3 p=0.3	R=-0.6 p=0.02	R=0.3 p=0.3	R=0.8 p<0.001	R=0.7 p<0.01	R=-0.02 p=1
	contra	R=0.4 p=0.2	R=0.02 p=1	R=-0.1 p=1	R=0.3 p=0.5	R=0.2 p=0.7	R=-0.2 p=0.6	R=0.3 p=0.3	R=-0.1 p=0.9	R=0.2 p=0.6	R=0.4 p=0.2	R=0.3 p=0.5	R=0.01 p=1

Table 9.2. Correlations of whole-tract FA/MD values with variables for both approaches. Spearman rho values (R) are shown with FDR corrected p-values (p) for each type of analysis (manual and automated). Boldface indicates significant effects. UF = uncinate fasciculus; PHWM = parahippocampal white matter bundle; FA = fractional anisotropy; MD = mean diffusivity; ipsi = ipsilateral; contra = contralateral.

9.3.3 Tract Profile Analysis (AFQ)

In contrast to the manual tractography method, AFQ software also allowed the automated analysis of FA/MD values along tract cores. A significantly reduced FA in a small area of the right UF in patients with right TLE relative to controls was found, while patients with left TLE had significantly increased MD in two small regions of the left UF and in large portions of the right UF relative to controls (Figure 9.4).

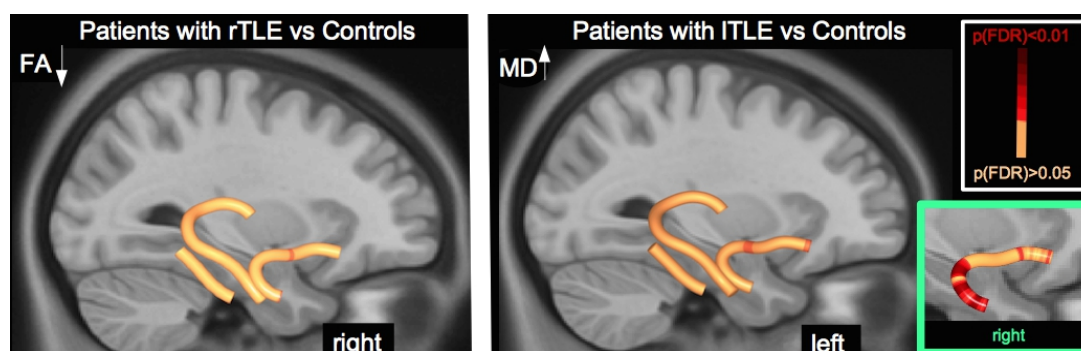


Figure 9.4. Comparison of Patients with right and left TLE versus controls.

The T1w overlay in standard space shows areas of the UF where patients had decreased FA (left, red areas) and increased MD (right and inset, red areas). rTLE = right TLE; lTLE = left TLE; FA = fractional anisotropy; MD = mean diffusivity.

Furthermore, patients with and without HS were compared to controls. There was significantly decreased FA in the frontal part of the ipsilateral UF and significantly increased MD in the frontal and temporal parts of the contralateral UF in patients with HS compared to controls (Figure 9.5). There were no significant differences between patients without HS and controls. Patients with HS had significantly decreased FA in the frontal part of the contralateral UF relative to patients without HS (Figure 9.5).

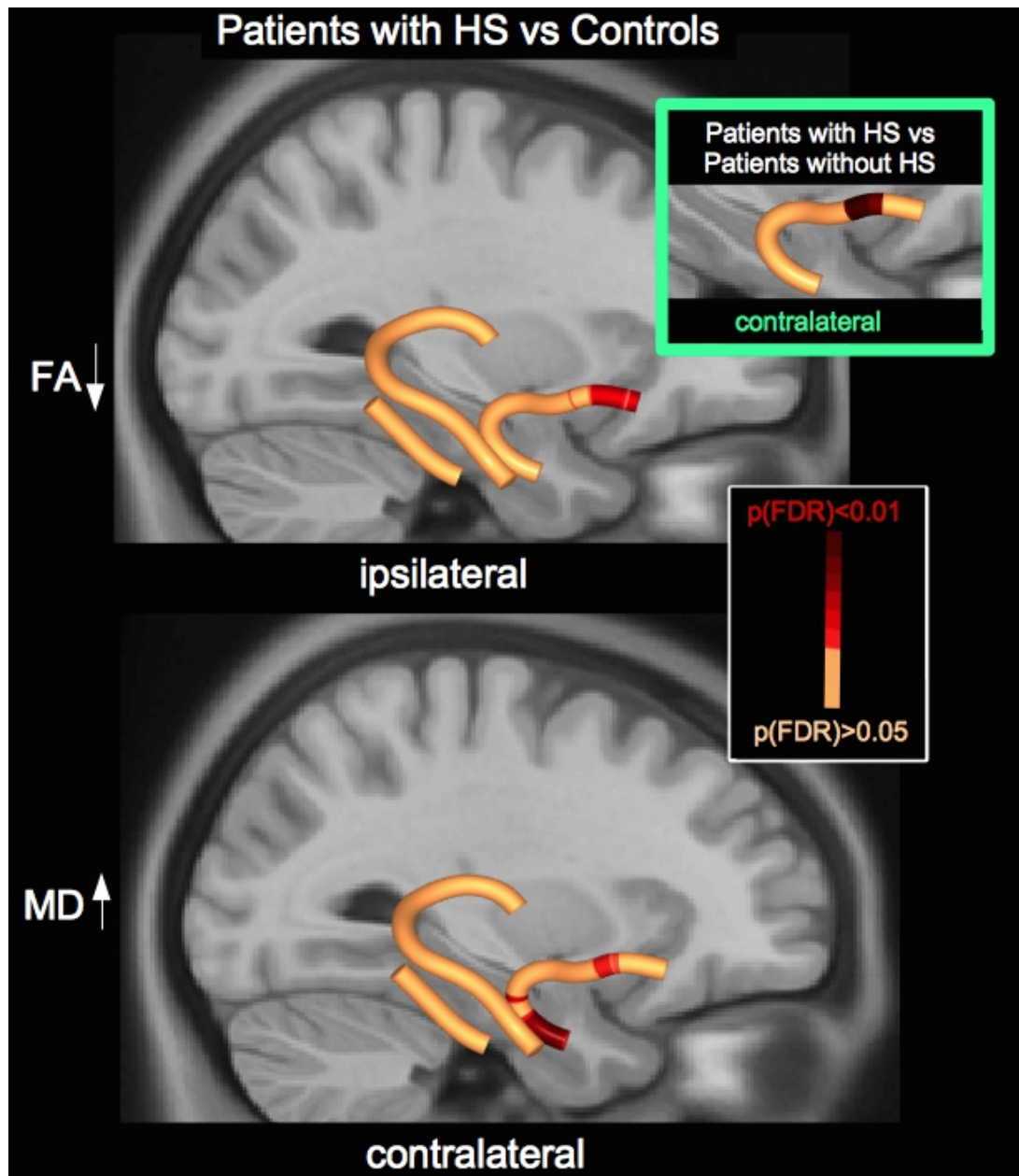


Figure 9.5. Patients with HS compared to controls and patients without HS (inset). The T1w overlay in standard space shows areas of the UF where patients with HS had decreased FA (top and inset, red areas) and increased MD (bottom, red areas). FA = fractional anisotropy; MD = mean diffusivity. HS = hippocampal sclerosis.

For all patients, correlations between FA/MD tract profile values and demographic / clinical variables were investigated. Several significant correlations were found, including age (ipsilateral decrease of FA in UF with increasing age), younger age at onset (decrease of FA in ipsilateral PHWM; increase of MD in ipsilateral PHWM and contralateral UF), increased seizure burden (correlated with a decrease in FA in a small posterior section of the contralateral PHWM) and a longer epilepsy duration corrected for age (correlated with a decrease of FA in ipsilateral and contralateral PHWM and an increase of MD in ipsilateral PHWM and contralateral UF). No correlations were found between FA/MD values of the FF and clinical variables (Figure 9.6).

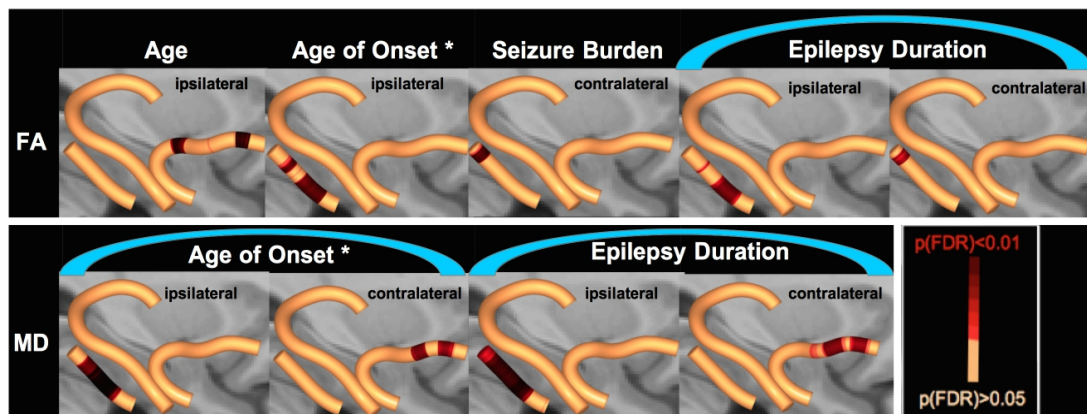


Figure 9.6. Correlations of DTI-metrics with demographic and clinical variables.

There were correlations between FA (top row) and age, age of onset, seizure burden and epilepsy duration corrected for age. All FA correlations were negative except for the correlation with age of onset, which was positive (marked with an asterisk, younger age of onset was associated with decrease in FA of the ipsilateral PHWM). There were also correlations between patient MD values (bottom row) and age of onset (negative, marked with an asterisk) and epilepsy duration corrected for age (positive).

9.4 Summary

There were two objectives for this study.

Objective 9.1

Agreement between manual and automated tractography

A whole-tract analysis approach is feasible with both tractography approaches (manual and AFQ). The analysis of consistency across approaches revealed a high degree of similarity in Dice Coefficients for the extracted tract shape, morphology and space (Dice coefficients at moderate to good agreement) and a strong correlation between FA/MD values extracted with both methods. The sensitivity of the tractography approaches differed within group FA/MD analysis regarding significant differences found across patients and controls. The manual approach revealed more differences than AFQ in group comparisons of whole-tract DTI-metrics. No correlations between whole-tract diffusion characteristics and clinical variables survived correction for multiple comparisons using the manual approach. In contrast to this, the whole-tract DTI-metrics determined using AFQ revealed correlations with clinical variables such as age of onset and duration of epilepsy corrected for age.

Objective 9.2

Along-the-tract diffusivity analysis of FF, UF and PHWM using automated tractography

The results obtained through conventional whole-tract diffusivity analysis between patients with left/right TLE and controls and correlation analysis were also confirmed through the along-the-tract analysis provided within AFQ. Overall, AFQ's along-the-tract analysis gave a more detailed description of localized diffusivity

changes that correlated with age, age of onset, seizure burden and epilepsy duration corrected for age. No correlations were found between FA/MD values of the FF and clinical variables. While there were significant diffusivity alterations in patients with HS compared to controls and compared to patients without HS, no abnormal diffusivity alterations were observed in patients without HS.

Chapter 10: Discussion and Conclusion

Chapter 10: Discussion and Conclusion.....	187
10.1 Organization of Chapter 10.....	187
10.2 Summary of Results	188
10.2.1 Automatic Hippocampal Subfield Segmentation in Patients with TLE and HS.....	188
10.2.2 Automated Tractography Analysis in Patients with TLE and HS.....	188
10.2.3 Neuroradiological Findings in Patients with 'Non-lesional' Focal Epilepsy.....	189
10.2.4 Automatic Detection of Focal Cortical Dysplasia.....	189
10.2.5 Automatic Fiber Quantification in Patients with TLE.....	190
10.3 Methodology, Strengths and Limitations.....	191
10.3.1 Cross-Sectional Study Design.....	191
10.3.2 Clinical Variables.....	192
10.3.3 In Vivo Hippocampal Subfield Mapping.....	193
10.3.4 Automated Tractography of Temporal Lobe Tracts.....	194
10.3.5 Voxel-based Analysis.....	197
10.4 Interpretations and Clinical Implications.....	200
10.4.1 Hippocampus and TLE.....	200
10.4.2 Temporal Lobe WM Tracts and TLE.....	202
10.4.3 Manual and Automated Tractography in Lesional and 'Non-lesional' TLE.....	207
10.4.4 Dysplasia and Focal Epilepsy.....	212
10.5 Future Directions and Conclusions.....	216
10.5.1 Automatic Hippocampal Subfield Segmentation in Patients with TLE and HS.....	216
10.5.2 Automated Tractography Analysis in Patients with TLE and HS.....	216
10.5.3 Automatic Fiber Quantification in Patients with TLE.....	218
10.5.4 Automatic Detection of Focal Cortical Dysplasia.....	218

10.1 Organization of Chapter 10

This chapter provides a detailed discussion on the quantitative results reported in Chapters 5-9, other than Chapter 7, the qualitative findings of which were discussed in that chapter. Chapter 10 starts with a summary of all results in Section 10.2, the methodological strengths and limitations are discussed in Section 10.3, the interpretations and implications of the studies are discussed in Section 10.4. Finally, future directions are discussed in Section 10.5, which also includes the conclusions

of this thesis. Information from Kreilkamp et al. (2017) has been included in this chapter.

10.2 Summary of Results

10.2.1 Automatic Hippocampal Subfield Segmentation in Patients with TLE and HS

The present study is the first to use a novel multi-contrast approach to improve automated hippocampal subfield segmentation in TLE and relate these measures to HIA ratings and clinical features. In this study, four primary findings have been reported. Firstly, patients with left TLE had decreased volume of the contralateral presubiculum and HATA relative to patients with right TLE. Conversely, patients with right TLE had significantly smaller contralateral hippocampal tail volumes relative to patients with left TLE. Secondly, ipsilateral and contralateral hippocampal subfield volumes did not correlate with duration of epilepsy, age of onset of epilepsy, epilepsy burden, a history of febrile seizures or prevalence of SGTCS. Thirdly, the volume of ipsilateral or contralateral hippocampal subfields was not associated with postoperative outcome. Finally, semi-quantitative hippocampal architecture ratings were significantly related to several hippocampal subfield volumes.

10.2.2 Automated Tractography Analysis in Patients with TLE and HS

There were four primary objectives of this study. Firstly, diffusion alterations of whole temporal lobe tracts were investigated in patients with TLE relative to healthy controls using an automated tractography approach. Whole-tract FA/MD abnormalities were observed in nearly all temporal lobe tracts investigated, the effects being observed bilaterally, but most strongly ipsilaterally. Tract diffusion alterations were more strongly bilaterally distributed in patients with left TLE. Secondly, an investigation of within-tract alterations using waypoint comparisons confirmed that ipsilateral tracts were more extensively affected than contralateral tracts. This approach also identified specific regions within tracts that demonstrated alterations in diffusion characteristics. Thirdly, the relationship between regional

tract alterations, the degree of the HA and clinical features of TLE (such as duration of epilepsy, seizure frequency) was assessed. This study showed that extent of HA was not related to (i) the degree of FA and MD alterations of temporal lobe tracts or (ii) the clinical characteristics of patients, whereas diffusion alterations of ipsilateral temporal lobe tracts were significantly related to age at onset of epilepsy, duration of epilepsy and epilepsy burden. Finally, the aim was to establish whether preoperative temporal lobe WM tract diffusivity measures differed between patients who were surgically rendered seizure free and those who had persistent postoperative seizures relative to controls. Outcome analysis revealed that patients with favorable outcomes and those experiencing postoperative seizures had a different pattern of FA/MD alterations along tracts relative to controls, to the extent that patients with postoperative seizures were affected more bilaterally relative to those rendered seizure free.

10.2.3 Neuroradiological Findings in Patients with 'Non-lesional' Focal Epilepsy

29 patients remained MRI-negative after reassessment by a neuroradiologist experienced in the evaluation of epileptogenic lesions. 33% of all patients had at least one potentially epileptogenic lesion (seven had HS, two had dual pathology (HS and FCD), two had dysplasia, one patient had amygdala enlargement, one had encephalocele and one patient had gliosis), which went undetected on previous clinical MRI. Of these 14 patients with lesions, eleven had lesions concordant with the likely epileptogenic region as identified by EEG. The full discussion and conclusions of these qualitative results can be found in Chapter 7.

10.2.4 Automatic Detection of Focal Cortical Dysplasia

CAT12 in SPM12 permitted the implementation of the previously published method by Huppertz et al. (2005) using a fully automated approach. This tool identified 100% of dysplastic lesions in previously non-lesional patients with epilepsy when both feature maps depicting the GM/WM junction and extent of GM thickness were used together. Additionally, two sites not previously identified were identified using the automated FCD detection technique. The number of false positives generated

through EXT/JCT images could be reduced by using a cluster threshold ($>3.5 \text{ cm}^3$) on EXT/JCT images and voxel-based analysis of all significant clusters in FA/MD/T2FLAIR and T2w images from 23 patients to twelve. All sites of dysplasia reported at the start of the study were detected using this technique, while also two additional sites could be identified. Of the twelve remaining patients with suspicious areas according to the individualized statistical testing, none were reported to be abnormal based on neuroradiological re-assessment.

10.2.5 Automatic Fiber Quantification in Patients with TLE

A whole-tract analysis approach is feasible with both tractography approaches (manual and AFQ). The analysis of consistency across approaches revealed a high degree of similarity in Dice Coefficients for the extracted tract shape and space (Dice coefficients at moderate to good agreement) and a strong correlation between FA/MD values extracted with both methods. The manual approach revealed more differences in FA/MD values than AFQ when comparing whole-tract DTI-metrics between patients and controls. When using the manual tractography approach, no correlations between whole-tract diffusion characteristics and clinical variables survived correction for multiple comparisons. In contrast to this, the whole-tract DTI-metrics determined using AFQ revealed correlations with clinical variables including age of onset of epilepsy and duration of epilepsy. These were also confirmed through AFQ's along-the-tract analysis, which provided a more detailed description of localized diffusivity changes along tracts, which correlated with age, age of onset of epilepsy, seizure burden and duration of epilepsy. Furthermore, imaging data was compared between patients with and without HS to controls. There was significantly decreased FA in the frontal part of the ipsilateral UF and significantly increased MD in the frontal and temporal parts of the contralateral UF in patients with HS compared to controls. There were no significant differences between patients without HS and controls. Patients with HS had significantly decreased FA in the frontal part of the contralateral UF relative to patients without HS.

10.3 Methodology, Strengths and Limitations

10.3.1 Cross-Sectional Study Design

Many publications to date have applied cross-sectional study designs to report on pathobiological processes and underlying brain alterations related to clinical features (e.g. seizure laterality, age of onset / duration of epilepsy) in patients with focal epilepsies (Ahmadi et al. 2009, Liu et al. 2016, Kemmotsu et al. 2011, Glenn et al. 2016) and those that underwent epilepsy surgery (Concha et al. 2007, Keller et al. 2017). Although a cross-sectional study design is a favorable choice concerning time-effectiveness and access to the same MR hardware and associated post-processing methods, it often comes at the cost of recruiting a heterogeneous patient population. Patients may differ in age, age of onset and duration of epilepsy, medication, types of seizures and seizure frequency. When these factors are not accounted for, they may mask the underlying pathological processes present in GM and WM that characterize focal epilepsy. In particular, a cross-sectional study design does not allow researchers to make causal inferences about time-dependent and specific disorder-related changes in either patient groups or individual patients when comparing them to healthy controls or among each other.

Longitudinal studies do not have these disadvantages and would allow more meaningful conclusions. However, longitudinal studies may suffer from participant attrition. Efforts to map structural and functional changes in study groups over time have been undertaken in neurodevelopment (Houston et al. 2014) and neurodegenerative diseases such as Alzheimer's disease (Wang et al. 2016b) or multiple sclerosis (Furby et al. 2010). Ongoing neurobiological processes contribute to progression of the brain development / disorder and this may also be true for epilepsy where time-dependent clinical patterns could be investigated in longitudinal studies. Neurobiological and pathological processes are interdependent and likely influence the outcomes of brain structural and functional studies. Longitudinal studies allow the investigation of different research questions, e.g. whether diffusivity alterations progress with continuing seizures (Keller et al. 2012) or

whether these may be reversible after surgery has been performed (Concha et al. 2007, Kemmotsu et al. 2014). Consequently, longitudinal studies may provide insights into the etiology of diffusion alterations in temporal lobe WM tracts.

10.3.2 Clinical Variables

It is important to investigate correlations of underlying brain alterations with clinical variables in order to assess whether brain alterations found in patients with focal epilepsy may be primary or secondary in nature. Studies to date have investigated whether certain brain areas are susceptible to damage resulting from the presence of febrile convulsions/SGTCS, certain types of seizures, recurrent seizures (seizure frequency), duration of epilepsy, age of onset or post-surgical outcomes and contradictory results have been reported. Some studies report that structural alterations correlate with duration (Keller et al. 2012, Keller et al. 2015b, Kreilkamp et al. 2017) and age of onset of epilepsy (Lin et al. 2008, Keller et al. 2002b). However, other studies were not able to establish relationships of GM/WM alterations with age of onset (Keller et al. 2015b) or with duration (Moran et al. 2001), which may be due to smaller sample sizes, the subtle nature of the alterations and the application of conservative statistical thresholds (Bernasconi et al. 2004). In this work, hippocampal subfield and gross hippocampal volume did not correlate with any clinical variables, whereas for the same dataset on patients with TLE and associated HS correlations between WM tract alterations and age of onset, duration and seizure burden were found. DTI waypoint analysis revealed where these alterations occurred, however correlations between tract measurements and clinical data cannot be attributed without caution. In particular, measures of seizure frequency may be biased as there is no objective way of measuring occurrence of seizures and this information is often only obtainable through reports given by relatives and friends observing the patient. Furthermore, the correlation of duration of epilepsy to seizure-induced brain damage does not allow inferences about causality given the cross-sectional nature of the present study. Longitudinal studies are required to characterize the multifactorial relationship between seizures, clinical features of the disorder, medication, co-morbidities and WM tract alterations.

10.3.3 In Vivo Hippocampal Subfield Mapping

The higher-resolution multi-contrast approach used in the present study clearly provided an improved segmentation of hippocampal subfields compared to an automated approach based solely on T1w images (Schoene-Bake et al. 2014). There are, however, important considerations that should be made. Firstly, it should be emphasized that it is currently impossible to obtain an estimate of neuronal density from MRI determined hippocampal subfields, and the goal of *in-vivo* imaging methods is to obtain an estimate volume of the approximate location of subfields. This likely explains the discrepancy between histopathology-outcome, imaging-clinical variable and imaging-outcome correlations in patients with TLE. The combination of standard T1w images with a higher resolution T2STIR sequence, as applied in the present study, improves the delineation of the approximate location of the subfields. A meta-analysis of studies reporting hippocampal subfield neuronal loss revealed statistically significant neuronal loss in all CA regions in patients with HS relative to control specimens and CA1 was preferentially affected (Steve et al. 2014). It is an important point to consider hippocampal subfields or regions separately when analyzing hippocampal volume metrics based on pre-surgical MRI in relation to outcome as different types of HS are related to different post-surgical outcomes (Blümcke et al. 2013). Unfortunately, due to the lack of healthy control data, this present study was unable to assess relationships between outcome and different types of HS as assessed by automated hippocampal subfield mapping. Healthy control data was not available because the high-resolution T2STIR sequence was acquired only for patients being considered for surgery. Even though all patients who participated in the present study were deemed to have unilateral HS, quantitative analysis of subfields did reveal some contralateral changes in patients with left/right TLE.

Other methodological issues that should be mentioned include the fact that hippocampal subfield mapping might be influenced by differences in image quality and motion across subjects (Iglesias et al. 2015). Some boundaries between structures might not be easily delineated as even in the training data some interfaces cannot be

detected (Yushkevich et al. 2015b). Furthermore, patients received individual epilepsy surgery as clinically indicated, for example with a trans-sylvian (~50%) or subtemporal (~50%) access to the pathologic hippocampus, which was then removed in sections (trans-sylvian) or in its entirety (subtemporal). Within this archival study, detailed microscopic information of intact hippocampal subfields from surgical specimens was not available for comparison to the automatically delineated hippocampal subfields based on MRI. However, this study is useful as it shows that in-vivo ipsilateral semi-quantitative continuous HIA ratings were significantly related to multiple automatically extracted ipsilateral hippocampal subfield volumes. This is an important finding and may indicate that automatic subfield mapping can reflect some clinical features present in different manifestations of HS. However, in the absence of a gold-standard procedure for in-vivo subfield mapping, estimation of hippocampal subfield volumes might only be used as an approximation for HS with inherent neuronal cell loss. Nevertheless, an automated technique for hippocampal volume extraction, which is sensitive to different patterns of HS could indeed complement patient clinical information in a reproducible and time-efficient way prior to surgery and further research in this direction using data from healthy controls and long-term surgical outcomes is warranted.

10.3.4 Automated Tractography of Temporal Lobe Tracts

The TRACULA results presented in Chapter 6 closely correspond to those of time-consuming manual tractography studies (Ahmadi et al. 2009, Yogarajah et al. 2008, Rodrigo et al. 2007, Diehl et al. 2008, Lin et al. 2008). The automated tractography approach utilized here has several advantages over manual approaches, including an improved reproducibility of measurements, increased time efficiency and no reliance on trained human anatomists. The utilization of automated image analysis techniques, particularly those that are performed in native space, is favorable over manual ones if such techniques are incorporated into clinical evaluation of patients, particularly given the high levels of reproducibility. TRACULA uses reproducible tracking protocols validated on a set of healthy training subjects and has been shown to be sensitive to WM changes in patients (Yendiki et al. 2011). Automated

techniques for tract reconstruction will have important implications for studies aiming to characterize side of seizure onset and develop individual diagnostics in a clinical setting (Martin et al. 2015) due to its low demands on time and higher reliability (Leergaard et al. 2012). TRACULA constrains tractography to WM voxels using an anatomically correct T1w based segmentation mask. Diffusion-weighted imaging may suffer from geometric distortions that can affect the accuracy of tract anatomy (Yendiki et al. 2011). The application of a b0/T1w co-registration approach can mitigate the effects of potentially distorted voxels so that tracts can be successfully reconstructed. Furthermore, SNR was computed and the analysis confirmed that mean SNR values for diffusion-weighted images were comparable across groups. However, motion was different across patients/controls and therefore the TMI for all participants was entered as a nuisance regressor into the analysis to mitigate confounding effects of motion differences between groups (Yendiki et al. 2013). Ultimately motion artifacts remain an important challenge for any DTI study, since macroscopic head motion can easily influence the microscopic diffusion measurements, which DTI studies aim to characterize. As DTI-derived scalar metrics are dependent on the SNR measures of the data (Farrell et al. 2007) and motion (Yendiki et al. 2013), this has implications for studies investigating subtle differences between different types of disorders or when comparing patients to controls. These measures should be computed and accounted for during statistical analysis as performed in the present study. Ultimately, a comparison to the gold-standard manual tractography approach should also be performed.

In Chapter 9 a direct comparison of manual and automated tractography (AFQ) approaches revealed that tracts generated by these two approaches spatially corresponded reasonably well given the results from Dice Coefficient analysis. However, minor differences were found (i) in tract volume, where the automated approach showed increased volume relative to the manual approach (ii) in group analysis where AFQ did not identify as many tracts with abnormal diffusivity values in patients with left TLE when compared to the manual approach and (iii) the whole-tract correlation analysis with clinical variables only showed significant results when

using AFQ relative to the manual approach. It is likely that the difference in tract volume stemmed from the fact that only the second-order Runge-Kutta algorithm was available for the manual approach, while for AFQ the default tractography algorithm had been set at the forth-order Runge-Kutta algorithm by the developers (Yeatman et al. 2012). As diffusion metrics were thus sampled from a larger tract volume within the automated approach, this may also explain why whole-tract diffusion alterations present in the manual approach were not detected with the automated approach in patients with left TLE. Another reason for these differences may be the fact that the manual approach was performed in patient native space, while the automated approach relied on co-registration of ROIs to define the tracts in standard space. Conversely, when investigating correlations between whole-tract diffusion metrics and clinical variables, these were only detected when using AFQ. These findings were replicated using AFQ's along-the-tract analysis. It is difficult to assess why some group results were not identified by AFQ, while clinical correlations with DTI-metrics could be found. Ultimately, studies aiming to compare these two tractography approaches in more detail should harmonize identical tractography algorithms to run in the same space (either subject-specific native or standard space) so that stronger conclusions may be justified and the automated approach with the closest correspondence to manual approaches (including waypoint analysis) can be identified.

In order to investigate the relationship between DTI-metrics and clinical variables and group diffusivity alterations across patients with and without HS and controls, the information obtained for each tract had to be side-flipped in patients with right TLE and a corresponding subset of controls in both studies (TRACULA and AFQ) reported within this thesis. This is a common procedure and often necessary, as the prevalence of right TLE is lower than that of left TLE (Giovagnoli 2001, Manaut et al. 2002, Njiokiktjien 2005). Although side-flipping has been performed in many previous studies aiming to assess correlations and group-wise differences in small sample sizes (Keller et al. 2015a, Coan et al. 2014, Imamura et al. 2015, Mueller et al. 2006, Fonseca et al. 2012), one limitation of this is that the analysis does not

allow judgements on diffusivity alterations that are dependent on right- or left-sided hemispheric differences.

10.3.5 Voxel-based Analysis

In the present study, a modified version of a previously published epileptogenic lesion detection algorithm was applied (MAP; Huppertz 2013). The aim was to use the novel segmentation algorithms within the newest version of SPM, which are superior to the previous SPM version used by MAP (Dahnke et al. 2012, Farokhian et al. 2017) and to maintain the same computational steps for T1w-derived feature maps (Huppertz et al. 2005, Huppertz et al. 2008, Huppertz 2013, Kassubek et al. 2002, Wilke et al. 2003) in order to determine the sensitivity of this approach when using automated voxel-based statistical analysis. Recently, Wang et al. (2016a) have emphasized the need for a statistical thresholding method to improve sensitivity, specificity and consistency of the applied automated approach in order to circumvent the need for extensive neuroradiological evaluation of feature maps. The strengths of the automated voxel-based approach include the fact that it does not entail manual lesion drawing unlike other semi-automatic tools requiring a priori information not available in patients with MRI-negative epilepsy. Furthermore, it is able to operate in 3D and identify multifocal lesions.

This is in contrast to a recently developed surface-based approach (Adler et al. 2017a), which is unable to identify multiple FCD sites in a patient as it makes reference to the corresponding contralateral region to evaluate deviations in cortical surface features such as folding and thickness. One important criticism to make here is that patients with epilepsy also show contralateral alterations in cortical surface features (Kemotsu et al. 2011, Kim et al. 2016) and extensive structural disorganization may be detectable using GM volume analysis (Sisodiya et al. 1995b). The pathological features of the disorder may compromise the ability of the surface-based approach developed by Adler et al. (2017a) to depict suspicious regions as the contralateral side cannot be used as a control. Therefore, a 3D voxel-based approach, which allows simultaneous analysis of multiple slices across the whole brain without

the use of a-priori information may be useful for patients with MRI-negative epilepsy who may show multi-focal lesion upon re-evaluation. It is important to account for age- and sex-matched healthy controls when assessing patients for possible epileptogenic lesions using any statistical tool. Within the study presented here, this had been considered, furthermore age and sex had been entered as covariates during voxel-based analysis. Other studies such as Adler et al. (2017a) have reported on differences in age between patients and controls where the mean age differed by three years between the two participant groups. Especially in a paediatric cohort this signifies a large heterogeneity as neurodevelopment is at very different stages at three and ten years of age for example (Giedd et al. 2015), which were the respective ages of the youngest patient and control (Adler et al. 2017a).

However, cortical surface mapping can afford additional information also relevant to FCDs such as 3D surface complexity including local gyrification, sulcal depth and curvature (Yotter et al. 2011, Thesen et al. 2011) and investigation of surrounding tissue by geodesic distance mapping (Hong et al. 2017). This additional information may render surface-based superior to voxel-based approaches when attempting to detect very subtle and small FCDs. The reasons for this are that voxel-based approaches are susceptible to partial volume effects (Kurth et al. 2015b) owing to their volume-based averaging procedures, thus the detection of spatially restricted lesions in folded cortex may be limited (Thesen et al. 2011). Even though these are features not obtainable with voxel-based techniques, the neuroradiologically verified approach used within this thesis was still able to detect suspicious areas suggestive of FCD with a sensitivity of 100%, which is 30% higher than those achieved by surface-based methods that have been histopathologically verified (Hong et al. 2014, Adler et al. 2017a). The high sensitivity achieved with the voxel-based approach in the present study has also been demonstrated by Huppertz et al. (2005). One other difference in the study conducted within this thesis and Adler et al. (2017a) was that data was acquired on a 3 Tesla magnet in the study presented within this thesis, while Adler and colleagues acquired the data on a 1.5 Tesla MRI scanner. Indeed, it cannot be ruled out that this may in part account for differences in results seen in sensitivity

73% (at 1.5 Tesla) versus 100% (3.0 Tesla) lesion detection rate. Consequently, differences in these results may not be solely attributed to the criticism raised on the surface-based approach but may also be due to improved segmentation based on 3.0 Tesla MRI with higher CNR as compared to 1.5 Tesla (Wagner et al. 2011). However, it is worth noting that Hong et al. (2014) have tested their data on 1.5 and 3 Tesla and have found similar sensitivity across field strengths for their automated surface-based approach.

The liberal threshold of $p < 0.01$ (voxel-level) and FWE $p < 0.05$ (cluster-level) may possibly be changed to $p < 0.001$ and FWE $p < 0.05$, a threshold that has been previously used in other publications (Focke et al. 2008b). The false positive rate was 1.5 to 2 times higher than the false positive rate reported by Wang et al. (2015) due to the liberal statistical threshold applied in this study. Applying a more stringent statistical threshold may help to avoid false positives and increase specificity when identifying a given pathology. In order to reduce the number of false positives the cluster extent threshold of 3.5 cm^3 was used as this was the smallest neuroradiologically confirmed FCD size found in the present dataset. As this threshold was inspired by the size of clinically defined FCD sites in this particular dataset, caution should be exercised when blindly applying this threshold to other datasets with potentially smaller FCDs. In particular, small FCDs found at the bottom of deep sulci may be overlooked by neuroradiologists (Besson et al. 2008) and may be left undetected by an automated voxel-based tool that has a high cluster size threshold. In contrast to this, surface-based approaches have been used to afford information on depth and curvature measures of the inner cortical surface with higher spatial resolution (Adler et al. 2017a, 2017b, Besson et al. 2008). However, these statistical and cluster-based thresholds can be adjusted in future studies and tested for their performance regarding specificity and sensitivity. Another fact that may have contributed to the high number of false positives found here and in a previous study (Wang et al. 2015), when using the approach developed by Huppertz et al. (2013), is that GM/WM intensities are estimated from whole brain MRI before masking out the cerebellum and deep GM nuclei. It is possible that the derived thresholds are

compromised by signal intensities derived from these subcortical and cerebellar regions as they do not reflect GM and WM intensities of areas within the cerebral cortex. Since the local adaptive segmentation offered in CAT12 takes local intensity differences into account (Dahnke et al. 2012), it would be contra-productive to discard this detailed information before computation of the GM/WM intensity boundary thresholds.

10.4 Interpretations and Clinical Implications

10.4.1 Hippocampus and TLE

Although left and right TLE do not differ in the extent of atrophy of the epileptogenic hippocampal subfields, patients with left TLE had significantly reduced volumes of the contralateral presubiculum and HATA relative to patients with right TLE. This is a new finding and suggests that left TLE may be associated with a bihemispheric hippocampal subfield alteration in these particular regions. For patients with right TLE, lower volumes in the contralateral hippocampal tail relative to patients with left TLE were found. There is an inconsistent literature on the effects of TLE laterality on the distribution of brain damage, with some indicating increasingly bilateral changes in left TLE (Keller et al. 2012, Coan et al. 2009), in right TLE (Garcia-Fiñana et al. 2006, Pail et al. 2010) and some studies suggesting equivalence (Liu et al. 2016). Just one of these studies (Liu et al. 2016) has entered the hippocampal asymmetry (right>left) found in healthy controls (Rogers et al. 2012, Pedraza et al. 2004) as a confounding factor during statistical analysis. It is possible that natural cerebral asymmetry of this structure may account for some differences found in patients, in particular since regional differences in bilateral hippocampal volume have been found in controls (Rogers et al. 2012). Unfortunately, since T2STIR images were not available for healthy controls, the present study was unable to resolve this, so that this would be a worthwhile addition to future studies. Differences in hippocampal subfield volume loss may be linked to different pathobiological processes, such as neuronal loss and altered microstructural organization (Keller et al. 2012) sensitive to age (Small et al. 2011) or may be related

to features inherent in natural hemispheric asymmetry as found in healthy controls' hippocampal volume with the right being larger than the left hippocampus (Szabo et al. 2001, Thompson et al. 2009) and function (Golby et al. 2001, Sepeta et al. 2016, Wei et al. 2016, Burgess et al. 2002). Further detailed research using structural, functional and histopathological data is needed in order to fully disentangle these different effects and to arrive at biologically meaningful conclusions.

Whether recurrent seizures cause progressive brain damage is a contentious issue. In the absence of longitudinal data, cross-sectional studies have correlated brain compartment volume with duration of epilepsy as a surrogate marker of progressive damage due to seizure chronicity. There is inconsistency in the literature with respect to hippocampal and extrahippocampal volume loss and duration of TLE (Fuerst et al. 2001, Salmenpera et al. 1998, Tasch et al. 1999, Theodore et al. 1999, Jack et al. 1992, Cendes et al. 1993, Keller et al. 2015b, Mueller et al. 2012, Keller et al. 2012). Given that duration of epilepsy and chronological age are related, it is important to correct clinical correlations for patient age to determine whether brain atrophy is driven by epilepsy-related factors or normal age-related maturation. In the present study it was reported that subfields of the epileptogenic and contralateral hippocampus are not correlated with clinical variables. These results suggest that hippocampal subfields are not susceptible to damage resulting from recurrent seizures, the general chronicity of the disorder, age of onset or the presence of febrile convulsions/SGTCS. This is consistent with previous work that indicates that HS may be a direct and immediate consequence of an initial precipitating injury (e.g. febrile seizures / infection / genetic defects) and hippocampal subfield volume loss may not be primarily influenced by the chronicity/severity of the disorder since the majority of neuron loss occurs during epileptogenesis before onset of seizures (Mathern et al. 1996, Pitkänen and Lukasiuk 2011, Davies et al. 1996). It is worth noting, however, that one study found an inverse relationship of epilepsy duration (corrected for age) and volumes of left CA1, presubiculum, and subiculum in left TLE and right CA1 in right TLE (Kim et al. 2015).

With respect to postoperative outcome, harmonizing results from histopathological studies of hippocampal subfield neuronal loss and imaging studies of hippocampal subfield volume loss is difficult because of the inherent differences in the resolution of tissue characteristics. Postoperative outcome has been shown to be superior in patients with TLE who, after resection, were retrospectively shown to have classical patterns of HS (i.e. preservation of CA2 neurons) or total HS (i.e. neuronal loss throughout the CA), whereas patients with circumscribed neuronal loss of CA1 or CA4 tend to have poorer outcomes (Blümcke et al. 2013, Blümcke et al. 2007, Thom et al. 2010, Giulioni et al. 2013, Na et al. 2015). Mathern et al. (1996) had previously reported that patients with initial precipitating injuries were more likely to benefit from surgery and had neuronal cell loss in CA1 and presubiculum regions. No volume differences in preoperative hippocampal subfields between 41 patients with an excellent postoperative outcome and 35 patients with a suboptimal outcome were identified. This is likely due to the fact that there is histopathological variability in HS across patients, which is not identifiable on MRI. To varying degrees, patients with left and right TLE both showed contralateral volume reduction and this may be interpreted to indicate increased bilateral mesial temporal damage, potentially reflecting a bihemispheric seizure disorder, which would be less amenable to surgical intervention. Specifically, contralateral hippocampal subfield volumetric changes confined to certain regions in patients with right or left TLE may have differential impact on surgical outcomes. In fact, this study showed that overall patients with right TLE were more likely to be seizure free, which is concordant with results showing that these patients are more likely to be affected in multiple hippocampal subfields ipsilaterally rather than bilaterally, and they only showed regional changes in one hippocampal subfield volume confined to the contralateral hippocampal tail when compared to patients with left TLE.

10.4.2 Temporal Lobe WM Tracts and TLE

Consistent with previous studies investigating diffusion characteristics of the ILF, SLF, cingulum and UF using manual DTI tractography approaches (Ahmadi et al. 2009, Yogarajah et al. 2008, Rodrigo et al. 2007, Diehl et al. 2008, Lin et al. 2008),

this study demonstrated significant alterations in bihemispheric temporal lobe tract diffusion characteristics in patients with unilateral TLE using the fully automated TRACULA tractography pipelines. Diffusion measurement analysis revealed that patients with left TLE are more bilaterally affected than patients with right TLE, which is a finding consistent with the literature (Ahmadi et al. 2009, Keller et al. 2012, Kemmotsu et al. 2011) and the contralateral hippocampal subfield volume loss found in patients with left TLE. Furthermore, DTI waypoint comparisons localized the bilateral diffusion changes more precisely within tracts. However, it should be noted that other studies investigating GM have reported increasingly bilateral brain alterations in patients with right TLE (Garcia-Fiñana et al. 2006, Pail et al. 2010). One explanation for this may be that the groups were heterogenous in the work of Pail et al. (2010) reporting that patients with left TLE took a greater number of AEDs than patients with right TLE who did not take as many drugs. The fact that patients with left TLE were prescribed a greater number of AEDs or the fact that their medical condition was probably worse than in the other patient group may have influenced structural degeneration of the brain. Garcia-Fiñana et al. (2006) reported that contralateral hippocampal volumes were reduced in patients with right TLE but not in patients with left TLE. However, no differences in clinical characteristics were found between patients with left and right TLE and these authors are one of the few in the field who also presented evidence of homoscedacity (normal distribution) of the data before performing statistical testing between groups. Generally however, it is now accepted that patients with left TLE are more bilaterally affected than patients with right TLE (McDonald et al. 2008, Keller et al. 2002a, Bonilha et al. 2007b).

FA and MD have proved to be useful in characterizing microstructural brain damage in patients with TLE (McDonald et al. 2008, Keller et al. 2012). FA is a measure of microstructural integrity computed through a normalized ratio of radial/axial diffusivities (Alexander et al. 2007, Soares et al. 2013) and could therefore imply multiple microstructural changes (e.g. demyelination, loss of axons, increased inter-axonal space). MD, as a directionally averaged value, that takes all diffusivity measures into equal account, may demonstrate the magnitude of fluid viscosity and is

sensitive to cellularity, edema and necrosis (Alexander et al. 2011). Therefore, MD may potentially permit inferences about microstructure regarding loss of axon membrane and thus provide in-vivo measurements that strongly relate to histopathology. In fact, a recent study on correlations between diffusion alterations (FA and MD) and histology found that preoperative diffusion alterations were related to an increase in extra-axonal fraction, reduced cumulative axonal membrane circumference and myelin of the resected tissue (Concha et al. 2010). Interestingly, MD was more sensitive than FA in determining differences between patients versus controls and was able to detect extensive bilateral effects. These findings are consistent with those reported in other studies that have employed within-tract analyses to demonstrate increased alterations in MD in patients with mesial TLE (Concha et al. 2012, Glenn et al. 2016, Keller et al. 2017), although similar findings have not been reported in patients with cryptogenic TLE (Keller et al. 2013). The inconsistencies may in part be explained by different types of analysis approaches, as, for example, a tract-based approach has been shown to be more sensitive than voxel-based ones (Focke et al. 2008a). Furthermore, some studies have found that diffusivity measures have a higher spatial correspondence with discharges from stereo-electroencephalography than anisotropy measures (Thivard et al. 2006, Guye et al. 2007), may be superior in detecting occult damage (Rugg-Gunn et al. 2001) and have been linked to dynamics of seizure activity (Yu and Tan 2008).

In contrast to recent publications using automated whole-tract tractography in standard space (Hagler et al. 2009) and in accordance with other deterministic automated (Glenn et al. 2016) and manual (Concha et al. 2012) along-the-tract approaches, the present study demonstrated that automated probabilistic tractography can detect alterations along temporal lobe tracts in native space. The study presented here revealed that TRACULA's waypoint analysis is sensitive to within-tract differences, which may have useful diagnostic (e.g. identification of occult damage) and prognostic (e.g. development of imaging biomarkers) applications. Along-the-tract analysis revealed no correlations with ipsilateral hippocampal volume, which is consistent with previously conducted manual deterministic tractography (Concha et

al. 2012) and ROI analysis (Keller et al. 2012, Bonilha et al. 2010). However, another study reported that extrahippocampal FA, approximately located in the ipsilateral superior segment of the cingulum and other extratemporal tracts not assessed in the present study, was correlated with hippocampal volume (Scanlon et al. 2013). These latter findings were also reported in the cohort of healthy controls within the same study.

An earlier age at onset of epilepsy, longer duration of epilepsy and increased epilepsy burden were related to greater diffusion alterations of temporal lobe WM tracts, but not the extent of HA. A correlation between duration of epilepsy and extrahippocampal alterations has been reported in studies (Chiang et al. 2016, Govindan et al. 2008, Lin et al. 2008, Keller et al. 2012). Given the relationships between clinical variables and tissue characteristics along WM tracts, and the absence of this relationship with hippocampal volume, these findings may suggest that the development of hippocampal and WM abnormalities are governed by independent developmental mechanisms. The development of mesial TLE is thought to begin with an initial precipitating injury or condition, such as febrile seizures, infection, genetic defects, trauma, stroke or hypoxic damage, which sets in process a period of epileptogenesis. This is a latent period of aberrant neuroplasticity that later supports the onset of spontaneous seizures (Mathern et al. 1996, Pitkänen and Lukasiuk 2011). It has been suggested that the initial precipitating event, and potentially the years of aberrant hippocampal plasticity, are the primary factors in the development of HS, which can be present prior to the onset of habitual seizures (Mathern et al. 1996). This may be the reason why the present study, like several other studies (Cendes et al. 1993, Davies et al. 1996, Keller et al. 2012, Keller et al. 2002b) report no relationships between the extent of HA and age at onset and duration of epilepsy. However, these clinical variables appear more significant in the development of extrahippocampal WM tract abnormalities, which may be influenced by the chronicity of TLE and therefore are likely to be secondary in nature. Other studies have reported relationships between diffusion characteristics of WM and the chronicity of TLE (Glenn et al. 2016, Keller et al. 2012). However, other studies

have failed to show a relationship between diffusivity measures and duration of epilepsy (Thivard et al. 2005) or age at onset of epilepsy (Thivard et al. 2005, Keller et al. 2012). The only other study to date investigating correlations between along-the-tract diffusion characteristics and seizure burden reported correlations only with diffusional kurtosis measures of microstructure, but not diffusion tensor measures (Glenn et al. 2016). However, this previous study was performed in standard space, while TRACULA outputs longer tracts in native space, which may account for the differences seen with respect to correlations with seizure burden.

This study showed the trend ($p=0.06$) that patients with right-sided TLE were more likely to be seizure-free after surgery, than those with left-sided TLE. In fact, this statistical test was significant ($p<0.05$) when more patients were included (Chapter 5). Patients with excellent outcomes had more ipsilaterally distributed WM tract diffusion alterations than patients with persistent postoperative seizures, who were affected more extensively and bilaterally. This is consistent with previous studies using DTI (Keller et al. 2017, Keller et al. 2015a). In particular, the study presented here reported that in patients with postoperative seizures, MD values of the contralateral SLFt were increased relative to controls, however, this change was not seen in patients without postoperative seizures. Altered diffusivity in the contralateral SLFt close to the insular cortex may indicate the presence of temporal plus epilepsy which would be less amenable to surgery than TLE (Section 1.3). A previously published study (Keller et al. 2017) using an automated deterministic tractography approach has found the contralateral PHWM to be more affected in patients with postoperative seizures. Although results of the study presented here did not corroborate this clearly, the posterior part of the contralateral PHWM seemed to be more extensively affected in these patients relative to patients who attained seizure freedom when comparing the patient groups to controls. These results indicate that patients with postoperative seizures have ipsi- and contralateral WM diffusion alterations. Therefore, these bilateral structural alterations may compromise attainment of excellent seizure outcomes in patients. Additionally, an FA decrease in the ipsilateral UF was found in patients with persistent seizures relative to controls,

whereas this change was not observed in patients who attained seizure freedom. Keller et al. (2017) have incorporated measures of surgical lacunae and found that insufficient resection of the ipsilateral UF could be a contributing factor to unfavorable surgical outcomes. Bonilha et al. (2007a) and Siegel et al. (1990) have found that the extent of entorhinal and parahippocampal resections were significantly related to outcome. It may therefore be especially important to account for sufficient resection in patients that have altered preoperative diffusion metrics in the vulnerable UF as found in the study presented in this thesis. These patients may belong to a particular subtype of refractory TLE that is less responsive to epilepsy surgery (Bonilha and Keller 2015).

10.4.3 Manual and Automated Tractography in Lesional and 'Non-lesional' TLE

In the present study, temporal lobe tracts were investigated with both manual and automated tractography approaches. When comparing patients with right TLE to controls, apart from an increase in MD in the left PHWM using manual tractography, no diffusion alterations were detected for the tracts analyzed (UF, PHWM and FF in the automated approach). In contrast to patients with right TLE, patients with left TLE showed multiple tracts with altered diffusion metrics when compared to controls. Previous research has suggested that early childhood left hemisphere damage predominates over right hemisphere damage and the left-right difference is also present in patients with unilateral TLE (Njiokiktjien 2005), which may indicate that the left temporal lobe is more vulnerable during development than the right temporal lobe. To explain this effect, it has been incorrectly argued and concluded that since the left hemisphere matures much slower than the right hemisphere, the structures within the left hemisphere would be more vulnerable to initial precipitating injuries (Keller et al. 2012, Kemmotsu et al. 2011, Miro et al. 2015). It is important to note that this fact has been cited from the original source (Corballis and Morgan 1978) incorrectly and the contrary is true: the left-right maturational gradient had been described by Corballis and Morgan (1978) as an earlier and more rapid development of the left hemisphere compared to the right. In consequence, the left hemisphere can no longer be considered to be vulnerable due to a slower maturation

compared to the right as this was not reported initially. More detailed longitudinal studies are necessary to make any such distinct statements and allow reasoning on neurodevelopmental factors influencing hemispheric vulnerability. Much like results in the work conducted on preterm newborns by Mullaart et al. (1995), Njiokiktjien (2005) has found that cerebral blood flow disturbances are a major cause of cerebral damage in the left hemisphere, Dabbs (1980) has stated that the right hemisphere (which is the non-verbal hemisphere in most people) receives more blood than the left in adults, and this may also be the case for children (Njiokiktjien 2005). Consequently, ischaemic insults to the brain render the left hemisphere more vulnerable and may cause damage to the hippocampal subfields (Schmidt-Kastner and Freund 1991) and immature WM that is especially vulnerable to oxygen deprivation (Njiokiktjien 2005). Furthermore, there is a significantly higher prevalence of HS in the left hemisphere relative to the right hemisphere in patients with TLE (Janszky et al. 2003). However, other pathobiological processes may be at play such as gene expression, differential biochemical and molecular processes and pathways that may be either activated or suppressed in certain populations of neurons and these could potentially influence neuronal response to stress rendering selective neuronal populations vulnerable or resistant to damage (Michaelis 2012, Bernaudin et al. 1998).

The study presented here included patients with left and right TLE previously thought to be non-lesional, but expert neuroradiological assessment of the novel MRI revealed unilateral HS in eight patients. This way, both of these patient groups with left- and right-sided TLE included patients with and without unilateral HS. This may have influenced the results presented within this study and may have biased the WM diffusivity alterations found in patients with left TLE, while these changes were not identified in the smaller group of patients with right TLE when compared to controls. Generally, results presented in this study still corroborate previous work, as it has appeared that patients with right TLE do not show the more extensive and severe WM disruption found in patients with left TLE (Ahmadi et al. 2009, Kreilkamp et al. 2017, Keller et al. 2012, Kemmotsu et al. 2011), which may be linked to the fact that

left and right TLE are etiologically and pathologically distinct subtypes of TLE (Ahmadi et al. 2009). However, there is a scarcity of publications separately analyzing data from patients with right TLE with and without associated HS without performing side-flipping, possibly due to the significantly lower prevalence of this structural abnormality in patients with right TLE (Janszky et al. 2003).

Mueller et al. (2006) have conducted a study on GM/WM volume on patients with and without HS and have reported on extensive volume decrease in patients with HS only, while no changes were found for patients without HS relative to controls. With respect to diffusion alterations, Concha et al. (2009), Liu et al. (2012) and Campos et al. (2015) have found that patients with TLE and associated HS had more widespread diffusion alterations than patients without HS. Results on waypoint diffusion alterations presented here corroborated this result for both patient groups when compared to controls, while it was also found that patients with HS had significantly decreased FA in the frontal part of the contralateral UF relative to patients without HS. This may indicate differential epileptogenic networks involved in lesional and non-lesional TLE (Liu et al. 2012) and that a pathologic hippocampus can influence WM tract integrity on the contralateral hemisphere, a finding that is consistent with other studies discussing patients with left TLE and HS (Kreilkamp et al. 2017, Keller et al. 2012, Kemmotsu et al. 2011, Ahmadi et al. 2009, Bonilha et al. 2007b). However, it should be noted that other studies have reported bilateral changes in patients with right TLE and HS (Liu et al. 2012, Garcia-Fiñana et al. 2006, Pail et al. 2010). So far, it is still undetermined why these results are not consistent for every study conducted on patients with left/right TLE and HS. In order to fully disentangle WM tract disruption in patients with and without HS and patients with left and right TLE, future studies should aim to incorporate a much larger number of these patients. One promising and encouraging step has been taken by the ENIGMA-Epilepsy project, which aims to harmonize neuroimaging analyses across different MRI research sites (<http://enigma.ini.usc.edu/ongoing/enigma-epilepsy/about-enigma-epilepsy/>).

Correlations between whole-tract/along-the-tract diffusivity metrics and clinical variables were investigated. The whole-tract DTI-metrics determined using AFQ revealed correlations with clinical variables. FA in the ipsilateral PHWM correlated positively, while MD correlated negatively with age of onset. Furthermore a positive correlation between MD and duration corrected for age was identified. Although these correlations did not survive multiple comparison correction within the manual tractography approach, the results obtained by the automated approach corroborate previous findings, which are detailed here separately for every correlation. Along-the-tract analysis within AFQ provided detailed information of localized diffusivity changes along tracts. In concordance with the whole-tract correlation analysis, a younger age of onset was associated with decrease in FA of the ipsilateral PHWM, which was also found by Kemmotsu et al. (2011) in patients with left TLE. Furthermore, these authors could identify a significant relationship between decreased FA of the ipsilateral/contralateral UF and age of onset, while in the present study there was a negative correlation between MD of the ipsilateral PHWM and contralateral UF with age of onset. These correlations may be expected, as there is abundant evidence in the literature of decreased cognitive functioning in patients with early onset epilepsies as this disorder disrupts brain maturation (Elger et al. 2004) and an early onset is likely associated with unfavorable postoperative outcomes (Kwan and Brodie 2000). There was a negative correlation of seizure burden with FA in the posterior part of the contralateral PHWM. Previously, a negative correlation of waypoint FA of the anterior portions of the ipsilateral UF and seizure burden has been identified (Kreilkamp et al. 2017, Chapter 6) and Glenn et al. (2016) were also able to establish a positive correlation for MD in the ipsilateral PHWM with seizure burden. In these studies, seizure burden had been defined as a function of seizure frequency and epilepsy duration. Within the study presented here, the same tract locations that showed a relationship with seizure burden also correlated with epilepsy duration. Consequently, it is difficult to state that these diffusivity alterations stem from either seizure burden (frequency) or epilepsy duration and often the information for seizure burden is not acquired as it is considered to be unreliable (Mueller et al. 2006) as it is dependent on patient

statements. There was also a negative correlation with epilepsy duration with FA in the ipsilateral and contralateral PHWM, while MD in the ipsilateral PHWM and contralateral UF correlated positively with epilepsy duration corrected for age. Previous studies have also found this negative correlation between duration corrected for age and FA of ipsilateral (Keller et al. 2012) and contralateral temporal lobe WM (Kemmons et al. 2011). Some other studies have not been able to determine correlations of diffusivity alterations with clinical variables (Thivard et al. 2005) and it has been argued that this may be due to small sample sizes (Keller et al. 2012). It should be added that performing conservative statistical testing taking non-normal distribution of the data and multiple testing into account, as performed within the present study (and similarly in Garcia-Fiñana et al. 2006) or not may also influence reports on significant correlations.

No correlations between clinical variables and fornical FA/MD diffusion characteristics were found, which is consistent with Concha et al. (2009), who only found a positive correlation between epilepsy duration corrected for age and perpendicular diffusivity. However, contrary to the results presented here, those authors also found that the patients with HS showed a bilateral reduction in fornical FA and increased perpendicular diffusivity in the FF when compared to controls and the non-lesional patients. Similarly, Campos et al. (2015) corroborated these results for patients with HS but did not find any diffusion alterations in patients with non-lesional TLE and in particular the FF did also not reveal any significant diffusion changes relative to controls or patients with HS. Concha et al. (2010) who performed a combined study of fornical FA and evaluation of electron microscopy images on patients with histologically confirmed HS, was able to show that patients with HS had decreased FA relative to patients without HS and that this reflected lower density and higher extra-axonal fraction. The reason for why these alterations were not found in the present study could lie in the fact that only few patients with HS (N=8) could be included.

10.4.4 Dysplasia and Focal Epilepsy

The automated voxel-based lesion detection technique identified 100% of all neuroradiologically defined dysplastic lesions in patients with previous MRI-negative epilepsy without time consuming neuroradiological assessment of multiple 3D feature maps and original 3D MRI as previously described by Huppertz et al. (2013) and Wang et al. (2015). Upon post-surgical histopathological investigation, FCD is the most common epileptogenic lesion found in patients with MRI-negative epilepsy (Wang et al. 2013). In patients with neuronal migratory disorders, such as FCDs, as many as 25% may have dual pathology and FCDs are likely accompanied by HS (Cendes et al. 1995, Colombo et al. 2003, Raymond et al. 1994, Kim et al. 2010) or by another FCD (Fauser et al. 2009). As this is one of the patient groups most likely to be refractory to surgery (Palmini et al. 1995, Fauser et al. 2009) the application of automated lesion detection approaches in these patients is most urgently indicated to identify subtle epileptogenic lesions. Importantly, the present study confirmed that it is able to identify lesions that were not previously identified on routine MRI inspection (Huppertz et al. 2005, Huppertz et al. 2008) and can be applied to find multiple FCD sites in patients with presumed non-lesional epilepsy. Reasons for this include the fact that voxel-based approaches allow analysis of the whole brain in three dimensions simultaneously, whereas the neuroradiologist relies on working memory to integrate information of consecutive 2D MRI slices. Although only a small number of patients had previously undetected FCDs (N=2) that could be neuroradiologically confirmed, the study presented here corroborated results of previous studies where the approach developed by Huppertz et al. (2013) has increased the diagnostic yield in MRI-negative patients (Huppertz et al. 2005, Wagner et al. 2011, Wang et al. 2014, Wang et al. 2016a). The approach used within the present study allows time-efficient and resourceful assessment of T1w images as it is less computationally expensive and does not require multi-feature cortical surface mapping. Previously, Hong et al. (2014) have used an automated algorithm trained on MRI-negative patients with histologically confirmed FCDs and achieved a sensitivity of 74% and specificity of 100%, where no controls were identified to have FCDs, although some false positive sites appeared in the patients. Other approaches

such as Adler et al. (2017a) may be useful in assessing various features of lesions that have already been visually identified and delineated manually, however, the sensitivity and specificity for this approach in MRI-negative patients where lesion masks are not readily available remains to be developed and tested.

The approach used here is especially useful for time-efficient assessment of patients with MRI-negative epilepsies and may be applicable to use in all patients with epilepsy undergoing MR imaging and pre-surgical evaluation. Wang et al. (2011) and Huppertz et al. (2005) using MAP, have found that the JCT image was superior to the EXT image in detecting FCD IIa and IIb, which are frequently associated with GM/WM blurring (Blümcke et al. 2011, Krsek et al. 2009, Muehlechner et al. 2012). The study presented here does not allow this conclusion, since histopathological data was not available and partly also because the sample size is so small. However, the results detailed in Chapter 8 confirm the importance of combining the information from both feature maps to identify lesions neuroradiologically. For example, the individual patient results showed that depending on the main feature of FCD found through the JCT/EXT maps (i.e. extensive GM/WM blurring / transmantle sign / cortical thickening), one feature map may be superior to the other. Although not specific to a given pathology, false positive results can be reduced by using a cluster threshold that reflects the lesion size and original MRIs can be re-reviewed using a single cluster map as a guide. Interestingly, more false positive sites were found in patients than in controls, a result also found by Wang et al. (2015), which may indicate that this approach is to some degree responsive to structural abnormalities not otherwise identifiable as FCDs, but that may reflect other variations in cortical structure as previously hypothesized (Colliot et al. 2006, Besson et al. 2008). Even when the FCD was not detected earlier on MRI, it is possible that the MAP approach highlights regions that may later be defined as an FCD through neuroradiological evaluation (Huppertz et al. 2008) as also evidenced by two cases within the study presented within this thesis. Thus, results shown by the automated lesion detection approach may indicate a structural abnormality (Hong et al. 2014) or an FCD that may be histologically verified after surgery. However, caution should be exercised

when applying invasive EEG studies based on MAP results, as sampling errors can occur and may fail to accurately identify the epileptogenic area (Tellez-Zenteno et al. 2010).

No noteworthy improvement to reduce false positives were found after FA/MD and T2w/T2FLAIR feature maps were added to the analysis. However, in some cases, the JCT/EXT map findings were confirmed by additional abnormal signal in FA/MD/T2w/T2FLAIR images and in exactly those areas already identified by the automated lesion detection tool. Especially FA and MD in WM and T2FLAIR JCT maps showed significantly reduced values when compared to controls. However, these results were not found consistently for all patients with neuroradiologically confirmed FCDs, corroborating findings of an earlier study stating that FA/MD values were unspecific (Eriksson et al. 2001). Nevertheless, these results indicate that in some patients FA and MD values may decrease in WM areas surrounding FCDs and that the GM/WM junction on T2FLAIR images is decreased due to blurring of signal between the two tissue types. While the study presented here reported on decrease in MD values within areas of FCD, Gross et al. (2005) found that while patients with obvious WM involvement based on hyperintense T2w signal had decreased FA and increased MD in underlying WM surrounding the FCD, patients with normal appearing WM below the identified FCD did not show any diffusion alterations. These results pertaining to FA maps were also confirmed by Princich et al. (2012), while diffusion abnormalities extended beyond visually determined boundaries of the FCDs as seen on T2FLAIR/T1w and FCDs were histopathological determined after patients received surgery. Studies like these have investigated WM tissue surrounding FCDs and found widespread FA decrease and MD increase (Gross et al. 2005, Eriksson et al. 2001), which may be related to the severity of the disorder or to the extent of the MRI-invisible portion of the lesion (Fonseca et al. 2012). In contrast to the study presented here, which reported on a decrease in MD, other publications investigating surrounding WM have found an increase in this diffusivity measure and linked it to defective neurogenesis or cell loss resulting in increased extracellular space (Eriksson et al. 2001). A possible explanation for this is that the

study presented within this thesis allowed extraction of FA/MD values at the immediate FCD location, whereas the previous studies have relied on whole-brain tract-based-spatial/voxel-based statistics and visual assessment of DTI-derived FA/MD maps providing an extensive analysis of more distal diffusivity alterations. FA and MD metrics from within FCDs have not yet been extensively tested as GM signal may be contaminated with CSF signal (Bhagat and Beaulieu 2004) and the tensor model was not specifically designed for areas with isotropic diffusion such as GM. So that generally, based on these and the current studies with limited sample sizes, alterations in FA/MD are not considered yet to be specific enough for lesion classification (Adler et al. 2017b). Nevertheless, since these steps were easily implemented within SPM, the present study has investigated FA/MD values at the exact FCD locations. However, analyses based on more advanced diffusion sequences may allow researchers to arrive at more detailed conclusions. For instance, one study has revealed intracellular volume fraction, a marker of neurite density, to be reduced in the area of dysplasia (Winston et al. 2014).

According to Colombo et al. (2003), neuroradiologically defined FCDs can usually be distinguished between Taylor's type (balloon cells) and those FCDs that do not have these large dysmorphic neurons. Automated lesion detection tools have not yet addressed the issue of identifying boundaries of FCDs (Wang et al. 2016a) and determining FCD subtypes based only on MRI, the latter of which is often achieved by neuroradiologists as long as the FCD is discernible on MRI. Identifying subtypes of FCDs will be especially challenging for automated MRI analysis approaches. In any case a neuroradiological assessment of MRI can contribute to pre-surgical evaluation. Apart from results obtained through neuroradiological assessment and automated lesion detection, measurements of electroencephalographic patterns may vary across different epileptogenic lesions (Perucca et al. 2014). However, the true gold standard remains the histopathological evaluation, which may also detect abnormalities consistent of FCD within tissue not found to be abnormal on MRI (Tassi et al. 2001). The subtype of FCD may even determine surgical outcomes, i.e. Taylor's type FCD IIb with balloon cells has been associated with a higher

probability of becoming seizure-free (Tassi et al. 2002).

10.5 Future Directions and Conclusions

10.5.1 Automatic Hippocampal Subfield Segmentation in Patients with TLE and HS

Studies based on analysis of surgically resected specimens have shown that different subtypes of HS are related to postoperative outcome in patients with refractory TLE. For these findings to have prospective predictive utility, they need to be translated to imaging approaches that can assess hippocampal subfields ahead of surgery. The present study has applied a novel automated multi-sequence hippocampal subfield segmentation technique to a large group of patients with refractory TLE. Neither semi-quantitative HIA ratings nor this technique, which performs well in mapping the approximate subfield locations, revealed any clear link between the respective properties of preoperative hippocampal subfields and postoperative outcome. Therefore, hippocampal features extracted from MRI are perhaps unlikely to stratify patients with HS according to outcome. However, the data presented here indicate that the reasons for favorable and poor outcomes depend on multiple preoperative factors, which may include side of seizure onset, focal unilateral EEG discharges (Ravat et al. 2016) and other factors not assessed within this particular study, e.g. ipsilateral and contralateral extrahippocampal atrophy (Bernhardt et al. 2010, Bernhardt et al. 2013) and differences in WM tract diffusivity (Glenn et al. 2016, assessed in Chapter 6). Future studies should endeavor to detail any bihemispheric epileptogenic activity and structural alterations in patients as this may well lead to predictive markers for post-surgical outcome in patients with this brain network disorder.

10.5.2 Automated Tractography Analysis in Patients with TLE and HS

Tractography is increasingly used to perform pre-surgical investigations regarding tract anatomy so that surgical damage to essential brain pathways can be avoided. In

particular, DTI is used for (i) pre-surgical tumor resection planning (Witwer et al. 2002, Jellison et al. 2004) and (ii) for identification of the optic radiations before temporal lobectomy in patients with TLE as damage to this tract may cause visual field deficits (Mansouri et al. 2012, Wiebe et al. 2001). Furthermore, tractographic analysis may contribute to the understanding of the underlying pathological mechanisms of epilepsy as a network disorder since it allows the investigation of structural brain connectivity and tract integrity. In epilepsy, tracts have been recognized as crucial components in seizure generation and propagation (Berg and Scheffer 2011, Richardson 2012) as they connect potentially epileptogenic GM regions with other GM areas, thus forming the structural connections of brain networks. Consequently, tractography may provide insight into different patterns of brain damage related to the laterality, type of epilepsy or epileptogenic lesion while along-the-tract analysis of diffusion metrics may also allow extraction of detailed information regarding neuropathology in epilepsy. It may have the potential to identify certain abnormal brain regions in individual patients (Martin et al. 2015), allow inferences about seizure onset zones or may even predict surgical outcomes (Keller et al. 2017). Future tractographic studies should aim to assess image quality, possible motion confounds and employ appropriate statistics so that subtle differences in diffusion metrics between individual patients, groups of patients and controls can be confidently identified and accurate diagnostic markers can be developed. TRACULA does not only provide detailed tractographic analysis strategies but also the possibility of detailed quality assurance and control giving researchers and clinicians a ready-to-use and sensitive tool for automated tractography. Future studies should consider different patterns of whole-tract and along-the-tract diffusivity alterations when designing algorithms that could stratify patients according to post-surgical outcomes based on preoperative diffusion imaging. A tool which can resolve subtle intra-tract microstructural changes and relationships with morphometric abnormalities will likely afford important clinical information for individual patients in the future.

10.5.3 Automatic Fiber Quantification in Patients with TLE

Even though there are limitations regarding investigation of WM disruption in patients with epilepsy due to the small sample size of the patient groups, the main objective of this study was to compare the manual and automated approaches. Compared to manual approaches, one of the major strengths when analyzing data via automated tractography, which performs similarly relative to time-consuming manual tractography, is the possibility of time-efficient reproducibility, detailed quality assurance and control giving researchers and clinicians a ready-to-use and sensitive tool. The present study using automated tractography was able to corroborate previous results found when patients with left/right TLE and patients with/without HS were compared to controls and when clinical correlations were assessed. Future studies should aim to perform comparisons of automated with manual tractography via same tractography algorithms implemented into harmonized protocols, which unfortunately was not feasible in the present study. This will also aid even larger multi-site research projects to arrive at conclusions and perhaps guide concrete recommendations on how to use automated tractography approaches to provide clinically significant information based on trajectory and integrity of the tracts.

10.5.4 Automatic Detection of Focal Cortical Dysplasia

Although surface-based approaches offer features not obtainable with voxel-based techniques, the approach used within this thesis was still able to detect suspicious areas suggestive of FCD. In the absence of histopathological data in the patient sample presented here, results could only be validated against neuroradiological assessment. Future studies on these patients should aim to evaluate the results obtained from automated lesion detection against histopathological data in order to demonstrate that neuroradiological, non-invasive/invasive electroclinical, histopathological and automated neuroimaging analysis complement each other as previously demonstrated (Adler et al. 2017b, Huppertz et al. 2005, Hong et al. 2014).

The developed MAP tool is still using segmentation algorithms based on SPM5 (Huppertz 2013), which is one of the older SPM packages (Wang et al. 2016a). However, since then considerable additions to segmentation algorithms have been performed to enable localization-specific tissue segmentation and these provide improvements over previous algorithms (Dahnke et al. 2012) that may render voxel-based results more accurate when investigating patients with epilepsy (Farokhian et al. 2017). Furthermore, Huppertz et al. (2013) have built GM/WM thresholds based on whole-brain GM/WM intensities. Future studies should compute the GM/WM thresholds only from cerebral cortex (without the inclusion of deep GM nuclei and cerebellum), also since local intensity differences are taken into account and computed during segmentation (Dahnke et al. 2012).

In the present study, sequential multimodal testing after generation of feature maps and computation of significant clusters using segmentation based on only T1w images did not increase specificity of the tool. Future studies should implement iterative search algorithms that can process multiple MRI or assess diagnostic yield rendered by simultaneous 3D multi-modal segmentation models. In addition to this, similar to Wilke et al. (2003), systematic comparisons of different statistical thresholds to identify the combination that is most sensitive and also specific to FCDs should be performed on newly developed automated lesion detection tools. It is likely that small lesions may be missed when concentrating on voxel-based approaches only. Voxel-based analysis alone does not allow direct comparison of surface-based or deformation-based features, which is an addition that should be implemented when using CAT12 in SPM12 with automated lesion detection approaches and should be subject to further development. Finally, machine-learning approaches such as those already used in TLE (Rudie et al. 2015, Kamiya et al. 2016) should be tested using a combination of voxel-based and surface-based approaches in a sufficient number of patients with histologically confirmed FCDs and age- and sex-matched controls.

REFERENCES

- Abd Rabou, A. (2013) From the Case: Focal Cortical Dysplasia. Available at: <https://radiopaedia.org/images/3366551> (accessed: 24/08/2017)
- Abou-Khalil, B. (2007) An update on determination of language dominance in screening for epilepsy surgery: the Wada test and newer noninvasive alternatives. *Epilepsia* 2007; 48: 442-55.
- Adler, S., Wagstyl, K., Gunny, R., Ronan, L., Carmichael, D., Cross, J. H. et al. (2017a). Novel surface features for automated detection of focal cortical dysplasia in pediatric epilepsy. *NeuroImage: Clinical*, 14 (December), 18-27. <http://doi.org/10.1016/j.nicl.2016.12.030>
- Adler, S., Lorio, S., Jacques, T. S., Benova, B., Gunny, R., Cross, J. H. et al. (2017b). Towards in vivo focal cortical dysplasia phenotyping using quantitative MRI. *NeuroImage: Clinical*, 15(March), 95-105. <http://doi.org/10.1016/j.nicl.2017.04.017>
- Agosta, F., Henry, R.G., Migliaccio, R., Neuhaus, J., Miller, B. L., Dronkers, N.F. et al. (2010) Language networks in semantic dementia. *Brain* 2010, 133: 286–299.
- Ahmadi, M.E., Hagler, D.J., McDonald, C.R., Tecoma, E.S., Iragui, V.J., Dale, A.M. et al. (2009) Side matters: Diffusion tensor imaging tractography in left and right temporal lobe epilepsy. *American Journal of Neuroradiology*, 30(9), 1740–1747. doi:10.3174/ajnr.A1650
- Ajtai, B., Lindzen, E., Madeu, J.C. (2015) Structural Imaging: Magnetic Resonance Imaging, Computed Tomography. In: *Neuroimaging, Chapter 33 A*. <http://clinicalgate.com/neuroimaging-structural-imaging-magnetic-resonance-imaging-computed-tomography/> (12/11/2016)
- Akanuma, N., Koutroumanidis, M., Adachi, N., Alarcon, G., Binnie, C.D. (2003) Presurgical assessment of memory-related brain structures: the Wada test and functional neuroimaging. *Seizure* 2003; 12: 346-58.
- Aldenkamp, A., Boon, P., Deblaere, K., Achten, E., Backes, W.H., Hofman, P. et al. (2003) Usefulness of language and memory testing during intracarotid amobarbital testing: observations from an fMRI study. *Acta Neurol Scand* 2003; 108: 147-52.
- Alexander, A.L., Hurley, S.A., Samsonov, A.A., Adluru, N., Hosseinbor, A.P., Mossahebi, P. et al. (2011) Characterization of Cerebral White Matter Properties Using Quantitative Magnetic Resonance Imaging Stains. *Brain Connectivity*, Volume 1, Number 6, 2011, DOI: 10.1089/brain.2011.0071
- Alexander, A.L., Lee, J.E., Lazar, M., Field, A.S. (2007) Diffusion Tensor Imaging of the Brain. *Neurotherapeutics*. July; 4(3): 316–329.
- Alexander, W.H., Brown, J.W. (2011) Medial prefrontal cortex as an action-outcome predictor. *Nature Neuroscience* (2011), volume 14, issue 10, p. 1338-1344
- Almeida, S.S., Naffah-Mazzacoratti, M.G., Guimarães, P.B., Wasinski, F., Pereira, F.E.G., Canzian, M. et al. (2012) Carbamazepine inhibits angiotensin I-converting enzyme, linking it

References

- to the pathogenesis of temporal lobe epilepsy. *Translational Psychiatry*, 2, e93. <http://doi.org/10.1038/tp.2012.21>
- Alonso, F., Sweet, J., Miller, J. (2016) Speech mapping using depth electrodes: The “electric Wada”. In *Clinical Neurology and Neurosurgery*, Volume 144, 2016, 88-90. <https://doi.org/10.1016/j.clineuro.2016.03.017>.
- Anastasopoulos, C., Reiser, M., Kiselev, V. G., Nguyen-Thanh, T., Schulze-Bonhage, A., Zentner, J. et al. (2014). Local and global fiber tractography in patients with epilepsy. *American Journal of Neuroradiology*, 35(2), 291-296. <http://doi.org/10.3174/ajnr.A3752>
- Andersen, P., Eccles, J. C., Loynning, Y. (1963). Recurrent inhibition in the hippocampus with identification of the inhibitory cell and its synapses. *Nature* 198:540-542.
- Andersson, J.L.R., Sotiropoulos, S.N. (2016). An integrated approach to correction for off-resonance effects and subject movement in diffusion MR imaging. *NeuroImage*, 125:1063-1078, 2016.
- Andersson, J.L.R., Skare, S., Ashburner, J. (2003) How to correct susceptibility distortions in spin-echo echo-planar images: application to diffusion tensor imaging. *NeuroImage*, 20(2):870-888, 2003.
- Annegers, J.F., Hauser, W.A., Elveback, L.R. (1979) Remission of seizures and relapse in patients with epilepsy. *Epilepsia*. 1979 Dec;20(6):729-37.
- Antel, S.B., Collins, D.L., Bernasconi, N., Andermann, F., Shinghal, R., Kearney, R.E. et al. (2003) Automated detection of focal cortical dysplasia lesions using computational models of their MRI characteristics and texture analysis, *NeuroImage*, 19(4), August 2003:1748-1759, ISSN 1053-8119, [http://dx.doi.org/10.1016/S1053-8119\(03\)00226-X](http://dx.doi.org/10.1016/S1053-8119(03)00226-X).
- Ardekani, S. and Sinha, U. (2005) Geometric distortion correction of high-resolution 3 T diffusion tensor brain images. *Magnetic Resonance in Medicine*, 54: 1163–1171. doi:10.1002/mrm.20651
- Ashburner, J., Friston, K.J. (2000) Voxel-based morphometry - the methods. *NeuroImage*. 2000;11:805–21.
- Ashburner J. (2007) A fast diffeomorphic image registration algorithm. *Neuroimage* 38(1):95-113.
- Ashburner J., Friston K.J. (2005) Unified segmentation. *NeuroImage*, 2005, 26:839–851.
- Bannerman, D. M., Grubb, M., Deacon, R. M. J., Yee, B. K., Feldon, J., Rawlins, J. N. P. (2003). Ventral hippocampal lesions affect anxiety but not spatial learning. *Behavioural Brain Research*, 139(1-2), 197-213. [http://doi.org/10.1016/S0166-4328\(02\)00268-1](http://doi.org/10.1016/S0166-4328(02)00268-1)
- Barba, C., Minotti, L., Job, A. S., & Kahane, P. (2017). The Insula in Temporal Plus Epilepsy. *Journal of Clinical Neurophysiology*, 34(4), 324-327. <http://doi.org/10.1097/WNP.0000000000000389>
- Barkovich, A.J., Guerrini, R., Kuzniecky, R.I., Jackson, G.D., Dobyns, W.B. (2012) A developmental and genetic classification for malformations of cortical development: Update 2012. *Brain* 135, no. 5: 1348-1369.

References

- Barkovich, A.J., Kuzniecky, R.I., Jackson, G.D., Guerrini, R., Dobyns, W.B. (2005) A developmental and genetic classification for malformations of cortical development. *Neurology* 65:1873–1887.
- Barkovich, A. J., Berkovic, S. F., Cascino, G. D., Chiron, C., Duncan, J. S., Gadian, D. G. et al. (1998). Guidelines for neuroimaging evaluation of patients with uncontrolled epilepsy considered for surgery. *Epilepsia*, 39(12), 1375–1376. <http://doi.org/10.1111/j.1528-1157.1998.tb01341.x>
- Barkovich, A.J., Kuzniecky, R.I., Bollen, A.W., Grant, P.E. (1997) Focal transmantle dysplasia: a specific malformation of cortical development. *Neurology* 49, 1148–1152.
- Barkovich, A.J. (2005) Chapter 7: Malformations of Cortical Development. In: Kuzniecky, R.I., Jackson, G.D. (2005) *Magnetic resonance in epilepsy: neuroimaging techniques*. Second Edition. Elsevier Academic Press. Burlington, California, London.
- Barr, W. (1997). Examining the right temporal lobe's role in nonverbal memory. *Brain Cog.*, 35, 26–41.
- Barry, D.S., Pakan, J.M., McDermott, K.W. (2014). Radial glial cells: key organisers in CNS development. *The international journal of biochemistry & cell biology*. 46: 76–9. doi:10.1016/j.biocel.2013.11.013.
- Basser, P.J., Pajevic, S., Pierpaoli, C., Duda, J., Aldroubi, A. (2000) In vivo fiber tractography using DT-MRI data. *Magnetic Resonance in Medicine* 44: 625– 632.
- Basser, P.J., Mattiello, J., Le Bihan, D. (1994) MR diffusion tensor spectroscopy and imaging. *Biophysical Journal* 66:259–267.
- Bast, T., Ramantani, G., Seitz, A., Rating, D. (2006). Focal cortical dysplasia: Prevalence, clinical presentation and epilepsy in children and adults. *Acta Neurologica Scandinavica*, 113(2), 72–81. <http://doi.org/10.1111/j.1600-0404.2005.00555.x>
- Bastos, A.C., Comeau, R.M., Andermann, F., Melanson, D., Cendes, F., Dubeau, F. et al. (1999) Diagnosis of subtle focal dysplastic lesions: curvilinear reformatting from three-dimensional magnetic resonance imaging. *Annals of Neurology*. 1999 Jul;46(1):88-94.
- Becker, A.J., Blümcke, I., Urbach, H., Hans, V., Majores, M. (2006) Molecular neuropathology of epilepsy-associated glioneuronal malformations. *Journal of Neuropathology and Experimental Neurology* 65:99–108.
- Bell, G.S., Sinha, S., de Tisi, J., Stephani, C., Scott, C.A., Harkness, W.F. et al. (2010) Premature mortality in refractory partial epilepsy: does surgical treatment make a difference? *Journal of Neurology Neurosurgery and Psychiatry* 2010; 81:716–718.
- Bello, L., Gambini, A., Castellano, A., Carrabba, G., Acerbi, F., Fava, E. et al. (2008) Motor and language DTI fiber tracking combined with intraoperative subcortical mapping for surgical removal of gliomas. *NeuroImage* 2008;39:369–82.
- Benjamini, Y., Hochberg, Y. (1995) Controlling the false discovery rate: a practical and powerful approach to multiple testing. *Journal of the Royal Statistical Society. Series B (Methodological)*, Vol. 57, No. 1 (1995), 289–300.
- Berbaum, K. S., Franken, E. A., Dorfman, D. D., Rooholamini, S. A., Kathol, M. H.,

References

- Barloon, et al. (1990). Satisfaction of search in diagnostic radiology. *Investigative Radiology*, 25, 133–140.
- Berg, A.T. (2009) Identification of pharmacoresistant epilepsy. *Neurol Clin.* Nov;27(4) 1003-1013. doi:10.1016/j.ncl.2009.06.001.
- Berg, A.T., Scheffer, I.E. (2011). New concepts in classification of the epilepsies: entering the 21st century. *Epilepsia*, 52(6), 1058–62. <http://doi.org/10.1111/j.1528-1167.2011.03101.x>
- Berg, A.T., Berkovic, S.F., Brodie, M.J., Buchhalter, J., Cross, J.H., Van Emde Boas, W., et al. (2010). Revised terminology and concepts for organization of seizures and epilepsies: Report of the ILAE Commission on Classification and Terminology, 2005-2009. *Epilepsia*, 51(4), 676–685. <http://doi.org/10.1111/j.1528-1167.2010.02522.x>
- Berg, A.T., Vickrey, B.G., Langfitt, J.T., Sperling, M.R., Walczak, T.S., Shinnar, S. et al. (2003) Multicenter Study of Epilepsy Surgery. The multicenter study of epilepsy surgery: recruitment and selection for surgery. *Epilepsia*. 2003;44(11):1425-1433
- Berkovic, S.F., McIntosh, A.M., Kalnins, R.M. (1995). Pre-operative MRI predicts outcome of temporal lobectomy. *Neurology* 1995; 45: 1358–63.
- Bernasconi, A., Antel, S.B., Collins, D.L., Bernasconi, N., Olivier, A., Dubeau, F., Pike, G.B., Andermann, F., Arnold, D.L. (2001) Texture analysis and morphological processing of magnetic resonance imaging assist detection of focal cortical dysplasia in extra-temporal partial epilepsy. *Annals of Neurology* 49:770–775.
- Bernasconi, A., Bernasconi, N., Bernhardt, B.C., Schrader, D. (2011) Advances in MRI for ‘cryptogenic’ epilepsies. *Nature Reviews Neurology* 7(2):99–108
- Bernasconi, N., Duchesne, S., Janke, A., Lerch, J., Collins, D.L., Bernasconi, A. (2004) Whole-brain voxel-based statistical analysis of gray matter and white matter in temporal lobe epilepsy. *NeuroImage* 23: 717–723.
- Bernaudo, M., Nouvelot, A., MacKenzie, E. T., Petit, E. (1998). Selective neuronal vulnerability and specific glial reactions in hippocampal and neocortical organotypic cultures submitted to ischemia. *Exp Neurol*, 150, 30–39.
- Bernhardt, B.C., Hong, S., Bernasconi, A., Bernasconi, N. (2013) Imaging structural and functional brain networks in temporal lobe epilepsy. *Frontiers in human neuroscience*. 2013;7:624.
- Bernhardt, B.C., Bernasconi, N., Concha, L., Bernasconi, A. (2010) Cortical thickness analysis in temporal lobe epilepsy: reproducibility and relation to outcome *Neurology*, 74 (2010), pp. 1776–1784
- Bernhardt, B.C., Worsley, K.J., Kim, H., Evans, A.C., Bernasconi, A., Bernasconi, N. (2009) Longitudinal and cross-sectional analysis of atrophy in pharmacoresistant temporal lobe epilepsy. *Neurology* 72:1747–1754.
- Bernhardt, B. C., Bonilha, L., Gross, D. W. (2015). Network analysis for a network disorder: The emerging role of graph theory in the study of epilepsy. *Epilepsy & Behavior : E&B*, 50, 162-170. <http://doi.org/10.1016/j.yebeh.2015.06.005>

References

- Besson, P., Bernasconi, N., Colliot, O., Evans, A., Bernasconi, A. (2008) Surface-Based Texture and Morphological Analysis Detects Subtle Cortical Dysplasia. In D. Metaxas et al. (Eds.): MICCAI 2008, Part I, LNCS 5241, pp. 645–652, 2008.
- Bettus, G., Bartolomei, F., Confort-Gouny, S., Guedj, E., Chauvel, P., Cozzone, P.J. et al. (2010). Role of resting state functional connectivity MRI in presurgical investigation of mesial temporal lobe epilepsy. *Journal of Neurology, Neurosurgery and Psychiatry*, 81(10), 1147–1154. <http://doi.org/10.1136/jnnp.2009.191460>
- Bhagat, Y. A., Beaulieu, C. (2004). Diffusion anisotropy in subcortical white matter and cortical gray matter: changes with aging and the role of CSF-suppression. *Journal of Magnetic Resonance Imaging : JMRI*, 20(2), 216-27. <http://doi.org/10.1002/jmri.20102>
- Bien, C.G., Szinay, M., Wagner, J., Clusmann, H., Becker, A.J., Urbach, H. (2009) Characteristics and surgical outcomes of patients with refractory magnetic resonance imaging-negative epilepsies. *Archives of Neurology* 2009; 66: 1491-1499.
- Binder, J. R. (2010). FMRI Is a Valid Noninvasive Alternative to Wada Testing, 48(Suppl 2), 1–6. <http://doi.org/10.1097/MPG.0b013e3181a15ae8.Screening>
- Bitar, R., Leung, G., Perng, R., Tadros, S., Moody, A. R., Sarrazin, J., et al. (2006). MR Pulse Sequences: What Every Radiologist Wants to Know but Is Afraid to Ask 1. <http://doi.org/10.1148/rg.262055063> *Radiographics* 2006; 26:512-537.
- Blaschke, A.J., Staley, K., Chun, J. (1996). Widespread programmed cell death in proliferative and postmitotic regions of the fetal cerebral cortex. *Development* 122: 1165–1174.
- Bloch, F. (1946) Nuclear Induction. *Physical Review*, 70-77.
- Blümcke, I., Thom, M., Aronica, E., Armstrong, D.D., Bartolomei, F., Bernasconi, A, et al. (2013) International consensus classification of hippocampal sclerosis in temporal lobe epilepsy: a Task Force report from the ILAE Commission on Diagnostic Methods. *Epilepsia*. 2013;54(7):1315-1329.
- Blümcke, I., Pauli, E., Clusmann, H., Schramm, J., Becker, A., Elger, C. et al (2007). A new clinico-pathological classification system for mesial temporal sclerosis. *Acta Neuropathologica*, 113(3), 235-244. <http://doi.org/10.1007/s00401-006-0187-0>
- Blümcke, I., Thom, M., Aronica, E., Armstrong, D. D., Vinters, H. V, Palmini, A., Spreafico, R. (2011). The clinicopathologic spectrum of focal cortical dysplasias: a consensus classification proposed by an ad hoc Task Force of the ILAE Diagnostic Methods Commission. *Epilepsia*, 52(1), 158-174. <http://doi.org/10.1111/j.1528-1167.2010.02777.x>
- Blume, W.T. (2006) The progression of epilepsy. *Epilepsia*, vol. 47, no. 1, supplement, 2006, 71–78.
- Boghi, A., Rasetti, R., Avidano, F., Manzone, C., Orsi, L., D'Agata, F. et al. (2006) The effect of gender on planning: An fMRI study using the Tower of London task. *Neuroimage*. 2006 Nov 15;33(3):999-1010.
- Bonelli, S.B., Powell, R.H.W., Yogarajah, M., Samson, R.S., Symms, M.R., Thompson, P.J., et al. (2010). Imaging memory in temporal lobe epilepsy: Predicting the effects of temporal

References

- lobe resection. *Brain*, 133(4), 1186–1199. <http://doi.org/10.1093/brain/awq006>
- Bonelli, S. B., Thompson, P. J., Yogarajah, M., Powell, R. H. W., Samson, R. S., McEvoy, A. W. et al. (2013). Memory reorganization following anterior temporal lobe resection: a longitudinal functional MRI study. *Brain*, 136(6), 1889–1900. <http://doi.org/10.1093/brain/awt105>
- Bonilha, L., Yasuda, C.L., Rorden, C., Li, L.M., Tedeschi, H., de Oliveira, E. et al. (2007a) Does resection of the medial temporal lobe improve the outcome of temporal lobe epilepsy surgery? *Epilepsia* 2007;48:571-578.
- Bonilha, L., Rorden, C., Halford, J.J., Eckert, M., Appenzeller, S., Cendes, F. et al. (2007b) Asymmetrical extra-hippocampal grey matter loss related to hippocampal atrophy in patients with medial temporal lobe epilepsy. *Journal of Neurology, Neurosurgery and Psychiatry* 78: 286–294.
- Bonilha, L., Keller, S.S. (2015) Quantitative MRI in refractory temporal lobe epilepsy: relationship with surgical outcomes. *Quantitative Imaging in Medicine and Surgery*, 5(2), 204–224. <http://doi.org/10.3978/j.issn.2223-4292.2015.01.01>
- Bonilha, L., Edwards, J.C., Kinsman, S.L., Morgan, P.S., Fridriksson, J., Rorden, C., et al. (2010). Extrahippocampal gray matter loss and hippocampal deafferentation in patients with temporal lobe epilepsy. *Epilepsia*, 51(4), 519-528. <http://doi.org/10.1111/j.1528-1167.2009.02506.x>
- Bonilha, L., Montenegro, M.A., Rorden, C., Castellano, G., Guerreiro, M.M., Cendes, F. et al. (2006). Voxel-based morphometry reveals excess gray matter concentration in patients with focal cortical dysplasia. *Epilepsia*, 47(5), 908-915. <http://doi.org/10.1111/j.1528-1167.2006.00548.x>
- Bonnici, H.M., Chadwick, M.J., Lutti, A., Hassabis, D., Weiskopf, N., Maguire, E.A. (2012) Detecting representations of recent and remote autobiographical memories in vmPFC and hippocampus. *Journal of Neuroscience*. 2012; 32:16982–16991.
- Braak H (1980) Architectonics of the human telencephalic cortex. *Studies of brain function*, vol 4. Springer, Berlin/Heidelberg/New York, 24–62.
- Braakman, H.M., Ijff, D.M., Vaessen, M.J., Debeij-van Hall, M.H., Hofman, P.A., Backes, W.H., et al. (2012) Cognitive and behavioural findings in children with frontal lobe epilepsy. *European Journal of Paediatric Neurology*. 16:707–715.
- Brodal, A. (1981). *Neurological Anatomy in Relation to Clinical Medicine*. Oxford University Press, 1981.
- Bronen, R.A., Vives, K.P., Kim, J.H., Fulbright, R.K., Spencer, S.S., Spencer, D.D. (1997). Focal cortical dysplasia of Taylor, balloon cell subtype: MR differentiation from low-grade tumors. *American Journal of Neuroradiology*, 18(6), 1141-1151.
- Buhl, E., Whittington, M. (2006) *Local Circuits*. DOI:10.1093/acprof:oso/9780195100273.003.0008; In: Andersen, P., Morris, R., Amaral, D., Bliss, T. and O'Keefe, J (2006) *The Hippocampus Book*. DOI: 10.1093/acprof:oso/9780195100273.001.0001

References

- Burgess, N., Maguire, E.A., O'Keefe, J. (2002) The human hippocampus and spatial and episodic memory. *Neuron* 35:625–641.
- Campos, B.M., Coan, A.C., Beltramini, G.C., Liu, M., Yasuda, C.L., Ghizoni, E., et al. (2015) White matter abnormalities associate with type and localization of focal epileptogenic lesions. *Epilepsia*. 2015;56(1):125–32.
- Cao, B., Li, W., Li, F., Li, H. (2016) Dissociable roles of medial and lateral PFC in rule learning. *Brain and Behavior*. 2016 Aug 19;6(11):e00551.
- Cascino, G.D. (2002). Video-EEG monitoring in adults. *Epilepsia*, 43(SUPPL. 3), 80–93. <http://doi.org/10.1046/j.1528-1157.43.s.3.14.x>
- Cascino, G.D., Jack, C.R., Jr., Parisi, J.E., Sharbrough, F.W., Hirschorn, K.A., Meyer, F.B. et al. (1991) Magnetic resonance imaging-based volume studies in temporal lobe epilepsy: pathological correlations. *Annals of Neurology*. 1991 Jul;30(1):31-36.
- Catani, M., Jones, D.K., Donato, R., Ffytche, D.H. (2003) Occipito-temporal connections in the human brain. *Brain*, 126: 2093–2107, 2003.
- Catani, M., Jones, D.K., Ffytche, D.H. (2005) Perisylvian language networks of the human brain. *Annals of Neurology*. 57, 8-16.
- Catani, M., Mesulam, M. (2008). The arcuate fasciculus and the disconnection theme in language and aphasia: History and current state. *Cortex*, 44(8), 953-961. <http://doi.org/10.1016/j.cortex.2008.04.002>
- Catani, M., Thiebaut de Schotten, M. (2008) A diffusion tensor imaging tractography atlas for virtual in vivo dissections, *Cortex*, Volume 44, Issue 8, September 2008, p. 1105-1132, <http://doi.org/10.1016/j.cortex.2008.05.004>.
- Cattaneo, L. (2013). Language. *Handbook of Clinical Neurology*, 116, 681-691. <http://doi.org/10.1016/B978-0-444-53497-2.00054-1>
- Cendes, F., Andermann, F., Gloor, P., Lopes-Cendes, I., Andermann, E., Melanson, D. et al. (1993) Atrophy of mesial structures in patients with temporal lobe epilepsy: cause or consequence of repeated seizures? *Annals of Neurology*. 1993;34(6):795-801.
- Cendes, F., Cook, M.J., Watson, C., Andermann, F., Fish, D.R., Shorvon, S.D. et al. (1995) Frequency and characteristics of dual pathology in patients with lesional epilepsy. *Neurology*. 1995 Nov;45(11):2058-64.
- Cendes, F., Theodore, W. H., Brinkmann, B. H., Sulc, V., Cascino, G. D. (2016). Neuroimaging of epilepsy. *Handbook of Clinical Neurology*, 136, 985–1014. <http://doi.org/10.1016/B978-0-444-53486-6.00051-X>
- Chiang, S., Levin, H.S., Wilde, E., Haneef, Z. (2016) White matter structural connectivity changes correlate with epilepsy duration in temporal lobe epilepsy. *Epilepsy Research*. 2016 Feb;120:37-46. doi: 10.1016/j.eplepsyres.2015.12.002.
- Christian, E.P., Dudek, F.E. (1988). Electrophysiological evidence from glutamate microapplications for local excitatory circuits in the CA1 area of rat hippocampal slices. *Neurophysiol*. 59:110-123.

References

- Cicchetti, D.L. (1994). Multiple comparison methods: Establishing guidelines for their valid application in neuropsychological research. *Journal of Clinical and Experimental Neuropsychology*, 16, 155–161.
- Coan, A.C., Appenzeller, S., Li, L.M., Cendes, F. (2009). Seizure frequency and lateralization affect progression of atrophy in temporal lobe epilepsy. *Neurology*, 73(11), 834–842. <http://doi.org/10.1212/WNL.0b013e3181b783dd>
- Coan, A.C., Campos, B.M., Yasuda, C.L., Kubota, B.Y., Bergo, F.P., Guerreiro, C.A., et al. (2014). Frequent seizures are associated with a network of gray matter atrophy in temporal lobe epilepsy with or without hippocampal sclerosis. *PloS One*, 9(1), e85843. <http://doi.org/10.1371/journal.pone.0085843>
- Cockerell, O.C., Johnson, A.L., Sander, J.W., Shorvon, S.D. (1997) Prognosis of epilepsy: a review and further analysis of the first nine years of the British National General Practice Study of Epilepsy, a prospective population-based study. *Epilepsia* 38, 31–46 (1997).
- Cockerell, O.C., Johnson, A.L., Sander, J.W., Hart, Y.M., Shorvon, S.D. (1995) Remission of epilepsy: results from the National General Practice Study of Epilepsy. *Lancet* 346, 140–144 (1995).
- Cohen-Gadol, A.A., Bradley, C.C., Williamson, A., Kim, J.H., Westerveld, M., Duckrow, R.B. et al. (2005) Normal magnetic resonance imaging and medial temporal lobe epilepsy: the clinical syndrome of paradoxical temporal lobe epilepsy. *Journal of Neurosurgery*. 102 (5), 902-909.
- Cohen, N., Ryan, J., Hunt, C., Romine, L., Wszalek, T., Nash, C. (1999). Hippocampal system and declarative (relational) memory: summarizing the data from functional neuroimaging studies. *Hippocampus*, 9, 83-98.
- Colliot, O., Bernasconi, N., Khalili, N., Antel, S.B., Naessens, V., Bernasconi, A. (2006) Individual voxel-based analysis of gray matter in focal cortical dysplasia. *NeuroImage*. 2006;29(1):162–171. <http://doi.org/10.1016/j.neuroimage.2005.07.021>
- Colombo, N., Salamon, N., Raybaud, C., Ozkara, C., Barkovich, A.J. (2009) Imaging of malformations of cortical development. *Epileptic Disorders* 2009; 11: 194–205.
- Colombo, N., Tassi, L., Galli, C., Citterio, A., Lo Russo, G., Scialfa, G. et al. (2003) Focal Cortical Dysplasias: MR Imaging, Histopathologic, and Clinical Correlations in Surgically Treated Patients with Epilepsy. *American Journal of Neuroradiology* 24:724–733, April 2003.
- Concha, L., Beaulieu, C., Gross, D.W. (2005) Bilateral limbic diffusion abnormalities in unilateral temporal lobe epilepsy. *Annals of Neurology*, 57:188–96.
- Concha, L., Kim, H., Bernasconi, A., Bernhardt, B.C., Bernasconi, N. (2012) Spatial patterns of water diffusion along white matter tracts in temporal lobe epilepsy. *Neurology*. 2012;79(5):455-462.
- Concha, L., Livy, D.J., Beaulieu, C., Wheatley, B.M., Gross, D.W. (2010) In vivo diffusion tensor imaging and histopathology of the fimbria-fornix in temporal lobe epilepsy. *Journal of Neuroscience*. 2010;30(3):996-1002.

References

- Concha, L., Beaulieu, C., Wheatley, B. M., Gross, D. W. (2007). Bilateral White Matter Diffusion Changes Persist after Epilepsy Surgery. *Epilepsia*, 48(5), 931-940. <http://doi.org/10.1111/j.1528-1167.2007.01006.x>
- Concha, L., Beaulieu, C., Collins, D. L., Gross, D. W. (2009). White-matter diffusion abnormalities in temporal-lobe epilepsy with and without mesial temporal sclerosis. *Journal of Neurology, Neurosurgery and Psychiatry*, 80(3), 312-319. <http://doi.org/10.1136/jnnp.2007.139287>
- Conover, W.J., Iman, R.L. (1982). Analysis of covariance using the rank transformation. *Biometrics*, 38(3), 715-24.
- Cooper, J. (2014). Molecules and mechanisms that regulate multipolar migration in the intermediate zone. *Frontiers In Cellular Neuroscience*, NOV 14, 2014, 8-11.
- Corballis, M.C., Morgan, M. (1978) On the Biological Basis of Human Laterality: I. Evidence for a Maturational Left-Right Gradient. *Behavioral and Brain Sciences*. 1978; 2:261-269.
- Culham, J.C., Valyear, K.F. (2006). Human parietal cortex in action. *Current Opinion in Neurobiology*. 16 (2): 205-212. doi:10.1016/j.conb.2006.03.005.
- Dabbs, J.M. (1980) Left-Right Differences in Cerebral Blood Flow and Cognition. *Psychophysiology*, 17: 548-551. doi:10.1111/j.1469-8986.1980.tb02295.x
- Dahnke, R., Yotter, R., Gaser, C. (2012). Cortical thickness and central surface estimation. *Neuroimage*, 65: 336-348.
- Damadian, R. (1971). Tumor detection by nuclear magnetic resonance. *Science* 171, 1151-1153. doi:10.1126/science.171.3976.1151
- Damadian, R. (1974) Apparatus and method for detecting cancer in tissue. U.S. Patent Office United States Patent no. 3789832. Filed 17 March 1972, awarded 5 February 1974.
- Dansereau, C.L., Bellec, P., Lee, K., Pittau, F., Gotman, J., Grova, C. (2014). Detection of abnormal resting-state networks in individual patients suffering from focal epilepsy: An initial step toward individual connectivity assessment. *Frontiers in Neuroscience*, 8(DEC), 1-21. <http://doi.org/10.3389/fnins.2014.00419>
- Davies, K.G., Hermann, B.P., Dohan, F.C., Foley, K.T., Bush, A.J., Wyler, A.R. (1996). Relationship of hippocampal sclerosis to duration and age of onset of epilepsy, and childhood febrile seizures in temporal lobectomy patients. *Epilepsy Research*, 24(2), 119-126. [http://doi.org/10.1016/0920-1211\(96\)00008-3](http://doi.org/10.1016/0920-1211(96)00008-3)
- de Tisi, J., Bell, G.S., Peacock, J.L. McEvoy, A.W., Harkness, W.F.J., Sander, J.W. et al. (2011) The long-term outcome of adult epilepsy & surgery, patterns of seizure remission, and relapse: a cohort study. *Lancet* 2011; 378:1388-1395.
- Deleo, F., Garbelli, R., Milesi, G., Gozzo, F., Bramerio, M., Villani, F. et al. (2016) Short- and long-term surgical outcomes of temporal lobe epilepsy associated with hippocampal sclerosis: Relationships with neuropathology. *Epilepsia*. 2016 Feb;57(2):306-15.
- Dewer, B., Rogers, P., Ricketts, J., Mukonoweshuro, W., Zeman, A. (2016). The radiological diagnosis of frontotemporal dementia in everyday practice: An audit of reports, review of

References

- diagnostic criteria, and proposal for service improvement. *Clinical Radiology*, 71(1), 40–47. <http://doi.org/10.1016/j.crad.2015.09.008>
- Deyo, S. N., Lytton, W. W. (1997). Inhibition can disrupt hypersynchrony in model neuronal networks. *Progress In Neuro-Psychopharmacology & Biological Psychiatry*, 21(5), 735-750.
- Dice, R. (1945) Measures of the Amount of Ecologic Association Between Species. *Ecology*, vol. 26, 1945, 297-302.
- Dichter, M.A., Brodie, M.J. (1996). New Antiepileptic Drugs. *New England Journal of Medicine*, 334(24), 1583–1590. <http://doi.org/10.1056/NEJM199606133342407>
- Diehl, B., Busch, R.M., Duncan, J.S., Piao, Z., Tkach, J., Luders, H.O. (2008) Abnormalities in diffusion tensor imaging of the uncinate fasciculus relate to reduced memory in temporal lobe epilepsy. *Epilepsia*. 2008;49(8):1409-1418.
- Dinner, S., Lüders, H.O., Klem, G. (1998). Chronic electrocorticography: cleveland clinic experience. *Electroencephalography and Clinical Neurophysiology. Supplement*, 1998, vol. 48, 58–69.
- Dobyns, W., Andermann, E., Andermann, F., Czapansky-Beilman, D., Dubeau, F., Dulac, O., et al. (1996). X-linked malformations of neuronal migration. *Neurology*, 47(2), 331-339.
- Draganski, B., Gaser, C., Kempermann, G., Kuhn, H. G., Winkler, J., Büchel, C. et al. (2006). Temporal and spatial dynamics of brain structure changes during extensive learning. *The Journal of Neuroscience*, 26(23), 6314-6317. <http://doi.org/10.1523/JNEUROSCI.4628-05.2006>
- Duncan, J.S. (2010). Imaging in the surgical treatment of epilepsy. *Nature Reviews Neurology* 6, 537-550 (October 2010) doi:10.1038/nrneurol.2010.131.
- Duncan, J.S. (1997) Imaging and epilepsy. *Brain*, 120(2), 339-377. <http://doi.org/10.1093/brain/120.2.339>
- Duncan, J. S., Winston, G. P., Koepp, M. J., Ourselin, S. (2016). Brain imaging in the assessment for epilepsy surgery. *The Lancet Neurology*, 15(4), 420-433. [http://doi.org/10.1016/S1474-4422\(15\)00383-X](http://doi.org/10.1016/S1474-4422(15)00383-X)
- Dunn, O.J. (1964) Multiple Comparisons using Rank Sums. *Technometrics* 6, 241-252.
- Duvernoy, H.M. (2005) Chapter 3: Brain Anatomy. In: Kuzniecky, R.I., Jackson, G.D. (2005) *Magnetic resonance in epilepsy: neuroimaging techniques*. Second Edition. Elsevier Academic Press. Burlington, California, London.
- Duvernoy, H.M., Cattin, F., Risold, P.-Y. (2013). *The Human Hippocampus. Functional anatomy, vascularization and serial sections with MRI*. Fourth Edition. Springer Berlin. DOI 10.1007/978-3-642-33603-4
- Duvernoy, H. (1998) *The human hippocampus. Functional anatomy, vascularization and serial sections with MRI*. Springer, Berlin Heidelberg.
- Dym, R.J., Burns, J., Freeman, K., Lipton, M.L. (2011) Is functional MR imaging assessment of hemispheric language dominance as good as the Wada test?: a meta-analysis. *Radiology*, 261 (2011), 446–455.

References

- Elger, C.E., Helmstaedter, C., Kurthen, M. (2004). Chronic epilepsy and cognition. *Lancet Neurology*, 3(11), 663-672. [http://doi.org/10.1016/S1474-4422\(04\)00906-8](http://doi.org/10.1016/S1474-4422(04)00906-8)
- Elkommos, S., Weber, B., Niehusmann, P., Volmering, E., Richardson, M.P., Goh, Y.Y. et al. (2016). Hippocampal internal architecture and postoperative seizure outcome in temporal lobe epilepsy due to hippocampal sclerosis. *Seizure*, 35, 65-71. <http://doi.org/10.1016/j.seizure.2016.01.007>
- Ellingson R.J., Wilken K., Bennett D.R. (1984) Efficacy of sleep deprivation as an activation procedure in epilepsy patients. *Journal of Clinical Neurophysiology*, vol. 1, no. 1, 1984, 83–101.
- Elster, A.D. (2017) IR: Introduction - What is the inversion recovery pulse sequence? Available at: <http://www.mri-q.com/what-is-ir.html> (accessed: 14/06/2017)
- Engel, J.Jr., Van Ness, P.C., Rasmussen, T.B., Ojemann, L.M. (1993) Outcome with respect to epileptic seizures. In: Engel, J. Jr., ed. (1993) *Surgical treatment of the epilepsies*. 2nd ed. New York, NY: Raven Press; 1993: 609–621.
- Englot, D.J., Chang, E.F., Auguste, K.I. (2011) Vagus nerve stimulation for epilepsy: a meta-analysis of efficacy and predictors of response; a review. *Journal of Neurosurgery* 2011; 115(6): 1248-1255.
- Epelbaum, S., Pinel, P., Gaillard, R., Delmaire, C., Perrin, M., Dupont, S. et al. (2008). Special issue: Original article: Pure alexia as a disconnection syndrome: New diffusion imaging evidence for an old concept. *Cortex*, 44 (Special Issue on "Brain Hodology - Revisiting disconnection approaches to disorders of cognitive function"), 962-974. doi:10.1016/j.cortex.2008.05.003
- Eriksson, P.S., Perfilieva, E., Björk-Eriksson, T., Alborn, A.M., Nordborg, C., Peterson, D.A. et al. (1998) Neurogenesis in the adult human hippocampus. *Nat Med* 4:1313–1317.
- Eriksson, S.H., Rugg-Gunn, F.J., Symms, M.R., Barker, G.J., Duncan, J.S. (2001) Diffusion tensor imaging in patients with epilepsy and malformations of cortical development. *Brain* 2001;124:617–26.
- Falconer, M.A. (1974) Mesial temporal (Ammon's horn) sclerosis as a common cause of epilepsy. Aetiology, treatment, and prevention, *Lancet* 2:767–770, 1974.
- Farokhian, F., Beheshti, I., Sone, D., Matsuda, H. (2017). Comparing CAT12 and VBM8 for Detecting Brain Morphological Abnormalities in Temporal Lobe Epilepsy. *Frontiers in Neurology* (8), 428. <http://doi.org/10.3389/fneur.2017.00428>
- Farrall, A. (2015) MRI Basics: T1, T2. Available at: <http://www.pebblepad.co.uk/personal/viewasset.aspx?oid=157902&type=webfolio&parentpageoid=173933&pageoid=177360y> (accessed 10/09/2017)
- Farrell, J.A.D., Landman, B.A., Jones, C.K., Smith, S.A., Prince, J.L., van Zijl, P.C.M. et al. (2007). Effects of signal- to- noise ratio on the accuracy and reproducibility of diffusion tensor imaging–derived fractional anisotropy, mean diffusivity, and principal eigenvector measurements at 1.5 T. *Journal of Magnetic Resonance Imaging* 26 (3), 756-767.

References

- Fauser, S., Becker, A., Schulze-Bonhage, A., Hildebrandt, M., Tuxhorn, I., Pannek, H.W. et al. (2004) CD34-immunoreactive balloon cells in cortical malformations. *Acta Neuropathol (Berl)*. 2004; 108:272–278.
- Fauser, S., Schulze-Bonhage, A. (2006) Epileptogenicity of cortical dysplasia in temporal lobe dual pathology: an electrophysiological study with invasive recordings. *Brain*. 2006; 129:82–95.
- Fauser, S., Sisodiya, S.M., Martinian, L., Thom, M., Gumbinger, C., Huppertz, H.-J. et al. (2009) Multi-focal occurrence of cortical dysplasia in epilepsy patients. *Brain* 2009; 132 (8): 2079-2090. doi: 10.1093/brain/awp145
- Fazio, L., Logroscino, G., Taurisano, P., Amico, G., Quarto, T., Antonucci, L.A., et al. (2016) Prefrontal Activity and Connectivity with the Basal Ganglia during Performance of Complex Cognitive Tasks Is Associated with Apathy in Healthy Subjects. *PLoS One*. 2016 Oct 31;11(10):e0165301. doi: 10.1371/journal.pone.0165301. ECollection 2016.
- Fernández, V., Llinares-Benadero, C., Borrell, V. (2016) Cerebral cortex expansion and folding: what have we learned? *EMBO J* 35:1021–1044, doi:10.15252/embj.201593701, pmid:27056680.
- Ffytche, D.H., Catani, M. (2005) Beyond localization: from hodology to function. *Philosophical Transactions of the Royal Society of London B Biological Sciences*, 360: 767–779, 2005.
- Fischer, D.B., Perez, D.L., Prasad, S., Rigolo, L., O'Donnell, L., Acar, D. et al. (2016). Right inferior longitudinal fasciculus lesions disrupt visual-emotional integration. *Social Cognitive and Affective Neuroscience*, 11(6), 945-951. <http://doi.org/10.1093/scan/nsw011>
- Fischl, B. (2012) FreeSurfer. *Neuroimage*. 2012 Aug 15;62(2):774-81.
- Fischl, B., Salat, D.H., Busa, E., Albert, M., Dieterich, M., Haselgrove, C., et al. (2002) Whole brain segmentation: automated labeling of neuroanatomical structures in the human brain. *Neuron*. 2002 Jan 31;33(3):341-55.
- Focke, N.K., Yogarajah, M., Bonelli, S.B., Bartlett, P.A., Symms, M.R., Duncan, J.S. (2008a). Voxel-based diffusion tensor imaging in patients with mesial temporal lobe epilepsy and hippocampal sclerosis. *NeuroImage*, 40(2), 728-737. <http://doi.org/10.1016/j.neuroimage.2007.12.031>
- Focke, N.K., Symms, M.R., Burdett, J.L., Duncan, J.S. (2008b). Voxel-based analysis of whole brain FLAIR at 3T detects focal cortical dysplasia. *Epilepsia*, 49(5), 786-793. <http://doi.org/10.1111/j.1528-1167.2007.01474.x>
- Focke, N. K., Bonelli, S. B., Yogarajah, M., Scott, C., Symms, M. R., Duncan, J. S. (2009). Automated normalized FLAIR imaging in MRI-negative patients with refractory focal epilepsy. *Epilepsia*, 50(6), 1484–1490. <http://doi.org/10.1111/j.1528-1167.2009.02022.x>
- Fogassi, L., Luppino, G. (2005). Motor functions of the parietal lobe. *Current Opinion in Neurobiology*, 15:626-631.
- Fonseca, V. de C., Yasuda, C.L., Tedeschi, G.G., Betting, L.E., Cendes, F. (2012). White Matter Abnormalities in Patients with Focal Cortical Dysplasia Revealed by Diffusion

References

- Tensor Imaging Analysis in a Voxelwise Approach. *Frontiers in Neurology*, 3, 121. <http://doi.org/10.3389/fneur.2012.00121>
- Friedman, E. (2014). Epilepsy imaging in adults: getting it right. *AJR. American Journal of Roentgenology*, 203(5), 1093–1103. <http://doi.org/10.2214/AJR.13.12035>
- Friedman, J.H., Chou, K.L. (2007). Mood, Emotion, and Thought. *Textbook of Clinical Neurology* (Third Edition). Elsevier Inc. <http://doi.org/10.1016/B978-141603618-0.10003-7>
- Fuerst, D., Shah, J., Kupsky, W.J., Johnson, R., Shah, A., Hayman–Abello, B. et al. (2001) Volumetric MRI, pathological, and neuropsychological progression in hippocampal sclerosis. *Neurology*. 2001 Jul 24;57(2):184-188.
- Furby, J., Hayton, T., Altmann, D., Brenner, R., Chataway, J., Smith, K. J. et al. (2010). A longitudinal study of MRI-detected atrophy in secondary progressive multiple sclerosis. *Journal of Neurology*, 257(9), 1508-1516. <http://doi.org/10.1007/s00415-010-5563-y>
- Fuster, J.M. (2002) Frontal lobe and cognitive development. *Journal of Neurocytology* 31, 373–385.
- Gaesser, B., Spreng, R.N., McLelland, V.C., Addis, D.R., Schacter, D.L. (2013) Imagining the future: Evidence for a hippocampal contribution to constructive processing. *Hippocampus*. 2013; 23:1150–1161.
- Gaillard, F. (2011) From the Case: Band Heterotopia (x-linked). Available at: <https://radiopaedia.org/images/1480237> (accessed: 24/08/2017)
- Gaitatzis, A., Trimble, M.R., Sander, J.W. (2004) The psychiatric comorbidity of epilepsy. *Acta Neurologica Scandinavica*. 2004;110(4):207–20. doi: 10.1111/j.1600-0404.2004.00324.x .
- Galazzo, I.B., Storti, S.F., Del Felice, A., Pizzini, F.B., Arcaro, C., Formaggio, E. et al. (2015). Patient-specific detection of cerebral blood flow alterations as assessed by arterial spin labeling in drug-resistant epileptic patients. *PLoS ONE*, 10(5), 1–24. <http://doi.org/10.1371/journal.pone.0123975>
- Garcia-Fiñana, M., Denby, C.E., Keller, S.S., Wieshmann, U.C., Roberts, N. (2006) Degree of hippocampal atrophy is related to side of seizure onset in temporal lobe epilepsy. *American Journal of Neuroradiology*. 2006 May;27(5):1046-52.
- Geva, T. (2006). Magnetic Resonance Imaging: Historical Perspective. *Journal of Cardiovascular Magnetic Resonance*, 8(4), 573–580. <http://doi.org/10.1080/10976640600755302>
- Giedd, J.N., Raznahan, A., Alexander-Bloch, A., Schmitt, E., Gogtay, N., Rapoport, J.L. et al. (2015) Child psychiatry branch of the National Institute of Mental Health longitudinal structural magnetic resonance imaging study of human brain development. *Neuropsychopharmacology* 40, 43–49.
- Gilliam, F., Hecimovic, H., Sheline, Y. (2003). Psychiatric comorbidity, health, and function in epilepsy. *Epilepsy and Behavior*. 4 Suppl 4, S26–30. <http://doi.org/10.1016/j.yebeh.2003.10.003>
- Giorgi, F. S., Guida, M., Caciagli, L., Maestri, M., Carnicelli, L., Bonanni, E., Bonuccelli, U.

References

- (2014). What is the role for EEG after sleep deprivation in the diagnosis of epilepsy? Issues, controversies, and future directions. *Neuroscience and Biobehavioral Reviews*, 47, 533–548. <http://doi.org/10.1016/j.neubiorev.2014.10.005>
- Giorgio, A., De Stefano, N. (2013) Clinical use of brain volumetry. *Journal of Magnetic Resonance Imaging*, 37: 1–14. doi: 10.1002/jmri.23671
- Giovagnoli, A.R. (2001) Relation of sorting impairment to hippocampal damage in temporal lobe epilepsy. *Neuropsychology*, 2001, 39, 140-150.
- Giulioni, M., Marucci, G., Martinoni, M., Volpi, L., Riguzzi, P., Marliani, A.F. et al. (2013) Seizure outcome in surgically treated drug-resistant mesial temporal lobe epilepsy based on the recent histopathological classifications. *Journal of Neurosurgery*. 2013 Jul;119(1):37-47.
- Glasser, M.F., Van Essen, D.C. (2011). Mapping human cortical areas in vivo based on myelin content as revealed by T1- and T2-weighted MRI. *The Journal of Neuroscience: The Official Journal of the Society for Neuroscience*, 31(32), 11597-11616. <http://doi.org/10.1523/JNEUROSCI.2180-11.2011>
- Gleissner, U., Helmstaedter, C., Schramm, J., Elger, C.E. (2004) Memory outcome after selective amygdalohippocampectomy in patients with temporal lobe epilepsy: one-year follow-up. *Epilepsia*. 2004;45:960–962.
- Glenn, G.R., Jensen, J.H., Helpert, J.A., Spampinato, M.V., Kuzniecky, R., Keller, S.S. et al. (2016). Epilepsy-related cytoarchitectonic abnormalities along white matter pathways. *Journal of Neurology, Neurosurgery & Psychiatry*. 87(9):930-936. <http://doi.org/10.1136/jnnp-2015-312980>
- Goh, Y.Y., Schoene-Bake, J.C., Marson, A.G., Richardson, M.P., Weber, B., Keller, S.S. (2014) Hippocampal volume and postsurgical outcome in intractable temporal lobe epilepsy. *Epilepsy Currents* 2014;14:232-233.
- Golby, A., Poldrack, R., Brewer, J., Spencer, D., Desmond, J., Aron, A. et al. (2001) Material-specific lateralization in the medial temporal lobe and prefrontal cortex during memory encoding. *Brain*, 124, 1841-1854. <https://doi.org/10.1093/brain/124.9.1841>
- Gold, G.E., Han, E., Stainsby, J., Wright, G., Brittain, J., Beaulieu, C. (2004) Musculoskeletal MRI at 3.0 T: relaxation times and image contrast. *AJR Am J Roentgenol* 2004;183(2):343–351.
- Goldberg, E.M., Coulter, D.A. (2013). Mechanisms of epileptogenesis: a convergence on neural circuit dysfunction. *Nature Reviews Neuroscience* 14(5)337-349.
- Govindan, R.M., Makki, M.I., Sundaram, S.K., Juhasz, C., Chugani, H.T. (2008) Diffusion tensor analysis of temporal and extra-temporal lobe tracts in temporal lobe epilepsy. *Epilepsy Research* 80:30–41.
- Gross, D.W. (2011). Diffusion tensor imaging in temporal lobe epilepsy. *Epilepsia*, 52 Suppl 4, 32–34. <http://doi.org/10.1111/j.1528-1167.2011.03149.x>
- Gross, D.W., Bastos, A., Beaulieu, C. (2005) Diffusion tensor imaging abnormalities in focal cortical dysplasia. *The Canadian journal of neurological sciences*. 32, 477-482.
- Grossi, D., Soricelli, A., Ponari, M., Salvatore, E., Quarantelli, M., Prinster, A. et al. (2014)

References

- Structural connectivity in a single case of progressive prosopagnosia: The role of the right inferior longitudinal fasciculus. *Cortex*, 56, 111-120. <http://doi.org/10.1016/j.cortex.2012.09.010>
- Guerrini, R., Marini, C. (2006) Genetic malformations of cortical development. *Experimental Brain Research*, 173(2), 322-333.
- Guye, M., Ranjeva, J.P., Bartolomei, F., Confort-Gouny, S., McGonigal, A., Régis J. et al. (2007). What is the significance of interictal water diffusion changes in frontal lobe epilepsies? *NeuroImage*, 35(1), 28-37. <http://doi.org/10.1016/j.neuroimage.2006.11.049>
- Hagler, D.J., Ahmadi, M.E., Kuperman, J., Holland, D., McDonald, C.R., Halgren, E. et al. (2009). Automated white-matter tractography using a probabilistic diffusion tensor atlas: Application to temporal lobe epilepsy. *Human Brain Mapping*, 30(5), 1535-1547. <http://doi.org/10.1002/hbm.20619>
- Haller, S., Kövari, E., Herrmann, F.R., Cuvinciuc, V., Tömm, A.-M., Zulian, G.B., et al. (2013). Do brain T2/FLAIR white matter hyperintensities correspond to myelin loss in normal aging? A radiologic-neuropathologic correlation study. *Acta Neuropathologica Communications*, 1, 14. <http://doi.org/10.1186/2051-5960-1-14>
- Hammers, A., Heckemann, R., Koepp, M. J., Duncan, J. S., Hajnal, J. V., Rueckert, D., & Aljabar, P. (2007). Automatic detection and quantification of hippocampal atrophy on MRI in temporal lobe epilepsy: A proof-of-principle study. *NeuroImage*, 36(1), 38-47. <http://doi.org/10.1016/j.neuroimage.2007.02.031>
- Harlow, J.M. (1868) Recovery after severe injury to the head. *Publication of the Massachusetts Medical Society*, 2, 327-346.
- Hashemi, R.H., Bradley, W.G. Jr., Chen, D.Y., Jordan, J.E., Queralt, J.A., Cheng, A.E. et al. (1995) Suspected multiple sclerosis: MR imaging with a thin-section fast FLAIR pulse sequence. *Radiology* 195; 196:505-510.
- Helmstaedter, C., Elger, C.E. (1996) Cognitive consequences of two-thirds anterior temporal lobectomy on verbal memory in 144 patients: a three-month follow-up study. *Epilepsia*, 37(2), 1996, 171-180.
- Helmstaedter, C., Grunwald, T., Lehnertz, K., Gleibner, U., Elger, C. (1997). Differential involvement of left temporolateral and temporomesial structures in verbal declarative learning and memory: evidence from temporal lobe epilepsy. *Brain Cog.*, 35, 110-131.
- Hermann, B.P., Wyler, A.R., Somes, G., Berry, A.D., Dohan, F.C. (1992). Pathological status of the mesial temporal lobe predicts memory outcome from left anterior temporal lobectomy. *Neurosurgery*, 31(4), 652-657.
- Hescham, S., Temel, Y., Schipper, S., Lagiere, M., Schönfeld, L., Jahanshahi, A. et al. (2017). Fornix deep brain stimulation induced long-term spatial memory independent of hippocampal neurogenesis. *Brain Structure And Function*, 222(2), 1069-1075. [doi:10.1007/s00429-016-1188-y](https://doi.org/10.1007/s00429-016-1188-y)
- Hittmair, K., Mallek, R., Prayer, D., Schindler, E.G., Kollegger, H. (1996) Spinal cord lesions in patients with multiple sclerosis: comparison of MR pulse sequences. *American Journal of Neuroradiology* 1996; 17:1555-1565.

References

- Holmes, M.D., Born, D.E., Kutsy, R.L., Wilensky, A.J., Ojemann, G.A., Ojemann L.M. (2000) Outcome after surgery in patients with refractory temporal lobe epilepsy and normal MRI. *Seizure*. 2000;9(6):407-411.
- Hong, S., Bernhardt, B.C., Caldairou, B., Hall, J.A., Guiot, M.C., Schrader, D. et al. (2017). Multimodal MRI profiling of focal cortical dysplasia type II, 1-10. <http://doi.org/10.1212/WNL.0000000000003632>
- Hong, S.J., Kim, H., Schrader, D., Bernasconi, N., Bernhardt, B.C., Bernasconi, A. (2014) Automated detection of cortical dysplasia type II in MRI-negative epilepsy. *Neurology*. 2014; 83(1):48–55.
- House, P.M., Lanz, M., Holst, B., Martens, T., Stodieck, S., Huppertz, H.-J. (2013). Comparison of morphometric analysis based on T1- and T2-weighted MRI data for visualization of focal cortical dysplasia. *Epilepsy Research*, 106(3), 403–409. <http://doi.org/10.1016/j.eplepsyres.2013.06.016>
- Houston, S.M., Herting, M.M., Sowell, E.R. (2014). The Neurobiology of Childhood Structural Brain Development: Conception Through Adulthood. *Current Topics in Behavioral Neurosciences*, 16, 3–17. http://doi.org/10.1007/7854_2013_265
- Howe, K.L., Dimitri, D., Heyn, C., Kiehl, T.R., Mikulis, D. and Valiante, T.A. (2010). Histologically confirmed hippocampal structural features revealed by 3T MR imaging: potential to increase diagnostic specificity of mesial temporal sclerosis. *American Journal of Neuroradiology*, 2010, 31(9), 1682–1689.
- Huang, Y., Coupland, N.J., Lebel, R.M., Carter, R., Seres, P., Wilman, A.H. et al. (2013) Structural Changes in Hippocampal Subfields in Major Depressive Disorder: A High-Field Magnetic Resonance Imaging Study. *Biological psychiatry*. 74(1).
- Human Anatomy Wiki (2017) Brain Lobes Anatomy and Function. Available at: <https://humananatomywiki.com/brain-lobes-anatomy-and-function/brain-lobes-anatomy-and-function-learn-the-four-lobes-of-the-brain-youtube/> (accessed 24/08/2017).
- Huppertz H.-J., Grimm C., Fauser S., Kassubek J., Mader I., Hochmuth A., et al. (2005). Enhanced visualization of blurred gray-white matter junctions in focal cortical dysplasia by voxel-based 3D MRI analysis. *Epilepsy Research*, 67(1-2), 35–50. <http://doi.org/10.1016/j.eplepsyres.2005.07.009>
- Huppertz, H. J., Kassubek, J., Altenmuller, D. M., Breyer, T., Fauser, S. (2008) Automatic curvilinear reformatting of three-dimensional MRI data of the cerebral cortex. *Neuroimage* 39, 80–86.
- Huppertz, H.-J. (2013). Morphometric MRI Analysis. In *MRI in Epilepsy, Medical Radiology. Diagnostic Imaging* (pp. 73–84). http://doi.org/10.1007/174_2012_564
- Huttenlocher, P.R. (1990) Morphometric study of human cerebral cortex development. *Neuropsychologia* 28, 517–527.
- Hutton, C., Draganski, B., Ashburner, J., Weiskopf, N. (2009). A comparison between voxel-based cortical thickness and voxel-based morphometry in normal aging. *Neuroimage*, 48(2-8), 371–380. <http://doi.org/10.1016/j.neuroimage.2009.06.043>

References

- Iglesias, J.E., Augustinack, J.C., Nguyen, K., Player, C.M., Player, A., Wright, M. et al. (2015) A computational atlas of the hippocampal formation using ex vivo, ultra-high resolution MRI: Application to adaptive segmentation of in vivo MRI. *Neuroimage*. 2015 Jul 15;115:117-37.
- ILAE: Commission on Classification and Terminology of the International League Against Epilepsy (1981) Proposal for revised clinical and electroencephalographic classification of epileptic seizures. From the Commission on Classification and Terminology of the International League Against Epilepsy.". *Epilepsia*. 22 (4): 489–501. doi:10.1111/j.1528-1157.1981.tb06159.x.
- ILAE: Commission on Classification and Terminology of the International League Against Epilepsy (1989) Proposal for revised classification of epilepsies and epileptic syndromes. *Epilepsia* 30, 389–399.
- ILAE: Commission on Neuroimaging of the International League Against Epilepsy (1997) Recommendations for neuroimaging of patients with epilepsy. *Epilepsia*. 1997 Nov. 38(11):1255-1256.
- Imamura, H., Matsumoto, R., Takaya, S., Nakagawa, T., Shimotake, A., Kikuchi, T. et al. (2015). Network specific change in white matter integrity in mesial temporal lobe epilepsy. *Epilepsy Research*, 120, 65-72 <http://doi.org/10.1016/J.EPLEPSYRES.2015.12.003>
- Immonen, A. (2010) Surgical treatment of refractory temporal lobe epilepsy: Preoperative evaluation and seizure outcome. Publications of the University of Eastern Finland. Dissertations in Health Sciences 7. 2010.
- Inoue, T., Ogasawara, K., Beppu, T., Ogawa, A., Kabasawa, H. (2005). Diffusion tensor imaging for preoperative evaluation of tumor grade in gliomas. *Clinical Neurology and Neurosurgery*, 107(3), 174-180. <http://doi.org/10.1016/j.clineuro.2004.06.011>
- Insausti, R., Amaral, D.G. (2012). Chapter 24 - Hippocampal Formation. In: *The Human Nervous System* (896-942). <http://doi.org/10.1016/B978-0-12-374236-0.10024-0>
- Insausti, R., Annese, J., Amaral, D.G., Squire, L.R. (2013). Human amnesia and the medial temporal lobe illuminated by neuropsychological and neurohistological findings for patient E.P. *Proceedings of the National Academy of Sciences*, 110(21), E1953-62. <http://doi.org/10.1073/pnas.1306244110>
- Jack, C.R. Jr. (1994). MRI-based hippocampal volume measurements in epilepsy. *Epilepsia*, 35 Suppl 6, S21-29. <http://doi.org/10.1111/j.1528-1157.1994.tb05986.x>
- Jack, C.R. Jr., Sharbrough, F.W., Cascino, G.D., Hirschorn, K.A., O'Brien, P.C., Marsh, W.R. (1992) Magnetic resonance image-based hippocampal volumetry: correlation with outcome after temporal lobectomy. *Annals of Neurology* 1992 Feb;31(2):138-146.
- Jackson, G.D., Berkovic, S.F., Tress, B.M., Kalnins, R.M., Fabinyi, G.C., Bladin, P.F. (1990) Hippocampal sclerosis can be reliably detected by magnetic resonance imaging. *Neurology*. 1990 Dec;40(12):1869-75. doi:10.1212/WNL.40.12.1869: 1526-632X
- Jackson, G.D., Kuzniecky, R.I., Cascino, G.D. (1994) Hippocampal sclerosis without detectable hippocampal atrophy. *Neurology* 1994;44:42–46.

References

- Jackson, G.D., Briellmann, R. S., Kuzniecky, R.I. (2005) Chapter 4: Temporal Lobe Epilepsy. In: Kuzniecky, R.I. And Jackson, G.D. (2005) Magnetic Resonance in Epilepsy (Second Edition) Neuroimaging Techniques 2005, Elsevier Academic Press Amsterdam. 99–176.
- Jacoby, A., Snape, D., Lane, S., Baker, G. A. (2015). Self-reported anxiety and sleep problems in people with epilepsy and their association with quality of life. *Epilepsy & Behavior*, 43, 149–158. <http://doi.org/10.1016/j.yebeh.2014.09.071>
- Jain, R.S., Sisodiya, M.S., Kookna, J.C., Bhana, I., Verma, Y.K. (2016) Deterioration of Pre-Existing Hemiparesis Following an Ipsilateral Corona Radiata Infarct: A Rare Entity. *Austin Journal of Cerebrovascular Disease & Stroke*. 2016; 3(1):1041.
- James, J.S., Radhakrishnan, A., Thomas, B., Madhusoodanan, M., Kesavadas, C., Abraham et al. (2015) Diffusion tensor imaging tractography of Meyer’s loop in planning resective surgery for drug-resistant temporal lobe epilepsy. *Epilepsy Res* 110:95–104.
- Janzsky, J., Janzsky, I., Schulz, R., Hoppe, M., Behne, F., Pannek, H.W. et al. (2005) Temporal lobe epilepsy with hippocampal sclerosis: predictors for long-term surgical outcome. *Brain*. 2005 Feb;128(Pt 2):395-404.
- Janzsky, J., Jokeit, H., Schulz, R., Hoppe, M., Ebner, A. (2000) EEG predicts surgical outcome in lesional frontal lobe epilepsy. *Neurology* 2000;54:1470-1476.
- Janzsky, J., Woermann, F.G., Barsi, P., Schulz, R., Halasz, P. et al. (2003) Right hippocampal sclerosis is more common than left after febrile seizures. *Neurology* 60: 1209-1210.
- Jehi, L.E., Najm, I., Bingaman, W., Dinner, D., Widdess-Walsh, P., Lüders, H. (2007) Surgical outcome and prognostic factors of frontal lobe epilepsy surgery. *Brain* 130:574–584.
- Jellison, B.J., Field, A.S., Medow, J., Lazar, M., Salamat, M.S., Alexander, A.L. (2004). Diffusion tensor imaging of cerebral white matter: a pictorial review of physics, fiber tract anatomy, and tumor imaging patterns. *AJNR. American Journal of Neuroradiology*, 25(3), 356–369.
- Johnson, G.D., Kuzniecky, R.I., Pell, G.S. (2005) Principles of Magnetic Resonance Imaging. Chapter 2. In: Magnetic Resonance in Epilepsy: Neuroimaging Techniques. Second Edition.
- Johnson, R.T., Yeatman, J.D., Wandell, B.A., Buonocore, M.H., Amaral, D.G., Nordahl, C.W. (2013) Diffusion properties of major white matter tracts in young, typically developing children. *Neuroimage*. 2013;88C:143-154.
- Kabat, J., Król, P. (2012) Focal cortical dysplasia - review. *Polish Journal of Radiology* 2012;77:35-43.
- Kaneda, T., Shigemune, Y., Tsukiura, T. (2017). Lateral and medial prefrontal contributions to emotion generation by semantic elaboration during episodic encoding. *Cognitive, Affective & Behavioral Neuroscience*, 17(1), 143-157. doi:10.3758/s13415-016-0468-6
- Kanner, A. M. (2009). Psychiatric issues in epilepsy: The complex relation of mood, anxiety

References

- disorders, and epilepsy. *Epilepsy and Behavior*, 15(1), 83–87. <http://doi.org/10.1016/j.yebeh.2009.02.034>
- Kamiya, K., Amemiya, S., Suzuki, Y., Kunii, N., Kawai, K., Mori H. et al. (2016) Machine Learning of DTI Structural Brain Connectomes for Lateralization of Temporal Lobe Epilepsy. *Magnetic Resonance in Medical Sciences*. 2016;15(1):121-9. doi:10.2463/mrms.2015-0027.
- Kassubek, J., Huppertz, H.-J., Spreer, J., Schulze-Bonhage, A. (2002). Detection and localization of focal cortical dysplasia by voxel-based 3-D MRI analysis. *Epilepsia*, 43(6), 596–602. <http://doi.org/10.1046/j.1528-1157.2002.41401.x>
- Keller, S.S., Schoene-Bake, J.C., Gerdes JS, Weber B, Deppe M. (2012) Concomitant fractional anisotropy and volumetric abnormalities in temporal lobe epilepsy: cross-sectional evidence for progressive neurologic injury. *PLoS One*. 2012;7(10):e46791.
- Keller, S.S., Roberts, N. (2008). Voxel-based morphometry of temporal lobe epilepsy: an introduction and review of the literature. *Epilepsia*, 49(5), 741–57. <http://doi.org/10.1111/j.1528-1167.2007.01485.x>
- Keller, S.S., Ahrens T., Mohammadi S., Gerdes J.S., Möddel G., Kellinghaus C. et al. (2013). Voxel-based statistical analysis of fractional anisotropy and mean diffusivity in patients with unilateral temporal lobe epilepsy of unknown cause. *Journal of Neuroimaging*, 23(3), 352–359. doi:10.1111/j.1552-6569.2011.00673.
- Keller, S.S., Glenn, G.R., Weber, B., Kreilkamp, B.A.K., Jensen, J.H., Helpert, J.A. et al. (2017). Preoperative automated fibre quantification predicts postoperative seizure outcome in temporal lobe epilepsy. *Brain*, Volume 140, Issue 1, 1 January 2017, 68–82, doi:<http://dx.doi.org/10.1093/brain/aww280>
- Keller, S.S., Richardson, M. P., Schoene-Bake, J.-C., O'Muircheartaigh, J., Elkommos, S., Kreilkamp, B. et al. (2015a) Thalamotemporal alteration and postoperative seizures in temporal lobe epilepsy. *Annals of neurology*. 77, 5, 760-774.
- Keller, S.S., Richardson, M.P., O'Muircheartaigh, J., Schoene-Bake, J.-C., Elger, C., Weber, B. (2015b). Morphometric MRI alterations and postoperative seizure control in refractory temporal lobe epilepsy. *Human Brain Mapping* 36(5):1637-1647. doi: 10.1002/hbm.22722.
- Keller, S.S., Mackay, C.E., Barrick, T.R., Wieshmann, U.C., Howard, M.A., Roberts, N. (2002a) Voxel-based morphometric comparison of hippocampal and extrahippocampal abnormalities in patients with left and right hippocampal atrophy. *Neuroimage* 2002;16:23–31.
- Keller, S.S., Wieshmann, U.C., Mackay, C.E., Denby, C.E., Webb, J., Roberts, N. (2002b). Voxel based morphometry of grey matter abnormalities in patients with medically intractable temporal lobe epilepsy: effects of side of seizure onset and epilepsy duration, *Journal of Neurology, Neurosurgery and Psychiatry*. 2002; 73(6):648-655.
- Kemmotsu, N., Girard, H. M., Bernhardt, B. C., Bonilha, L., Lin, J. J., Tecoma, E. S. et al. (2011). MRI analysis in temporal lobe epilepsy: cortical thinning and white matter disruptions are related to side of seizure onset. *Epilepsia*, 52(12), 2257-2266. <http://doi.org/10.1111/j.1528-1167.2011.03278.x>

References

- Kemmotsu, N., Kucukboyaci, N. E., Leyden, K. M., Cheng, C. E., Girard, H. M., Iragui, V. J. et al. (2014). Frontolimbic brain networks predict depressive symptoms in temporal lobe epilepsy. *Epilepsy Research*, 108(9), 155-163. <http://doi.org/10.1016/j.eplepsyres.2014.08.018>
- Kensinger, E.A., Ullman, M.T., Corkin, S. (2001) Bilateral medial temporal lobe damage does not affect lexical or grammatical processing: evidence from amnesic patient H.M. *Hippocampus* 11:347–360.
- Kesner, R.P., Goodrich-Hunsaker, N.J. (2010). Developing an animal model of human amnesia: The role of the hippocampus. *Neuropsychologia*, 48(8), 2290-2302. <http://doi.org/10.1016/j.neuropsychologia.2009.10.027>
- Kerchner, G.A., Hess, C.P., Hammond-Rosenbluth, K.E., Xu, D., Rabinovici, G. D., Kelley, D.A.C. et al. (2010). Hippocampal CA1 apical neuropil atrophy in mild Alzheimer disease visualized with 7-T MRI. *Neurology*, 75(15), 1381-1387. <http://doi.org/10.1212/WNL.0b013e3181f736a1>
- Khan, A.R., Goubran, M., de Ribaupierre, S., Hammond, R.R., Burneo, J.G., Parrent, A.G. et al. (2014). Quantitative relaxometry and diffusion MRI for lateralization in MTS and non-MTS temporal lobe epilepsy. *Epilepsy Research*, 108(3), 506-516. <http://doi.org/10.1016/j.eplepsyres.2013.12.012>
- Kiernan, J.A. (2012). Anatomy of the Temporal Lobe. *Epilepsy Research and Treatment*, 2012(3), 1-12. <http://doi.org/10.1155/2012/176157>
- Kim, D.W., Lee, S.K., Nam, H., Chu, K., Chung, C.K., Lee, S.-Y. et al. (2010), Epilepsy with dual pathology: Surgical treatment of cortical dysplasia accompanied by hippocampal sclerosis. *Epilepsia*, 51: 1429–1435. doi:10.1111/j.1528-1167.2009.02403.x
- Kim, D.W., Lee, S.K., Chung, C.K., Koh, Y.C., Choe, G., Lim, S.D. (2012) Clinical features and pathological characteristics of amygdala enlargement in mesial temporal lobe epilepsy. *Journal of Clinical Neuroscience*. 2012, 19 (4): 509-512. 10.1016/j.jocn.2011.05.042.
- Kim, J.Bin, Suh, S.il., Kim, J.H. (2015). Volumetric and shape analysis of hippocampal subfields in unilateral mesial temporal lobe epilepsy with hippocampal atrophy. *Epilepsy Research*, 117, 74–81. <http://doi.org/10.1016/j.eplepsyres.2015.09.004>
- Kim, J.S., Koo, D.L., Joo, E.Y., Kim, S.T., Seo, D.W., Hong, S.B. (2016). Asymmetric gray matter volume changes associated with epilepsy duration and seizure frequency in temporal-lobe-epilepsy patients with favorable surgical outcome. *Journal of Clinical Neurology (Korea)*, 12(3), 323-331. <http://doi.org/10.3988/jcn.2016.12.3.323>
- Kipps, C.M., Davies, R.R., Mitchell, J., Krilc, J.J., Hallidayd, G.M., Hodgesa, J.R. (2007) Clinical significance of lobar atrophy in frontotemporal dementia: application of an MRI visual rating scale. *Dementia and Geriatric Cognitive Disorders* 2007;23(5):334-342.
- Klöppel, S., Büchel, C. (2005) Alternatives to the Wada test: a critical view of functional magnetic resonance imaging in preoperative use *Current Opinion in Neurology*, 18 (2005), 418–423.
- Kojovic, M., Cordivari, C., Bhatia, K. (2011). Myoclonic disorders : a practical approach for diagnosis and treatment, 47–62. <http://doi.org/10.1177/1756285610395653>

References

- Kral, T., Clusmann, H., Urbach, J., Schramm, J., Elger, C.E., Kurthen, M. et al. (2002) Preoperative evaluation for epilepsy surgery (Bonn Algorithm). *Zentralblatt Für Neurochirurgie*, 63(3), 106–10. <http://doi.org/10.1055/s-2002-35826>
- Krebs, C., Bodnar, T., Holman, P., Weinberg, J. (2014) Hypothalamus and Limbic System - UBC Neuroanatomy - Season 1 - Ep 4. <https://www.youtube.com/watch?v=ErpxEwIWww4> . 6:01 mins.
- Kreilkamp, B.A.K., Weber, B., Richardson, M.P., Keller, S.S. (2017). Automated tractography in patients with temporal lobe epilepsy using TRActs Constrained by UnderLying Anatomy (TRACULA). *NeuroImage: Clinical*, 14, 67-76. <http://doi.org/10.1016/j.nicl.2017.01.003>
- Krishnan, S.S., Panigrahi, M., Jayalakshmi, S., Varma, D.R. (2011) Neuroplasticity in hemispheric syndrome: An interesting case report. *Neurology India*, 2011; 59:601-604. <http://www.neurologyindia.com/text.asp?2011/59/4/601/84346> (23/08/2017)
- Krsek, P., Pieper, T., Karlmeier, A., Hildebrandt, M., Kolodziejczyk, D., Winkler, P. et al. (2009) Different presurgical characteristics and seizure outcomes in children with focal cortical dysplasia type I or II. *Epilepsia* 2009; 50: 125-137.
- Kurth, F., Gaser, C., Luders, E.A. (2015a) A 12-step user guide for analyzing voxel-wise gray matter asymmetries in statistical parametric mapping (SPM). *Nature Protocols* 10, 293–304 (2015) doi:10.1038/nprot.2015.014
- Kurth, F., Luders, E., Gaser, C. (2015b) Voxel-Based Morphometry. *Brain Mapping: An Encyclopedic Reference*, (2015), vol. 1, 345-349.
- Kuzniecky, R.I., Jackson, G.D. (2005) MRI in Special Conditions Associated with Epilepsy. Chapter 6. In: *Magnetic Resonance in Epilepsy: Neuroimaging Techniques*. Second Edition.
- Kuzniecky, R.I. (2015). Epilepsy and malformations of cortical development: new developments. *Current Opinion In Neurology*, 28(2), 151-157. doi:10.1097/WCO.0000000000000175.
- Kuzniecky, R.I. (2002). Neuroimaging of Epilepsy. *Brain*, 22(3), 279-288. <http://doi.org/10.1055/s-2002-36647>
- Kwan, P., Brodie, M.J. (2000). Early Identification of Refractory Epilepsy. *New England Journal of Medicine*, 342(5), 314–319. <http://doi.org/10.1056/NEJM200002033420503> 2.
- Lamparello, P., Baybis, M., Pollard, J., Hol, E.M., Eisenstat, D.D., Aronica, E. et al. (2007) Developmental lineage of cell types in cortical dysplasia with balloon cells. *Brain* 2007; 130: 2267-2276.
- Le Bihan, D. (2014). Diffusion MRI: What water tells us about the brain. *EMBO Molecular Medicine*, 6(5), 569-573. <http://doi.org/10.1002/emmm.201404055>.
- Le Bihan, D., Poupon, C., Amadon, A., Lethimonnier, F. (2006). Artifacts and pitfalls in diffusion MRI. *Journal of Magnetic Resonance Imaging*, 24(3), 478-488. <http://doi.org/10.1002/jmri.20683>
- Le Duigou, C., Simonnet, J., Telenczuk, M., Fricker, D., Miles, R. (2014). Recurrent synapses and circuits in the CA3 region of the hippocampus: an associative network.

References

Frontiers In Cellular Neuroscience, 7, 7-13.

Lee, S.H., Coutu, J.P., Wilkens, P., Yendiki, A., Rosas, H.D., Salat, D.H., Alzheimer's disease Neuroimaging Initiative (ADNI). (2015a) Tract-based analysis of white matter degeneration in Alzheimer's disease. *Neuroscience*. 2015 Aug 20;301:79-89. doi: 10.1016/j.neuroscience.2015.05.049.

Lee, S. A., Kim, M. J., Lee, H. W., Heo, K., Shin, D. J., Song, H. K. et al. (2015b). The effect of recurrent seizures on cognitive, behavioral, and quality-of-life outcomes after 12 months of monotherapy in adults with newly diagnosed or previously untreated partial epilepsy. *Epilepsy and Behavior*, 53, 202–208. <http://doi.org/10.1016/j.yebeh.2015.10.020>

Lee, T.M., Yip, J.T., Jones-Gotman, M. (2002) Memory deficits after resection from left or right anterior temporal lobe in humans: a meta-analytic review. *Epilepsia*. 2002;43:283–291.

Lee, S. K., Kim, D. I., Mori, S., Kim, J., Kim, H. D., Heo, K. et al. (2004). Diffusion tensor MRI visualizes decreased subcortical fiber connectivity in focal cortical dysplasia. *NeuroImage*, 22(4), 1826-1829. <http://doi.org/10.1016/j.neuroimage.2004.04.028>

Lee, S.E., Han, Y., Park, H. (2016) Neural Activations of Guided Imagery and Music in Negative Emotional Processing: A Functional MRI Study. *Journal of Music Therapy*. 2016; 53(3):257-78. doi: 10.1093/jmt/thw007.

Leemans, A., Jones, D.K. (2009) The B-matrix must be rotated when correcting for subject motion in DTI data. *Magnetic Resonance in Medicine*. 61, 1336–1349.

Leergaard, T.B., Hilgetag, C.C., Sporns, O. (2012). Mapping the connectome: multi-level analysis of brain connectivity. *Frontiers in Neuroinformatics*, 6, 14. <http://doi.org/10.3389/fninf.2012.00014>

Lerner, J.T., Salamon, N., Hauptman, J., Velasco, T.R., Hemb, M., Wu, J.Y. et al. (2009) Assessment and surgical outcomes for mild type I and severe type II cortical dysplasia: A critical review and the UCLA experience. *Epilepsia*. 2009;50(6):1310-1336.

Lhatoo, S. D., Solomon, J.K., McEvoy, A.W., Kitchen, N.D., Shorvon, S.D., Sander, J.W. (2003). A prospective study of the requirement for and the provision of epilepsy surgery in the United Kingdom. *Epilepsia* 44(5): 673-676.

Libero, L.E., DeRamus, T.P., Lahti, A.C., Deshpande, G., Kana, R.K. (2015). Multimodal neuroimaging based classification of autism spectrum disorder using anatomical, neurochemical, and white matter correlates. *Cortex; a Journal Devoted to the Study of the Nervous System and Behavior*, 66, 46–59. <http://doi.org/10.1016/j.cortex.2015.02.008>

Lim, C., Blume, H.W., Madsen, J.R., Saper, C.B. (1997) Connections of the hippocampal formation in humans: I. the mossy fiber pathway. *Journal of Computational Neurology*, 385 (1997), 325–351.

Lin, J.J., Riley, J.D., Juranek, J., Cramer, S.C. (2008) Vulnerability of the frontal-temporal connections in temporal lobe epilepsy. *Epilepsy Research*. 2008;82(2-3):162-170.

Liu, M., Bernhardt, B.C., Bernasconi, A., Bernasconi, N. (2016) Gray matter structural compromise is equally distributed in left and right temporal lobe epilepsy. *Hum Brain Mapp*. 2016 Feb;37(2):515-524.

References

- Liu, Z., Xu, Y., An, J., Wang, J., Yin, X., Huang, R., et al. (2014). Altered Brain White Matter Integrity in Temporal Lobe Epilepsy: A TBSS Study. *Journal of Neuroimaging*, 1–5. <http://doi.org/10.1111/jon.12154>
- Liu, M., Concha, L., Lebel, C., Beaulieu, C., Gross, D.W. (2012). Mesial temporal sclerosis is linked with more widespread white matter changes in temporal lobe epilepsy. *NeuroImage: Clinical*, 1(1), 99-105. <http://doi.org/10.1016/j.nicl.2012.09.010>
- Lorente de No, R. (1934) Studies on the structure of the cerebral cortex. II. Continuation of the study of the Ammonic system. *Journal of Psychology and Neurology* 46(2):113–177.
- Loring, D. W. (2007), It's About Time: Long-term Memory Outcome Following Temporal Lobectomy. *Epilepsy Currents*, 7: 38–40. doi:10.1111/j.1535-7511.2007.00162.x
- Lossi, L., Merighi, A. (2003). In vivo cellular and molecular mechanisms of neuronal apoptosis in the mammalian CNS. *Progress in Neurobiology* 69: 287–312.
- Lv, R., Sun, Z., Cui, T., Guan, H., Ren, H., Shao, X. (2014) Temporal lobe epilepsy with amygdala enlargement: a subtype of temporal lobe epilepsy. *BMC Neurology* 201414:194. DOI: 10.1186/s12883-014-0194-z
- MacIntosh, B.J., Graham, S.J. (2013). Magnetic resonance imaging to visualize stroke and characterize stroke recovery: A review. *Frontiers in Neurology*, 4 (May), 1-14. <http://doi.org/10.3389/fneur.2013.00060>
- Mackay, C., Webb, J., Eldridge P., Chadwick, D.W., Whitehouse, G.H., Roberts, N. (2000) Quantitative magnetic resonance Neuroimaging in consecutive patients evaluated for surgical treatment of temporal lobe epilepsy. *Magnetic Resonance Imaging*. 2000;18:1187–99.
- Maguire, E.A., Nannery, R., Spiers, H.J. (2006). Navigation around London by a taxi driver with bilateral hippocampal lesions. *Brain*, 129(11), 2894-2907. <http://doi.org/10.1093/brain/awl286>
- Malone, I.B., Leung, K.K., Clegg, S., Barnes, J., Whitwell, J.L., Ashburner, J. et al. (2015): Accurate automatic estimation of total intracranial volume: a nuisance variable with less nuisance. *Neuroimage* 104:366-372.
- Malykhin, N.V., Lebel, R.M., Coupland, N.J., Wilman, A.H., Carter, R. (2010) In vivo quantification of hippocampal subfields using 4.7 T fast spin echo imaging. *Neuroimage*. 2010 Jan 15;49(2):1224-1230.
- Manaut, E., Gómez, C.M., Vaquero, E., Rodriguez, E. (2002) Hemispheric lateralization of language in epileptic right-handed children with unihemispheric discharge. *Journal of Child Neurology*, 2002, vol. 17, 505-509.
- Mandonnet, E., Nouet, A., Gatignol, P., Capelle, L., Duffau, H. (2007). Does the Left Inferior Longitudinal Fasciculus Play a Role in Language? A Brain Stimulation Study. *Brain*, 130(3), 623-629.
- Mansouri, A., Fallah, A., Valiante, T.A. (2012). Determining Surgical Candidacy in Temporal Lobe Epilepsy. *Epilepsy Research and Treatment*, 2012, 1-16. <http://doi.org/10.1155/2012/706917>

References

- Marcus, D.S., Harwell, J., Olsen, T., Hodge, M., Glasser, M.F., Prior, F. et al.(2011). Informatics and data mining tools and strategies for the human connectome project. *Frontiers in Neuroinformatics*. 5:4. doi: 10.3389/ fninf.2011.00004
- Mark, L.P., Daniels, D.L., Naidich, T.P., Borne, J.A. (1993) Limbic system anatomy: an overview. *American Journal of Neuroradiology* 1993;14:349–352.
- Marsh, L., Morrell, M.J., Shear, P.K., Sullivan, E.V, Freeman, H., Marie, A. et al. (1997). Cortical and hippocampal volume deficits in temporal lobe epilepsy. *Epilepsia*, 38(5), 576–87. <http://doi.org/9184604>
- Martin, P., Bender, B., Focke, N.K. (2015) Post-processing of structural MRI for individualized diagnostics. *Quantitative Imaging in Medicine and Surgery* 2015;5(2):188-203. doi: 10.3978/j.issn.2223-4292.2015.01.10
- Martin, P., Winston, G.P., Bartlett, P., de Tisi, J., Duncan, J.S., Focke, N.K. (2017). Voxel-based magnetic resonance image postprocessing in epilepsy. *Epilepsia*, 1-12. <http://doi.org/10.1111/epi.13851>
- Mathern, G.W., Babb, T.L., Leite, J.P., Pretorius, J.K., Yeoman, K.M., Kuhlman, P.A. (1996). The pathogenic and progressive features of chronic human hippocampal epilepsy. *Epilepsy Research*, 26(1), 151–161. [http://doi.org/10.1016/S0920-1211\(96\)00052-6](http://doi.org/10.1016/S0920-1211(96)00052-6)
- Matsufuji, M., Utsunomiya, H., Inoue, T., Yasumoto, S., Takashima, S., Mitsudome, A. (2012). Magnetic resonance imaging volumetry and clinical analysis of epilepsy patients with unilateral hippocampal abnormality. *Pediatrics International*, 54(1), 19–26. <http://doi.org/10.1111/j.1442-200X.2011.03444.x>
- McDonald, C.R., Ahmadi, M.E., Hagler, D.J., Tecoma, E.S., Iragui, V.J., Gharapetian, L. et al. (2008). Diffusion tensor imaging correlates of memory and language impairments in temporal lobe epilepsy. *Neurology*, 71(23), 1869-1876. <http://doi.org/10.1212/01.wnl.0000327824.05348.3b>
- McMillan, A.B., Hermann, B.P., Johnson, S.C., Hansen, R.R., Seidenberg, M., Meyerand, M.E. (2004). Voxel-based morphometry of unilateral temporal lobe epilepsy reveals abnormalities in cerebral white matter. *NeuroImage*, 23(1), 167–174. <http://doi.org/10.1016/j.neuroimage.2004.05.002>
- McNamara, J.O. (1999) Emerging insights into the genesis of epilepsy. *Nature*. 1999 Jun 24;399(6738 Suppl):A15-22.
- Meierkord, H., Holtkamp, M. (2007). Non-convulsive status epilepticus in adults: clinical forms and treatment. *Lancet Neurol*, 6(4), 329–339. [http://doi.org/10.1016/S1474-4422\(07\)70074-1](http://doi.org/10.1016/S1474-4422(07)70074-1)
- Meiners, L.C., Van Gils, A., Jansen, G.H., De Kort, G., Witkamp, T.D., Ramos, L.M.P. et al. (1994). Temporal lobe epilepsy: The various MR appearances of histologically proven mesial temporal sclerosis. *American Journal of Neuroradiology*, 15(8), 1547–1555.
- Merschhemke, M., Mitchell, T.N., Free, S.L., Hammers, A., Kinton, L., Siddiqui, A. et al. (2003) Quantitative MRI detects abnormalities in relatives of patients with epilepsy and malformations of cortical development. *Neuroimage* 18:642–649.

References

- Mesulam, M.M. (2002). The Human Frontal Lobes: Transcending the Default Mode through Contingent Coding. *Principles of Frontal Lobe Function*, (2002), 8-30. <http://doi.org/10.1093>
In: *Principles of Frontal Lobe Function*, edited by Stuss, D.T. and Knight, R.T. Oxford University Press, 2002. ProQuest Ebook Central, <http://ebookcentral.proquest.com/lib/liverpool/detail.action?docID=281470>.
- Metzler-Baddeley, C., Jones, D.K., Belaroussi, B., Aggleton, J.P., O'Sullivan, M.J. (2011). Frontotemporal connections in episodic memory and aging: a diffusion MRI tractography study. *The Journal of Neuroscience : The Official Journal of the Society for Neuroscience*, 31(37), 13236-13245. <http://doi.org/10.1523/JNEUROSCI.2317-11.2011>
- Michaelis, E. (2012). Selective Neuronal Vulnerability in the Hippocampus: Relationship to Neurological Diseases and Mechanisms for Differential Sensitivity of Neurons to Stress. In: *The Clinical Neurobiology of the Hippocampus: An integrative view*. Oxford University Press.
- Miles, R., Wong, R.K.S. (1986). Excitatory synaptic interactions between CA3 neurons in the guinea-pig hippocampus. *Physiology* 373:397-418.
- Miro, J., Gurtubay-Antolin, A., Ripolles, P., Sierpowska, J., Juncadella, M., Fuentemilla, L. et al. (2015). Interhemispheric microstructural connectivity in bitemporal lobe epilepsy with hippocampal sclerosis. *Cortex*, 67 (May), 106-121. <http://doi.org/10.1016/j.cortex.2015.03.018>
- Mishkin, M. 1978. Memory in monkeys severely impaired by combined but not separate removal of amygdala and hippocampus. *Nature*, 273, 297-298.
- Miyata, H., Hori, T., Vinters, H. (2013). Surgical pathology of epilepsy-associated non-neoplastic cerebral lesions: A brief introduction with special reference to hippocampal sclerosis and focal cortical dysplasia. *Neuropathology*, 33: 442-458. doi:10.1111/neup.12028
- Moran, N.F., Lemieux, L., Kitchen, N.D., Fish, D.R., Shorvon, S. D. (2001). Extrahippocampal temporal lobe atrophy in temporal lobe epilepsy and mesial temporal sclerosis. *Brain : A Journal of Neurology*, 124(1), 167-175. <http://doi.org/10.1093/brain/124.1.167>
- Mori, S., Oishi, K., Faria, A.V. (2009). White matter atlases based on diffusion tensor imaging. *Current Opinion in Neurology*, 22(4), 362-369. <http://doi.org/10.1097/WCO.0b013e32832d954b>
- Morimoto, K., Fahnestock, M., Racine, R.J. (2004). Kindling and status epilepticus models of epilepsy: Rewiring the brain. *Progress in Neurobiology*, 73(1), 1-60. <http://doi.org/10.1016/j.pneurobio.2004.03.009>
- Mosewich, R.K., So, E.L., O'Brien, T.J., Cascino, G.D., Sharbrough, F.W., Mars, W. R. et al. (2000). Factors Predictive of the Outcome of Frontal Lobe Epilepsy Surgery. *Epilepsia*, 41(7), 843-849. <http://doi.org/10.1111/j.1528-1157.2000.tb00251.x>
- Mrzljak, L., Uylings, H.B.M., Van Eden, C.G., Judas, M. (1990) Neuronal development in human pre-frontal cortex in prenatal and postnatal stages. In: *The Pre-frontal Cortex: Its Structure, Function and Pathology* (edited by Uylings, H.B.M., Van Eden, C.G., De Bruin,

References

- J.P.C., Corner, M.A., Feenstra, M.G.P.) Amsterdam: Elsevier. 185–222.
- Mueller, C.-A., Scorzin, J., von Lehe, M., Fimmers, R., Helmstaedter, C., Zentner, J. et al. (2012) Seizure outcome 1 year after temporal lobe epilepsy: an analysis of MR volumetric and clinical parameters. *Acta Neurochirurgica* (Wien) 2012;154(8):1327-1336.
- Mueller, S.G., Chao, L.L., Berman, B., Weiner, M.W. (2011) Evidence for functional specialization of hippocampal subfields detected by MR subfield volumetry on high resolution images at 4 T. *Neuroimage*. 2011 Jun 1;56(3):851-857.
- Mueller, S.G., Laxer, K.D., Barakos, J., Cheong, I., Garcia, P., Weiner, M.W. (2009) Subfield atrophy pattern in temporal lobe epilepsy with and without mesial sclerosis detected by high-resolution MRI at 4 Tesla: preliminary results. *Epilepsia*. 2009 Jun;50(6):1474-1483.
- Mueller, S.G., Stables, L., Du, A.T., Schuff, N., Truran, D., Cashdollar, N. et al. (2007) Measurement of hippocampal subfields and age-related changes with high resolution MRI at 4T. *Neurobiol Aging*. 2007 May;28(5):719-726.
- Mueller, S.G., Weiner, M.W. (2009) Selective effect of age, Apo e4, and Alzheimer's disease on hippocampal subfields. *Hippocampus*. 2009 Jun;19(6):558-564.
- Mueller, S.G., Laxer, K.D., Barakos, J., Ian, C., Garcia, P., Weiner, M. W. (2010). Widespread Neocortical Abnormalities in Temporal Lobe Epilepsy With And Without Mesial Sclerosis, 46(2), 353–359. <http://doi.org/10.1016/j.neuroimage.2009.02.020>. Widespread
- Mueller, S.G., Laxer, K.D., Cashdollar, N., Buckley, S., Paul, C., Weiner, M. W. (2006). Voxel-based optimized morphometry (VBM) of gray and white matter in temporal lobe epilepsy (TLE) with and without mesial temporal sclerosis. *Epilepsia*, 47(5), 900-907. <http://doi.org/10.1111/j.1528-1167.2006.00512.x>
- Muehlechner, A., Coras, R., Kobow, K., Feucht, M., Czech, T., Stefan, H., et al. (2012) Neuropathologic measurements in focal cortical dysplasias: validation of the ILAE 2011 classification system and diagnostic implications for MRI. *Acta Neuropathologica*. 123, 259-272.
- Mullaart, R.A., Daniëls, O., Hopman, J.C., De Haan, A.F., Stoeltinga, G.B., Rottevel, J.J. (1995) Asymmetry of the Cerebral Blood Flow: An Ultrasound Doppler Study in Preterm Newborns. *Pediatric Neurology* 1995;13:319-322.
- Na, M., Ge, H., Shi, C., Shen, H., Wang, Y., Pu, S. et al. (2015) Long-term seizure outcome for international consensus classification of hippocampal sclerosis: a survival analysis. *Seizure*. 2015 Feb;25:141-146.
- Nadarajah, B., Parnavelas, J.G. (2002) Modes of neuronal migration in the developing cerebral cortex *Nature Reviews Neuroscience* 3, 423-432 (June 2002) doi:10.1038/nrn845
- National Institutes of Health (2012) Paediatric MRI Data Repository. Available at: https://pediatricmri.nih.gov/nihpd/info/Documents/PedsMRI_Brochure_June2012.pdf (accessed 13/06/2017)
- Neligan, A., Hauser, W.A., Sander, J.W. (2012) The epidemiology of the epilepsies. *Handbook of clinical neurology*. 2012;107:113-133.

References

- Newberry, N.R., Nicoll, R.A. (1984). A bicuculline-resistant inhibitory post-synaptic potential in rat hippocampal pyramidal cells in vitro. *Journal of Physiology*. 348:239-254.
- Ngugi A.K., Bottomley C., Kleinschmidt I., Sander J.W., Newton C.R. (2010) Estimation of the burden of active and life-time epilepsy: a meta-analytic approach. *Epilepsia*. 2010;51(5):883-890.
- Njiokiktjien, C. (2005). Differences in vulnerability between the hemispheres in early childhood and adulthood. *Human Physiology*, 32(1), 37-42. <http://doi.org/10.1134/S0362119706010051>
- Noguchi, K., Ogawa, T., Inugami, A., Toyoshima, H., Okudera, T., Uemura, K. (1995) Acute subarachnoid hemorrhage: MR imaging with fluid attenuated inversion recovery pulse sequences. *Radiology* 1995; 196:773-777.
- Novais-Santos, S., Gee, J., Shah, M., Troiani, V., Work, M., Grossman, M. (2007) Resolving sentence ambiguity with planning and working memory resources: Evidence from fMRI. *Neuroimage*. 2007 Aug 1;37(1):361-378.
- Okuda, T., Korogi, Y., Shigematsu, Y., Sugahara, T., Hirai, T., Ikushima, I. et al. (1999) Brain lesions: when should fluid-attenuated inversion-recovery sequences be used in MR evaluation? *Radiology*. 1999;212 (3): 793-798.
- Oppenheim, C., Dormont, D., Biondi, A., Lehericy, S., Hasboun, D., Clemenceau, S. et al. (1998) Loss of digitations of the hippocampal head on high-resolution fast spin-echo MR: a sign of mesial temporal sclerosis. *American Journal of Neuroradiology* 1998;19:457-463.
- Otte, W. M., Van Eijdsden, P., Sander, J. W., Duncan, J. S., Dijkhuizen, R. M., Braun, K. P. J. (2012). A meta-analysis of white matter changes in temporal lobe epilepsy as studied with diffusion tensor imaging. *Epilepsia*, 53(4), 659-667. <http://doi.org/10.1111/j.1528-1167.2012.03426.x>
- Pail, M., Brazdil, M., Marecek, R., Mikl, M. (2010). An optimized voxel-based morphometric study of gray matter changes in patients with left-sided and right-sided mesial temporal lobe epilepsy and hippocampal sclerosis (MTLE/HS). *Epilepsia*, 51(4), 511-518. <http://doi.org/10.1111/j.1528-1167.2009.02324.x>
- Palmini, A., Najm, I., Avanzini, G., Babb, T., Guerrini, R., Foldvary-Schaefer, N. et al. (2004). Terminology and classification of the cortical dysplasias. *Neurology*, 62(6 Suppl 3), S2-S8. <http://doi.org/10.1212/01.WNL.0000114507.30388.7E>
- Palmini, A. (2011) Revising the classification of focal cortical dysplasias. *Epilepsia*, 52: 188-190. doi:10.1111/j.1528-1167.2010.02923.x
- Palmini, A., Gambardella, A., Andermann, F., Dubeau, F., da Costa, J.C., Olivier, A., et al. (1995) Intrinsic epileptogenicity of human dysplastic cortex as suggested by corticography and surgical results. *Ann Neurol* 1995; 37: 476-487.
- Papageorgiou, V., Vargiami, E., Kontopoulos, E., Kardaras, P., Economou, M., Athanassiou-Mataxa, M. et al. (2015). Association between iron deficiency and febrile seizures. *European Journal of Paediatric Neurology*, 19(5), 591-596. <http://doi.org/10.1016/j.ejpn.2015.05.009>
- Papagno, C., Casarotti, A., Comi, A., Pisoni, A., Lucchelli, F., Bizzi, A. et al. (2016). Long-

References

- term proper name anomia after removal of the uncinate fasciculus. *Brain Structure & Function*, 221(1), 687-694. doi:10.1007/s00429-014-0920-8
- Pedraza, O., Bowers, D., Gilmore, R. (2004). Asymmetry of the hippocampus and amygdala in MRI volumetric measurements of normal adults. *Journal of the International Neuropsychological Society*. 10, 664–678.
- Pelletier, I., Sauerwein, H.C., Lepore, F., Saint-Amour, D., Lassonde, M. (2007). Non-invasive alternatives to the Wada test in the presurgical evaluation of language and memory functions in epilepsy patients. *Epileptic Disorders*, 9(2), 111–126. <http://doi.org/10.1684/epd.2007.0109>
- Penfield, W., Rasmussen, T. (1950). *The cerebral cortex of a man: A clinical study of localization of function*. New York: Macmillan.
- Perucca, P., Dubeau, F., Gotman, J. (2014) Intracranial electroencephalographic seizure-onset patterns: effect of underlying pathology. *Brain* 2014; 137 (1): 183-196. doi: 10.1093/brain/awt299
- Phal, P.M., Usmanov, A., Nesbit, G.M., Anderson, J.C., Spencer, D., Wang, P. et al. (2008). Qualitative comparison of 3-T and 1.5-T MRI in the evaluation of epilepsy. *American Journal of Roentgenology*, 191(3), 890–895. <http://doi.org/10.2214/AJR.07.3933>
- Piao, X., Basel-Vanagaite, L., Straussberg, R., Grant, P. E., Pugh, E. W., Doheny, K. et al. (2002). An Autosomal Recessive Form of Bilateral Frontoparietal Polymicrogyria Maps to Chromosome 16q12.2-21. *American Journal of Human Genetics*, 70(4), 1028–1033.
- Pillai, J., Sperling, M.R. (2006), Interictal EEG and the Diagnosis of Epilepsy. *Epilepsia*, 47:14–22. doi:10.1111/j.1528-1167.2006.00654.x
- Pipitone, J., Park, M.T., Winterburn, J., Lett, T.A., Lerch, J.P., Pruessner, J.C. et al. (2014) Multi-atlas segmentation of the whole hippocampus and subfields using multiple automatically generated templates. *Neuroimage*. 2014 Nov 1;101:494-512.
- Pitkänen, A., Lukasiuk, K. (2011) Mechanisms of epileptogenesis and potential treatment targets. *Lancet Neurol*. 2011;10(2):173-186.
- Poduri, A., Evrony, G.D., Cai, X., Walsh, C.A. (2013) Somatic Mutation, Genomic Variation, and Neurological Disease. *Science* 05 Jul 2013:Vol. 341, Issue 6141, 1237758 DOI: 10.1126/science.1237758
- Poustchi-Amin, M., Mirowitz, S.A, Brown, J.J., McKinstry, R.C., Li, T. (2001). Principles and Applications of Echo-planar Imaging : A Review for the General Radiologist. *Radiographics : A Review Publication of the Radiological Society of North America, Inc*, 21, 767-779. DOI: 10.1148/radiographics.21.3.g01ma23767
- Preacher, K.J. (2001). Calculation for the chi-square test: An interactive calculation tool for chi-square tests of goodness of fit and independence [Computer software]. Available from <http://quantpsy.org>.
- Princich, J.P., Consalvo, D., Kauffman, M., Seifer, G., Blenkman, A., Kochen, S. (2012) Contribución de las imágenes de resonancia magnética por tensor de difusión al diagnóstico de displasias corticales focales. *Revista de neurologia* 2012; 54: 453-460.

References

- Prudent, V., Kumar, A., Liu, S., Wiggins, G., Malaspina, D., Gonen, O. (2010) Human hippocampal subfields in young adults at 7.0 T: feasibility of imaging. *Radiology*. 2010 Mar;254(3):900-906.
- Purcell, E., Torrey, H., Pound, R. (1946) Resonance absorption by nuclear magnetic moments in a solid. *Phys Rev* 1946;69:37–38.
- Quarto, T., Blasi, G., Maddalena, C., Viscanti, G., Lanciano, T., Soleti, E. et al. (2016) Association between Ability Emotional Intelligence and Left Insula during Social Judgment of Facial Emotions. *PLoS One*. 2016 Feb 9;11(2):e0148621. doi: 10.1371/journal.pone.0148621.
- Quigg, M., Bertram, E.H., Jackson, T., Laws, E. (1997) Volumetric magnetic resonance imaging evidence of bilateral hippocampal atrophy in mesial temporal lobe epilepsy. *Epilepsia* 1997;38:588-94.
- Rakic, P., Schwab D.F. (1988) Defects of neuronal migration and the pathogenesis of cortical malformations. *Progress in Brain Research* 73, 15–37 (1988).
- Ramon y Cajal, S. (1893) Estructura del asta de Ammon y fascia dentata. *Anales de la Sociedad Espanola de Historia Natural*, 22, 1893
- Ramon y Cajal, S. (1928) Degeneration and Regeneration of the Nervous System (ed. May, R. M.) 656–692 (Oxford Univ. Press, London, 1928).
- RANZCRPart1 (2015) White matter: Fornix and forniceal commissure. Available at: http://ranzcrpart1.wikia.com/wiki/White_matter:Fornix_and_forniceal_commissure (accessed 10/09/2017)
- Rasmussen, T., Olszewski, J., Lloyd-Smith, D.K. (1958) Focal seizures due to chronic localized encephalitis. *Neurology* 8, 435–455.
- Ravat, S., Rao, P., Iyer, V., Shah, U., Shah, S., Jain, N., et al. (2016). Surgical outcomes with non-invasive presurgical evaluation in MRI determined bilateral mesial temporal sclerosis: A retrospective cohort study. *International Journal of Surgery*, 36, 429-435. <http://doi.org/10.1016/j.ijssu.2015.09.006>
- Raymond, A.A., Fish, D.R., Sisodiya, S.M., Alsanjari, N., Stevens, J.M., Shorvon, S.D. (1995) Abnormalities of gyration, heterotopias, tuberous sclerosis, focal cortical dysplasia, microdysgenesis, dysembryoplastic neuroepithelial tumour and dysgenesis of the archicortex in epilepsy. Clinical, EEG and neuroimaging features in 100 adult patients. *Brain*, 118(3), 1995. 629–660.
- Raymond, A.A., Fish, D.R., Stevens, J.M., Cook, M.J., Sisodiya, S.M., Shorvon, S.D. (1994) Association of hippocampal sclerosis with cortical dysgenesis in patients with epilepsy. *Neurology*, 44(10), 1994. 1841–1845.
- Richardson, M.P. (2012) Large scale brain models of epilepsy: dynamics meets connectomics. *Journal of Neurology, Neurosurgery & Psychiatry*, 1238–1248. <http://doi.org/10.1136/jnnp-2011-301944>
- Rizvi, S.A.A., Hernandez-Ronquillo, L., Wu, A., Tellez Zenteno, J.F. (2014). Is rapid withdrawal of anti-epileptic drug therapy during video EEG monitoring safe and efficacious?

References

- Epilepsy Research, 108(4), 755–764. <http://doi.org/10.1016/j.epilepsyres.2014.01.022>
- Roberts, N., Garden, A.S., Cruz-Orive, L.M., Whitehouse, G.H., Edwards, R.H.T. (1994) Estimation of fetal volume by MRI and stereology. *British Journal of Radiology*. 1994;67:1067–1077.
- Rodrigo, S., Oppenheim, C., Chassoux, F., Golestani, N., Cointepas, Y., Poupon, C. et al. (2007) Uncinate fasciculus fiber tracking in mesial temporal lobe epilepsy. Initial findings. *European Radiology*. 2007 Jul;17(7):1663-1668.
- Rodríguez-Cruces, R., Concha, L. (2015). White matter in temporal lobe epilepsy: clinico-pathological correlates of water diffusion abnormalities. *Quantitative Imaging in Medicine and Surgery*, 5(2), 264–278. <http://doi.org/10.3978/j.issn.2223-4292.2015.02.06>
- Rogers, B.P., Sheffield, J.M., Luksik, A.S., Heckers, S. (2012) Systematic Error in Hippocampal Volume Asymmetry Measurement is Minimal with a Manual Segmentation Protocol. *Frontiers in Neuroscience*, 2012 6 (December), 179. <http://doi.org/10.3389/fnins.2012.00179>
- Rogers, S.W., Andrews, P.I., Gahring, L.C., Whisenand, T., Cauley, K., Crain, B.(1994) Autoantibodies to glutamate receptor GluR3 in Rasmussen's encephalitis. *Science* 265, (1994), 648–651.
- Ronan, J.L., Wu, W., Crabtree, G.R. (2013) From neural development to cognition: unexpected roles for chromatin. *Nature Reviews Genetics* 14, 347–359 (2013) [doi:10.1038/nrg3413](http://doi.org/10.1038/nrg3413)
- Rosenow, F., Lüders, H. (2001). Presurgical evaluation of epilepsy. *Brain*, 124(Pt 9), 1683-1700. <http://doi.org/10.4103/1817-1745.40593>
- Rudie, J.D., Colby, J.B., Salamon, N. (2015) Machine learning classification of mesial temporal sclerosis in epilepsy patients. *Epilepsy Res*. 2015 Nov;117:63-69. [doi:10.1016/j.epilepsyres.2015.09.005](http://doi.org/10.1016/j.epilepsyres.2015.09.005).
- Rugg-Gunn, F.J., Eriksson, S.H., Symms, M.R., Barker, G.J., Duncan, J.S. (2001). Diffusion tensor imaging of cryptogenic and acquired partial epilepsies. *Brain*, 124, 627–636.
- Rugg-Gunn, F.J., Boulby, P.A., Symms, M.R., Barker, G.J., Duncan, J.S. (2005) Whole-brain T2 mapping demonstrates occult abnormalities in focal epilepsy. *Neurology* 64:318–325.
- Saavalainen, T., Jutila, L., Mervaala, E., Kälviäinen, R., Vanninen, R., Immonen, A. (2015). Temporal anteroinferior encephalocoele. *Neurology*, 2015, 85(17), 1467-1474.
- Sacchet, M.D., Prasad, G., Foland-Ross, L.C., Joshi, S.H., Hamilton, J.P., Thompson, P.M. et al. (2014a). Structural abnormality of the corticospinal tract in major depressive disorder. *Biology of Mood & Anxiety Disorders*, 4:8. <http://doi.org/10.1186/2045-5380-4-8>
- Sacchet, M.D., Prasad, G., Foland-Ross, L.C., Joshi, S.H., Hamilton, J.P., Thompson, P.M., et al. (2014b). Characterizing white matter connectivity in depressive disorder: Automated fiber quantification and maximum density paths. *Proceedings / IEEE International Symposium on Biomedical Imaging: From Nano to Macro. IEEE International Symposium on Biomedical Imaging*, 11, 592–595. <http://doi.org/10.1109/ISBI.2014.6867940>

References

- Salmenpera, T., Kalviainen, R., Partanen, K., Pitkanen, A. (1998) Hippocampal damage caused by seizures in temporal lobe epilepsy. *Lancet*. 1998 Jan 3;351(9095):35.
- Salmond, C. H., Ashburner, J., Vargha-Khadem, F., Connelly, A., Gadian, D. G., Friston, K. J. (2002). Distributional assumptions in voxel-based morphometry. *NeuroImage*, 17(2), 1027-1030. [http://doi.org/10.1016/S1053-8119\(02\)91153-5](http://doi.org/10.1016/S1053-8119(02)91153-5)
- Samsonsen, C., Sand, T., Bråthen, G., Helde, G., Brodtkorb, E. (2016) The impact of sleep loss on the facilitation of seizures: A prospective case-crossover study, In *Epilepsy Research*, 127, 260-266. <https://doi.org/10.1016/j.eplepsyres.2016.09.014>.
- Sarkisian, M.R., Bartley, C.M., Rakic, P. (2008) Trouble making the first move: interpreting arrested neuronal migration in the cerebral cortex. *Trends Neurosci*2008;31:54-61.
- Sarubbo, S., De Benedictis, A., Merler, S., Mandonnet, E., Balbi, S., Granieri, E. et al. (2015) Towards a functional atlas of human white matter. *Human Brain Mapping*. 2015 Aug; 36(8):3117-36. doi: 10.1002/hbm.22832.
- Scanlon, C., Mueller, S. G., Cheong, I., Hartig, M., Weiner, M. W., Laxer, K. D. (2013). Grey and white matter abnormalities in temporal lobe epilepsy with and without mesial temporal sclerosis. *Journal of Neurology*, 260(9), 2320–9. <http://doi.org/10.1007/s00415-013-6974-3>.
- Scarpazza, C., Sartori, G., De Simone, M. S., Mechelli, A. (2013). When the single matters more than the group: Very high false positive rates in single case Voxel Based Morphometry. *NeuroImage*, 70 (January), 175–188. <http://doi.org/10.1016/j.neuroimage.2012.12.045>
- Schacter, D., Curran, T., Reiman, E., Chen, K., Bandy, D., Frost, J. (1999). Medial temporal lobe activation during episodic encoding and retrieval: A PET study. *Hippocampus*, 9, 575-581.
- Schaffer, K. (1892) Beitrag zur Histologie der Ammonshornformation. *Archiv für mikroskopische Anatomie* 39:611–632.
- Scheltens, P., Launer, L.J., Barkhof, F., Weinstein, H.C., van Gool, W.A. (1995) Visual assessment of medical temporal lobe atrophy on magnetic resonance imaging; interobserver reliability. *Journal of Neurology* 1995, 242(9). 557–560.
- Schmidt-Kastner, R., Freund, T.F. (1991) Selective vulnerability of the hippocampus in brain ischemia. *Neuroscience*. 1991;40(3):599–636.
- Schmolck, H., Kensinger, E.A., Corkin, S., Squire, L.R. (2002). Semantic knowledge in patient H.M. and other patients with bilateral medial and lateral temporal lobe lesions. *Hippocampus*, 12(4), 520-533. <http://doi.org/10.1002/hipo.10039>
- Schoene-Bake, J.-C., Keller, S.S., Niehusmann, P., Volmering, E., Elger, C., Deppe, M. et al. (2014) In vivo mapping of hippocampal subfields in mesial temporal lobe epilepsy: relation to histopathology. *Human Brain Mapping* 2014;35(9):4718-4728.
- Schuele, S.U., Lüders, H.O. (2008) Intractable epilepsy: management and therapeutic alternatives. *Lancet Neurology* 2008; 7: 514–524.
- Scimemi, A., Schorge, S., Kullmann, D.M., Walker, M.C. (2006). Epileptogenesis is

References

- associated with enhanced glutamatergic transmission in the perforant path. *Journal Of Neurophysiology*, 95(2), 1213-1220.
- Scott, C.A., Fish, D.R., Smith, S.J., Free, S.L., Stevens, J.M., Thompson, P. et al. (1999) Presurgical evaluation of patients with epilepsy and normal MRI: role of scalp video-EEG telemetry. *Journal of Neurology, Neurosurgery and Psychiatry*. 1999;66(1):69-71.
- Seiam, A.H., Dhaliwal, H., Wiebe, S. (2011) Determinants of quality of life after epilepsy surgery: systematic review and evidence summary. *Epilepsy and Behavior* 2011; 21:441–445.
- Sepeta, L.N., Berl, M.M., Wilke, M., You, X., Mehta, M., Xu, B. et al. (2016). Age-Dependent Mesial Temporal Lobe Lateralization in Language fMRI. *Epilepsia*, 57(1), 122–130. <http://doi.org/10.1111/epi.13258>
- Sharif, M.R., Kheirhah, D., Madani, M., Kashani, H.H. (2015). The Relationship Between Iron Deficiency and Febrile Convulsion: A Case-Control Study. *Global Journal of Health Science*, 8(2), 185–189. <http://doi.org/10.5539/gjhs.v8n2p185>
- Shinoura, N., Suzuki, Y., Tsukada, M., Katsuki, S., Yamada, R., Tabei, Y. et al. (2007). Impairment of Inferior Longitudinal Fasciculus plays a Role in Visual Memory Disturbance. *Neurocase (Psychology Press)*, 13(2), 127-130. doi:10.1080/13554790701399254
- Shinoura, N., Suzuki, Y., Tsukada, M., Yoshida, M., Yamada, R., Tabei, Y. et al. (2010). Deficits in the left inferior longitudinal fasciculus results in impairments in object naming. *Neurocase*, 16(2), 135-139.
- Shinoura, N., Yamada, R., Tabei, Y., Midorikawa, A., Itoi, C., Saito, S. et al. (2013). Damage to the left ventral, arcuate fasciculus and superior longitudinal fasciculus-related pathways induces deficits in object naming, phonological language function and writing, respectively. *International Journal Of Neuroscience*, 123(7), 494-502. doi:10.3109/00207454.2013.765420
- Shiono, T., Teshima, Y., Iwasaki, N. (1996) Advantages and disadvantages of fast fluid-attenuated inversion recovery sequences in the evaluation of brain infarction. *Nippon Igaku Hoshasen Gakkai Zasshi* 1996; 56:625–628.
- Sidhu, M.K., Stretton, J., Winston, G.P., Bonelli, S., Centeno, M., Vollmar, C. et al. (2013). A functional magnetic resonance imaging study mapping the episodic memory encoding network in temporal lobe epilepsy. *Brain*, 136(6), 1868–1888. <http://doi.org/10.1093/brain/awt099>
- Siegel, A.M., Cascino, G.D., Meyer, F.B., McClelland, R.L., So, E.L., Marsh, W.R. et al. (2004) Resective reoperation for failed epilepsy surgery: seizure outcome in 64 patients. *Neurology* 63, 2298-2302.
- Siegel, A.M., Wieser, H.G., Wichmann, W., Yasargil, G.M. (1990) Relationships between MR-imaged total amount of tissue removed, resection scores of specific mediobasal limbic subcompartments and clinical outcome following selective amygdalohippocampectomy. *Epilepsy Research* 1990;6:56-65.
- Sisodiya, S.M., Free, S.L., Fish, D.R., Shorvon, S.D. (1995a) Increasing the yield from volumetric MRI in patients with epilepsy. *Magnetic Resonance Imaging* 13:1147–1152.

References

- Sisodiya, S.M., Free, S.L., Stevens, J.M., Fish, D.R., Shorvon, S.D. (1995b) Widespread cerebral structural changes in patients with cortical dysgenesis and epilepsy. *Brain* 1995; 118: 1039-1050.
- Sisodiya, S.M., Moran, N., Free, S.L., Kitchen, N.D., Stevens, J.M., Harkness, W.F.J. et al. (1997) Correlation of widespread preoperative magnetic resonance imaging changes with unsuccessful surgery for hippocampal sclerosis. *Annals of Neurology* 1997;41:490-496.
- Sisodiya, S.M. (2004) Malformations of cortical development: burdens and insights from important causes of human epilepsy. *Lancet Neurology* 3:29–38.
- Sivakanthan, S., Neal, E., Murtagh, R., Vale, F.L. (2016). The evolving utility of diffusion tensor tractography in the surgical management of temporal lobe epilepsy: a review. *Acta Neurochirurgica* 2158-2185. doi:10.1007/s00701-016-2910-5.
- Small, S.A., Schobel, S.A., Buxton, R.B., Witter, M.P., Barnes, C.A. (2011) A pathophysiological framework of hippocampal dysfunction in ageing and disease. *Nature Reviews Neuroscience* 12:585-601. doi:10.1038/nrn3085
- Smith, S.J.M. (2005) EEG in the diagnosis, classification, and management of patients with epilepsy. *Journal of Neurology, Neurosurgery and Psychiatry* 2005;76:suppl 2 ii2-ii7 doi:10.1136/jnnp.2005.069245
- Smith, S.M., Jenkinson, M., Woolrich, M.W., Beckmann, C.F., Behrens, T.E. J., Johansen-Berg, H. et al. (2004). Advances in functional and structural MR image analysis and implementation as FSL. *NeuroImage*, 23, 208-219. <http://doi.org/10.1016/j.neuroimage.2004.07.051>
- Smith, S.M. (2002) Fast robust automated brain extraction. *Human Brain Mapping*, 17, 143–155.
- Soares, J.M., Marques, P., Alves, V., Sousa, N. (2013). A hitchhiker's guide to diffusion tensor imaging. *Frontiers in Neuroscience*, 7(7), 1-14. <http://doi.org/10.3389/fnins.2013.00031>
- Sølsnes, A. E., Sripada, K., Yendiki, A., Bjuland, K. J., Østgård, H. F., Aanes, S. et al. (2016). Limited microstructural and connectivity deficits despite subcortical volume reductions in school-aged children born preterm with very low birth weight. *NeuroImage*, 130, 24–34. <http://doi.org/10.1016/j.neuroimage.2015.12.029>
- Sone, D., Sato, N., Maikusa, N., Ota, M., Sumida, K., Yokoyama, K. et al. (2016). Automated subfield volumetric analysis of hippocampus in temporal lobe epilepsy using high-resolution T2-weighted MR imaging. *NeuroImage: Clinical*, 12(July), 57-64. <http://doi.org/10.1016/j.nicl.2016.06.008>
- Sormaz, M., Jefferies, E., Bernhardt, B. C., Karapanagiotidis, T., Mollo, G., Bernasconi, N., Smallwood, J. (2017). Knowing what from where: Hippocampal connectivity with temporoparietal cortex at rest is linked to individual differences in semantic and topographic memory. *NeuroImage*, 152(November 2016), 400-410. <http://doi.org/10.1016/j.neuroimage.2017.02.071>
- Spencer, S.S. (1994) The relative contributions of MRI, SPECT, and PET imaging in epilepsy. *Epilepsia*, 35, supplement 6, 1994, S72–S89.

References

- Spencer, S.S. (2002) When should temporal-lobe epilepsy be treated surgically?. *The Lancet Neurology*, 1(6), 2002, 375–382.
- Spencer, S.S., Berg A.T., Vickrey B.G., Sperling M.R., Bazil C.W., Shinnar S. et al. (2005). Predicting long-term seizure outcome after resective epilepsy surgery: the multicenter study. *Neurology*, 65(6), 912–918. <http://doi.org/10.1212/01.wnl.0000176055.45774.71>
- Spencer S.S., Williamson P.D., Bridgers S.L. (1985) Reliability and accuracy of localization by scalp ictal EEG. *Neurology*, vol. 35(11), 1985, 1567–1575.
- Sprooten, E., Barrett, J., McKay, D.R., Knowles, E.E., Mathias, S.R., Winkler, A.M. et al. (2016) A comprehensive tractography study of patients with bipolar disorder and their unaffected siblings. *Human Brain Mapping*, 37: 3474–3485. doi:10.1002/hbm.23253
- Squire, L.R., Schmolck, H., Stark, S. (2001) Impaired auditory recognition memory in amnesic patients with medial temporal lobe lesions. *Learning and Memory* 8:252–256.
- Squire, L. (1992) Memory and hippocampus: A synthesis from findings with rats, monkeys and humans. *Psychological Review*, 99, 195–231.
- Squire, L. R., Wixted, J. T. (2011). The Cognitive Neuroscience of Human Memory Since H.M. *Annual Review of Neuropsychology* (Vol. 34). <http://doi.org/10.1146/annurev-neuro-061010-113720>.
- Squire, L.R., Stark, C.E.L., Clark, R.E. (2004). The Medial Temporal Lobe. *Annual Review of Neuroscience*, 27(1), 279–306. <http://doi.org/10.1146/annurev.neuro.27.070203.144130>
- Squire, L., Amaral, D., Press, G. (1990) Magnetic resonance imaging of the hippocampal formation and mamillary nuclei distinguish medial temporal lobe and diencephalic amnesia. *J. Neurosci.*, 10, 3106–3117.
- Steve, T.A., Jirsch, J.D., Gross, D.W. (2014) Quantification of subfield pathology in hippocampal sclerosis: a systematic review and meta-analysis. *Epilepsy Res.* 2014 Oct;108(8):1279–1285.
- Storsve, A.B., Fjell, A.M., Yendiki, A., Walhovd, K.B. (2016). Longitudinal Changes in White Matter Tract Integrity across the Adult Lifespan and Its Relation to Cortical Thinning. *PLoS ONE*, 11(6), e0156770. <http://doi.org/10.1371/journal.pone.0156770>
- Strange, B. A., Fletcher, P. C., Henson, R. N., Friston, K. J., Dolan, R. J. (1999). Segregating the functions of human hippocampus. *Proceedings of the National Academy of Sciences of the United States of America*, 96(March), 4034–4039. <http://doi.org/10.1073/pnas.96.7.4034>
- Surges, R., Elger, C.E. (2013) Reoperation after failed resective epilepsy surgery. *Seizure* 22:493–501 doi:10.1016/j.seizure.2013.04.020
- Surguladze, S.A., Brammer, M.J., Young, A.W., Andrew, C., Travis, M.J., Williams, S.C. et al. (2003) A preferential increase in the extrastriate response to signals of danger. *Neuroimage*. 2003 Aug;19(4):1317–1328.
- Szabo, C.A., Xiong, J., Lancaster, J. L., Rainey, L., Fox, P. (2001). Amygdalar and hippocampal volumetry in control participants: Differences regarding handedness. *American Journal of Neuroradiology*, 22(7), 1342–1345.

References

- Szirmai, I., Buzsaki, G., Kamondi, A. (2012). 120 years of Hippocampal Schaffer Collaterals, 1516, 1508-1516. <http://doi.org/10.1002/hipo.22001>
- Tasch, E., Cendes, F., Li, L.M., Dubeau, F., Andermann, F., Arnold, D.L. (1999) Neuroimaging evidence of progressive neuronal loss and dysfunction in temporal lobe epilepsy. *Annals of Neurology*. 1999 May;45(5):568-576.
- Tassi, L., Colombo, N., Garbelli, R., Francione, S., Lo Russo, G., Mai, R. et al. (2002) Focal cortical dysplasia: neuropathological subtypes, EEG, neuroimaging and surgical outcome. *Brain* 2002;125(Pt 8):1719–1732.
- Tassi, L., Pasquier, B., Minotti, L., Garbelli, R., Kahane, P., Benabid, A.L. et al. (2001) Cortical dysplasia: electroclinical, imaging, and neuropathologic study of 13 patients. *Epilepsia* 2001;42:1112–1123.
- Tau, G. Z., Peterson, B. S. (2010). Normal Development of Brain Circuits. *Neuropsychopharmacology*, 35(1), 147–168. <http://doi.org/10.1038/npp.2009.115>
- Taylor, D.C., Falconer, M.A., Bruton, C.J., Corsellis, J.A.N. (1971) Focal dysplasia of the cerebral cortex in epilepsy. *Journal of Neurology, Neurosurgery and Psychiatry* 1971;34:369-387.
- Téllez-Zenteno, J.F., Hernández Ronquillo, L., Moien-Afshari, F., Wiebe, S. (2010) Surgical outcomes in lesional and non-lesional epilepsy: a systematic review and meta-analysis. *Epilepsy Research* 2010; 89:310–318
- Theodore, W.H., Bhatia, S., Hatta, J., Fazilat, S., DeCarli, C., Bookheimeret, S.Y. et al. (1999) Hippocampal atrophy, epilepsy duration, and febrile seizures in patients with partial seizures. *Neurology*. 1999 Jan 1;52(1):132-136.
- Thesen, T., Quinn, B.T., Carlson, C., Devinsky, O., DuBois, J., McDonald, C.R. et al. (2011) Detection of epileptogenic cortical malformations with surface-based MRI morphometry. *PLoS One* 2011; 6(2): e16430.
- Thiebaut de Schotten, M., Cohen, L., Amemiya, E., Braga, L., Dehaene, S. (2014). Learning to Read Improves the Structure of the Arcuate Fasciculus. *Cerebral Cortex*, 24(4), 989-995.
- Thiebaut de Schotten, M., Kinkingnehun, S., Delmaire, C., Lehericy, S., Duffau, H., Thivard, L., et al. (2008) Visualization of disconnection syndromes in humans. *Cortex*, 44, 2008, 1097–1103.
- Thivard, L., Adam, C., Hasboun, D., Clemenceau, S., Dezamis, E., Lehericy, S. et al. (2006). Interictal diffusion MRI in partial epilepsies explored with intracerebral electrodes. *Brain*, 129(2), 375–385. <http://doi.org/10.1093/brain/awh709>
- Thivard, L., Lehericy, S., Krainik, A., Adam, C., Dormont, D., Chiras, J. et al. (2005). Diffusion tensor imaging in medial temporal lobe epilepsy with hippocampal sclerosis. *NeuroImage*, 28(3), 682–690. <http://doi.org/10.1016/j.neuroimage.2005.06.045>
- Thom, M., Liagkouras, I., Elliot, K.J., Martinian, L., Harkness, W., McEvoy, A. et al. (2010) Reliability of patterns of hippocampal sclerosis as predictors of postsurgical outcome. *Epilepsia*. 2010 Sep;51(9):1801-1808.
- Thompson, D.K., Wood, S.J., Doyle, L.W., Warfield, S.K., Egan, G.F., Inder, T.E. (2009)

References

- MR-determined hippocampal asymmetry in full-term and preterm neonates. *Hippocampus*. 2009 Feb;19(2):118-123. doi: 10.1002/hipo.20492.
- Toldo, I., Perissinotto, E., Menegazzo, F., Boniver, C., Sartori, S., Salviati, L. et al. (2010) Comorbidity between headache and epilepsy in a pediatric headache center. *Journal of Headache and Pain*. 2010;11:235–240.
- Toledano, R., Jimenez-Huete, A., Campo, P., Poch, C., Garcia-Morales, I., Angulo, J.C.G. et al. (2016). Small temporal pole encephalocele : A hidden cause of “normal” MRI temporal lobe epilepsy, 841-851. <http://doi.org/10.1111/epi.13371>
- Tombini, M., Squitti, R., Cacciapaglia, F., Ventriglia, M., Assenza, G., Benvenga A. et al. (2013). Inflammation and iron metabolism in adult patients with epilepsy: Does a link exist? *Epilepsy Research*, 107(3), 244–252. <http://doi.org/10.1016/j.eplepsyres.2013.09.010>
- Toosy, A.T., Ciccarelli, O., Parker, G.J., Wheeler-Kingshott, C.A., Miller, D.H., Thompson A.J. (2004) Characterizing function-structure relationships in the human visual system with functional MRI and diffusion tensor imaging. *Neuroimage*. 2004 Apr;21(4):1452-1463.
- Traub, R., Miles, R. (1991a). The hippocampus in Context. In: *Neuronal Networks of the Hippocampus* (pp. 1-33). Cambridge: Cambridge University Press. doi:10.1017/CBO9780511895401.002
- Traub, R., Miles, R. (1991b). Collective behaviors of the CA3 network: experiment and model. In: *Neuronal Networks of the Hippocampus* (pp.119-156). Cambridge: Cambridge University Press. doi:10.1017/CBO9780511895401.002
- Travis, K. E., Adams, J. N., Ben-Shachar, M., Feldman, H. M. (2015a). Decreased and Increased Anisotropy along Major Cerebral White Matter Tracts in Preterm Children and Adolescents. *PLoS ONE*, 10(11), e0142860. <http://doi.org/10.1371/journal.pone.0142860>
- Travis, K.E., Golden, N.H., Feldman, H.M., Solomon, M., Nguyen, J., Mezer, A. et al. (2015b). Abnormal white matter properties in adolescent girls with anorexia nervosa. *NeuroImage : Clinical*, 9, 648–659. <http://doi.org/10.1016/j.nicl.2015.10.008>
- Travis, K.E., Ben-Shachar, M., Myall, N.J., Feldman, H.M. (2016). Variations in the neurobiology of reading in children and adolescents born full term and preterm. *NeuroImage : Clinical*, 11, 555–565. <http://doi.org/10.1016/j.nicl.2016.04.003>
- Tschampa, H.J., Urbach, H., Malter, M., Surges, R., Greschus, S., Gieseke, J. (2015). Magnetic resonance imaging of focal cortical dysplasia: Comparison of 3D and 2D fluid attenuated inversion recovery sequences at 3T. *Epilepsy Research*, 116, 8–14. <http://doi.org/10.1016/j.eplepsyres.2015.07.004>
- Tsuchiya, K., Inaoka, S., Mizutani, Y., Hachiya, J. (1997) Fast fluid-attenuated inversion-recovery MR of intracranial infections. *AJNR* 1997; 18:909– 913.
- Van Essen, D.C., Ugurbil, K., Auerbach, E., Barch, D., Behrens, T.E.J., Bucholz, R. et al. (2012). The Human Connectome Project: a data acquisition perspective. *NeuroImage*, 62(4), 2222-2231. <http://doi.org/10.1016/j.neuroimage.2012.02.018>
- Van Leemput, K., Bakkour, A., Benner, T., Wiggins, G., Wald, L.L., Augustinack, J. et al. (2009) Automated segmentation of hippocampal subfields from ultra-high resolution in vivo

References

- MRI. *Hippocampus*. 2009 Jun;19(6):549-557.
- Vargas, M.I., Vulliemoz, S., Rosset, A., Seeck, M., Delavelle, J. (2008) Temporal anterior encephalocele. *Neurology* 2008 (71), 1293 DOI10.1212/01.wnl.0000327602.65933.79
- Vaswani, A.K., Nizamani, W.M., Ali, M., Aneel, G., Shahani, B.K., Hussain, S. (2014) Diagnostic Accuracy of Contrast-Enhanced FLAIR Magnetic Resonance Imaging in Diagnosis of Meningitis Correlated with CSF Analysis. *ISRN Radiol.* 2014;2014: 578986. doi:10.1155/2014/578986
- Ver Hoef, L.W., Williams, F.B., Kennedy, R.E., Szaflarski, J.P., Knowlton, R.C. (2013a) Predictive value of hippocampal internal architecture asymmetry in temporal lobe epilepsy. *Epilepsy Res* 2013a;106:155–163.
- Ver Hoef, L.W., Paige, A.L., Riley, K.O., Cure, J., Soltani, M., Williams, F.B. et al. (2013b) Evaluating hippocampal internal architecture on MRI: inter-rater reliability of a proposed scoring system. *Epilepsy Res* 2013b;106:146–154.
- Vogt, B.A. (2005) Pain and Emotion Interactions in Subregions of the Cingulate Gyrus. *Nature Reviews Neuroscience* (2005), 6(7), 533-544.
- Vogt, B.A., Finch, D.M., Olson, C.R. (1992) Functional heterogeneity in cingulate cortex: the anterior executive and posterior evaluative regions. *Cerebral Cortex* (1992), 2(6), 435-443.
- Von Der Heide, R.J., Skipper, L.M., Klobusicky, E., Olson, I.R. (2013). Dissecting the uncinate fasciculus: disorders, controversies and a hypothesis. *Brain: A Journal Of Neurology*, 136(6), 1692.
- Von Oertzen, T.J. (2014). Imaging and treatment decision in seizures and epilepsy. *EMJ Neurology*, (July), 59-64.
- Von Oertzen, T.J., Urbach, H., Jungbluth, S., Kurthen, M., Reuber, M., Fernandez, G. et al. (2002). Standard magnetic resonance imaging is inadequate for patients with refractory focal epilepsy. *Journal of Neurology, Neurosurgery, and Psychiatry*, 73(6), 643-647. <http://doi.org/10.1136/jnnp.73.6.643>
- Wada, J., Rasmussen, T. (1960) Intracarotid injection of sodium Amytal for the lateralization of cerebral speech dominance. *Journal of Neurosurgery* 1960 17:266-282.
- Wagner, J., Weber, B., Urbach, H., Elger, C., Huppertz, H. (2011) Morphometric MRI analysis improves detection of focal cortical dysplasia type II. *Brain* 134(10):2844–2854.
- Wakana, S., Caprihan, A., Panzenboeck, M.M., Fallon, J.H., Perry, M., Gollub, R.L. et al. (2007) Reproducibility of quantitative tractography methods applied to cerebral white matter. *Neuroimage* 36: 630–644.
- Walsh, S., Donnan, J., Fortin, Y., Sikora, L., Morrissey, A., Collins, K. et al (2017). A systematic review of the risks factors associated with the onset and natural progression of epilepsy. *NeuroToxicology*, 61, July 2017, 64-77.
- Wang, I.Z., Alexopoulos, A.V., Jones, S.E., Najm, I.M., Ristic, A., Wong, C. et al. (2014) Linking MRI post-processing with magnetic source imaging in MRI-negative epilepsy. *Annals of Neurology*. 75(5):759–770.

References

- Wang, I.Z., Suwanpakdee, P., Jones, S.E., Jaisani, Z., Moosa, A.N.V, Najm, I.M., Alexopoulos, A.V. (2016a). Re-review of MRI with post-processing in non-lesional patients in whom epilepsy surgery has failed. *Journal of Neurology*, 263(9), 1736-1745. <http://doi.org/10.1007/s00415-016-8171-7>
- Wang, X., Shen, D., Huang, H. (2016b). Prediction of memory impairment with MRI data: A longitudinal study of Alzheimer's disease. In *Medical Image Computing and Computer-Assisted Intervention - MICCAI 2016 - 19th International Conference, Proceedings* (Vol. 9900 LNCS, pp. 273-281). (Lecture Notes in Computer Science (including subseries Lecture Notes in Artificial Intelligence and Lecture Notes in Bioinformatics); Vol. 9900 LNCS). Springer Verlag. DOI:10.1007/978-3-319-46720-7_32
- Wang, I.Z., Alexopoulos, A.V., Jones, S.E., Jaisani, Z., Najm, I.M., Prayson, R.A. (2013) The Pathology of Magnetic-Resonance-Imaging-Negative Epilepsy. *Mod Pathol*. 2013;26(8):1051-1058.
- Wang, Z. I., Jones, S. E., Jaisani, Z., Najm, I. M., Prayson, R. A., Burgess, R. C. et al. (2015). Voxel-based morphometric magnetic resonance imaging (MRI) postprocessing in MRI-negative epilepsies. *Annals of Neurology*, 77(6), 1060–1075. <http://doi.org/10.1002/ana.24407>
- Wansapura, J. P., Holland, S. K., Dunn, R. S., Ball, W. S. (1999) NMR relaxation times in the human brain at 3.0 tesla. *J. Magn. Reson. Imaging*, 9: 531–538.
- Wei, W., Chen, C., Dong, Q., Zhou, X. (2016). Sex Differences in Gray Matter Volume of the Right Anterior Hippocampus Explain Sex Differences in Three-Dimensional Mental Rotation. *Mental Rotation. Frontiers in Human Neuroscience* 10:580. doi: 10.3389/fnhum.2016.00580
- Welker, K.M., Patton, A. (2012). Assessment of normal myelination with magnetic resonance imaging. *Seminars in Neurology*, 32(1), 15-28. <http://doi.org/10.1055/s-0032-1306382>
- Wheeler, M., De Herdt, V., Vonck, K., Gilbert, K., Manem, S., Mackenzie, T. et al. (2011). Efficacy of vagus nerve stimulation for refractory epilepsy among patient subgroups: A re-analysis using the Engel classification. *Seizure: European Journal Of Epilepsy*, 20331-20335. doi:10.1016/j.seizure.2011.01.002
- White, W.F., Nadler, J.V., Hamberger, A., Cotman, C.W., Cummins, J.T. (1977). Glutamate as transmitter of hippocampal perforant path. *Nature*, 270(5635), 356-357.
- Widjaja, E., Blaser, S., Miller, E., Kassner, A., Shannon, P., Chuang, S. H. et al. (2007). Evaluation of subcortical white matter and deep white matter tracts in malformations of cortical development. *Epilepsia*, 48(8), 1460-1469. <http://doi.org/10.1111/j.1528-1167.2007.01105.x>
- Widjaja, E., Mahmoodabadi, S.Z., Otsubo, H., Snead, O.C., Holowka, S., Bells, S. et al. (2009). Subcortical alterations in tissue microstructure adjacent to focal cortical dysplasia: detection at diffusion-tensor MR imaging by using magnetoencephalographic dipole cluster localization. *Radiology*, 251(1), 206-215. <http://doi.org/10.1148/radiol.2511081092>
- Wiebe, S., Blume, W.T., Girvin, J.P., Eliasziw, M. (2001) Effectiveness, Efficiency of

References

- Surgery for Temporal Lobe Epilepsy Study G. A randomized, controlled trial of surgery for temporal-lobe epilepsy. *New England Journal of Medicine*. 2001 Aug 2;345(5):311-318.
- Wiebe, S., Gafni, A., Blume, W.T., Girvin, J.P. (1996) Letter to the Editor: The economics of surgery for temporal lobe epilepsy. *Journal of Epilepsy* 1996; 9:144-145.
- Wiebe, S., Jette, N. (2012a) Pharmacoresistance and the role of surgery in difficult to treat epilepsy. *Nature Reviews Neurology* 8, 669-677 (December 2012) | doi:10.1038/nrneurol.2012.181
- Wiebe, S., Jette, N. (2012b). Epilepsy surgery utilization: who, when, where, and why? *Current opinion in neurology* 25(2): 187-193.
- Wieser, H.G., Blume, W.T., Fish, D., Goldensohn, E., Hufnagel, A., King, D. et al. (2001) ILAE Commission Report. Proposal for a new classification of outcome with respect to epileptic seizures following epilepsy surgery. *Epilepsia* 2001;42:282-286.
- Wieshmann, U.C., Larkin, D., Varma, T., Eldridge, P. (2008). Predictors of outcome after temporal lobectomy for refractory temporal lobe epilepsy. *Acta Neurologica Scandinavica*, 118(5), 306-312. <http://doi.org/10.1111/j.1600-0404.2008.01043.x>
- Wieshmann, U.C., Free, S.L., Everitt, A.D., Bartlett, P.A., Barker, G.J., Tofts, P.S. et al. (1996) MR imaging in epilepsy with a fast FLAIR sequence. *Journal of Neurology, Neurosurgery and Psychiatry* 1996;61:357-361.
- Wilke, M., Kassubek, J., Ziyeh, S., Schulze-Bonhage, A., Huppertz, H. J. (2003). Automated detection of gray matter malformations using optimized voxel-based morphometry: A systematic approach. *NeuroImage*, 20(1), 330-343. [http://doi.org/10.1016/S1053-8119\(03\)00296-9](http://doi.org/10.1016/S1053-8119(03)00296-9)
- Winston, G. P., Cardoso, M. J., Williams, E. J., Burdett, J. L., Bartlett, P. A., Espak, M., Ourselin, S. (2013a). Automated hippocampal segmentation in patients with epilepsy: Available free online. *Epilepsia*, 54(12), 2166-2173. <http://doi.org/10.1111/epi.12408>
- Winston, G.P., Micallef, C., Kendell, B.E., Bartlett, P.A., Williams, E.J., Burdett, J.L. et al. (2013b). The value of repeat neuroimaging for epilepsy at a tertiary referral centre: 16 years of experience. *Epilepsy Research*, 105(3), 349-355. <http://doi.org/10.1016/j.eplepsyres.2013.02.022>
- Winston, G.P., Micallef, C., Symms, M. R., Alexander, D. C., Duncan, J. S., Zhang, H. (2014). Advanced diffusion imaging sequences could aid assessing patients with focal cortical dysplasia and epilepsy. *Epilepsy Research*, 108(2), 336-339. <http://doi.org/10.1016/j.eplepsyres.2013.11.004>
- Wisse, L.E., Biessels, G.J., Geerlings, M.I. (2014) A Critical Appraisal of the Hippocampal Subfield Segmentation Package in FreeSurfer. *Frontiers in aging neuroscience*. 2014;6:261.
- Wisse, L.E., Gerritsen, L., Zwanenburg, J.J., Kuijf, H.J., Luijten, P.R. Biessels, G.J. et al. (2012) Subfields of the hippocampal formation at 7 T MRI: in vivo volumetric assessment. *NeuroImage*. 2012 Jul 16;61(4):1043-1049.
- Wisse, L.E., Kuijf, H.J., Honingh, A.M., Wang, H., Pluta, J.B., Das, S.R. et al. (2016) Automated Hippocampal Subfield Segmentation at 7T MRI. *American Journal of*

References

- Neuroradiology, June 2016, 37 (6), 1050-1057; DOI: <https://doi.org/10.3174/ajnr.A4659>
- Witwer, B.P., Moftakhar, R., Hasan, K.M., Deshmukh, P., Haughton, V., Field, A., et al. (2002) Diffusion-tensor imaging of white matter tracts in patients with cerebral neoplasm. *J Neurosurg* 2002;97:568–575.
- Woermann, F.G., Barker, G.J., Birnie, K.D., Meencke, H.J., Duncan, J.S. (1998) Regional changes in hippocampal T2 relaxation and volume: a quantitative magnetic resonance imaging study of hippocampal sclerosis. *Journal of Neurology, Neurosurgery and Psychiatry* 1998; 65: 656–664.
- Woermann, F.G., Vollmar, C. (2009). Clinical MRI in children and adults with focal epilepsy: a critical review. *Epilepsy and Behavior*: 15(1), 40-49. <http://doi.org/10.1016/j.yebeh.2009.02.032>
- WHO (2016) World Health Organization. Epilepsy Fact sheet N°999 February 2016. <http://www.who.int/mediacentre/factsheets/fs999/en/> (accessed 16/10/2016)
- Wozniak, J.R., Mueller, B.A., Lim, K.O., Hemmy, L.S., Day, J.W. (2014) Tractography reveals diffuse white matter abnormalities in Myotonic Dystrophy Type 1. *Journal of the Neurological Sciences*, 341(0), 73–78. <http://doi.org/10.1016/j.jns.2014.04.005>
- Wyler, A.R., Hermann, B.P., Richey, E.T. (1989) Results of reoperation for failed epilepsy surgery. *Journal of Neurosurgery* 71:815–819.
- Yamamuro, T., Senzaki, K., Iwamoto, S., Nakagawa, Y., Hayashi, T., Hori, M., et al. (2010). Neurogenesis in the dentate gyrus of the rat hippocampus enhanced by tickling stimulation with positive emotion. *Neuroscience Research*, 68(4), 285-289. doi:10.1016/j.neures.2010.09.001
- Yang, F.C., Liang, K.C. (2014). Interactions of the dorsal hippocampus, medial prefrontal cortex and nucleus accumbens in formation of fear memory: Difference in inhibitory avoidance learning and contextual fear conditioning. *Neurobiology of Learning and Memory*, 112, 186-194. <http://doi.org/10.1016/j.nlm.2013.07.017>
- Yates, F. (1934). Contingency tables involving small numbers and the chi-square test. *Journal of the Royal Statistical Society*, 1, 217-235.
- Yeatman, J.D., Dougherty, R.F., Myall, N.J., Wandell, B.A., Feldman, H.M. (2012). Tract profiles of white matter properties: automating fiber-tract quantification. *PloS One*, 7(11), e49790. <http://doi.org/10.1371/journal.pone.0049790>
- Yendiki, A., Panneck, P., Srinivasan, P., Stevens, A., Zöllei, L., Augustinack, J. et al. (2011). Automated Probabilistic Reconstruction of White-Matter Pathways in Health and Disease Using an Atlas of the Underlying Anatomy. *Frontiers in Neuroinformatics*, 5, 23. <http://doi.org/10.3389/fninf.2011.00023>
- Yendiki, A., Koldewyn, K., Kakunoori, S., Kanwisher, N., Fischl, B., (2013). Spurious group differences due to headmotion in a diffusionMRI study. *NeuroImage* 88C:79–90. <http://dx.doi.org/10.1016/j.neuroimage.2013.11.027>.
- Yogarajah, M., Powell, H.W., Parker G.J., Alexander D.C., Thompson P.J., Symms M.R. et al. (2008). Tractography of the parahippocampal gyrus and material specific memory

References

- impairment in unilateral temporal lobe epilepsy. *Neuroimage*. 2008;40(4):1755-1764.
- Yotter, R.A., Ziegler, G., Nenadic, I., Thompson, P.M., Gaser, C. (2011): Local cortical surface complexity maps from spherical harmonic reconstructions. *Neuroimage*, 56(3): 961-973.
- Yu, J.T., Tan, L. (2008) Diffusion-weighted magnetic resonance imaging demonstrates parenchymal pathophysiological changes in epilepsy. *Brain Research Reviews* 2008;59:34–41.
- Yushkevich, P. A., Pluta, J. B., Wang, H., Xie, L., Ding, S.-L., Gertje, E. C., Mancuso, L., Kliot, D., Das, S. R. and Wolk, D. A. (2015a), Automated volumetry and regional thickness analysis of hippocampal subfields and medial temporal cortical structures in mild cognitive impairment. *Hum. Brain Mapp.*, 36: 258–287.
- Yushkevich, P.A., Amaral, R.S.C., Augustinack, J.C., Bender, A.R., Bernstein, J.D., Boccardi, M. et al. (2015b). *NeuroImage Quantitative comparison of 21 protocols for labeling hippocampal subfields and parahippocampal subregions in in vivo MRI : Towards a harmonized segmentation protocol*, 111, 526–541. <http://doi.org/10.1016/j.neuroimage.2015.01.004>
- Zachenhofer, I., Novak, K., Baumgartner, C., Prayer, D., Czech, T. (2011). Reoperation after selective amygdalohippocampectomy: an MRI analysis of the extent of temporomesial resection in ten cases. *Acta Neurochirurgica* (2011) 153:239–248.
- Zeidman, P., Maguire, E.A. (2016). Anterior hippocampus : the anatomy of perception, imagination and episodic memory , 17 (3) , 173 - 182 . <http://doi.org/10.1038/nrn.2015.24>.Anterior
- Zhang, Z., Liao, W., Bernhardt, B., Wang, Z., Sun, K., Yang, F. et al. (2014). Brain iron redistribution in mesial temporal lobe epilepsy: a susceptibility-weighted magnetic resonance imaging study. *BMC Neuroscience*, 15(1), 117. <http://doi.org/10.1186/s12868-014-0117-3>
- Zijdenbos, A.P., Dawant, B.M., Margolin, R.A., Palmer, A.C. (1994) Morphometric analysis of white matter lesions in MR images: method and validation. *IEEE Trans Med Imaging*, vol. 13, 716-724.
- Zola-Morgan, S., Squire, L., Amaral, D. (1986). Human amnesia and the medial temporal region: Enduring memory impairment following a bilateral lesion limited to field CA1 of the hippocampus. *Journal of Neuroscience*, 6, 2950-2967.
- Zola-Morgan, S., Squire, L., Amaral, D. (1989). Lesions of the amygdala that spare adjacent cortical regions do not impair memory or exacerbate the impairment following lesions of the hippocampal formation. *Journal of Neuroscience*, 9, 1922-1936.

APPENDIX I: Raw Data

Chapter 2: Materials and Objectives

ID	Finding	Analysis	FC	Onset	Duration	Type	Frequency	Outcome	Age	Sex	ID	Age	Sex
L3009	IHS	T2STIR	0	6	18	CPS	1	2	24	f	c0039	24	f
L3044	IHS	T2STIR	1	24	32	CPS, SGTCS	3	1	56	m	c0056	27	f
L3210	IHS	T2STIR	1	11	14	CPS, SGTCS	5	2	25	f	c0067	22	f
L3214	IHS	T2STIR	0	33	18	CPS, SGTCS	3	1	51	m	c0132	47	f
L3258	IHS	T2STIR + DTI		25	27				52	m	c0136	26	m
L3287	IHS	T2STIR	0	32	1	SPS, CPS, SGTCS	10	2	33	f	c0137	30	m
L3310	IHS	T2STIR	0	16	13	CPS, SGTCS	5	1	29	f	c0187	36	f
L3332	IHS	T2STIR	0	2	33	SPS, CPS	4	1	35	f	c0303	48	f
L3405	IHS	T2STIR	1	13	26	CPS, SGTCS	3		39	f	c0306	51	f
L3534	IHS	T2STIR	0	1	52	SPS, CPS, SGTCS	6	1	53	m	c0324	60	f
L3663	IHS	T2STIR	0	14	50	CPS	3	1	64	f	c0331	59	m
L4099	IHS	T2STIR + DTI		34	22				56	f	c0337	47	m
L4187	IHS	T2STIR	0	2	51	SPS, CPS, SGTCS	8	2	53	m	c0349	50	m
L4194	IHS	T2STIR	1	19	9	CPS, SGTCS	7	2	28	m	c0359	46	f
L4195	IHS	T2STIR	1	5	42	CPS, SGTCS	4	2	47	m	c0389	27	f
L4248	IHS	T2STIR	0	0	22	CPS	30	1	22	f	c0442	24	f
L4258	IHS	T2STIR	1	15	5	SPS, CPS	60		20	f	c0443	29	m
L4417	IHS	T2STIR	0	3	14	SPS, CPS	1	1	17	f	c0449	26	f
L4553	IHS	T2STIR	1	2	47	SPS, CPS	1	1	49	f	c0474	24	f
L4635	IHS	T2STIR	0	29	10	CPS, SGTCS	3	1	39	f	c0542	44	m
L4695	IHS	T2STIR + DTI		5	18				23	f	c0627	50	m
L4781	IHS	T2STIR	1	6	26	SPS, CPS, SGTCS	7	2	32	f	c0660	62	f
L4969	IHS	T2STIR + DTI		29	19				48	f	c0688	24	f
L4974	IHS	DTI	0	15	29	SPS, CPS	4	1	44	f	c0773	28	m
L4984	IHS	T2STIR	0	33	23	SPS, CPS	30	2	56	f	c0923	23	f
L4995	IHS	T2STIR + DTI	0	1	42	CPS, SGTCS	2	2	43	f	c1088	35	m
L5018	IHS	T2STIR + DTI		12	15				27	m	c3318	58	f
L5041	IHS	T2STIR + DTI	0	21	24	CPS	15	1	45	f	c3422	18	f
L5091	IHS	T2STIR	0	9	33	SPS, CPS	60	1	42	f	c3457	61	f
L5110	IHS	T2STIR	1	13	14	SPS, CPS	2	1	27	f	c3466	45	m
L5125	IHS	T2STIR + DTI		26	26				52	m	c3614	39	f
L5187	IHS	T2STIR	1	18	12	CPS, SGTCS	5	1	30	f	c3614	39	f
L5214	IHS	T2STIR	0	18	3	CPS	4	2	21	m	c3660	60	f
L5222	IHS	T2STIR + DTI	0	13	10	CPS, SGTCS	1	2	23	f	c3667	55	f
L5242	IHS	T2STIR + DTI	0	13	20	SPS, CPS, SGTCS	2	2	33	f	c3728	61	f
L5302	IHS	DTI	0	12	42	CPS, SGTCS	6	2	54	f	c3734	27	m
L5303	IHS	DTI	1	15	34	CPS	1	2	49	f	c3768	37	m
L5309	IHS	T2STIR + DTI	1	3	43	SPS, CPS	8	2	46	m	c3789	44	m
L5351	IHS	T2STIR + DTI		28	17				45	f	c3790	48	m
L5416	IHS	T2STIR + DTI	1	13	19	SPS, CPS	4	2	32	m	c3826	42	f
L5424	IHS	T2STIR + DTI	0	5	36	SPS, SGTCS	3	1	41	m	c3891	59	m
L5433	IHS	T2STIR	0	11	33	SPS, CPS	3	2	44	m	c3955	46	f
L5436	IHS	T2STIR + DTI	1	3	42	CPS	3	1	45	f	c4064	32	m
L5438	IHS	T2STIR + DTI	1	9	18	CPS, SGTCS	4	1	27	m	c4130	38	f
L5447	IHS	T2STIR + DTI	0	30	18	SPS, CPS, SGTCS	15	1	48	f	c4277	22	m
L5449	IHS	T2STIR	0	34	23	SPS, CPS, SGTCS	20	1	57	m	c4279	23	f
L5480	IHS	T2STIR + DTI	0	29	3	SPS	8	2	32	f	c4335	45	m
L5537	IHS	T2STIR	0	5	46	SPS, CPS	5	2	51	m	c4594	67	f
L5606	IHS	T2STIR + DTI	0	9	17	SPS, CPS	4	2	26	f	c4597	41	m
L5658	IHS	T2STIR + DTI							44	m	c4901	46	m
L5702	IHS	T2STIR	1	42	9	SPS, CPS, SGTCS	5	2	51	m	c4928	45	f
L5757	IHS	T2STIR	0	26	24	SPS, CPS	5	1	50	m	c4932	31	f
L5777	IHS	T2STIR + DTI	0	1	21	SPS, CPS	12	1	22	m	c5236	25	f
L5842	IHS	T2STIR	1	3	28	SPS, CPS	1	2	31	m	c5377	25	f
L5948	IHS	T2STIR + DTI		2	34				36	f	c5412	48	m
L5959	IHS	T2STIR	1	16	8	CPS	90	2	24	f	c5511	19	m
L6017	IHS	T2STIR + DTI	1	15	35	CPS, SGTCS	6	2	50	f	c5673	36	m
L6023	IHS	T2STIR + DTI	0	34	36	CPS	6	2	70	f	c7174	48	f

Table 2.A. Raw data for patients and controls (Studies 1 & 2). FC = febrile convulsions, l = left, c = control, HS = hippocampal sclerosis, CPS = complex partial seizure, SPS = simple partial seizure, SGTCS = secondary-generalized tonic-clonic seizure, m/f = male / female, Onset/Age/Duration in years, frequency per month. 0/1 = no/yes. Empty cells indicate missing data. DTI = diffusion tensor imaging, T2STIR = T2 Short TI Inversion Recovery.

APPENDIX

ID	Finding	Analysis	FC	Onset	Duration	Type	Frequency	Outcome	Age	Sex
L6077	IHS	T2STIR + DTI	0	14	40	SPS, CPS, SGTCS	1	1	54	f
L6078	IHS	T2STIR + DTI	1	18	9	SPS, SGTCS	5	1	27	m
L6116	IHS	T2STIR + DTI		14	11				25	f
L6126	IHS	T2STIR + DTI	0	35	2	CPS, SGTCS	10	1	37	m
L6178	IHS	T2STIR + DTI	0	30	5	CPS	2	1	35	m
L6189	IHS	T2STIR + DTI	0	17	22	CPS, SGTCS	3		39	m
L6300	IHS	T2STIR + DTI	0	36	3	CPS	4	2	39	f
L6369	IHS	T2STIR + DTI		17	11				28	f
L6522	IHS	T2STIR + DTI	0	21	41	SPS, CPS	2	2	62	f
L6541	IHS	T2STIR + DTI	0	47	21	SPS, SGTCS	10		68	f
L6549	IHS	T2STIR + DTI	1	15	14	CPS	6	2	29	f
L6794	IHS	T2STIR + DTI	0	5	38	CPS	3	2	43	f
L7064	IHS	T2STIR + DTI		46	4				50	m
L7193	IHS	T2STIR		35	16				51	f
L7220	IHS	T2STIR + DTI		21	41				62	f
R1087	rHS	DTI	0	39	12	SPS, CPS	1	1	51	m
R3221	rHS	T2STIR	0	21	15	CPS	3	1	36	m
R3444	rHS	T2STIR	0	25	5	CPS, SGTCS	6	1	30	m
R3463	rHS	T2STIR	0	44	14	CPS	5	1	58	m
R3498	rHS	T2STIR	1	2	21	CPS	30	2	23	f
R4119	rHS	T2STIR	0	31	17	CPS	4	1	48	m
R4523	rHS	T2STIR + DTI	1	7	18	CPS	3	1	25	m
R4585	rHS	T2STIR + DTI		14	8				22	m
R4700	rHS	T2STIR + DTI	1	1	15	CPS, SGTCS	8	2	16	f
R4751	rHS	T2STIR	1	20	23	CPS, SGTCS	4	1	43	f
R4858	rHS	T2STIR + DTI	1	11	8	SPS, CPS	10	1	19	m
R4972	rHS	T2STIR		25	30				55	f
R4993	rHS	T2STIR	0	38	3	SPS, CPS	10	1	41	f
R5051	rHS	T2STIR	0	6	59	CPS	4	2	65	f
R5141	rHS	T2STIR + DTI		4	52				56	f
R5208	rHS	T2STIR + DTI	0	5	29	CPS	3	1	34	m
R5219	rHS	T2STIR + DTI	0	22	14	SPS, CPS, SGTCS	4	2	36	f
R5249	rHS	T2STIR		1	51				52	m
R5346	rHS	T2STIR + DTI		6	31				37	m
R5412	rHS	T2STIR	1	15	32	CPS	0	1	47	m
R5425	rHS	T2STIR	1	12	12	SPS	4		24	m
R5492	rHS	T2STIR	0	1	20	CPS	1	1	21	m
R5505	rHS	T2STIR	0	17	38	SPS, CPS	1	2	55	f
R5844	rHS	T2STIR + DTI	0	1	44	CPS, SGTCS	2	1	45	m
R5968	rHS	T2STIR + DTI		22	18				40	m
R5973	rHS	T2STIR + DTI	0	7	55	CPS, SGTCS	1	2	62	f
R5974	rHS	DTI	0	34	12	SPS, SGTCS	1	1	46	m
R6058	rHS	T2STIR + DTI	1	33	4	CPS	5	2	37	m
R6081	rHS	T2STIR + DTI	0	24	6	SPS, CPS	90	1	30	m
R6091	rHS	DTI							48	f
R6297	rHS	T2STIR + DTI	0	11	13	CPS, SGTCS	3	1	24	f
R6426	rHS	T2STIR	0	7	30	SPS, CPS	3	1	37	m
R6580	rHS	T2STIR		44	16				60	m
R6596	rHS	T2STIR + DTI	0	19	7	SPS, CPS	4	2	26	m
R6671	rHS	T2STIR + DTI		18	49				67	f
R6770	rHS	T2STIR + DTI		27	29				56	f
R6774	rHS	T2STIR + DTI	1	12	47	SPS, CPS	4	1	59	f
R6800	rHS	T2STIR	1	19	7	CPS, SGTCS	2	1	26	m
R7192	rHS	T2STIR + DTI	0	13	35	CPS	2	1	48	f
R7231	rHS	DTI							50	m

Table 2.A. (continued). Raw data for patients (Studies 1 & 2). FC = febrile convulsions, r = right, l = left, HS = hippocampal sclerosis, CPS = complex partial seizure, SPS = simple partial seizure, SGTCS = secondary-generalized tonic-clonic seizure, m/f = male / female, Onset/Age/Duration in years, frequency per month. 0/1 = no/yes. Empty cells indicate missing data. DTI = diffusion tensor imaging, T2STIR = T2 Short TI Inversion Recovery.

ID	Finding	Comorbidity	CB	FC	Infection	Onset	Duration	Localization	Type	Frequency	Family	Age	Sex	Surgery
REF005	0	0	0	0	0	47	14	ITL	GS-A, CPS	4	0	61	f	
REF007	0	0	0	0	0	19	9	ITL	CPS	14	0	28	m	
REF010	0	depression	0	0	0	3	22	ITL	CPS	3.5	1	25	f	
REF011	0	0	1	0	1	10	12	rTL	GS-A	1	1	22	m	
REF014	0	0	0	0	0	12	10	IFL	GS-A, SGTCS, CPS	1	0	22	m	
REF015	0	0	0	0	0	6	12	IFL	CPS, SGTCS	2.5	0	18	f	
REF017	0	N/A	0	0	0	17	10	biFL	CPS	46	0	27	f	
REF019	0	0	0	0	0	29	12	rTL	CPS, SGTCS	2	1	41	f	
REF021	0	depression	0	0	0	14	27	ITL	GS-A; SGTCS	3.5	1	41	m	
REF022	SVD, rHS	0	0	0	0	5	50	rTL	SPS, SGTCS, CPS	2	1	54	f	Right temporal lobectomy
REF024	rHS	anxiety	0	1	1	36	2.5	rTL	SGTCS	0.5	1	39	f	
REF025	biHS	anxiety	0	0	0	34	13	biTL	GS-A, SGTCS, CPS	2	0	47	m	
REF027	IHS	0	0	1	0	7	31	ITL	CPS, SGTCS	0.5	1	38	f	
REF030	0	0	0	0	0	12	7	ITL	CPS, SGTCS	1	0	19	f	
REF031	0	0	0	0	0	6	13	IFL	SGTCS, SPS	7	0	19	m	
REF032	0	0	0	0	0	29	6	unknown	SPS, SGTCS	7	0	35	f	
REF034	0	depression	0	0	1	9	43	rFL	SPS, SGTCS	3	0	52	m	
REF038	IHS	0	unsure	0	0	15	15	ITL	SGTCS	1	1	30	f	Left temporal lobectomy
REF042	0	0	0	0	0	17	4	IFL	SGTCS	0.5	1	21	f	
REF044	0	N/A	unsure	0	0	28	6	rTL	SPS	14	0	34	f	
REF049	0	0	0	0	0	17	12	rFL	SGTCS	2	1	29	f	
REF051	IHS + FCD	anorexic	0	1	0	6	37	ITL	CPS, SGTCS	2	0	43	f	
REF052	0	0	1	0	0	16	3	rTL	CPS, SGTCS	2	0	19	m	
REF054	0	depression, anxiety	0	0	0	4	41	FL, side unknown	SPS	1	1	45	f	
REF056	rHS + FCD	depression	0	0	1	6	17	rTL	GS-A, CPS	2.5	0	23	f	Right anterior temporal lobectomy
REF058	0	0	0	0	0	23	15	FL, side unknown	SPS, SGTCS	0.06	1	38	m	
REF059	FCD	depression	0	0	0	6	21	left FCD involved	SGTCS, CPS	7	1	27	f	
REF061	left encephalocele	0	0	1	0	30	6	LTL	SGTCS	2 per year	0	36	f	
REF062	0	0	0	0	0	28	11	ITL	SGTCS, CPS	1	1	39	m	
REF064	0	depression	1	0	0	13	12	rFL	SGTCS, CPS, GS-A	2	0	25	f	
REF065	FCD	depression, memory	0	0	0	5	17	rFL	SGTCS, SPS, CPS, GS-A	6	1	22	m	
REF066	IHS	0	0	0	0	10	8	ITL	SGTCS, CPS, SPS	1	1	18	m	
REF068	0	anxiety, low mood	0	0	0	19	9	possibly rTP	GS-A, SGTCS	7	0	28	f	
REF069	right-sided gliosis	0	1	0	0	10	19	rTP	CPS, SGTCS	7	0	29	m	
REF079	0	0	0	0	0	13	16	ITL	SGTCS	0.25	0	29	m	
REF080	0	0	0	0	0	28	22	TL, side unknown	CPS	1	0	50	f	
REF081	IHS	0	0	1	0	7	33	ITL	CPS-A	2	0	40	f	Planned: left hippocampectomy
REF082	0	0	0	0	0	13	22	left, lobe unknown	CPS, SGTCS	2	0	35	m	
REF084	enlarged left amygdala	0	0	0	0	18	1	ITL	CPS, SGTCS	35	1	19	f	
REF085	0	0	1	1	0	1	21	IFL	CPS, SGTCS	35	1	22	f	
REF086	0	migraine	0	0	0	4	17	ITL	CPS	4	0	21	f	
REF087	0	0	0	0	1	15	7	rTL	SPS, CPS, SGTCS	2 per year	1	22	m	
REF089	0	0	0	0	0	19	8	ITL	CPS, SGTCS	1	0	27	m	

Table 2.B. Raw data for patients (Studies 3-5). CB = Complications at birth, FC = febrile convulsions, SVD = Small Vessel Disease, r = right, l = left, HS = hippocampal sclerosis, FCD = focal cortical dysplasia, TL = temporal lobe, FL = frontal lobe, TP = temporoparietal, GS = generalized seizure, A = absence, CPS = complex partial seizure, SPS = simple partial seizure, SGTCS = secondary-generalized tonic-clonic seizure, m/f = male / female, Family = Family history of epilepsy. Onset/Age/Duration in years, frequency per week. 0/1 = no/yes. Boldface: presence of potentially epileptogenic lesion (neuroradiological assessment, epilepsy research dedicated MRI).

APPENDIX

Participant	Age	Sex
REF001	24	f
REF002	22	m
REF003	23	m
REF004	23	m
REF006	22	m
REF008	27	f
REF009	37	m
REF012	25	f
REF013	60	f
REF018	26	f
REF020	50	f
REF023	32	m
REF026	38	f
REF028	28	f
REF029	41	f
REF033	21	f
REF035	33	f
REF036	32	f
REF037	34	f
REF039	37	m
REF040	35	m
REF041	45	f
REF043	26	m
REF045	38	m
REF046	27	f
REF047	45	m
REF048	34	f
REF050	43	m
REF053	25	m
REF055	38	m
REF063	39	f
REF067	26	f
REF071	28	f
REF072	25	f
REF073	32	f
REF074	39	m
REF075	27	f
REF076	34	m
REF077	25	f
REF078	24	f
REF083	24	f
REF088	43	m

Table 2.B. (continued). Raw data for controls (Studies 3-5). m/f = male / female. Age in years. Controls with IDs REF001 (no T1w FSPGR) and REF072 (structural lesion) had to be excluded from further imaging analysis (Section 2.3.2.2).

APPENDIX II: Supplementary Material

Chapter 9: Manual and Automated Tractography Approaches in Patients with 'non-lesional' and lesional Temporal Lobe Epilepsy

Tract		M (SD)			p-values (Bonferroni)			Statistics	
		ITLE	C	rTLE	ITLE vs C	ITLE vs rTLE	C vs rTLE	χ^2 -statistic	p-value
Manual									
UF	l	0.46 (0.03)	0.48 (0.03)	0.45 (0.08)	<0.05	1	0.7	7.8	<0.05
FA	r	0.45 (0.03)	0.47 (0.03)	0.45 (0.02)	-	-	-	5	0.08
UF	l	0.86 (0.04)	0.82 (0.03)	0.85 (0.05)	<0.05	1	0.27	9.7	<0.01
MD	r	0.9 (0.04)	0.86 (0.04)	0.88 (0.03)	<0.05	1	0.85	8.6	<0.05
PHWM	l	0.42 (0.05)	0.43 (0.03)	0.42 (0.02)	-	-	-	1.9	0.4
FA	r	0.43 (0.04)	0.45 (0.04)	0.43 (0.05)	<0.05	1	1	6.8	<0.05
PHWM	l	0.9 (0.08)	0.88 (0.06)	0.97 (0.12)	0.4	0.8	<0.05	6.7	<0.05
MD	r	0.9 (0.1)	0.84 (0.07)	0.91 (0.1)	<0.05	1	0.26	8.7	<0.05
AFQ									
UF	l	0.45 (0.03)	0.47 (0.04)	0.47 (0.03)	-	-	-	3.7	0.2
FA	r	0.44 (0.02)	0.45 (0.03)	0.44 (0.02)	-	-	-	3.1	0.2
UF	l	0.84 (0.05)	0.82 (0.03)	0.81 (0.03)	-	-	-	5.2	0.07
MD	r	0.88 (0.03)	0.85 (0.06)	0.87 (0.03)	<0.05	1	0.7	6.4	<0.05
PHWM	l	0.39 (0.04)	0.4 (0.03)	0.4 (0.02)	-	-	-	1.3	0.5
FA	r	0.4 (0.03)	0.42 (0.02)	0.41 (0.04)	<0.05	0.69	1	7.02	<0.05
PHWM	l	0.97 (0.07)	0.95 (0.07)	0.95 (0.07)	-	-	-	1.2	0.5
MD	r	0.9 (0.05)	0.91 (0.1)	0.91 (0.1)	-	-	-	0.25	0.8

Table 9.A. Whole-tract diffusion measures for manual (top) versus AFQ (bottom) tractography.

Abbreviations: M = Mean; SD = Standard Deviation; TLE = Temporal Lobe Epilepsy; C = Control; l = left; r = right; AFQ = Automated Fiber Quantification; FA = fractional anisotropy; MD = mean diffusivity (in 10^{-3} mm²/s); UF = uncinate fasciculus; PHWM = parahippocampal white matter bundle

APPENDIX

	UF FA		UF MD (in $10^{-3}\text{mm}^2/\text{s}$)		PHWM FA		PHWM MD (in $10^{-3}\text{mm}^2/\text{s}$)	
	lpsi	Contra	lpsi	Contra	lpsi	Contra	lpsi	Contra
MANUAL								
female	0.45 (0.03)	0.44 (0.05)	0.87 (0.05)	0.89 (0.06)	0.4 (0.04)	0.42 (0.02)	0.92 (0.08)	0.92 (0.09)
male	0.46 (0.03)	0.46 (0.03)	0.86 (0.03)	0.89 (0.04)	0.4 (0.05)	0.44 (0.04)	0.9 (0.13)	0.94 (0.14)
Z; $p(\text{FDR})$	0; 1	-0.8; 0.8	0.5; 1	-0.4; 1	-1.3; 0.67	-1.2; 0.68	1.1; 0.69	0.15; 1
SGTCS	0.46 (0.04)	0.45 (0.06)	0.87 (0.05)	0.88 (0.04)	0.44 (0.05)	0.43 (0.03)	0.89 (0.07)	0.91 (0.08)
SGTCS No	0.46 (0.01)	0.44 (0.02)	0.85 (0.03)	0.91 (0.06)	0.41 (0.04)	0.42 (0.03)	0.95 (0.12)	0.96 (0.14)
Z; $p(\text{FDR})$	0.5; 1	1.4; 0.67	0.96; 0.78	-1.6; 0.67	1.67; 0.67	1.67; 0.67	-1.46; 0.67	-0.76; 0.84
HS	0.45 (0.04)	0.45 (0.03)	0.88 (0.05)	0.89 (0.05)	0.41 (0.05)	0.42 (0.04)	0.95 (0.08)	0.92 (0.08)
HS No	0.46 (0.02)	0.45 (0.05)	0.86 (0.04)	0.89 (0.05)	0.43 (0.05)	0.43 (0.03)	0.9 (0.1)	0.93 (0.12)
Z; $p(\text{FDR})$	-0.2; 1	-0.03; 1	0.6; 0.98	0.03; 1	-1.2; 0.68	-0.2; 1	1.6; 0.67	0.18; 1
Febrile	0.45 (0.04)	0.45 (0.03)	0.87 (0.05)	0.89 (0.06)	0.39 (0.04)	0.41 (0.03)	0.97 (0.07)	0.94 (0.07)
Febrile No	0.46 (0.03)	0.45 (0.05)	0.86 (0.04)	0.89 (0.05)	0.43 (0.05)	0.43 (0.03)	0.9 (0.1)	0.93 (0.1)
Z; $p(\text{FDR})$	0.16; 1	-0.3; 1	0.16; 1	0; 1	-1.4; 0.67	-1; 0.78	1.8; 0.67	0.8; 0.8
AFQ								
female	0.44 (0.02)	0.45 (0.02)	0.86 (0.05)	0.85 (0.04)	0.39 (0.04)	0.39 (0.01)	0.95 (0.08)	0.91 (0.05)
male	0.47 (0.03)	0.46 (0.04)	0.85 (0.03)	0.87 (0.05)	0.42 (0.03)	0.42 (0.04)	0.93 (0.06)	0.92 (0.09)
Z; $p(\text{FDR})$	-2.2; 0.6	-0.1; 1	0.2; 1	-0.84; 0.87	-1.6; 0.63	-1.6; 0.63	0.34; 1	0.03; 1
SGTCS	0.45 (0.03)	0.46 (0.03)	0.86 (0.05)	0.85 (0.04)	0.4 (0.04)	0.41 (0.03)	0.94 (0.08)	0.91 (0.06)
SGTCS No	0.45 (0.01)	0.45 (0.02)	0.83 (0.02)	0.87 (0.04)	0.4 (0.03)	0.4 (0.02)	0.95 (0.07)	0.9 (0.07)
Z; $p(\text{FDR})$	-0.65; 0.87	0.47; 0.97	1.4; 0.7	-0.79; 0.87	0.3; 1	1; 0.87	-0.2; 1	-1; 0.87
HS	0.44 (0.04)	0.45 (0.03)	0.87 (0.06)	0.87 (0.03)	0.38 (0.04)	0.39 (0.02)	0.99 (0.08)	0.92 (0.05)
HS No	0.45 (0.02)	0.45 (0.03)	0.84 (0.03)	0.86 (0.04)	0.41 (0.03)	0.41 (0.03)	0.92 (0.06)	0.92 (0.07)
Z; $p(\text{FDR})$	-0.7; 0.87	-0.7; 0.87	0.67; 0.87	0.5; 0.97	-1.87; 0.6	-0.77; 0.87	1.7; 0.63	0.03; 1
Febrile	0.44 (0.03)	0.44 (0.01)	0.86 (0.06)	0.86 (0.04)	0.37 (0.04)	0.39 (0.02)	0.97 (0.1)	0.92 (0.05)
Febrile No	0.45 (0.03)	0.46 (0.03)	0.85 (0.04)	0.86 (0.04)	0.41 (0.04)	0.41 (0.03)	0.94 (0.6)	0.92 (0.07)
Z; $p(\text{FDR})$	-0.3; 1	-1.1; 0.87	0; 1	0; 1	-1.6; 0.63	-1.4; 0.7	0.7; 0.87	0.14; 1

Table. 9.B. Comparison of FA/MD values from all tracts between patient groups according to sex, presence of HS, SGTCS and history of febrile seizures. Mean and standard deviations (in brackets) are presented for each tract. No significant effects were observed for either manual or AFQ generated tracts. UF = uncinate fasciculus; PHWM = parahippocampal white matter bundle; FA = fractional anisotropy; MD = mean diffusivity; ipsi = ipsilateral; contra = contralateral; HS = hippocampal sclerosis; SGTCS = secondary-generalized tonic-clonic seizures.